NAVAL POSTGRADUATE SCHOOL

MONTEREY, CALIFORNIA

DISSERTATION

FRESHWATER EXPORT FROM THE ARCTIC OCEAN AND ITS DOWNSTREAM EFFECT ON LABRADOR SEA DEEP CONVECTION IN A HIGH-RESOLUTION NUMERICAL MODEL

by

Timothy P. McGeehan

December 2010

Dissertation Supervisor: Wieslaw Maslowski

Approved for public release; distribution is unlimited

THIS PAGE INTENTIONALLY LEFT BLANK

REPORT DOCUMENTATION PAGE		*Form Approved OMB No. 0704-0188*
Public reporting burden for this collection of information is estimated to average 1 hour per response, including the time for reviewing instruction, searching existing data sources, gathering and maintaining the data needed, and completing and reviewing the collection of information. Send comments regarding this burden estimate or any other aspect of this collection of information, including suggestions for reducing this burden, to Washington headquarters Services, Directorate for Information Operations and Reports, 1215 Jefferson Davis Highway, Suite 1204, Arlington, VA 22202-4302, and to the Office of Management and Budget, Paperwork Reduction Project (0704-0188) Washington DC 20503.		

1. AGENCY USE ONLY *(Leave blank)*	2. REPORT DATE December 2010	3. REPORT TYPE AND DATES COVERED Dissertation

4. TITLE AND SUBTITLE: Freshwater Export from the Arctic Ocean and Its Downstream Effect on Labrador Sea Deep Convection in a High-Resolution Numerical Model	5. FUNDING NUMBERS
6. AUTHOR(S) Timothy P. McGeehan	

7. PERFORMING ORGANIZATION NAME(S) AND ADDRESS(ES) Naval Postgraduate School Monterey, CA 93943-5000	8. PERFORMING ORGANIZATION REPORT NUMBER

9. SPONSORING / MONITORING AGENCY NAME(S) AND ADDRESS(ES) N/A	10. SPONSORING / MONITORING AGENCY REPORT NUMBER

11. SUPPLEMENTARY NOTES The views expressed in this thesis are those of the author and do not reflect the official policy or position of the Department of Defense or the U.S. Government. IRB Protocol number _____.

12a. DISTRIBUTION / AVAILABILITY STATEMENT Approved for public release; distribution is unlimited	12b. DISTRIBUTION CODE A

13. ABSTRACT (maximum 200 words)

The Labrador Sea is one of the only known locations of deep open ocean convection, a process determined to play a significant role in regulating global thermohaline circulation and climate. The main hypothesis of this study is that low salinity water from the Arctic Ocean, particularly outflow through the Canadian Arctic Archipelago (CAA), may affect Labrador Sea deep convection. To address it, output from a pan-Arctic high-resolution coupled ice-ocean model was examined. Volume and freshwater fluxes through the CAA for 1979-2004 were found in good agreement with the observations. Further analyses suggest that the flow through the major CAA channels depends on the sea surface height gradient between the Arctic Ocean and northern Baffin Bay. Freshwater flux anomalies entering the Labrador Sea through Davis Strait do not immediately affect deep convection. Instead, eddies and sea ice acting on shorter time scales can move freshwater to locations of active convection and halt the process, which underscores the importance of high-resolution. Also, changing ice conditions revealed the Northwest Passage was a possible shipping route in three summers. Finally, preliminary results from an eddy-resolving model configuration suggest that many of the shortcomings in this model may be rectified with higher spatial resolution.

14. SUBJECT TERMS Arctic Ocean, Labrador Sea, Canadian Arctic Archipelago, climate change, deep convection, sea ice, freshwater, eddies, oceanography, numerical modeling, Northwest Passage	15. NUMBER OF PAGES 209
	16. PRICE CODE

17. SECURITY CLASSIFICATION OF REPORT Unclassified	18. SECURITY CLASSIFICATION OF THIS PAGE Unclassified	19. SECURITY CLASSIFICATION OF ABSTRACT Unclassified	20. LIMITATION OF ABSTRACT UU

i

THIS PAGE INTENTIONALLY LEFT BLANK

FRESHWATER EXPORT FROM THE ARCTIC OCEAN AND ITS DOWNSTREAM EFFECT ON LABRADOR SEA DEEP CONVECTION IN A HIGH-RESOLUTION NUMERICAL MODEL

Timothy P. McGeehan
Lieutenant Commander, United States Navy
B.S., United States Naval Academy, 2000
M.S., Naval Postgraduate School, 2008

Submitted in partial fulfillment of the
requirements for the degree of

DOCTOR OF PHILOSOPHY IN PHYSICAL OCEANOGRAPHY

from the

NAVAL POSTGRADUATE SCHOOL
December 2010

Author: _____
Timothy P. McGeehan

Approved by:

_____ _____
Wieslaw Maslowski   Peter Chu
Research Professor of Oceanography Professor of Oceanography
Dissertation Supervisor,
Committee Chair

_____ _____
Timothy Stanton   Rebecca Stone
Research Associate   Military Faculty
Professor of Oceanography

_____
Peter Guest
Research Professor of Meteorology

Approved by: _____
Jeffrey Paduan, Chair, Department of Oceanography

Approved by: _____
Douglas Moses, Vice Provost for Academic Affairs

iii

THIS PAGE INTENTIONALLY LEFT BLANK

ABSTRACT

The Labrador Sea is one of the only known locations of deep open ocean convection, a process determined to play a significant role in regulating global thermohaline circulation and climate. The main hypothesis of this study is that low salinity water from the Arctic Ocean, particularly outflow through the Canadian Arctic Archipelago (CAA), may affect Labrador Sea deep convection. To address it, output from a pan-Arctic high-resolution coupled ice-ocean model was examined. Volume and freshwater fluxes through the CAA for 1979-2004 were found in good agreement with the observations. Further analyses suggest that the flow through the major CAA channels depends on the sea surface height gradient between the Arctic Ocean and northern Baffin Bay. Freshwater flux anomalies entering the Labrador Sea through Davis Strait do not immediately affect deep convection. Instead, eddies and sea ice acting on shorter time scales can move freshwater to locations of active convection and halt the process, which underscores the importance of high-resolution. Also, changing ice conditions revealed the Northwest Passage was a possible shipping route in three summers. Finally, preliminary results from an eddy-resolving model configuration suggest that many of the shortcomings in this model may be rectified with higher spatial resolution.

THIS PAGE INTENTIONALLY LEFT BLANK

TABLE OF CONTENTS

THIS PAGE INTENTIONALLY LEFT BLANK

LIST OF FIGURES

xiv

LIST OF TABLES

THIS PAGE INTENTIONALLY LEFT BLANK

LIST OF ACRONYMS AND ABBREVIATIONS

AMSA	Arctic Marine Shipping Assessment
AO	Arctic Oscillation
CAA	Canadian Arctic Archipelago
CNA	Center for Naval Analyses
ECMWF	European Center for Medium range Weather Forecasting
EEZ	Economic Exclusive Zone
EKE	Eddy Kinetic Energy
IBCAO	International Bathymetric Chart of the Arctic Ocean
NAO	North Atlantic Oscillation
NATO	North Atlantic Treaty Organization
NOAA	National Oceanic and Atmospheric Administration
NSIDC	National Snow and Ice Data Center
NWP	Northwest Passage
OWSB	Ocean Weather Station Bravo
S	Salinity
SSH	Sea Surface Height
SSHA	Sea Surface Height Anomaly
SSS	Sea Surface Salinity
SST	Sea Surface Temperature
T	Temperature
TKE	Total Kinetic Energy
UNCLOS	United Nations Convention on the Law of the Sea
USCG	United States Coast Guard

USGS	United States Geological Survey
WGC	West Greenland Current
WMO	World Meteorological Organization

ACKNOWLEDGMENTS

First and foremost, I'd like to thank my wife Kristi, who has been so supportive of this endeavor and held down the fort while I was working. I thank Aidan and Erin for sacrificing some time with Daddy so I could finish.

At NPS, I'd like to thank my advisor Wieslaw Maslowski for his patience, advice, and keeping this train on the tracks where I might have gone off on a tangent. I am deeply indebted to Jackie Clement-Kinney for her help with data, programming, and all things IT. I also thank Robert Osinski, who patiently walked me through the 2 km modeling process, even though we were separated by nine time zones. I also thank Peter Chu, Tim Stanton, Rebecca Stone, and Peter Guest who did me the honor of sitting on my committee.

Funding for the development and integration of the coupled ice-ocean model was provided by the ARCSS Program of the National Science Foundation, the Climate Change Prediction Program of the Department of Energy, and the Office of Naval Research. Computer resources were provided by the Arctic Region Supercomputer Center (ARSC) and the Navy DOD Supercomputing Resource Center (DSRC).

Finally, I'd like to thank my long-time "patron," the U.S. Navy, which recognizes the value of a well educated officer corps and has sponsored my education from BS to MS to PhD. Hopefully these opportunities will continue to expand for others, as the following quote was never more applicable than it is today:

> A nation that draws too broad a distinction between its warriors and its scholars will have its thinking done by cowards and its fighting done by fools.
>
> -Thucydides

THIS PAGE INTENTIONALLY LEFT BLANK

I. GENERAL INTRODUCTION

Our main object was to explore the unknown Polar Sea.

-Fridtjof Nansen, 1902

Despite centuries of exploration, much about the Arctic Ocean remains unknown. It is a remote and harsh environment, hindering attempts at both in situ and remote data collection. However, long-term human perseverance and advances in technology have allowed for expanded data gathering, shedding new light on the region. The Arctic Ocean is surrounded by land with narrow openings to the North Pacific and North Atlantic oceans. It has vast shelves and two deep basins, the Eurasian and Canada Basin, which are separated by the Lomonosov Ridge. While there are shallow connections via the Barents Sea opening, Bering Strait, and Canadian Arctic Archipelago (CAA), the only deep connection to the world ocean is via Fram Strait (Figure 1).

Arctic sea ice plays important roles in regulating climate. Sea ice moderates the exchange of radiation, sensible heat, and momentum between the atmosphere and ocean (McBean et al. 2005). Its formation and ablation also affect water density and stratification by alternately removing and adding freshwater to the ocean surface and brines on freezing. Major climate modeling studies have predicted that the Arctic will experience some of the largest changes in response to current global warming trends and the perennial sea ice is expected to disappear (Solomon et al. 2007). The science community is trying to observe and model the Arctic and its variability in order to better understand this complex and highly non-linear system. New insight could lead to better prediction of changes in the Arctic region. Furthermore, due to the interconnected nature of the global climate system, better understanding of the Arctic would allow enhanced prediction of downstream effects that may occur elsewhere in the world.

The Arctic Ocean has also long been recognized as a potential shortcut for maritime trade between Europe and the Far East. However, the presence of its perennial

ice cap has been a barrier to transpolar shipping. In recent years the ice has been observed both thinning and receding. Navigable stretches of open water are appearing.

The Arctic seafloor has also been shown to be rich in natural resources, especially oil and natural gas. Extraction of these resources was previously considered impractical due to the environmental conditions and low cost of oil and gas. However, as the ice reduces, Arctic resource extraction becomes more viable. With rising costs of energy and an unstable Middle East, the Arctic option is becoming even more attractive.
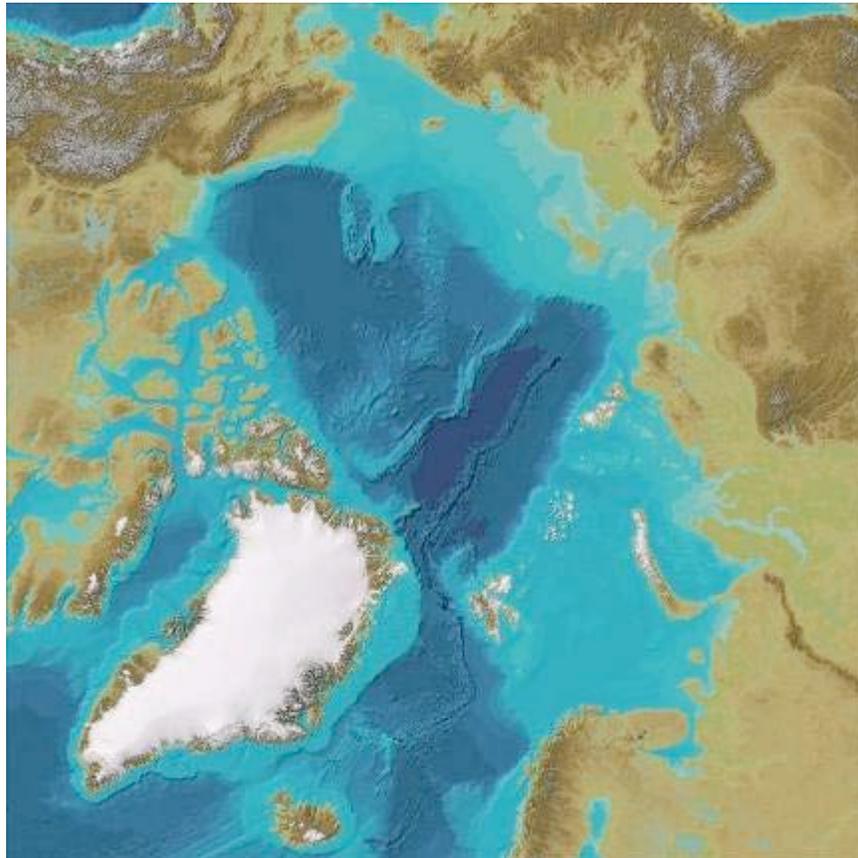
Figure 1.　Bathymetry of the Arctic Ocean (from IBCAO; Jakobsson et al. 2008).

National governments have realized that there may be future competition for both the Arctic trade routes and the resources. In the past, wars have been fought elsewhere over trade routes and resources. As such, militaries are now working to enhance their capabilities to operate and exert sovereignty in the region. During the Cold War, militaries planned and executed operations in the Arctic because its location made it

strategically valuable, a status it lost after the fall of the USSR and the end of the Cold War. However, with further ice retreat being forecast, eyes are turning to the Arctic once again.

A.   HISTORIC BACKGROUND

For centuries, European nations sought a sea route between the North Atlantic and Pacific Ocean, linking Europe with the Far East. Traveling via this "Northwest Passage" would have been a significantly shorter alternative to the long and dangerous voyages around the Cape of Good Hope or Cape Horn. This would have allowed increased trade in exotic goods and spices from the Far East, greatly benefiting their economies. Simply put, finding a route was in their national interests.

Among those early explorers who sought the Northwest Passage were Cartier, Frobisher, Davis, Hudson, and Baffin. These men left their names upon the map but did not achieve their missions. In 1845, almost 350 years after Cabot first landed in Newfoundland, Sir John Franklin set off into the Canadian Arctic to conquer the passage (Lehane 1981). His ships were beset in the ice and ultimately he and his men perished. However, his legacy is profound because of the numerous rescue expeditions (both British and American) that were launched after his disappearance. Although these expeditions did not rescue Franklin, they added extensively to the body of knowledge of the Arctic, mapping the previously unknown regions of the Canadian Arctic Archipelago. Ultimately, it was the Norwegian Roald Amundsen who first completed the Northwest Passage by sea in 1906. His ordeal proved the existence of a navigable passage but it also proved that it was not a viable trade route. It took him over two years due to sea ice often blocking his way and trapping his ship, sometimes for entire seasons (Lehane 1981).   Recent observations of diminishing ice conditions suggest the "non-viable" conclusion may soon be challenged.

B.   OBSERVED CHANGES

The Arctic environment is changing. Many of these changes affect one another and sometimes the associated feedbacks are highly non-linear. An example of this is ice-

albedo feedback. In the Arctic Ocean, snow covered sea ice can have an extreme albedo of ~0.9 and open water has a value of ~0.06 (NSIDC 2010a). As such, the Arctic has some of the highest and lowest albedo values observed anywhere on earth, and they can occur right next to one another. Ice-albedo feedback occurs when the amount of ice is reduced, increasing the open water fraction. With more open water, the effective albedo decreases so the ocean absorbs more radiation (than it would have if the ice were present). This causes the ocean to heat up and melt more ice. Additionally, increasing heat storage in the ocean makes it more difficult to form new ice over the next winter, which in turn leads to less ice and more open water the next year. In this way, the reduction of ice can accelerate. It is important to note that the loop can start at any point in the cycle (i. e. increased radiation/unusually warm conditions can precede the ice loss or the ice loss can happen first, followed by the increased absorption of radiation).

The Arctic sea ice reached its minimum recorded extent in 2005 and again in 2007 (Figure 2). This was due to a number of factors including warming air temperatures (Kauker et al. 2009), favorable persistent atmospheric pressure systems which generated winds ideal for exporting ice from the Arctic (Overland et al. 2008), preconditioning ice by long term thinning (Lindsay et al. 2009), basal melting (Perovich et al. 2008), ice-albedo feedback (Zhang et al. 2008), and increased heat from Pacific Water inflow (Shimada et al. 2006). Negative ice extent anomalies have continued. The 2008 minimum ice extent was second only to that of 2007. There appeared to be signs of recovery but the 2009 minimum still qualified as the third lowest (up until that time). The ice extent minimum in the summer of 2010 restarted the downward trend and was only exceeded by 2007 and 2008 (NSIDC 2010b).

The Northwest Passage and the Northern Sea Route (which skirts the edge of the Arctic Ocean along the northern Russian coast) have briefly opened in recent years. In 2005, the Northern Sea Route was open. In 2006, neither route was passable. In 2007, with the minimum ice extent on record, the Northwest Passage was open for the first time in recorded history. However, the Northern Sea Route was not. In 2008, both routes were open (Figure 3). In 2009, the Northwest Passage was briefly open but not the Northern Sea route (NSIDC 2009). Both routes opened again in 2010 (NSIDC 2010b).
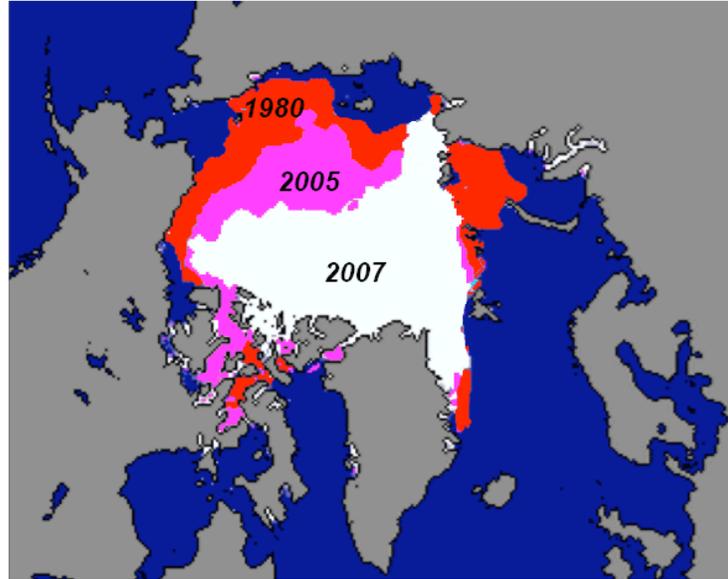
Figure 2.   Minimum summer ice extent from 1980, 2005, and 2007 (From Kruse 2009).

Figure 3.   Summer 2008 sea ice minimum with both Northwest Passage and Northern
Sea Route open (From Kruse 2009).

However, the reduction of ice extent is only part of the story. To more accurately
describe the total amount of ice lost one needs to calculate its change in volume. This
requires knowledge of the vertical dimension, ice thickness.   Thin first year ice is

becoming more common and thicker multiyear ice (which has survived freeze and melt cycles) is becoming scarce (Kwok 2009). Observations of ice draft and freeboard reveal that the thinning of the icepack is accelerating (Kwok and Rothrock 2009).

The glacial ice sheet on Greenland is also thinning (e. g. Mote 2007). Glaciers with outlets at coastal fjords are accelerating their rate of ice loss, apparently due to interaction with the warming ocean (Holland et al. 2008; Rignot et al. 2010; Straneo et al. 2010; Holland 2010). In northwest Greenland, the tongue of Petermann Glacier has been calving into the Hall Basin of Nares Strait; an ice island four times the size of Manhattan broke off on August 5, 2010 (University of Delaware 2010).

Another climate buffer, permafrost, is also melting in the Arctic. As the permafrost melts, heat will be transferred directly from the atmosphere to the land. Permafrost is melting not only on the land but below the ocean as well. This may have serious consequences because of the possible increase in the release of methane that is trapped within permafrost. Gram for gram, methane is 30 times more potent as a greenhouse gas than carbon dioxide (NSF 2010). Its release may contribute to yet another positive feedback loop whereby warming melts permafrost, releasing methane, which causes more warming, which melts more permafrost.

There has also been accelerated coastal erosion along the Arctic Ocean associated with the ice edge retreat. A dramatic example is unfolding in northern Alaska. Previously, the ice edge extended close enough to shore (even in the summer) that the waves generated by the wind blowing over the stretch of open water (between the ice and the shore) were fetch limited. That is, the waves couldn't exceed a certain size because the wind couldn't act over a long enough distance. Now, as wider stretches of open water appear, the waves are growing and hitting the shoreline with more energy. Coupled with the fact that much of this shoreline contains melting permafrost, where cavities are forming and weakening the land, rates of erosion are increasing. For the period 2002-2007, the rate of coastal erosion observed along a 60 km stretch of Alaskan Beaufort Sea coastline was 13.6 meters per year, double the rate observed between 1955 and 1979 (Jones et al. 2009).

There have also been significant biological responses to the changing Arctic environment. Arctic species that require sea ice are being replaced (Lubchenko 2009). Polar bears, which depend on dwindling sea ice for hunting, are now on the endangered species list. Warming waters have led to an increase in non-native species moving into the Arctic Ocean. Salmon normally seen to the west of Alaska in the Bering Sea have been spotted as far north as Barrow (Lubchenko 2009). Potentially the change most threatening to biology is the decreasing pH of the ocean. The world ocean is becoming more acidic due to increased uptake of CO_2. Ocean acidification and its effects are expected to be the most pronounced in the polar regions (Feely et al. 2009). The ultimate effect of ocean acidification on marine ecosystems remains unclear (Doney et al. 2009) but many individual Arctic species are thought to be at risk (Fabry et al. 2009).

C.   ARCTIC STAKEHOLDERS

Due to the inter-related nature of climate components, changes in the Arctic affect everyone to some degree. However, some are more affected than others. Key Arctic stakeholders are described here.

1.   Indigenous Peoples

The indigenous people of the Arctic bear much of the immediate brunt of Arctic change. Their culture and way of life are interconnected with the ice. Loss of the sea ice is drastically changing traditions integral to their identity, such as whaling. Their villages are threatened by melting permafrost (which causes buckling foundations and structural failure of buildings) and coastal erosion. These stressors are though to be a contributing factor to high suicide rates of indigenous peoples in Canada, where the Inuit suicide rate is more than 11 times the Canadian average (Silversides 2010).

2.   Oil/Mineral Companies

The Arctic is a storehouse of energy. A 2008 United States Geological Survey report estimated that the Arctic holds undiscovered reserves containing 90 billion barrels of oil, 1,669 trillion cubic feet of natural gas, and 44 billion barrels of natural gas liquids

(USGS 2008). These represent 22% of the world's undiscovered, recoverable hydrocarbons. Furthermore, the USGS estimated that approximately 84% of the undiscovered oil and gas occurs offshore. New technology and high demand have made oil and mineral companies keen to expand operations to the region. Most areas of interest are shallow, with depths less than 100m. The Chukchi shelf is particularly promising. Worldwide, commercial oil or gas is only found in about 3% of all wells drilled; 2 out of 5 drilled on the Chukchi shelf were viable (Noble 2008).

3.   Fisheries

Arctic fisheries are very important economically. The Bering Sea supports a $4 billion per year fishing industry (Hufford 2009). However, the fisheries are sensitive to changes as well. Cold water species of fish are moving north (Sigler 2009). At least six species have extended their range from Bering Sea to the Beaufort Sea (Logerwell 2008). In 2009, the North Pacific Fisheries Management Council closed the Arctic Ocean to fishing north of Bering Strait until the situation is better understood (Lubchenko 2009).

4.   Shipping

The Northwest Passage (through the CAA) and the Northern Sea Route (over the top of Russia) may finally become consistently passable to shipping as the Arctic sea ice recedes. The savings in terms of time, distance, and ultimately money cannot be overstated. The Northern Sea Route would cut the distance between Rotterdam and Yokohama (via the Suez Canal) by 4,700 nm (Borgerson 2008). The Northwest Passage would cut the distance from Rotterdam to Seattle (via the Panama Canal) by 2,000 nm. The route between Europe and Asia via the Northwest Passage is 12,000 nm shorter than around Cape Horn (Falkingham 2000). When considering fuel, canal fees, etc, as much as $3.5 million could be saved on the cost of a single transit by a large container ship (Borgerson 2008).

These alternative routes could also provide better security for merchant shipping. Major established shipping routes include transits through the Straits of Malacca, Straits of Hormuz, Suez Canal, and Panama Canal. These choke points are areas with high threat of piracy or terrorist attack.

The near term prognosis for the shipping industry due to reduced ice cover is mixed. Neither the Arctic Marine Shipping Assessment (AMSA) (Ellis and Bingham 2009) nor the report released by the Center for Naval Analyses (CNA) (Bowes 2009) predicts a viable commercial shipping route through the Northwest Passage before 2020. They regard the Northwest Passage as too shallow, unsurveyed, unpredictable, with only a maximum narrow two-month time window to allow shipping. Furthermore, thinner ice is easier to deform. This can increase ridging and make it more difficult to pass through. There is also a lack of infrastructure such as ports, refueling depots, repair facilities, and rescue assets (Bowes 2009). The Northern Sea Route has some infrastructure but the schedule is unreliable, the fees are suspect, icebreaker escort is required, and many portions of it are still draft limited (Bowes 2009).

However, the AMSA and CNA report did predict that destination traffic for local supply, transport, and tourism will increase (Ellis and Bingham 2009; Bowes 2009). The shipping industry is planning on exploiting the Arctic. In the summer of 2004, ~6000 ships were in the Arctic at some point (Ellis and Bingham 2009). Shipyards around the world are producing ice capable ships. In 2005, there were 262 active ice capable ships and 234 more on order (Borgerson 2008). In 2009, two merchant ships from the German Beluga Group completed the Northern Sea Route, traveling from South Korea to Rotterdam (Kramer and Revkin 2009). It must also be kept in mind that either the Northwest Passage or the Northern Sea Route (or both) has been observed to open in five of the last six summers.

5.   **Tourism**

Arctic tourism provides a paradox. Lured by the chance to see the sensitive ecosystem "before it completely changes," tourists flock to observe the wildlife close-up. In order to get people as close as possible, ships risk damaging the fragile ecosystem the

tourists are paying to see. Between 2000 and 2008, polar (both Arctic and Antarctic) cruise ships established an appalling record: 5 ships sunk, 16 groundings, 42 environmental or pollution violations, and 28 ships disabled by collision, fire, or propulsion loss (Snyder 2009). Furthermore, these ships are seeking out more and more remote areas to visit, getting further and further from rescue assets (Ellis and Bingham 2009). Ashore, longer ice free seasons mean longer tourist stays, overwhelming local facilities. In 2008, Greenland, population 56,901, played host to 24,999 cruise ship tourists (Snyder 2009).

6.   Governments

Russia, Canada, Denmark, Norway, and the United States have territorial claims in the Arctic. Several of these claims are overlapping, leading to boundary disputes. The United Nations Convention on the Law of the Sea (UNCLOS) is the legal framework for adjudicating these claims. Although the UNCLOS treaty was negotiated in 1982, the U.S. still has not ratified the treaty, placing it on a short list in company with Libya, Iran, and North Korea. As such, the U.S. can neither make claims nor participate in the adjudication process. However, the U.S. does observe the treaty in most cases.

UNCLOS gives nations complete control over their territorial waters that extend 12 nm from the low water mark of their coastline. The Exclusive Economic Zone (EEZ) extends 200 nm from the coastline and nations can control and exploit those resources. Articles 76 and 77 allow a nation to claim additional seabed resources on the continental shelf if it extends beyond 200 nm (Baker 2010). Undersea features are considered an extension of the continental shelf if the structure is geologically similar to their continental landmass (Gove 2009). This provision for extended continental shelf claims has led to a flurry of surveying and forthcoming claims by nations hoping to extend their territory. This inspired Russia in 2001 to claim an additional 460,000 square miles of seafloor, including the Lomonosov Ridge which extends across the Arctic Ocean and later the North Pole itself with the highly publicized underwater flag planting in August of 2007 (Borgerson 2008). Counterclaims have been made by Canada and Denmark (via Greenland) who claim that the ridge and associated territory is really an extension of their

shelves (Gove 2009). The U.S. has launched an interagency effort of NOAA, USGS, and USCG to map the extended continental shelf north of Alaska in preparation for an extended continental shelf claim (assuming the U.S. does ratify UNCLOS). However, even with geological evidence for extended claims, the fact remains that no amount of science alone will settle these disputes.

There is hope that there will be a peaceful resolution to every Arctic dispute. Most of the energy reserves already lie in uncontested EEZs (USGS 2008). The Illulissat Declaration produced by the Arctic nations in 2008 confirmed that UNCLOS will be used to arbitrate additional claims. However, it is important to note that every Arctic nation but Norway has opted out of binding arbitration (Article 298), effectively saying that they will not accept the final decision from UNCLOS if they don't like it (Andres 2009). The agreements and diplomacy are tenuous and nations are hedging their bets with military deterrence.

7.   Military (Strategic)

During the Cold War, the Arctic region was of vital strategic importance. As the shortest distance between the USSR and the U.S., it was the likely path for a strike of one nation against the other. The Arctic Ocean provided a patrol area for Soviet ballistic missile submarines that lurked beneath the relative safety of the ice pack, ready to break through and launch nuclear weapons. U.S. and UK attack submarines would attempt to track and trail the submarines, prepared to engage them before they could release their payload. The Distant Early Warning (DEW) Line was created as a string of radar sites high in the Canadian Arctic which could detect an incoming Soviet strike in time to intercept it or at least ensure enough time to launch a counterstrike. The U.S. Strategic Air Command (SAC) had bombers carrying nuclear payloads aloft 24 hours a day, ready to go over the pole and attack the USSR. After the fall of the Soviet Union and subsequent period of disarmament, the Arctic lost its strategic importance. Now, with the current and forecast changes coupled with the current geopolitical situation, the Arctic is regaining its previous status.

From the current military point of view, the Arctic Ocean represents a potentially contentious wide-open region with little or no infrastructure. It is ringed by four NATO states and their primary adversary, Russia. Access is controlled by only two choke points, the Bering Strait and the Greenland-Iceland-United Kingdom (GIUK) Gap. Currently, many navies are experiencing tight fiscal restraints and can not afford to build new hull designs to operate in the Arctic Ocean. Armed conflict in the region is of low risk but could have large consequences, making the argument for significant military presence (Willett 2009).

a. Russia

The resurgence of the Russian military has been highly publicized and provocative towards the U.S.. Russian bombers conducted overflights of a U.S. aircraft carrier in the Pacific (Roberts 2008), have flown undetected through U.S. airspace (Bowes 2009), and hunter killer submarines have resumed patrols off of America's eastern seaboard after a 15 year hiatus (Mazzetti and Shanker 2009).

The U.S. is not the only nation to receive attention from the Russian military. Norway has been the object of recent intimidation. Russian planes have invaded Norwegian airspace, Russian warships have charged their oilrigs, and Russian bombers executed a mock bombing run on the Norwegian military headquarters in Bodo for the first time since the end of the Cold War (Bowes 2009; Andres 2009).

NATO remains their primary adversary but while NATO is engaged in Afghanistan, Russia can focus more on the Arctic. They are upgrading their nuclear triad and Vladimir Putin sees the Navy, particularly the submarine force as a primary tool for re-asserting Russian strength. They have resumed permanent patrols in the Northern Fleet. 75% of their submarines are based in the Arctic (Willett 2009). In 2008, Russia released a public statement regarding a submarine's recent transit across Arctic from the Barents to the Pacific while submerged, signaling to the rest of the world that the Russian Navy still has the expertise to operate under the ice (Bowes 2009).

However, all may not be as sinister as it sounds. Russia has a historic interest in Arctic. They have been exploring it since the 16th century. They have more miles of coastline bordering the Arctic Ocean than they have land border with any other country. The Northern Fleet has always been large and active because it had so much ocean access. They are not building up but renewing infrastructure that had fallen into disrepair after fall of USSR (Fedoroff 2009). Russia already has the bulk of known and expected resources in their undisputed EEZ (USGS 2008). There would probably be no conflict over resources unless EEZs are directly challenged (Fedoroff 2009).

There is evidence that Russia will act within the rule of law in the Arctic region. Russia was the first nation to submit a formal claim for an extended continental shelf within the rules, abiding by internationally agreed upon procedures (Baker 2010). Furthermore, in September 2010, Russia and Norway formally agreed on their maritime boundary that had led to fisheries disputes for decades (BBC 2010). They also have a boundary dispute with the U.S. regarding the maritime boundary in the Bering Sea. At stake is 18,000 square miles of Bering Sea and associated fisheries (Gove 2009). In 1990, there was agreement to effectively split the difference. The U.S. ratified the treaty but the USSR collapsed before ratification. The U.S. and Russia are applying the treaty on a provisional basis pending ratification by the Russian parliament (DOS 2009). Thus, although there are potential disputes, there are also opportunities for peaceful cooperation in the Arctic.

b.   *Canada*

Most of Canada's Arctic disputes are with the U.S.. The biggest of these is over sovereignty of the Northwest Passage. In fact, in order to bolster their claim that it is not an international strait, since 2006 Canada has discontinued use of the term "Northwest Passage," referring to it instead as "Canadian Internal Waters" (VanderKlippe 2006). In July 2007, Canadian Prime Minister Brian Harper said, "The first principle of Arctic Sovereignty is use it or lose it." The Canadian government then placed orders for up to eight new ice strengthened ships to enforce sovereignty, the refurbishment of a deepwater port on Baffin Island, establishment of a cold-weather army

training base at Resolute, and announced plans to increase the number of troops in the region (BBC 2007). In 2008, the Canadian government blocked the sale of the company operating RADARSAT-2 (an ice imaging satellite) to a U.S. company citing national security concerns, as the satellite is used to maintain surveillance of the Canadian Arctic (CBC 2008).

Much of the Canadian resistance to the Northwest Passage being declared an international strait is due to environmental concerns. An oil tanker incident on the scale of the Exxon Valdez could be catastrophic to the pristine ecosystem (as it was in Alaska). However, non-tankers can still be dangerous. Container ships routinely carry up to 3 million gallons of fuel just to operate the ship itself (Allen 2008). If there were an accident, Canada would likely bear the brunt of the damage and the cost of the clean up. The recent example of the British Petroleum oil spill in the Gulf of Mexico and subsequent fallout for the U.S. gulf coast suggests that the Canadians do have reason to worry. Ice could complicate the cleanup of oil as well; much of the breakdown and dispersal mechanisms relied upon in the Gulf of Mexico such as the sun, winds, the addition of chemical additives or outright burning would not be options.

Canada is involved in other Arctic boundary disputes. The other ongoing dispute with the U.S. is over the extension of the line separating Alaska from the Yukon Territory into the Beaufort Sea. It is based on an 1825 Convention between Great Britain and Russia (Bowes 2009). Canada also disputes the status of Hans Island with Denmark (which administers Greenland). Hans Island lies in Nares Strait. Even though it is only about the size of a football field, the nation who controls it expands its EEZ at the expense of the other. The Canadian Navy routinely lands on Hans Island and raises their flag. The Danish Navy does the same. Although it may seem trivial and probably won't lead to shooting war, Canada sees their claim on Hans Island as a critical precedent. If they give on Hans Island then the will be expected to yield on the Northwest Passage too. As such, they believe that they must stand firm on Hans Island (Reynolds 2005).

### c.	*United States*

The U.S. has been widely criticized for not taking a more active role in the Arctic (Borgerson 2008). With 1000 miles of Arctic coastline and potential rights to several hundred thousand square miles of area, the U.S. has an interest in the region. This was acknowledged in 2009 with the release of National Security Presidential Directive 66. Included was the order to "Project a sovereign maritime presence in the Arctic." The U.S. Navy subsequently stood up Task Force Climate Change to examine national security issues associated with observed and forecast climate change. Their first deliverable was the Arctic Roadmap which provided guidance out to FY 2014 regarding operations, training, environmental assessment and prediction, identifying gaps, and investing in sensors and platforms.

Nonetheless, the U.S. is playing catch up in the Arctic. This is illustrated by the number of Arctic capable U.S. ships. In 2008, the U.S. had a navy as large as the next 17 in the world combined. However, it had only one seaworthy oceangoing icebreaker, placing it on par with China (which operates one), and significantly behind Russia, with 18 (Borgerson 2008).

### 8.	Military (Tactical)

There are several tactical implications of the changes in the Arctic. As the summer ice reduces the marginal ice zone will increase in size, raising ambient noise levels and making passive sonar detection more difficult. As the pH lowers, there is less absorption of sound, so sound may propagate further, resulting in potentially increased ambient noise levels (Hester et al. 2008). This is already having some effect the 10 kHz frequency range (Hester et al. 2008). As the underside of the ice cover changes from rough multiyear ice to smooth first-year ice, there may be less acoustic scattering and improved sound propagation ranges. However, in regions of heavy ridging, first year ice will deform more and cause rougher ice and more scattering, reducing propagation ranges. As the surface waters freshen, submarines may find it more difficult to achieve the positive buoyancy necessary to surface the boat through the remaining ice. Surface ships will have to contend with more mobile ice that can quickly envelop them. Hulls

will have to be ice strengthened to deal with those situations and to pass safely through ridged ice. Furthermore, vessel icing and stability issues will have to be addressed.

For the foreseeable future, Arctic sea ice will continue to form during the winter due to the tilt of the Earth, which prevents the Arctic from receiving solar radiation during the dark winter months. As a result, militaries will have to deal with a more seasonally variable environment. Areas may be open water in summer and ice covered in winter. Acoustic propagation will be further affected by the seasonal variation of open water versus ice as an upper boundary condition and by seasonal changes in seawater density caused by ice formation and ablation.

Arctic search and rescue missions will become more frequent as shipping, tourism, fishing, drilling, and military traffic increase in the region. However, there is little local infrastructure. Search and rescue assets are randomly distributed throughout the Arctic; often those nominally responsible are not in the Arctic at all (Newton 2009). Furthermore, the limited survival times associated with the harsh environment do not allow for a long wait for distant rescue assets to arrive. As larger cruise ships head into the region there is concern that the sheer number of passengers is beyond the current capability of the rescue assets from any one nation (Newton 2009). International cooperation will be required and there is talk of establishing an Arctic Emergency Liaison Office, which could coordinate search and rescue efforts. There is precedence for this sort of cooperation: the International Submarine Emergency Rescue Liaison Office (ISMERLO) was created after the loss of the Russian submarine Kursk. ISMERLO later coordinated assets from Russia, Japan, the U.S. and UK in the rescue of a Russian submersible in 2004 (Newton 2009).

Finally, the thick ice cap has long been a barrier to non-Arctic navies. With less ice to contend with, other navies may commence Arctic patrols. This has even caused some to speculate about a possible commencement of Chinese SSBN patrols in the Arctic (Willett 2009).

D.   CONCLUSION

With so much at stake, there is an urgent need to significantly advance the understanding of the Arctic Ocean environment and its downstream effects. National decisions, policy, and strategy require it. Given sampling difficulties in the Arctic and the scarcity of data, numerical models can provide valuable insights into the processes and controls of Arctic and sub-Arctic waters and identify key areas and parameters where more observations are needed. However, the global climate models have been shown to be too conservative with their prediction of Arctic sea ice loss (Stroeve et al. 2007), which has so far proceeded faster than the models predicted. Much of the problem may lie in the relatively coarse resolution of global climate models and subsequently the representation of critical but small sale physical processes affecting Arctic climate change.

This study uses a high-resolution numerical model to address some of the problems faced by global climate models at coarse resolution. Specifically, it examines downstream effects of changes in the Arctic Ocean, including volume and freshwater fluxes, their controls and ultimate effects on Labrador Sea deep convection. The results of this study advance the understanding of key physical processes relevant to understanding climate and will hopefully guide future research and decisions.

THIS PAGE INTENTIONALLY LEFT BLANK

II. MODEL DESCRIPTION

I am never content until I have constructed a mechanical model of the subject I am studying. If I succeed in making one, I understand; otherwise I do not.

-Lord Kelvin, 1904

This study utilized the Naval Postgraduate School Arctic Modeling Effort (NAME) model, a coupled ice-ocean model with horizontal resolution of $1/12^o$ (~9 km). The model domain (Figure 4) includes the North Pacific and North Atlantic as well as the Arctic, thus permitting exchanges between the Arctic and sub-Arctic. The grid measures 1280 x 720 points and has 45 vertical fixed-depth layers, with thickness ranging from 5 m near the surface to 300 m at depths (Table 1). Model bathymetry of the central Arctic is derived from the 2.5 km resolution International Bathymetric Chart of the Arctic Ocean (IBCAO (Jakobsson et al. 2000)) and for the region south of 64^oN from ETOPO5 at 5-min resolution. Model calculations are based on an Arakawa B grid. In this configuration, model temperature (T) and salinity (S) are specified at the corners of each grid cell while the velocity is calculated in the center. A no slip boundary condition stipulates that if any of the four points surrounding a velocity point is land then the velocity is set to zero (Figure 5). The 9 km horizontal resolution of the domain allows narrow straits and passages to be represented and still have flow while satisfying the no slip boundary condition. In rare cases, the straits are so narrow that slight modifications were made to the grid to artificially widen them and allow realistic flow (Marble 2001). However, these changes were minor. Overall, the 9 km resolution allows the realistic depiction of the Canadian Arctic Archipelago (Figure 4), which figures prominently in this study.

The ocean model is a regional application of the Parallel Ocean Program (POP) of Los Alamos National Laboratory (LANL). It assumes hydrostatic balance and the Boussinesq approximation. The model resolves a free surface (i.e. no rigid lid) allowing

19

the use of high-resolution bathymetry and the determination of actual sea surface height and gradients. Vertical mixing and a convective adjustment scheme are described in Smith and Gent (2002).

The model was initialized with three-dimensional temperature and salinity fields from the Polar Science Center Hydrographic Climatology (PHC) (Steele et al. 2000) and integrated for 48 years in a spinup mode before the production run which was forced with daily averaged ECMWF data from 1979–2004. The upper 5m of the ocean was restored to monthly PHC climatology on a monthly time scale. Surface salinity restoring in particular is a common approach used in many ocean models to prevent artificial salinity drift (e. g. Yeager and Jochum 2009) in part due to missing surface buoyancy forcing related to precipitation minus evaporation (P-E) and river runoff (e. g. in Hudson Bay). A vertical 'curtain' 48 points thick along the southern boundary and 24 points thick along the eastern and western boundaries is restored to PHC T and S on a 10 day time scale. Moving from the lateral curtain towards the center of the domain, model restoring continues over the next 24 points at a time scale decreasing linearly from 10 days to 240 days.
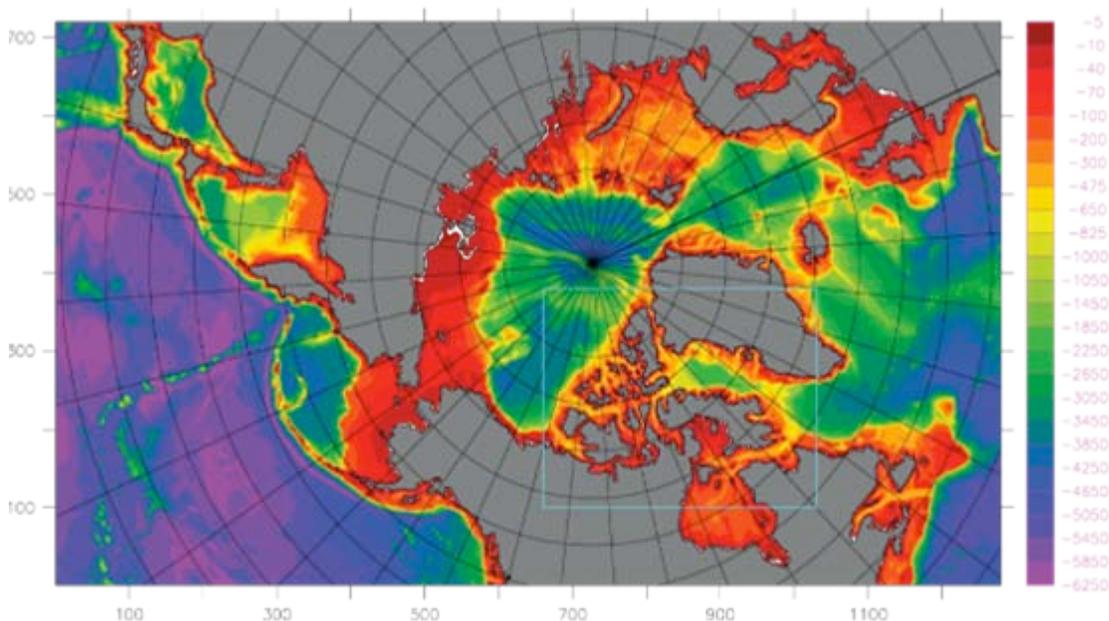
Figure 4.   Model bathymetry (m). Light blue box denotes Canadian Archipelago region.

The dynamic-thermodynamic sea ice model is based on the work of Hibler (1979) with modifications by Zhang and Hibler (1997). Additional model information including further descriptions of sea ice, river runoff, and of restoring have been provided elsewhere (Marble 2001; Maslowski and Lipscomb 2003; Maslowski et al. 2004; Maslowski et al. 2007).

For this study, all calculated fluxes are presented in the form of monthly means. All calculations of freshwater use a reference salinity of 34.8 and liquid equivalent fluxes assume the salinity of sea ice to be 4. Fluxes are given in Sv (1 Sv=1x10^6 m^3/s) or mSv (1 mSv=1x10^3 m^3/s). Positive flux values are from the Arctic towards the Labrador Sea. Anomalies discussed henceforth are determined by removing the annual cycle from the data (i.e. the volume flux anomaly for June 2002 is calculated by removing the 26-year mean June volume flux from the June 2002 volume flux value). Values listed as ± are standard deviations based on the time series of monthly means except where explicitly specified.
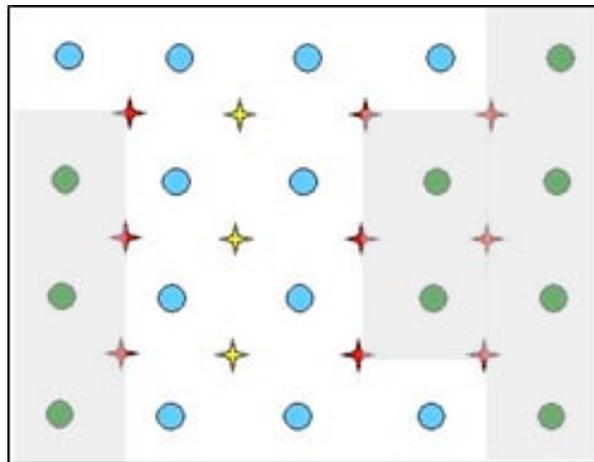
Figure 5. Hypothetical channel configuration on an Arakawa B grid. Circles indicate temperature and salinity grid points, stars = velocity grid points. Green circles = land points, blue circles = ocean points; red stars = zero velocity points; and yellow stars = non-zero velocity points, allowing flow through the channel. Gray shading represents land (From Marble 2001).

21

Layer	Thickness (m)	Lower Depth (m)	Midpoint (m)
1	5.0	5.0	2.5
2	5.0	10.0	7.5
3	5.0	15.0	12.5
4	5.0	20.0	17.5
5	6.0	26.0	23.0
6	7.3	33.3	29.7
7	8.8	42.1	37.7
8	10.6	52.7	47.4
9	12.8	65.4	59.1
10	15.4	80.8	73.1
11	18.6	99.4	90.1
12	22.4	121.8	110.6
13	27.0	148.9	135.4
14	32.6	181.5	165.2
15	39.3	220.8	201.2
16	47.5	268.3	244.6
17	57.3	325.5	296.9
18	69.1	394.6	360.1
19	83.3	477.9	436.3
20	100.5	578.4	528.2
21	121.6	700.0	639.2
22	150.0	850.0	775.0
23	200.0	1050.0	950.0
24	200.0	1250.0	1150.0
25	200.0	1450.0	1350.0
26	200.0	1650.0	1550.0
27	200.0	1850.0	1750.0
28	200.0	2050.0	1950.0
29	200.0	2250.0	2150.0
30	200.0	2450.0	2350.0
31	200.0	2650.0	2550.0
32	200.0	2850.0	2750.0
33	200.0	3050.0	2950.0
34	250.0	3250.0	3150.0
35	250.0	3500.0	3375.0
36	250.0	3750.0	3625.0
37	250.0	4000.0	3875.0
38	250.0	4250.0	4125.0
39	250.0	4500.0	4275.0
40	250.0	4750.0	4625.0
41	300.0	5050.0	4900.0
42	300.0	5350.0	5200.0
43	300.0	5650.0	5500.0
44	300.0	5950.0	5800.0
45	300.0	6250.0	6100.0

Table 1.   Model vertical levels with associated thicknesses and depths.

III. VOLUME AND FRESHWATER FLUXES THROUGH THE CANADIAN ARCTIC ARCHIPELAGO

> Baffin's Bay and the Hudson and Greenland seas, constitute the only uniform outlet to the polar basin. It is by these avenues, then, that the enormous masses of floating ice, with the deeply immersed berg, and the still deeper belt of colder water, are conveyed outward.
>
> -Elisha Kent Kane, 1853

The Labrador Sea is one of the few known locations of open ocean deep convection (e.g. Marshall and Schott 1999). This deep convection is an integral part of the Atlantic meridional overturning circulation (AMOC), a key component of the global climate system often described as the "great ocean conveyor" (Broecker 1991). Model simulations of AMOC have shown it to be sensitive to freshwater exiting the Arctic Ocean (Hakkinen 1999; Jungclaus et al. 2005; Hu et al. 2008). In particular, freshwater exiting the Arctic Ocean through the Canadian Arctic Archipelago (CAA) has been shown to significantly affect modeled AMOC (e.g., Gosse et al. 1997; Wadley and Bigg 2002; Cheng and Rhines 2004; Komuro and Hasumi 2005). Observational studies (Belkin et al. 1998; Houghton and Visbeck 2002) have also concluded that CAA outflow was most likely a major contributor of low salinity anomalies in the Labrador Sea, such as the "Great Salinity Anomaly" in the 1980s. However, due to coarse spatial resolution in most global ocean models the CAA cannot be accurately represented. In reality the CAA has complex morphology and coastline with numerous narrow and/or shallow sections for which the exact bathymetry is still poorly known despite centuries of exploration (this was underscored by the 1976 discovery of Landsat Island, which lies just 20 km off the NE coast of Labrador but was only recently discovered using Landsat satellite imagery (Rocchio 2006)). In today's ocean models, the CAA is often represented as a wide single channel or it is completely closed, thereby distorting or completely preventing the direct flow of low salinity water from the Arctic to Baffin Bay and onwards to the Labrador Sea via this pathway (Gosse et al. 1997; Wadley and Bigg 2002; Komuro and Hasumi 2005; Koberle and Gerdes 2007; Jahn et al. 2010).

The other oceanic freshwater pathway is a much less direct route from the Arctic, transiting Fram Strait and circumnavigating Greenland before arriving in the Labrador Sea. The freshwater signal takes longer to transit to the Labrador Sea and can be diffused and modified significantly along this route (Williams 2004) through mixing with warm and salty Atlantic water in the Nordic and Irminger seas. If a model has an overly wide single channel in lieu of a realistic CAA, too much Arctic freshwater may drain out through that channel, causing an unrealistically large freshwater flux to the Labrador Sea and raising the salinity of the outflow at Fram Strait (Wadley and Bigg 2002). If a model has the CAA closed altogether, the freshwater must all come through Fram Strait, unrealistically lowering the salinity at Fram Strait. In addition to influencing the freshwater fluxes leaving the Arctic, the width of a modeled CAA channel may also affect the magnitude of Atlantic water input into the Arctic (Joyce and Proshutinsky 2007). To understand the freshwater input to the Labrador Sea and its impact on deep convection there, both pathways need to be realistically represented in a model.

The explicit modeling of sea ice and ocean as a coupled system responding to atmospheric forcing is also critical to understanding the timing, phase (i.e. solid vs liquid) and location of freshwater export from the Arctic because most of the freshwater flux through Fram Strait is in the form of sea ice, which later undergoes a phase change as it is advected around Greenland. Conversely, the flow through the CAA is predominately in the liquid phase due to the tight constrictions on sea ice drift imposed by bathymetry and topography. In addition, the extent of ice cover and location of a marginal ice zone affects momentum transport from the atmosphere and vertical mixing in the ocean by modulating stresses and heat fluxes (both latent and sensible).

Prediction of future states of the Arctic and North Atlantic may depend heavily on realistic representation of these phase changes and the CAA pathway. A study by Haak and the MPI Group (cited by Vellinga et al. 2008) suggests that by 2070–2099 freshwater flux through the CAA will increase by 48% whereas the Fram Strait branch will increase only 3% due to the loss of the sea ice component (which currently dominates the Fram Strait outflow). Koenigk et al. (2007) came to a similar conclusion, where the relative importance of Fram Strait to the total Arctic freshwater export decreased while the

importance of the CAA grew.   Such changes contributed to significantly reduced convection in the Labrador Sea and a 6 Sv decrease in their modeled AMOC.

Although the main focus of this paper is on freshwater flux, volume flux is also closely examined because it often controls the former.   Figure 6 denotes several subregions which will be discussed in the text and provides a higher resolution image of the CAA bathymetry. Figure 7 is included as a reference to help navigate the names of islands, bays, straits, and channels within the CAA (note that it is rotated compared to the other figures).
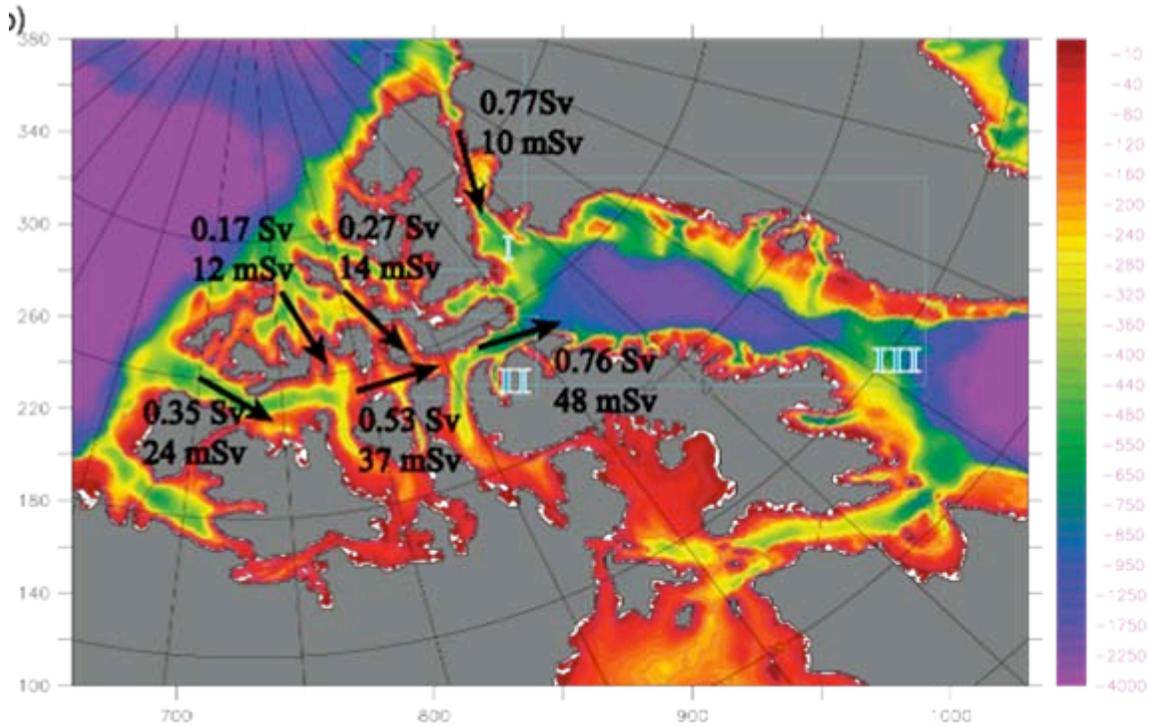
Figure 6.   CAA bathymetry (m). Box I=Nares Strait region, box II=Lancaster Sound region, box III=Baffin Bay region. Volume and freshwater fluxes are presented in Sv and mSv, respectively.

Figure 7.　Canadian Arctic Archipelago model geography and place names. PPI =
Prince Patrick Isl. MI = Melville Isl. MKI = Mackenzie King Isl. BHI =
Bathurst Isl. ERI/ARI = Ellef/Amund Ringness Isl. AHI = Axel Heiberg Isl. CI
= Cornwallis Isl. PWI = Prince of Whales Isl. KWI = King William Isl. SI =
Somerset Isl. BI = Bylot Isl. (from Marble 2001).

A.   NARES STRAIT

1.   Nares Strait Setting

Nares Strait is located in the northeast corner of the CAA, providing a connection from Lincoln Sea in the north to Baffin Bay in the south (Figure 8). It is bordered by Ellesmere Island to west and Greenland to its east. Nares Strait is over 500 km long and with its width ranges from ~35 km in the narrow channels to ~130 km in Kane Basin. Its depth varies from 600m to ~220m at the sill in Kane Basin. Nares Strait is a major outflow point for water exiting the Arctic Ocean, with its estimated net volume accounting for up to half of the total CAA outflow (Prinsenberg and Hamilton 2005; Dickson et al. 2007).

2.   Nares Strait Fluxes

The observed and modeled volume flux is almost entirely one way with net flow directed out of the Arctic Ocean (Munchow et al. 2006; Munchow et al. 2007; Munchow and Melling 2008). The model's strongest southbound flow is confined to a strong subsurface jet on the western side of the strait, similar to observations (Munchow et al. 2006; Munchow et al. 2007; Munchow and Melling 2008). There is some recirculation in Kane Basin and occasionally very weak northward flow along the eastern side of the strait, also in line with observations (Munchow et al. 2007; Munchow and Melling 2008).

The modeled 26-year mean net volume flux through Kennedy Channel (Figure 9a) is 0.77 Sv $\pm$ 0.17 Sv. There is considerable interannual variation. The modeled net liquid freshwater flux through Kennedy Channel (Figure 9b) has a 26-year mean value of 10.38 mSv $\pm$ 1.67 mSv. The 26-year freshwater flux time series shows an increasing trend, especially towards the end of the record. This increase is not reflected in the volume flux time series, but rather is due to decreasing upstream salinity, possibly associated with the modeled accelerated melt of multiyear ice to the north. The 26-year mean net ice flux (liquid equivalent) is 0.80 mSv $\pm$ 0.75 mSv, giving a combined freshwater flux of 11.18 $\pm$ 2.11 mSv. The ice component is relatively small, most probably due to restrictions imposed by topography and the development of ice arches.
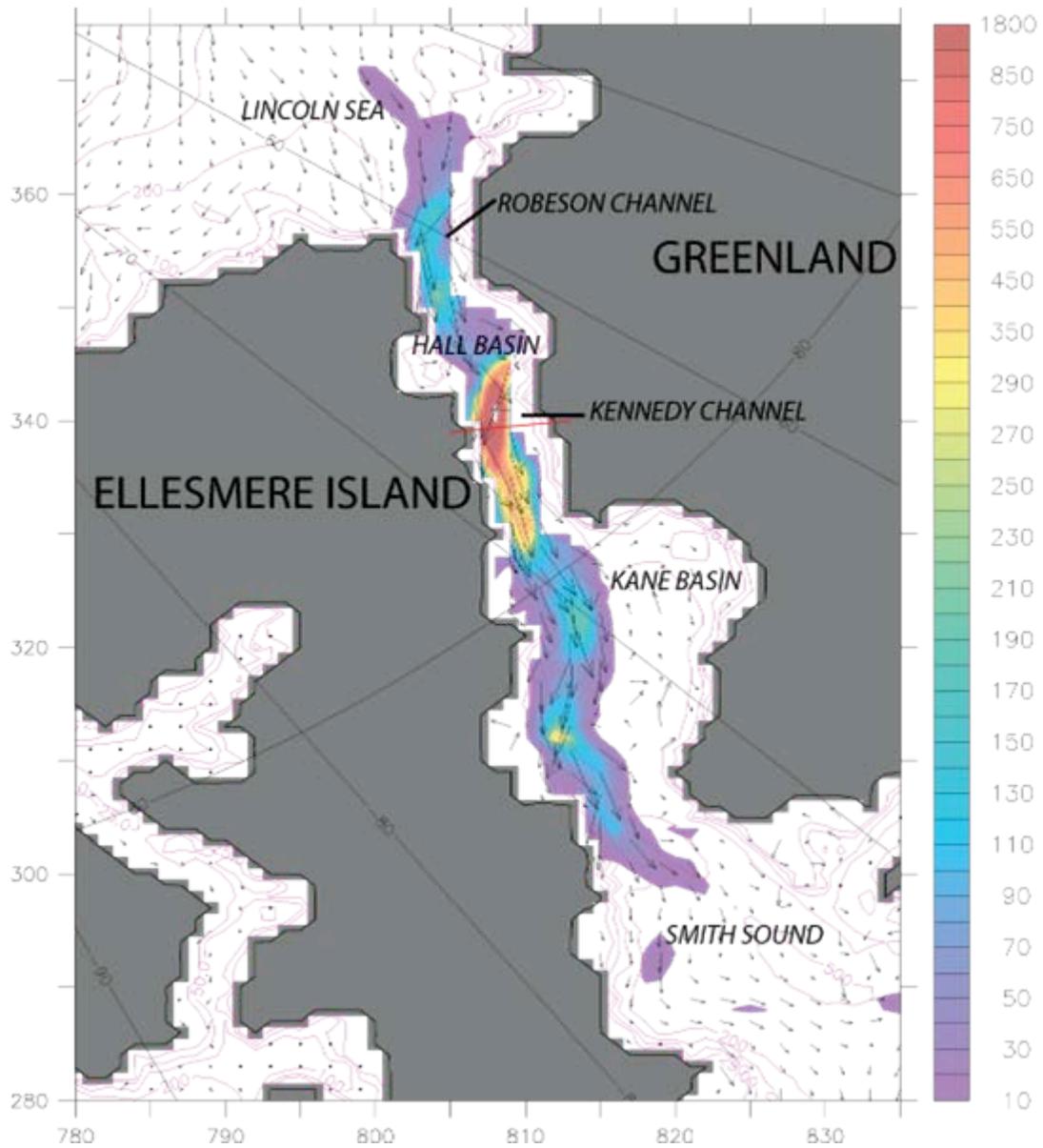
Figure 8.   Nares Strait 0-122m 26-year mean velocity (vectors) and TKE (shading) (cm^2/s^2). Red line is location of Kennedy Channel flux measurement.
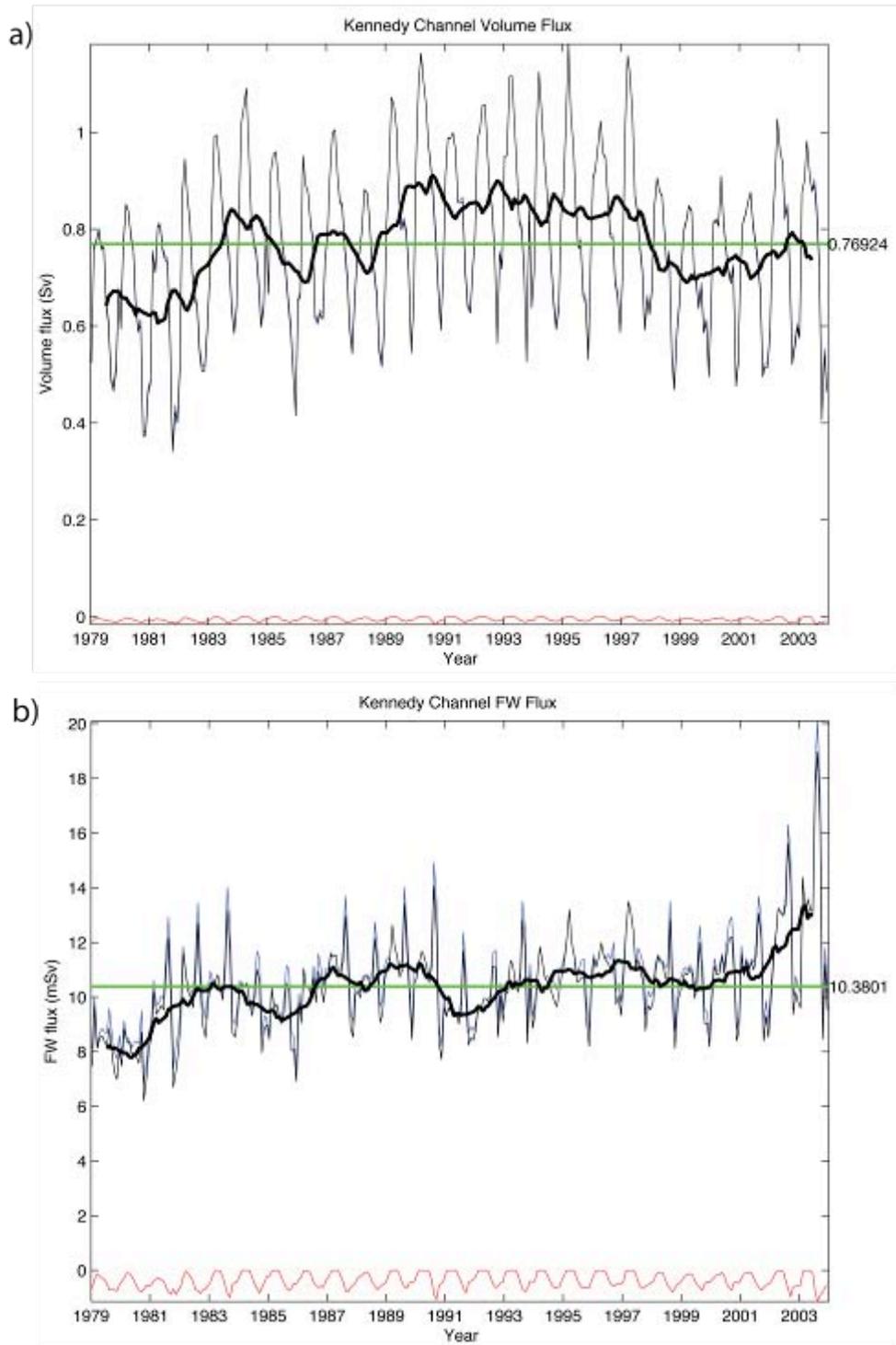
Figure 9.   Model 26-year fluxes through Kennedy Channel (blue=southward, red=northward, black=net, thick black=13-month running mean of the net). a) volume and b) freshwater (liquid).

The annual cycle of volume flux (Figure 10a) peaks in April and has a minimum in October. This is somewhat surprising as the maximum occurs when the strait has its thickest ice. However, Munchow and Melling (2008) observed the along channel vertically averaged flow near Ellesmere Island (which dominates the overall volume flux) to have a southward pulse from January to June and then diminish the rest of the year. This agrees with our model results. The origin of this pulse of volume flux will be further discussed in Chapter IV. The annual freshwater flux cycle (Figure 10b) differs from the volume flux cycle as it has two peaks: one associated with the volume peak in March and a larger one in August due to seasonal ice melt and subsequent decrease of salinity.

Observations from this location are rare but some contemporary data do allow for limited comparisons. The August 2003 model volume and freshwater (liquid) flux estimates were 0.83 Sv and 18.97 mSv, in close agreement with the observations of Munchow et al. (2006) of 0.8 Sv ± 0.3 Sv and 25 mSv ± 12 mSv respectively. Munchow and Melling (2008) analyzed August 2003-August 2006 fluxes through central Nares Strait in Kennedy Channel but excluded the upper 30m, where measurements were not obtained due to hazards of ice drift. Extrapolation of flow to the surface was deemed impractical due to complexities of the near surface flow in the under ice boundary layer. Their mean volume flux was 0.57 Sv ± 0.09 Sv. Unfortunately, model results were unavailable for the exact same time period for direct comparison. However, model output calculated over the same depths for one year of overlap (August 2003-August 2004) yielded a 1 year mean volume flux of 0.54 Sv ± 0.11 Sv and the 26-year mean volume flux was 0.61 mSv ± 0.13 Sv, both in close agreement with the observations. Kwok (2005) estimated the 1996-2002 mean solid freshwater flux though Nares Strait to be ~4 mSv, much greater than the 0.11 mSv ± 0.30 mSv values for contemporary model results. This discrepancy is most likely due to a combination of ice arching (discussed further in the next section) and the lack of high resolution wind forcing, specifically the effect of topographic funneling. Samelson and Barbour (2008) describe intense wind events generated in the region using a high resolution atmospheric model and Samelson
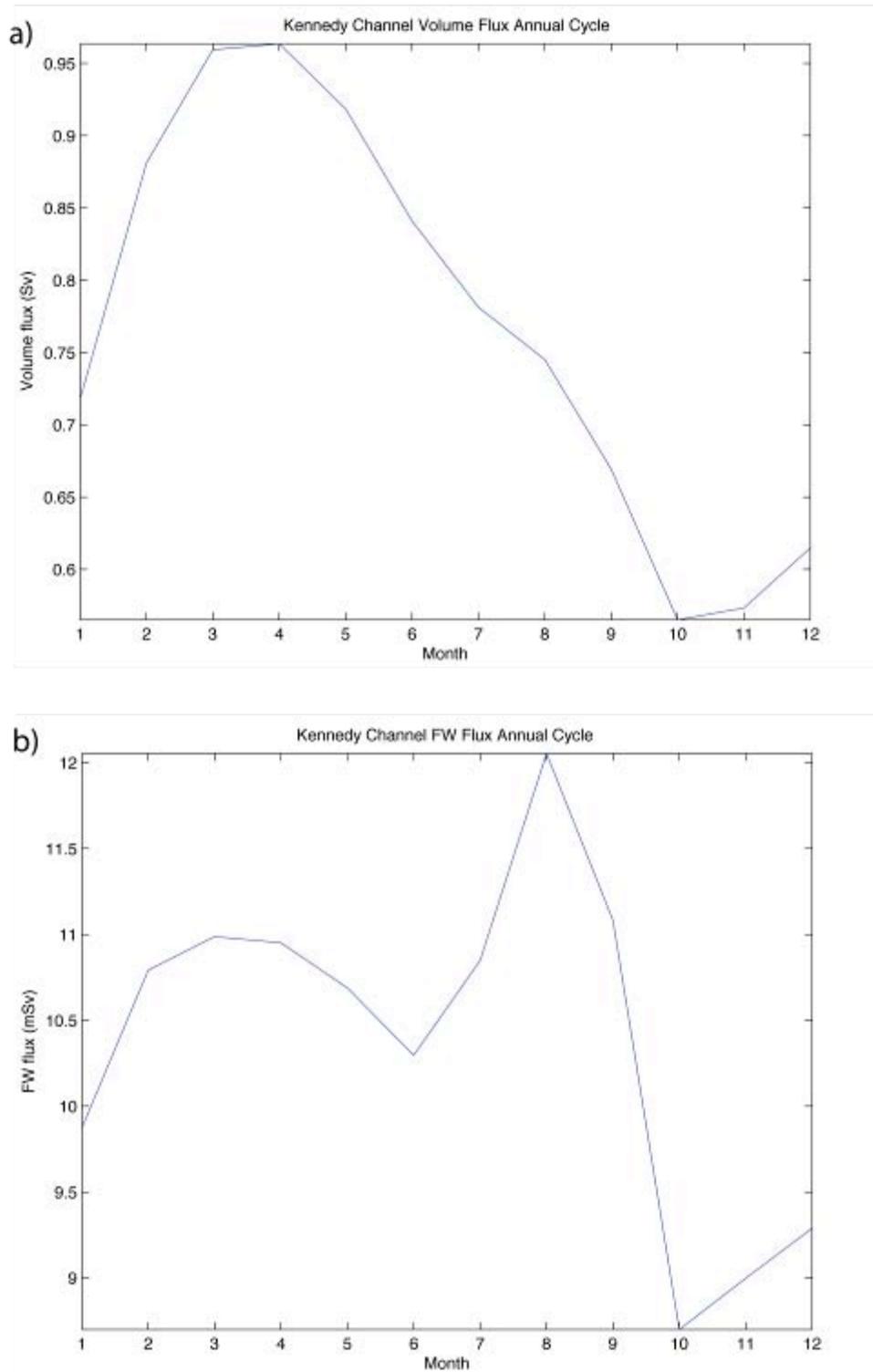
Figure 10.   Kennedy Channel net flux annual cycles. a) volume and b) freshwater (liquid).

et al. (2006) combine satellite observations and simulation to show evidence for atmospheric control of ice motion through Nares Strait.

Munchow and Melling (2008) also described a linear trend in the average volume flux below 30m, with an increase of 20 % ± 10 % between 2003 and 2006. The model results also show an increasing trend in volume flux at these depths at the end of the record (where there is some overlap with the observations). The benefit of the model is that this trend can be put into context within a 26-year period. The modeled increase appears to be the flow simply recovering from of a period of anomalously low volume flux from 1998-2002, still well below previous maxima of 1990 and 1995 and inside the range of variability for the time series (Figure 9a). Munchow and Melling (2008) also showed that the observed flow below 30 m is independent of the local wind forcing. The modeled time series of volume flux measured from 0-30 m was highly correlated (R=0.99 at zero lag) with the values from 30m to the bottom. When coupled with the fact that this part of Nares Strait is almost continually ice covered, the model also supports the hypothesis that the wind has little influence on the Nares Strait volume fluxes, relying instead upon other forcing mechanisms, such as mass continuity and/or sea surface height gradients.

3.   Nares Strait Sea Ice

Sea ice conditions within Nares Strait were also analyzed. Ice thickness and concentration within Nares Strait decline over the last 10 years of the study period. The model also realistically represents the North Water Polynya forming south of Smith Sound. Modeled ice concentration and thickness are high where ice is confined in narrow Kennedy Channel, resulting in a recurring ice arch that prevents further southward motion. To the north in Hall Basin a small polynya becomes more frequent and larger over the time period. Reduced ice coverage there may become increasingly important as this is the area that interacts with Petermann Glacier as it outflows from Greenland. The lower albedo of open water could facilitate local warming of the ocean

and possibly accelerate glacial melting. Towards the end of the study period, modeled thick ice is surviving in late summer only on the eastern side of Kane Basin, with the ice thinning over the length of western Nares Strait.

Usually the ice in Nares Strait is observed to consolidate between December and March in Smith Sound, forming an ice arch which prevents the export of thick multiyear ice from the Arctic to Baffin Bay (Dunbar 1973; Barber et al. 2001; Kwok 2005). Another ice arch typically develops above Robeson Channel at the northern extent of Nares Strait (Kwok et al. 2010). Our model reproduces the ice arches above Robeson Channel, in Smith Sound, and one in Kennedy Channel (Figure 11). However, these ice arches are most likely overrepresented, as model ice strength is based upon the mean thickness of the ice, rather than the thinner ice which experiences more deformation. The modeled ice arch above Robeson Channel is perennial; it moves slightly north and south throughout the time period but it is always there. This could be partially due to excessive ice strength and could possibly explain why our modeled ice flux is consistently lower than in reality: as far as ice goes there is no connection with the Arctic Ocean via Nares Strait, and the small amount of sea ice exported through the southern end in Smith Sound has been created within the strait. The modeled ice arch in Smith Sound is more variable; in several years the North Water Polynya expands northwards across the arching location. The final simulated ice arch appears in Kennedy Channel. This has been observed (Kwok et al. 2010) but does not appear to last as long as it does in the model. In 2007, no ice arches formed, resulting in the highest ice flux observed in the 1997-2009 record, much of it thick multiyear ice (Kwok et al. 2010). Although this model simulation does not run long enough to show these most recent developments, it does show a progression towards that state with ice becoming thinner and less concentrated.
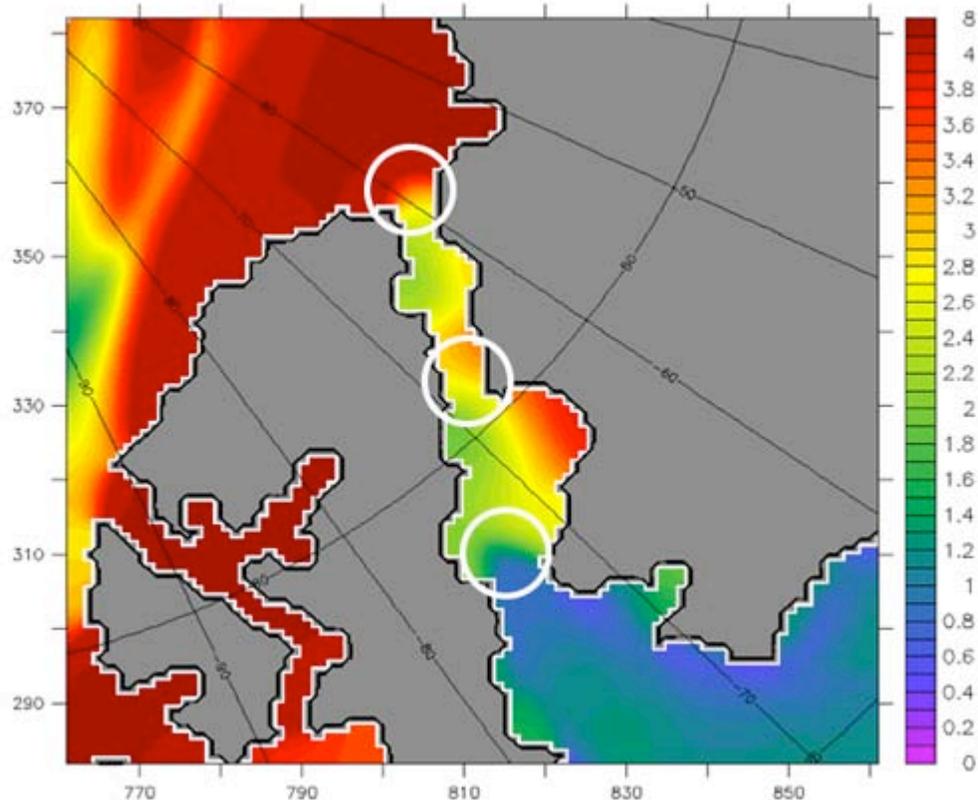
Figure 11. December 1998 Nares Strait sea ice thickness (m). Circles are locations of frequent ice arches described in text.

B.   LANCASTER SOUND

1.   Lancaster Sound Setting

Lancaster Sound is the other location for major CAA outflow (Figure 12). It opens to western Baffin Bay and is due north of Baffin Island. Its opening is about 100 km wide and it is 700-800m deep at its mouth. Flow though Lancaster Sound comes from the west, as a combination of the inputs from several gateways from the Arctic Ocean to the CAA (see Figures 6 and 7). Moving from west to east, flow originates in McClure Strait, gets an addition from Byam Martin Channel in the north, continues eastward flowing through Barrow Strait, receives more input from Penny Strait to the north, and then proceeds through Lancaster Sound to Baffin Bay. Deep flow is restricted

by the presence of shallow sills located in the vicinity of Byam Martin Channel, Barrow Strait, and Penny Strait. Volume and freshwater fluxes for several straits in the CAA shown on Figure 6

.
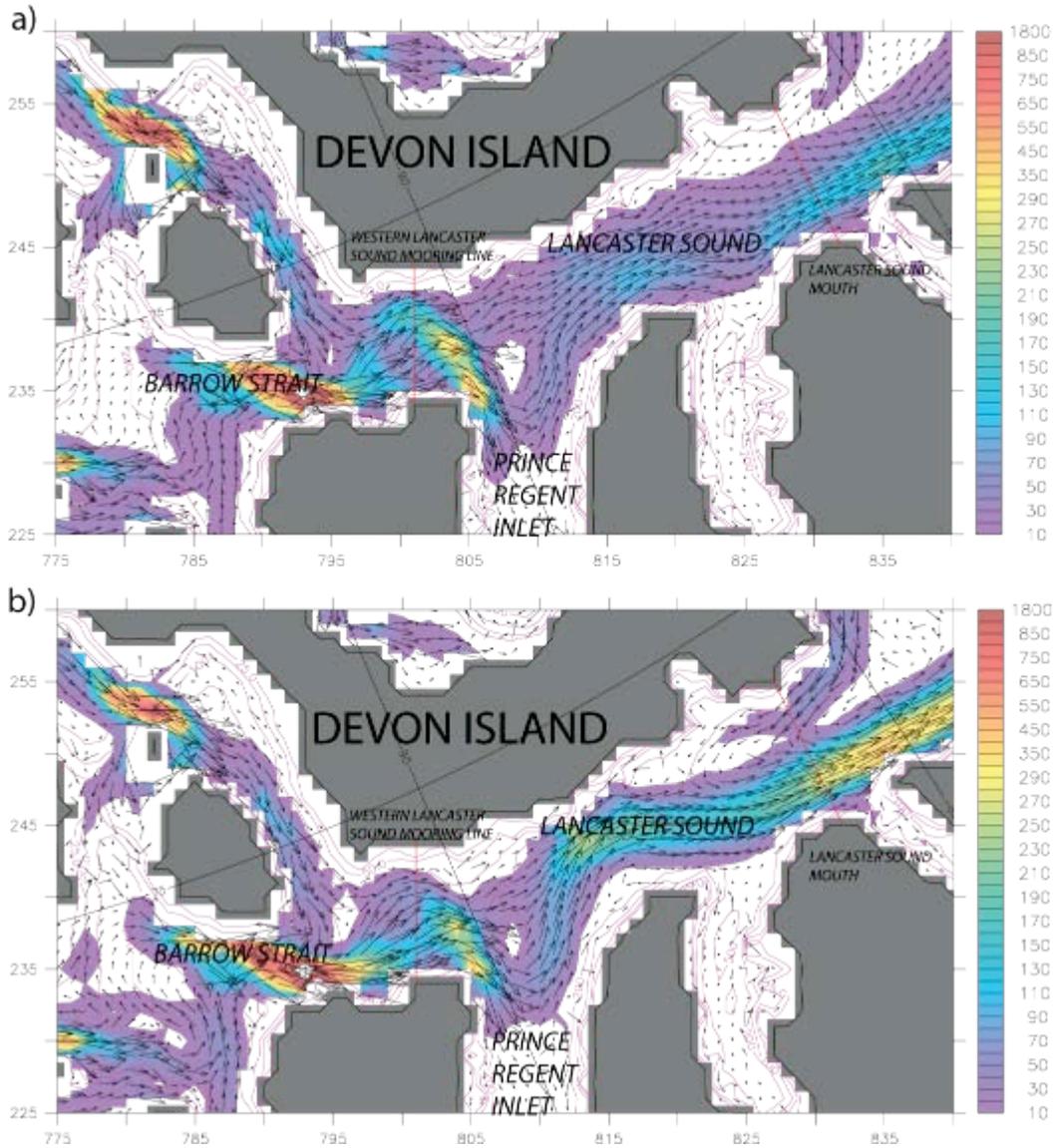
Figure 12. Lancaster Sound 0-122m 26-year mean velocity (vectors) and TKE (shading). a) March and b) August.

2. Lancaster Sound Fluxes

The modeled net volume flux through the mouth of Lancaster Sound is into Baffin Bay, but there is a deep inflow on its northern side that seasonally extends to the surface in summer (Fig 12b). In the model, this flow recirculates and heads back out towards Baffin Bay well before it reaches Prince Regent Inlet, in agreement with summertime drifter and mooring observations (Fissel et al. 1982).

At the mouth of Lancaster Sound where the flow enters Baffin Bay, the model 26-year mean net volume (Figure 13a) and liquid freshwater fluxes (Figure 13b) were 0.76 Sv ± 0.12 Sv and 48.45 mSv ± 7.83 mSv respectively. Ice fluxes accounted for an additional freshwater liquid equivalent of 1.24 mSv ± 1.55 mSv, bringing the combined freshwater flux to 49.69 mSv ± 8.61 mSv. Liquid freshwater fluxes are mostly a function of the volume fluxes, which is reflected in the model correlation between the volume and freshwater flux time series (R=0.85 at 0 lag) and in agreement with the model study of Jahn et al. (2010). It is important to note that although Lancaster Sound accounts for slightly less volume flux (26-year mean) than Nares Strait, it accounts for almost 5 times its long-term mean freshwater flux. This is probably due to a combination of more direct linkage to low salinity Pacific water, large freshwater input of the Mackenzie River, and seasonal input of water derived from the melting of ice in the Beaufort Sea.
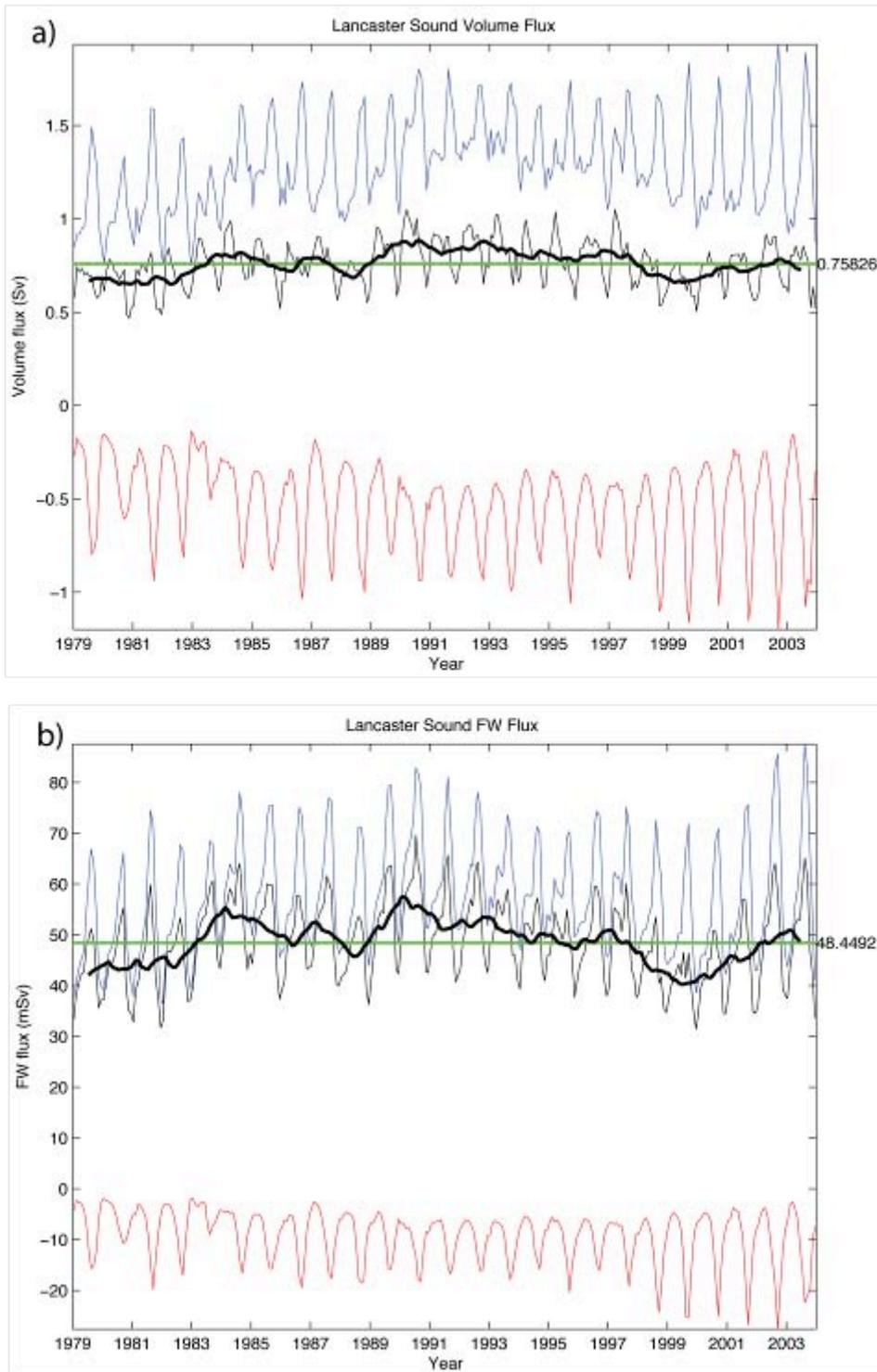
Figure 13.   Lancaster Sound fluxes (blue=southward, red=northward, black=net, thick black=13-month running mean of the net). a) volume and b) freshwater (liquid).

The annual net volume flux cycle has dual maxima, the larger one in March and the secondary maximum in July (Figure 14a). The minimum flux is in November with a secondary minimum in June. Like in Nares Strait, the overall maximum volume flux occurs when the strait has its thickest ice cover. The origin of both pulses in volume flux will be further discussed in Chapter IV. Unlike in Nares Strait, the annual freshwater flux cycle has only one peak at the end of summer, not one associated with the overall volume maximum (Figure 14b). This is due to a loss of about 4.5 mSv of freshwater southwards through Prince Regent Inlet in February/March. This reduces the winter peak in the freshwater annual cycle, which is visible in the model throughout the CAA as far as the western Lancaster Sound mooring array (Figure 12). Without this loss, the freshwater cycle would have two peaks.
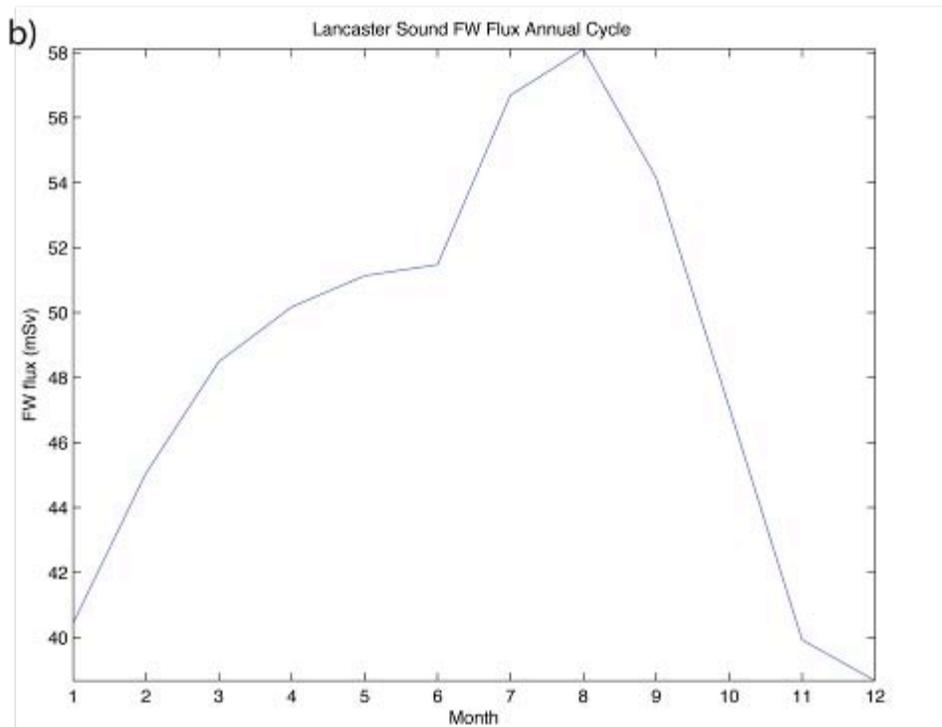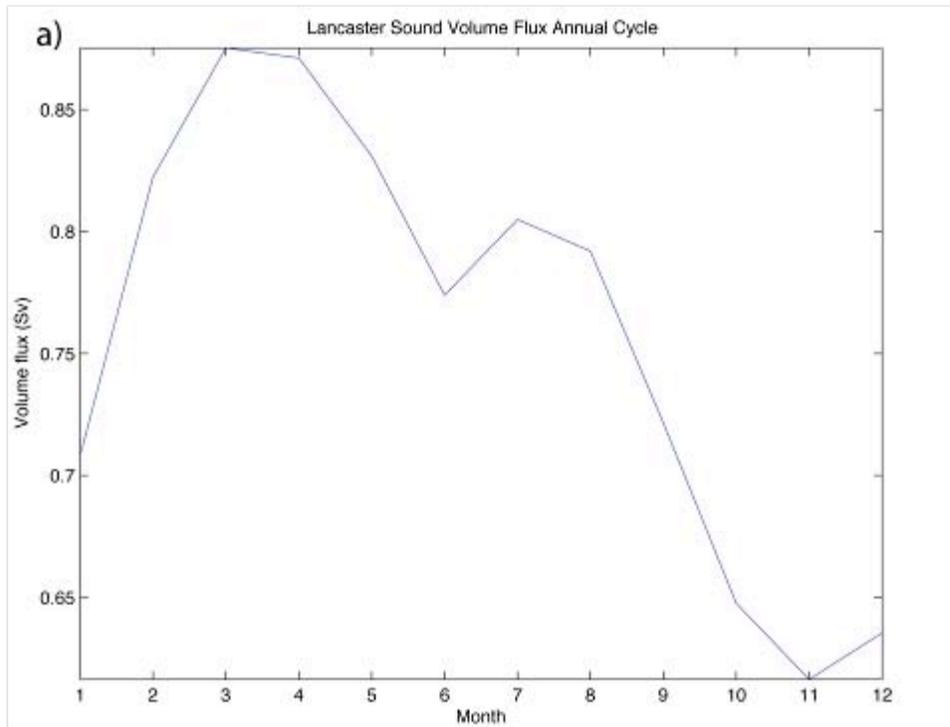
Figure 14. Lancaster Sound net flux annual cycles a) volume and b) freshwater (liquid).

3.   Western Lancaster Sound Fluxes

Observational data is most abundant in the western Lancaster Sound and Barrow Strait region (Figure 12).   As such, model fluxes were calculated for the western Lancaster Sound section only to allow for comparisons.   Prinsenberg and Hamilton (2005) determined the 1998-2001 western Lancaster Sound annual mean volume flux to be 0.75 Sv ± 0.25 Sv, which was close to the modeled 0.72 Sv ± 0.04 Sv (annual standard deviation).   However, it should be noted that the observed standard deviation was much larger.   Using a longer dataset from August 1998-2004 yielded similar results.   The mean annual volume flux was observationally determined to be 0.7 Sv with a range from 0.4-1.0 Sv (Melling et al. 2008) compared with model results of 0.74 Sv and a much smaller range of 0.69 and 0.78 Sv.   Further extending the observational dataset from 1998-2006 yielded nearly identical results as the 1998-2004 period (Prinsenberg et al. 2009).   In general, the smaller modeled standard deviations could be due to the large scale smoothed atmospheric forcing, which misses small-scale (spatial and temporal) variation.   Gustiness of winds, funneling due to topography, and intense drainage (katabatic) phenomena are not represented in the model.   However, they may have significant effects on the observations, especially since the observations are based on few points.

A concern raised by Prinsenberg and Hamilton (2005) was that their freshwater fluxes were based on 1998-2001 data gathered from a CTD instrument at 30 m depth and therefore not sufficient to represent the highly stratified water column above it.   However, their 3-year annual mean liquid flux value of 46.3 mSv compared closely with the modeled 44.31 mSv that took into account salinity at all levels.   For 2001-2004, an ICYCLER instrument was used to extend measurements to the surface.   For the combined dataset from 1998-2004, the observed 6-year annual mean freshwater flux was 48 mSv in close agreement with the modeled 47.18 mSv.   An extended observational dataset from 1998-2006 yielded nearly identical results as the 1998-2004 period (Prinsenberg et al. 2009).   As with the model data, freshwater flux appears to be almost entirely a function of volume flux (Melling et al. 2008; Prinsenberg et al. 2009).

40

It is generally accepted that volume flux through Barrow Strait / western Lancaster Sound peaks in late summer. After geostrophic calculations from an August 1998 hydrographic section showed an eastward current extending 2/3 of the distance across the sound with the highest speed near the southern shore, it was concluded that the flow peaks in August on the southern side of the strait (Melling et al. 2008). Flow on the northern side of the strait was shown to be quite variable and contributed little to the net flux on a long-term average (Prinsenberg and Hamilton 2005; Melling et al. 2008; Prinsenberg et al. 2009). As a result, estimated fluxes for the entire section were based on weighted observations from the southern moorings (Prinsenberg and Hamilton 2005).

To investigate the flow on either side of the strait, modeled annual volume flux cycles were calculated for the entire western Lancaster Sound section and separately for the north and south sections of the line (Figure 15). The modeled flow on the southern side of the channel (Figure 15c) peaks in August in agreement with the observations (Prinsenberg and Hamilton 2005; Melling et al. 2008; Prinsenberg et al. 2009). However, model flow on the northern side of the channel (Figure 15b) has an annual peak in March. This is particularly evident in long term monthly mean model cross sections, where the core of the flow is observed to change sides of the channel (Figure 16). At the time of the August 1998 hydrographic section, flow along the northern side of the channel was decreasing towards the minimum of its annual cycle (Figure 15b, Figure 16), which possibly lead to the determination of flow there as being variable and contributing little to the net flux.
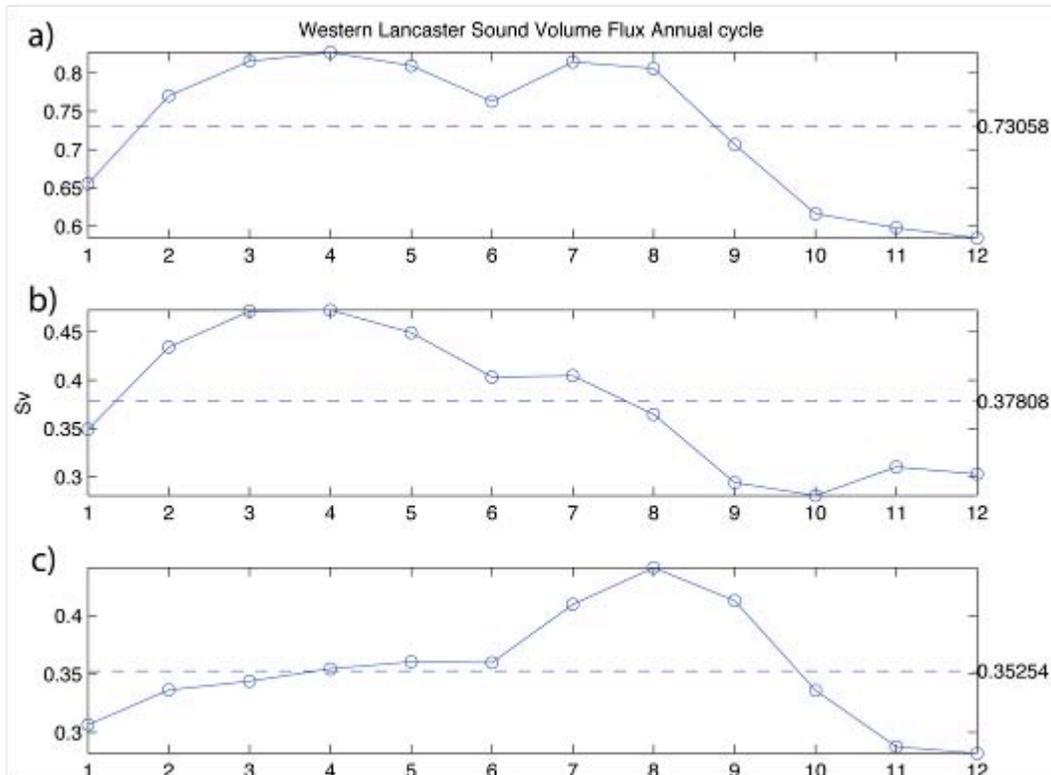
Figure 15.   Model annual cycle (based on August 1998-2004) of volume transport across western Lancaster Sound line of moorings. a) total section, b) northern half of section, and c) southern half of the section.

Using only moorings data from the southern half of the transect from 2001 to 2004, Melling et al. (2008) present velocity peaks only in August/September (see their Figure 9.5). This is in agreement with model results when considering the same area (i.e. only the southern portion). Furthermore, under closer investigation one can make an argument that as one moves across the mooring array towards the northern side that the volume flux regime changes from one with a summertime peak to one with a wintertime peak. Additionally, observed volume fluxes in western Lancaster Sound (Prinsenberg and Hamilton 2005) reveal not only a late summer maximum but also some evidence of a relative maximum in spring (~March). Using data from the same moorings, Peterson et al. (2008) briefly mention that there is some evidence of a secondary maximum in the transport annual cycle in February (see their Figure 2a and 3a) and there also appears to

be a February/March relative maximum in the mooring data as presented by Melling et al. (2008) (see their Figure 9.7). Prinsenberg et al. (2009) noted that the northern flow is generally directed towards the west in summertime and to the east in wintertime. These observations of wintertime eastward flow are in agreement with our model results. The observed negative (westward) flow along the northern edge in summer has been attributed to a coastal buoyancy current. This feature may require higher resolution to simulate, beyond the capabilities of our 9 km model.
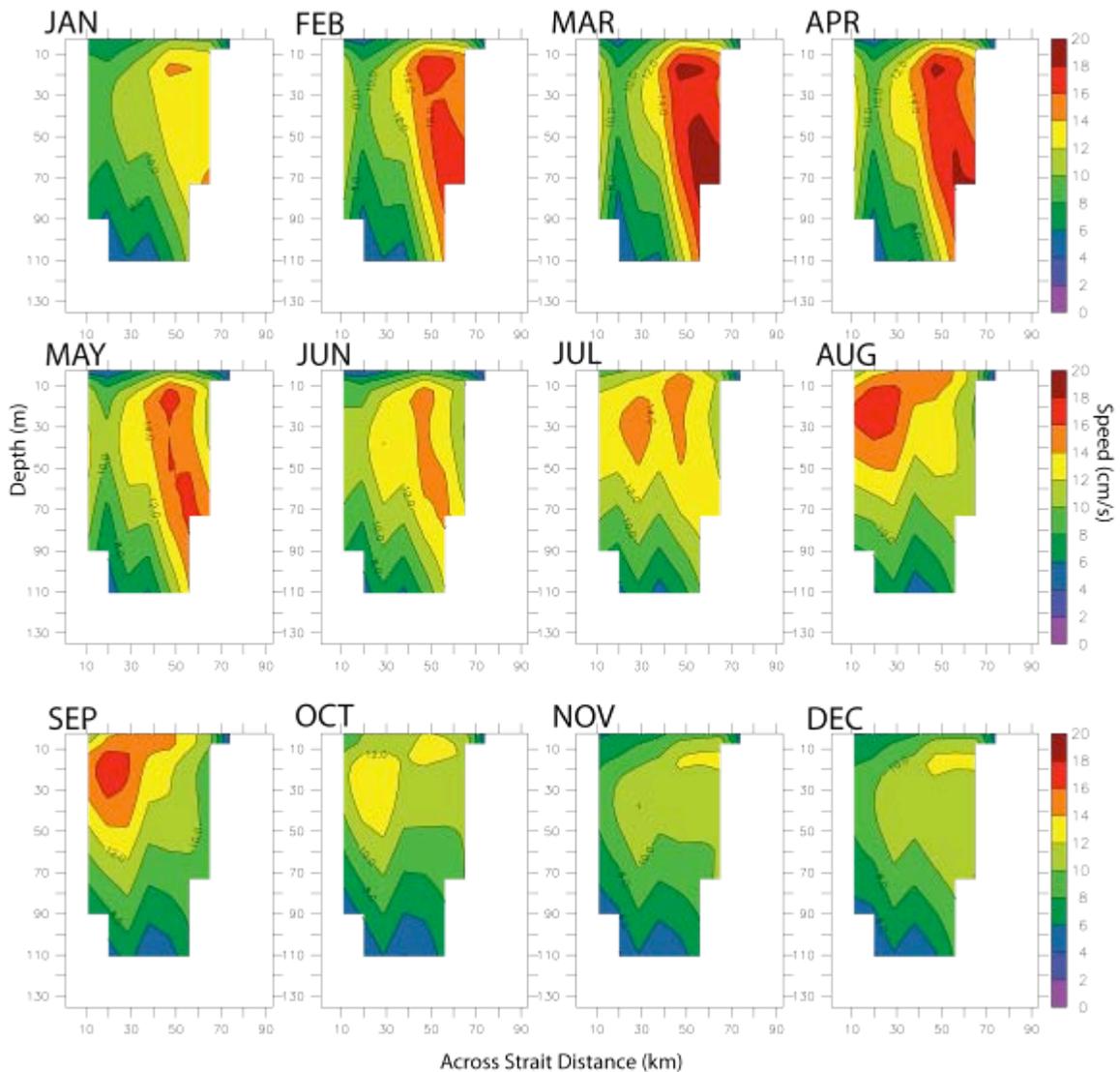
Figure 16. Monthly cross sections of flow (cm/s) through western Lancaster Sound. Southern side of the section is on the left and northern end is on the right. Positive values indicate flow moving towards the east.

Given that the structure of the modeled flow in western Lancaster Sound differs significantly from the scaled up observations, it is difficult to explain the agreement in volume and freshwater flux values. Additional details on how the observations of the southern end of the strait were scaled to represent the total section would be necessary for a more detailed comparison.

C.   CAA ICE

CAA ice cover undergoes a large annual cycle (Figure 17). The CAA forms and melts sea ice locally. Wintertime ice concentration routinely reaches 100% but the summertime minimum area decreases, especially towards the end of the study period. Likewise, ice volume decreases with accelerated loss towards the end of the record. Modeled thick multiyear ice is confined to the north due to ice arching above Penny Strait and Byam Martin Channel and cannot enter the Northwest Passage from that direction. However, the model shows a tongue of thick ice entering via McClure Strait in the west, blocking that end of the Northwest Passage. Satellite based ice flux estimates from recent years (Kwok 2006; Kwok 2007; Agnew et al. 2008) have shown the CAA to not only create but also export sea ice via Lancaster Sound, Amundsen Gulf, and McClure Strait. In the model, ice is exported through Lancaster Sound, Amundsen Gulf imports and exports ice, but McClure Strait imports a small amount. The discrepancies are likely due to modeled ice being less mobile than has been observed (Kwok et al. 2008). Lietaer et al. (2008) used a finite element grid numerical model that yielded a CAA ice export to Baffin Bay 1979-2005 annual mean of 125 km^3/yr. Our model results accounted for just over 1/3 of that value, again suggesting that ice mobility could be an issue. Their ice volume was dominated by the Smith Sound outflow (~70%), followed by Lancaster Sound (~20%) and Jones Sound (~10%) whereas our ice outflow was dominated by Lancaster Sound (~70%), followed by Smith Sound (~20%) and Jones Sound (~10%). Further details about ice in the CAA can be found in Chapter VI.
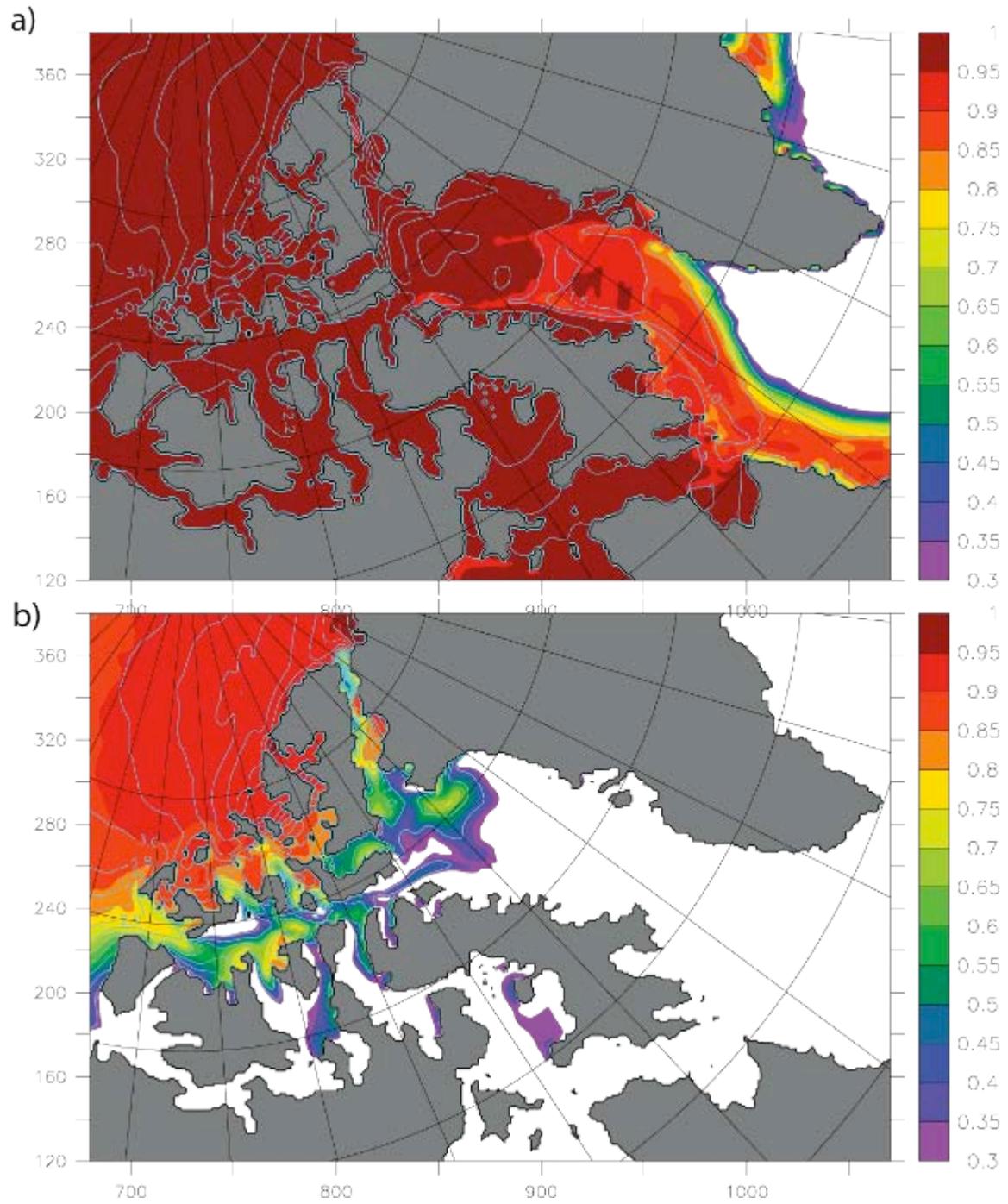
Figure 17.   26-year model mean sea ice concentration (shading) and thickness (contours).
a) March and b) September.

45

D.   BAFFIN BAY

1.   Baffin Bay Setting

Baffin Bay is located between Baffin Island and Greenland and opens to the Labrador Sea in the south. It is about 1000 km long, 400 km wide and its depths exceed 2300m. It is the collection point for CAA outflow as it continues enroute to the Labrador Sea. It receives inputs from Nares Strait, Jones Sound, and Lancaster Sound. It also receives volume input from the West Greenland Current (WGC) flowing north through eastern Davis Strait and loses volume as the Baffin Island Current flows southwards along western side of Davis Strait. This current system gives Baffin Bay a cyclonic circulation regime (Figure 18). The waters in the Baffin Island Current are mostly of Arctic origin and cold and fresh while those flowing in the opposite direction in the WGC are warmer and saltier due to the Irminger Water it carries. Deep flow between Baffin Bay and the Labrador Sea is prevented by a ~670m deep sill in Davis Strait.

2.   Baffin Bay Circulation

Baffin Bay's circulation changes strength seasonally. When the bay is ice covered in winter the ocean is insulated from much of the wind effects and currents are weaker (Figure 18a). In summer the ice has retreated and the ocean is exposed to the atmosphere and the currents are stronger (Figure 18b). These findings are similar to the observations of Tang et al. (2004) who found weaker currents in winter/spring and stronger currents in summer/fall.   The modeled currents in eastern (especially northeastern) Baffin Bay are much stronger during the summer open water period, a finding consistent with the model experiments of Dunlap and Tang (2006), who showed that the strongest effects of wind forcing (for September only) were confined to eastern Baffin Bay, (particularly to the northeast). The long-term model volume fluxes into and out of Baffin Bay balance, as expected by continuity. The modeled freshwater fluxes (combined liquid and solid) into and out of Baffin Bay are nearly balanced, with more freshwater going out than coming in being due to net precipitation (~ 7 mSv) accounted for in the model by restoring.
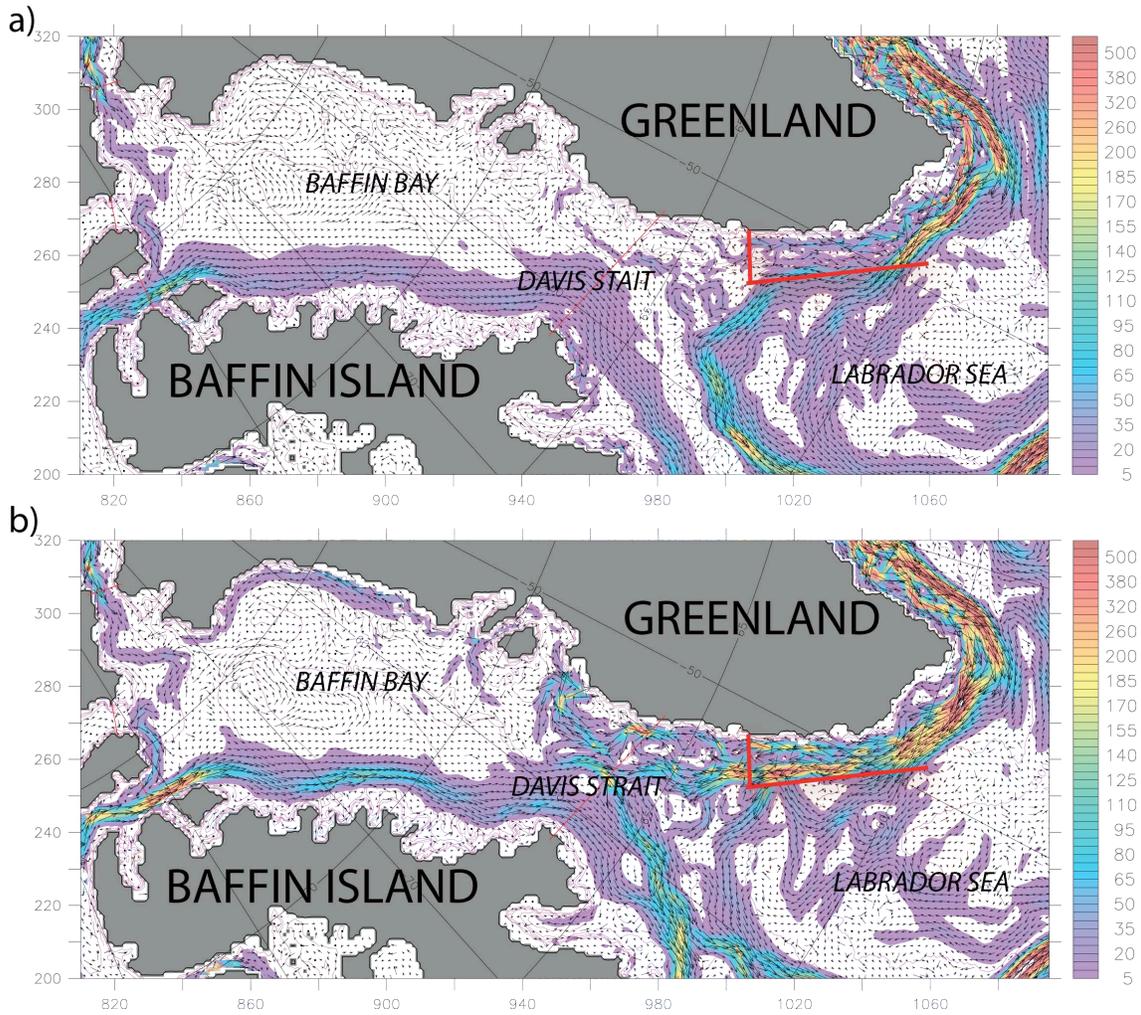
Figure 18.   Baffin Bay 0-122m 26-year mean velocity (vectors) and TKE (shading). a) March and b) September.

3.   Baffin Bay Sea Ice

Sea ice coverage is highly variable, with the bay covered in the winter by first year ice that almost completely disappears in summer. Winter ice covers all of Baffin Bay except the region in eastern Davis Strait that receives heat from the WGC (Tang et al. 2004). The model does reproduce this feature, as well as the previously mentioned North Water Polynya that occurs in the north near Smith Sound (Barber et al. 2001). Observations (Tang et al. 2004) show that a small amount of ice does survive the summer

melt. Estimates of that minimum ice area correspond well with our model results (see Figure 6 from Tang et al. 2004).

E. DAVIS STRAIT

1. Davis Strait Setting

Davis Strait lies between southern Baffin Island and Greenland. It divides Baffin Bay in the north from the Labrador Sea to the south. There is a sill that constricts the flow in the vertical as well as the horizontal narrowing of the strait. Opposing currents flow north and south on either side of the strait.

2. Davis Strait Fluxes

After CAA outflow moves into Baffin Bay, it is exported southwards to the Labrador Sea via Davis Strait. The modeled 26-year mean net volume (Figure 19a) and liquid freshwater fluxes (Figure 19b) through Davis Strait (positive values are southward into the Labrador Sea) are 1.55 Sv ± 0.29 Sv and 62.66 mSv ± 11.67 mSv respectively. Ice flux accounts for an additional liquid equivalent flux of 12.81 mSv ± 13.09 mSv giving a total mean freshwater flux of 75.48 ± 9.73 mSv. Cuny et al. (2005) estimated September1987-1990 Davis Strait volume, freshwater and ice fluxes to be 2.6 Sv ± 1.0 Sv, 92 mSv ± 34 mSv, and 16.7 mSv (when converted from km^3 /year) respectively (these values include an extrapolation of flow along the West Greenland shelf). Contemporary model results fit well within these bounds with volume, freshwater and ice fluxes of 1.7 Sv ± 0.3 Sv, 66 mSv ± 14 mSv, and 14.8 mSv respectively.

Model volume and liquid freshwater flux anomalies correlated with R=0.75, less than the correlation at Lancaster Sound (R=0.85), suggesting modification of the signal within Baffin Bay. Recalculating the correlation using the combined freshwater flux anomaly (including the ice component instead of just the liquid freshwater) yields a value of R=0.81, capturing an additional 10% of the variance. Thus our freshwater and volume flux anomalies are highly correlated at Davis Strait.

The annual cycle of volume flux (Figure 20a) shows that the net peak outflow southwards through Davis Strait occurs in the winter months (February/March/April), when both northward and southward fluxes are at their minimum (the northward flux happens to reduce much more than the southbound flux, leaving the net at its maximum) (Figure 20a). This is similar to Cuny et al. (2005) who observed that the northwards volume flux was at a minimum in March/April and the minimum southward flux was in March. The most vigorous fluxes across the strait occur when the area is ice free in September but largely cancel one another in the net sense. Cuny et al. (2005) also observed from 1987-1990 that the highest northward and southward fluxes (volume and freshwater) to occur concurrently, but in November. Tang et al. (2004) observed the strongest northward flux in eastern Davis Strait to occur in fall as well. The annual cycle of freshwater flux peaks in September (Figure 20b).
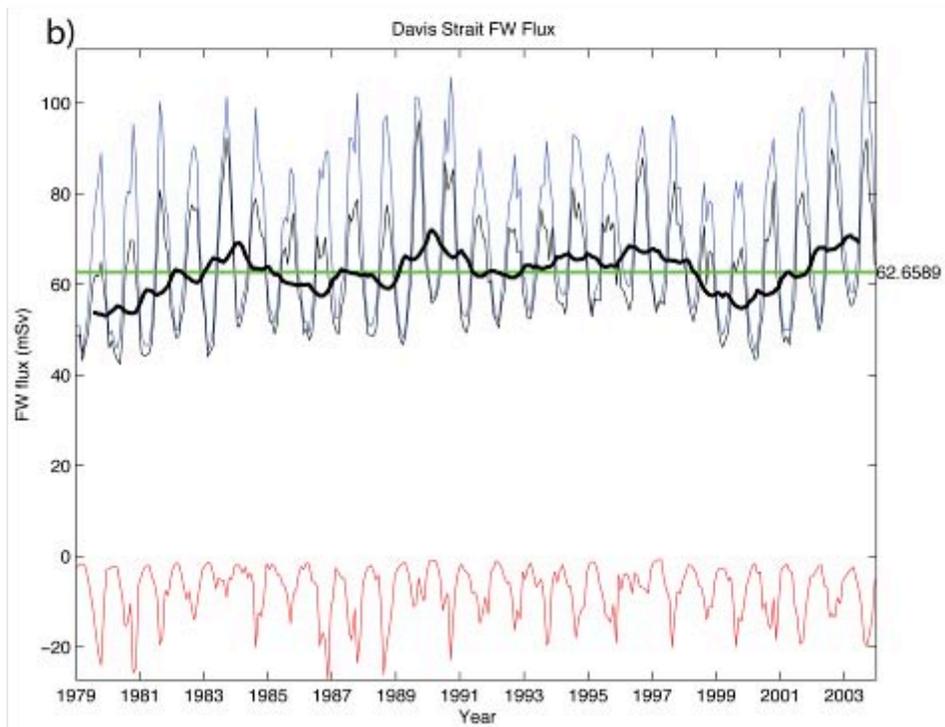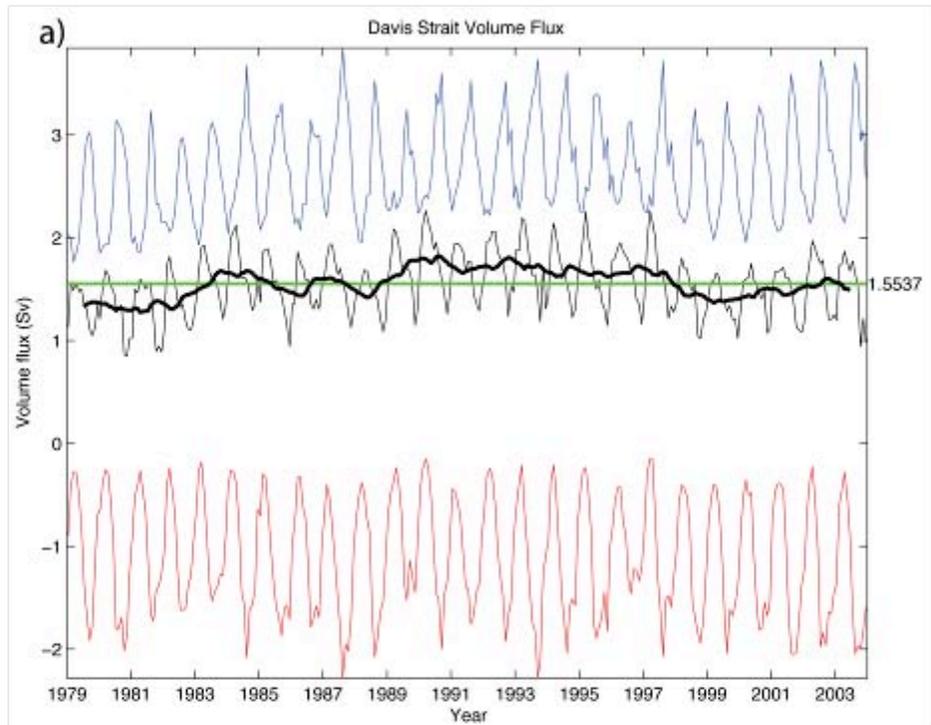
Figure 19.   Davis Strait fluxes (blue=southward, red=northward, black=net, thick black=13-month running mean of net). a) volume and b) freshwater (liquid).
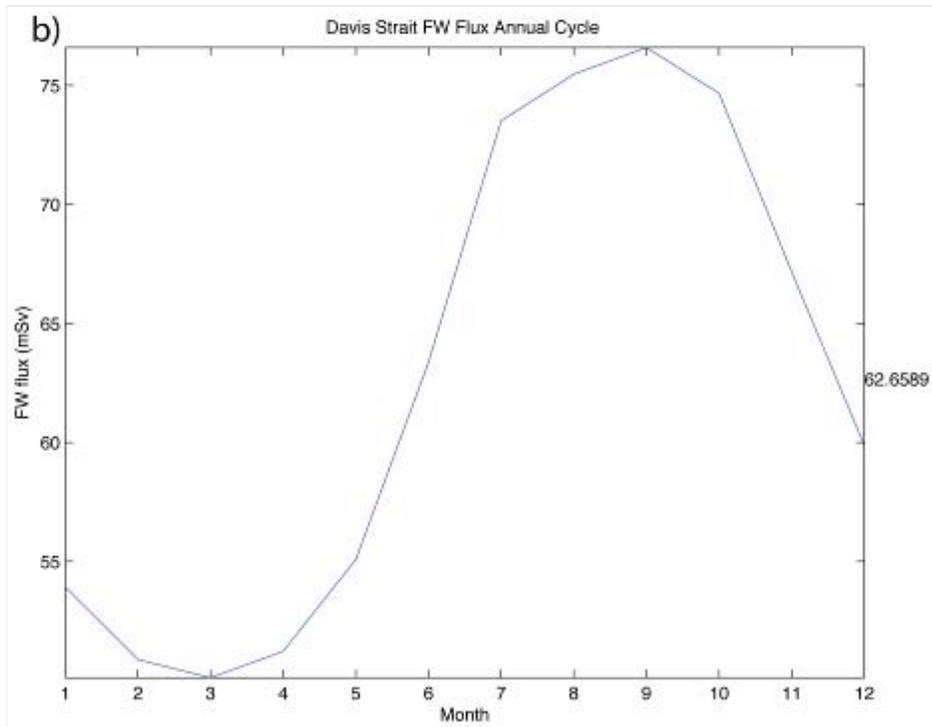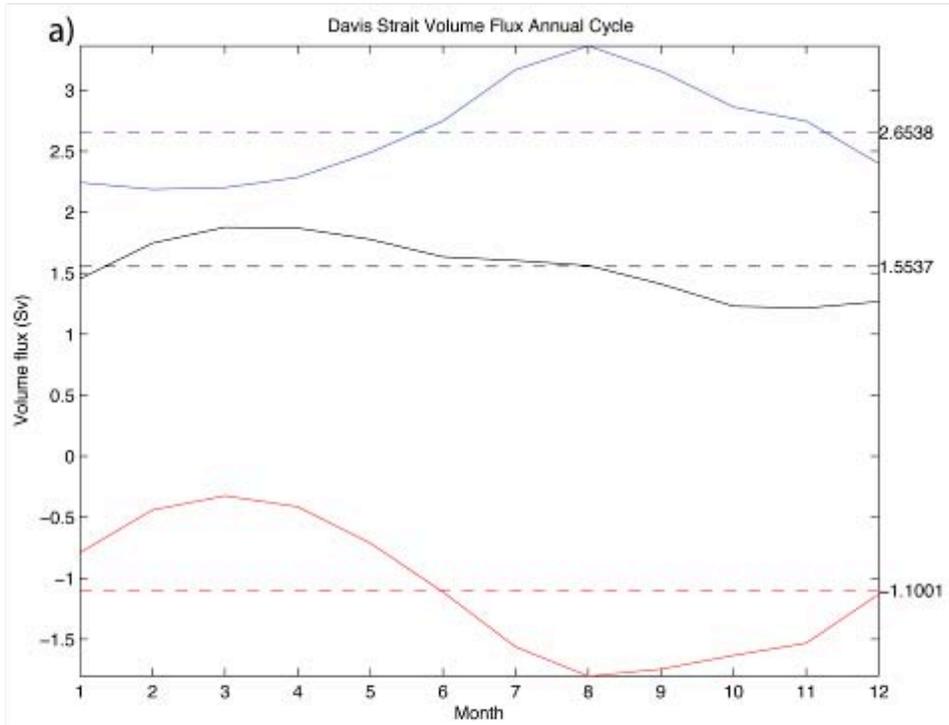
Figure 20.   Davis Strait flux annual cycles. a) volume (blue=southward, red=northward,
black=net) and b) net freshwater (liquid).

F.   FRAM STRAIT

1.   Fram Strait Setting

The other pathway for freshwater to exit the Arctic Ocean is via Fram Strait. Fram Strait lies with Greenland to its west and Svalbard to its east. It is a both an entry and exit point for volume fluxes of the Arctic Ocean. On its eastern side the West Spitsbergen Current flows northward along Svalbard into the Arctic Ocean and to the west the East Greenland Current flows southwards out of the Arctic Ocean.

2.   Fram Strait Fluxes

In the net volumetric sense Fram Strait is an export pathway. The model 26-year mean volume flux (from the Arctic Ocean to the south) through Fram Strait is 2.33 Sv ± 0.57 Sv. This is within the bounds of the observational estimates of Schauer et al. (2004) who specified net volume fluxes between 2 Sv ± 2 Sv and 4 Sv ± 2 Sv. The 26-year mean freshwater (liquid) flux is 12.17 mSv ± 5.24 mSv. However, most of the freshwater comes out as ice which accounts for an additional flux of 51.54 mSv ± 37.41 mSv, making the combined freshwater export to be 63.72 ± 39.18 mSv. This is in reasonable agreement with Kwok et al. (2004), who estimated the ice outflow to be equivalent to ~70 mSv. To summarize (in the 26-year mean sense), Fram Strait exports about 1.5 times more net volume from the Arctic than does the CAA through Davis Strait. However, the CAA exports about 20% more FW than Fram Strait. It is important to note the large variability of the Fram Strait freshwater fluxes. Most of this variability is due to the ice component, which is largely wind controlled (Kwok et al. 2004).

The annual cycle of Fram Strait's net volume flux is at a minimum in April/May and is at a maximum in November. It is nearly out of phase with the net volume flux through Nares Strait that is at a maximum in April and minimum in October.

3.   Fram Strait Freshwater Pathway

Most the freshwater exported from Fram Strait is lost as it circles around Greenland towards the Labrador Sea. Much of it is lost towards the east soon after it

crosses Fram Strait. This happens due to recirculation from the East Greenland Current back towards the northbound West Spitsbergen Current. Also, the model advects ice too far to the east in the Iceland Sea. The freshwater is continually mixed and diffused as it is carried south towards Denmark Strait, especially with the northward flowing warm and salty Irminger Current. There the relative amount of freshwater flux continues to shift from being predominantly solid to liquid phase. Further to the south, mixing continues in the Irminger Sea and some of the remaining flow retroflects to the east at Cape Farewell so very little of the original freshwater exported from Fram Strait makes it to the Labrador side of Greenland (1.70 mSv ± 2.07 mSv compared to the 63.72 mSv ± 39.18 mSv that transited Fram Strait). This surviving freshwater then either splits into a branch moving westwards as it traverses the northern rim of the Labrador Sea or it continues to the north through Davis Strait. In this model, the Fram Strait branch provides very little freshwater to the vicinity of the Labrador Sea compared with the CAA pathways that deliver 75.48 mSv ± 9.73 mSv via Davis Strait.

G.   HUDSON BAY

1.   Hudson Bay Setting

Hudson Bay is another freshwater source to the Labrador Sea. While not usually regarded as a connection between the Arctic Ocean and the Labrador Sea or even passageway of the CAA, it does have connections to the CAA (via the very narrow Fury and Hecla Strait) and it opens onto the Labrador shelf.

2.   Hudson Bay Fluxes

The Hudson Strait 26-year mean net volume flux is nearly balanced, accounting for just 0.17 Sv of net flow towards the Labrador Sea. However, the net liquid freshwater flux is 9.58 mSv and the ice flux is 0.67 mSv, bringing the combined freshwater flux to 10.25 mSv. This is drastically lower than the observed outflow only value of 78-88 mSv (Straneo and Saucier 2008). Our outflow only mean value was 15.31 mSv. Dickson et al. (2007) proposed a net freshwater flux to the Labrador Sea of 42 mSv, of which 35

mSv was river discharge through Hudson Bay and 7 mSv was from the CAA via Fury and Hecla Strait. Our data are in reasonable agreement when considering that our model has no explicit river input to Hudson Bay, except the surface salinity restoring, which does not appear to be sufficient to make up for the entire riverine source. Other model limitations at 9 km resolution prevent complete depiction of flows in Hudson Bay and Hudson Strait, particularly their coastal currents. However, limited representation of those 35 mSv may be acceptable here, especially if much of the water leaving Hudson Bay may be confined to the inner branches of the Labrador Current on the Labrador shelf and cannot influence convective regions of deep water formation. In any event, Hudson Bay provides a significant input to the Labrador shelf, especially in comparison to the Fram Strait branch.

H.   CONCLUSIONS

This portion of the study examined the 1979-2004 volume and freshwater fluxes through the Canadian Arctic Archipelago using a high-resolution (~9 km) numerical model. It was determined that the 26-year mean volume and freshwater fluxes through Nares Strait were 0.77 Sv ± 0.17 Sv and 10.38 mSv ± 1.67 mSv respectively, while those through Lancaster Sound amounted to 0.76 Sv ± 0.12 Sv and 48.45 mSv ± 7.83 mSv respectively. Thus the volume fluxes through the two main passages were nearly the same but the freshwater flux was much greater for Lancaster Sound. The 26-year mean volume and freshwater fluxes through Davis Strait were 1.55 mSv ± 0.29 Sv and 62.66 mSv ± 11.67 mSv.

When compared to available observations, it is apparent that the model does provide realistic volume and freshwater fluxes, as well as ice thickness and concentration in the CAA. However, limitations include the lack of high resolution atmospheric forcing (especially the effects of local topography), low mobility of modeled ice, incomplete depiction of ice arching, and possible lack of coastal buoyancy currents. Many of these issues could possibly be addressed with increased resolution. As future freshwater fluxes through the CAA are expected to increase with climatic implications, it is imperative that models are capable of resolving them.

IV. CONTROLS ON VOLUME FLUXES THROUGH THE CANADIAN ARCTIC ARCHIPELAGO

When one tugs at a single thing in nature, he finds it attached to the rest of the world.

-John Muir

From a modeling standpoint, simulating flow through the CAA is a difficult task. The CAA is a network of many bays and inlets connected by narrow straits and shallow sills. Its complex bathymetry and coastline require high horizontal and vertical resolution for full description. Only after the CAA is accurately represented can its through-flow be simulated and analyzed. The actual quantification of fluxes and their variability through the CAA were examined in Chapter III. This chapter examines their controls.

Freshwater flux through the CAA is largely a function of volume flux (Melling et al. 2008; Prinsenberg et al. 2009). As such, it is imperative to identify controls on the volume flux in order to understand freshwater flux. Volume flux through the CAA is generally believed to be due to a background sea surface height (SSH) gradient between the northern Pacific Ocean, Arctic Ocean, and northern Atlantic Ocean. It is due in large part to steric height, i.e. fresher less dense water in the North Pacific that increases in salinity (causing increased density and decreased SSH) as it moves through the Arctic and into the North Atlantic (Steele and Ermold 2007). The modeled 26 year mean SSH plot (Figure 21) shows this background SSH gradient across the CAA. The annual cycle of volume flux through western Lancaster Sound has been attributed to a seasonal modulation of the SSH gradient (Prinsenberg and Bennett 1987). Recent analyses correlating Arctic winds and oceanic volume fluxes through western Lancaster Sound suggest that summer winds located along the CAA's Beaufort coast blowing towards the northeast cause an Ekman transport of mass towards the CAA. This in turn leads to increased setup and ultimately increased volume flux through the CAA, resulting in a summertime flux maximum (Petersen et al. 2008, Prinsenberg et al. 2009). However, studies of the forcing behind the volume flux through the CAA passages are severely

limited by a lack of SSH measurements across the CAA. This model provides contemporary SSH and flux information so the two can be investigated together. Additionally, it provides 26 years of output, allowing for examination of seasonal cycles and interannual variability.
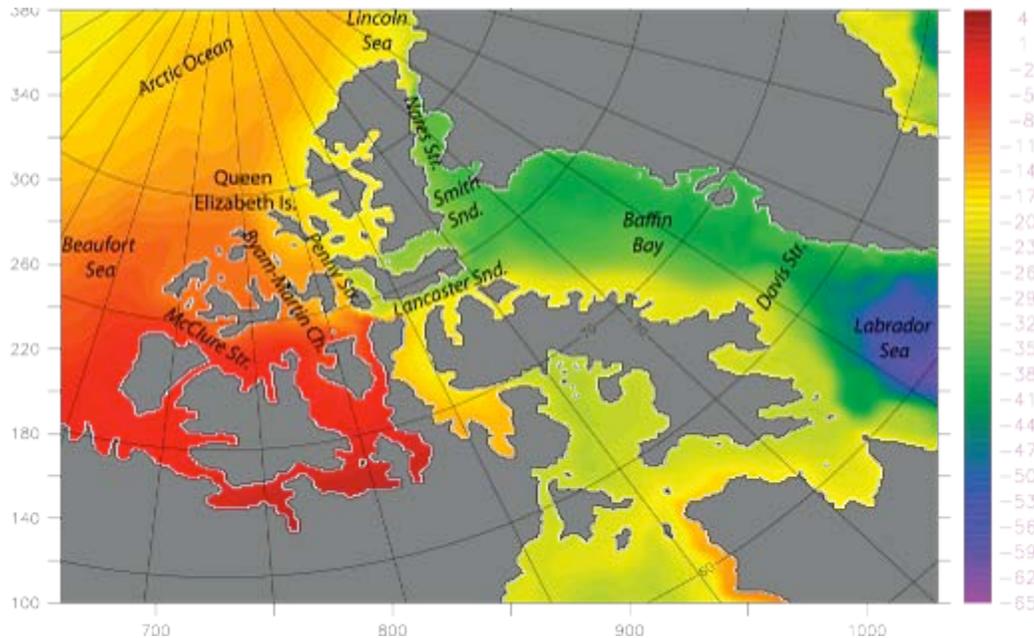
Figure 21.   Model 26-year mean CAA SSH (cm).

A.   SUMMER VOLUME FLUX MAXIMUM

Model results for volume flux through Lancaster Sound reveal two peaks in the annual cycle: one in March and a smaller one in July (Figure 14a). The relative maximum occurring in the late summertime is consistent with observations. Furthermore, the peak does appear due to the wind. When only considering volume fluxes for the upper 25m, both peaks in the annual cycle are still present but the larger one occurs during the late summer instead of during the late winter (as it does when considering all depths). This occurs for the length of the CAA, with annual cycles of the upper 25m volume flux at McClure Strait, Byam Martin Channel, and Penny Strait all behaving like Lancaster Sound with the larger peaks occurring in late summer. This is the time with the climatological wind most favorable to flow through the CAA (excluding Nares Strait) and the time when the ice has retreated, allowing wind to act

more on the ocean surface. This also explains why there isn't a late summer pulse of volume through Nares Strait. The wind direction is not conducive to increased summertime flow and Nares Strait retains more of its ice cover than the Northwest Passage, insulating the ocean from the overlying winds.

B. WINTER VOLUME FLUX MAXIMUM

The annual cycle of volume flux through Nares Strait has only one maximum, in March/April (Figure 10a). This coincides with the larger maximum volume flux through Lancaster Sound (Figure 14a). Munchow and Melling (2008) describe enhanced volume flux in Nares Strait from January to June and several studies mention evidence of a winter pulse in eastward volume flux through western Lancaster Sound (Peterson et al. 2008; Melling et al. 2008; Prinsenberg et al. 2009). See Chapter III for further details.

When considering fluxes integrated over all depths, this annual peak in modeled volume flux does not appear related to the wind forcing. This is consistent with the findings of Munchow and Melling (2008) who determined that Nares Strait volume fluxes below 30m were independent of the wind. Furthermore, when the time series of volume fluxes for both locations are plotted together (Figure 22), it becomes apparent that although the annual cycles are different (one or two volume peaks), most of the variability is common to both locations (correlation R=0.94). This suggests a common large scale forcing. Although the upstream ends of both locations are different, they do share their downstream endpoint: i.e. northern Baffin Bay.
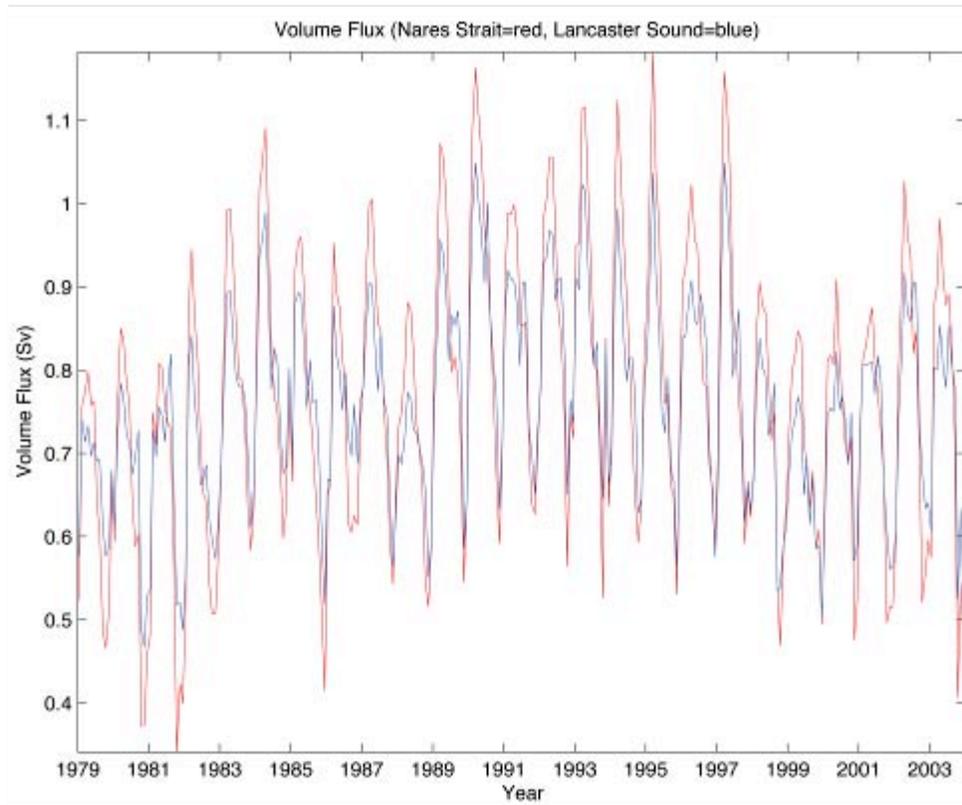
Figure 22.   26-year net volume fluxes. Nares Strait (red) and Lancaster Sound (blue).

C.   SSH GRADIENTS

Results from a modeling study by Kliem and Greenberg (2003) suggested that the volume flux through the CAA is a function of the Arctic to Baffin Bay SSH gradient, whereby the fluxes are modulated by a change in SSH in Baffin Bay. They calculated that decreasing the SSH in Baffin Bay by 5 cm would double the volume flux through the CAA. Unfortunately they only simulated summertime conditions in the CAA, leaving the question of annual cycles and interannual variation unaddressed.

Our model results based on 26-years of simulation demonstrate that SSH gradients do explain the annual peak volume fluxes (around March) through both Nares Strait (Figure 23c) and Lancaster Sound (Figure 23f). The volume flux anomalies and SSH gradient anomalies are also highly correlated. Volume flux anomalies through

58

Nares Strait (Figure 24a) and anomalies of the SSH gradient (measured from the Lincoln Sea to Smith Sound) (Figure 24b) were highly correlated (R=0.89). Volume flux anomalies through the mouth of Lancaster Sound (Figure 24c) and anomalies of the SSH gradient (measured between the Queen Elizabeth Islands and western Baffin Bay) (Figure 24d) were also highly correlated (correlation R=0.85).
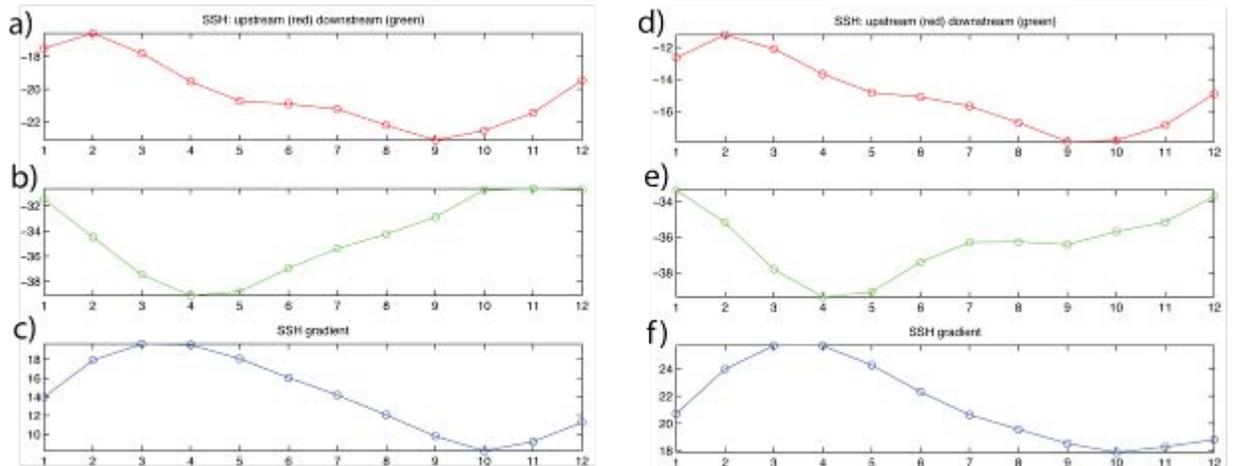
Figure 23. Annual cycle of SSH in a) Lincoln Sea, b) Smith Sound, and c) the gradient between them. Annual cycle of SSH in d) Queen Elizabeth Islands, e) Baffin Bay, and f) the gradient between them.

For Nares Strait, about half of the variance in the SSH gradient anomalies corresponded to SSH anomalies upstream in the Lincoln Sea and the other half corresponded to negative SSH anomalies downstream in Smith Sound. For Lancaster Sound, the negative downstream SSH anomalies in western Baffin Bay correlated better with the SSH gradient anomalies than the SSH anomalies upstream in the Queen Elizabeth Islands (QEI). These findings confirm what Kliem and Greenburg (2003) had proposed: that the gradient is just as much if not more controlled by the sea surface drop in Baffin Bay as it is by an increase in the Arctic Ocean.

For Lancaster Sound, the upstream end of the SSH gradient is traditionally considered to lie at the edge of the Beaufort Sea near McClure Strait. However, volume flux anomalies were better correlated with anomalies of the SSH gradient measured from above the QEI to western Baffin Bay (R=0.85) as opposed to being measured from the

Beaufort Gyre to western Baffin Bay (R=0.48). Cross sections of flow through western Lancaster Sound (Figure 16) show the summertime maximum velocities are near the surface towards the southern side of the strait (consistent with wind forcing), whereas the wintertime maximum velocities are more evenly distributed over the water column (consistent with more of a barotropic response to a large scale gradient) on the northern side of the strait (consistent with control by the input from the QEI region vice Beaufort Gyre).
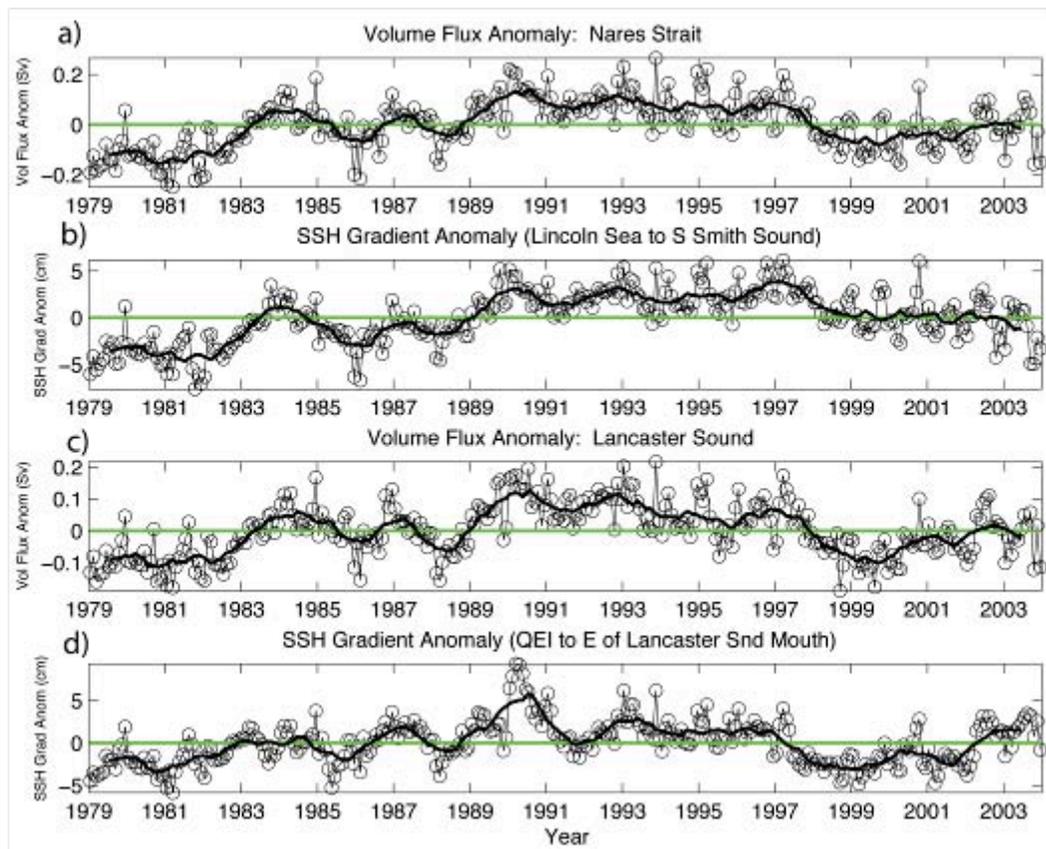
Figure 24.   a) volume flux anomalies through Nares Strait, b) SSH gradient (from the Lincoln Sea to Baffin Bay), c) volume flux anomalies through Lancaster Sound, and d) SSH gradient (from the Queen Elizabeth Islands to Baffin bay). Thick black line=13-month running mean.

The upstream ends of the calculated SSH gradients were located in the Arctic Ocean. As such, those SSH's and SSH anomalies were the product of a complex

circulation north of the CAA. There the currents are highly variable along the slope, shelf, and coast, as well as possibly being affected by the major large-scale Arctic Ocean circulation patterns. The SSH and SSH anomaly time series' were correlated with the AO and NAO on monthly, seasonal, and annual time scales but only a small portion of variance could be explained (~10%). The Arctic dipole anomaly (Wu et al. 2006; Wu et al. 2008) does not appear to explain the time series variability either. Furthermore, there is a lack of observational data in this region leaving its circulation and hydrography largely unknown. However, examination of the downstream ends of the SSH gradients (locations in northern Baffin Bay) sheds light on the volume fluxes through the major CAA passages.

D.   BAFFIN BAY SSH AND VOLUME

Based on the model-derived annual cycle, Baffin Bay's sea surface drops from February to April and then rises back up for the rest of the year. The effect is most evident on the eastern side of the bay. This is not just a redistribution of mass across the bay: the actual volume of Baffin Bay fluctuates over this cycle. The Baffin Bay volume anomaly leads both the Lancaster Sound and Nares Strait volume flux anomalies by one month with correlations of R= -0.73 (for each) suggesting that the volume decrease which controls SSH in Baffin Bay drives increased fluxes through the CAA. Moreover, the decreases in Baffin Bay SSH and volume coincide with a decrease in the northward volume transport by the West Greenland Current (WGC) into Baffin Bay from the south (Figure 18a). In fact, net flow along the western Greenland shelf north of Davis Strait actually turns southwards from February to April (some weak northbound flow does continue on the eastern side of Davis Strait but it is dominated by the southbound flow in the net sense). Using a mooring in eastern Davis Strait, Tang et al. (2004) observed that the northward current was strongest in fall and weakest in winter, sometimes even changing direction to indicate southward flow. Rykova (2010) determined the WGC to be widest and fastest in November and slowest in April/March. Both of these studies are consistent with our simulated seasonal variability of flow in eastern Davis Strait.

E. THE WEST GREENLAND CURRENT NEAR CAPE DESOLATION

The possible cause of variability in the northward flow can be traced all the way back to Cape Desolation in the south. Near Cape Desolation, the WGC fractures into three branches with one continuing north along the West Greenland coast and the others following the bathymetry to the west around the northern rim of the Labrador basin (Cuny et al. 2002). Previous comparison of results from this model with available data show similar spatial distribution and magnitude of eddy kinetic energy (Maslowski et al. 2008a) suggesting agreement not just with the linear branch of the current but also with the magnitude and frequency of eddies separating from the WGC. This is in fact a site of observed eddy production (Prater 2002; Lilly et al. 2003; Hatun et al. 2007). Eddies enter the Labrador Sea in the recirculating branches and are thought to play significant roles in the preconditioning, deep convection, and restratification processes (Katsman et al. 2004; Chanut et al. 2008; Rykova 2010). In a modeling study, Eden and Boning (2002) found that eddies shed near Cape Desolation were formed by instability in the WGC southwards of that location. The instability and eddy generation was seasonal, peaking in January/February/March, consistent with the time period when recirculaton (offshore branching and eddy flux into the Labrador Sea interior) is strongest in our model. Over the annual cycle, the model shows that as the across shelf volume flux peaks (Figure 25a) the northwards volume transport in the WGC decreases (Figure 25b). Conversely, when the across shelf volume flux is at its minimum the northwards flux builds up again.
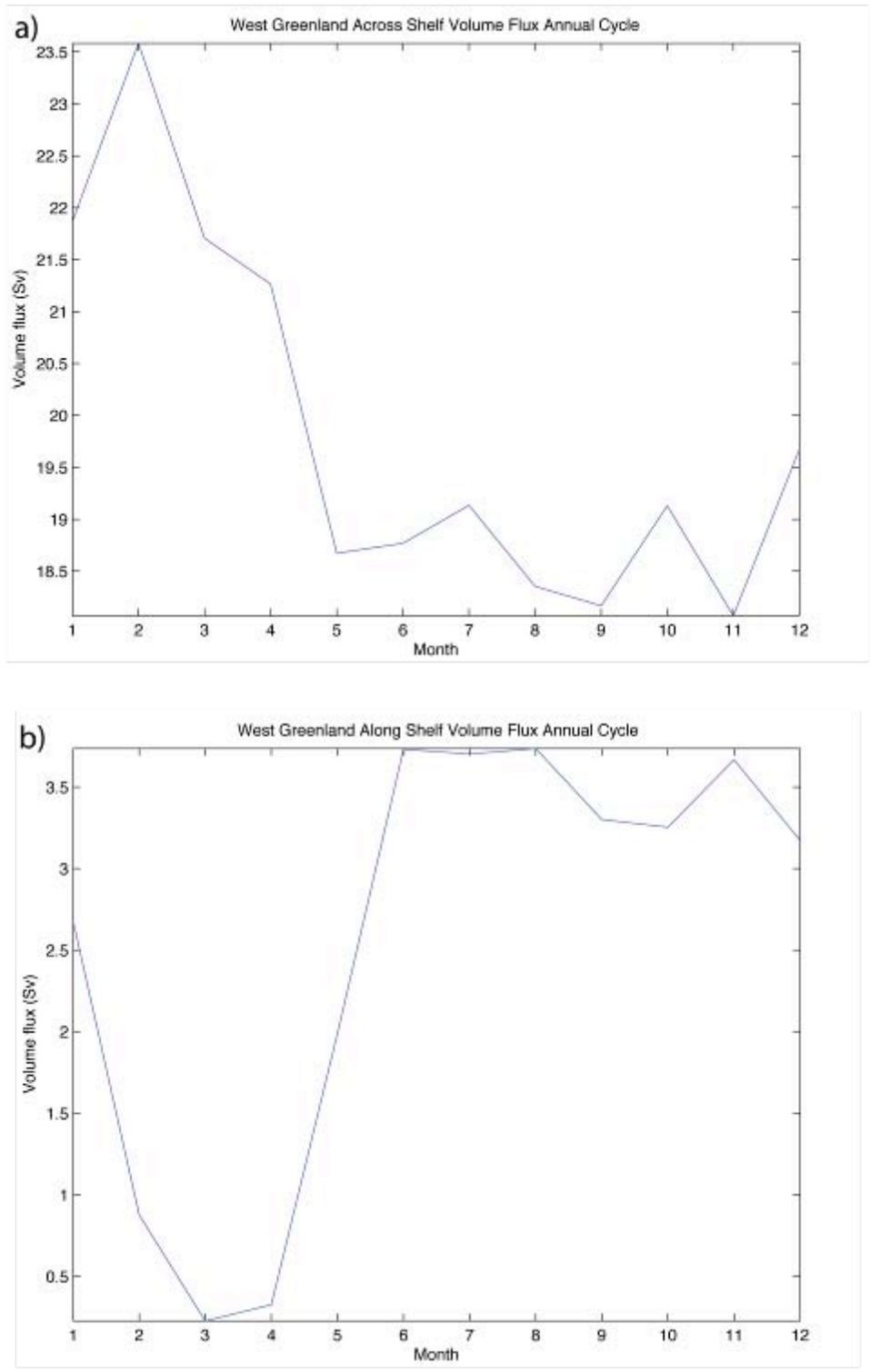
Figure 25.   Western Greenland net annual volume flux cycles. a) across shelf and b) along shelf (downstream of the across shelf region).

There is very little correlation in volume flux anomalies (measured along the shelf) between successive locations while moving northwards up the western coast of Greenland. Most of the variance in the volume flux anomaly signal can be tracked moving across the shelf into the interior of the Labrador Sea rather than continuing northwards along Greenland. The variable dynamics that control the volume directed offshore make it impossible for volume flux anomalies to propagate northward with their overall signal intact. Dunlap and Tang (2006) used a model to show that increasing the volume flux south of Greenland (rounding Cape Farewell) "mostly affects the part of the WGC that branches westward at about 64 N." Possibly related, Houghton and Visbeck (2002) showed that freshwater anomalies observed near Cape Farewell are much different than those moving northward through eastern Davis Strait. As the anomalies are continually removed, the annual cycle is all that is left for comparison. The annual peak of cross shelf flow corresponds to a slack period in the northward flow. This contributes to the volume and SSH variation in Baffin Bay.

Of particular interest is what causes the recirculation branches to leave the west Greenland shelf. Plots of wind stress and wind stress curl show that when the most recirculation is occurring (January/February/March), the winds exert a cyclonic torque on the upper ocean over the region where they move offshore (Figure 26a). This area is ice free in the model and observations, allowing the wind to act on the open water. Eden and Boning (2002) found that wind stress does play a role on the instability of the WGC and eddy formation during this season. There is cyclonic torque exerted on the surface in other regions along the west Greenland shelf and eastern Baffin Bay. However, those areas are covered by smooth first year ice at the time, effectively de-coupling the ocean from the atmosphere. Later, after the ice has receded, the winds are favorable to flow along the western Greenland coast (Figure 26b), and the flow does increase there (Figure 18b, Figure 26b).
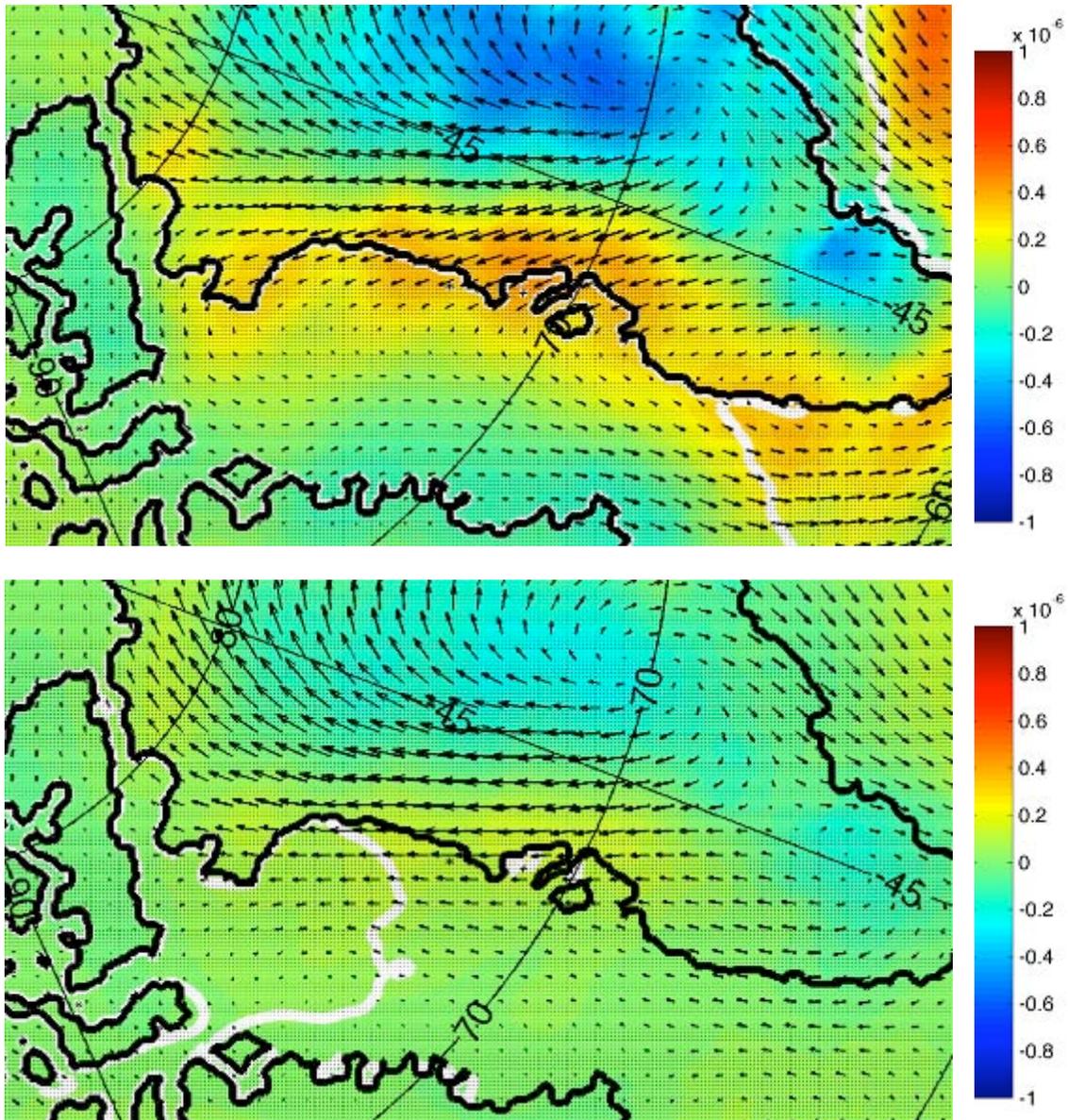
Figure 26.   Wind stress (vectors), wind stress curl (N/m^3) (shading) and 30% ice
concentration (white contour) for March (top) and August (bottom).

However, it is difficult to completely attribute the SSH drop to any one event.
Other factors possibly causing SSH to drop in northeast Baffin Bay are local cooling of
the water and the input of brine as a result of ice formation, both of which increase
density and lower SSH. In fact, the time series of ice volume anomalies in Baffin Bay
correlates with the liquid volume anomalies in Baffin Bay at R= -0.5 at zero lag.

Furthermore, during the time of the lowest SSH, the area with the lowest SSH experiences the highest sea surface salinity in any region of Baffin Bay over the entire annual cycle.

F.   DAVIS STRAIT SSH GRADIENTS AND OUTFLOW

After CAA outflow moves into Baffin Bay, it is exported southward to the Labrador Sea via Davis Strait. While the actual fluxes were presented in Chapter III, their controls are examined here. There is an across strait SSH gradient of approximately 10 cm across Davis Strait, with the western side of the strait sitting higher than the eastern side. The western side of the strait changes little whereas the eastern side exhibits large variability. Using the annual cycle of SSH gradients calculated between northern Baffin Bay and various points along the Davis Strait section (Figure 27), it becomes evident that the SSH gradients are most variable on the eastern side of Davis Strait. There, the gradient goes positive and negative (Figure 27c). It is positive (oriented w/ northern Baffin Bay higher than eastern Davis Strait) in the winter months during which time the volume transport is weakest in the WGC, allowing the maximum net volume outflow from Davis Strait south to the Labrador Sea. During the late summer/ fall, the SSH gradient has switched signs (with eastern Davis Strait higher than northern Baffin Bay), which coincides with the peak volume inflow from the WGC, resulting in the minimum net outflow from Davis Strait. Thus, sign changes in this gradient are associated with flood and ebb of WGC into and out of Baffin Bay.
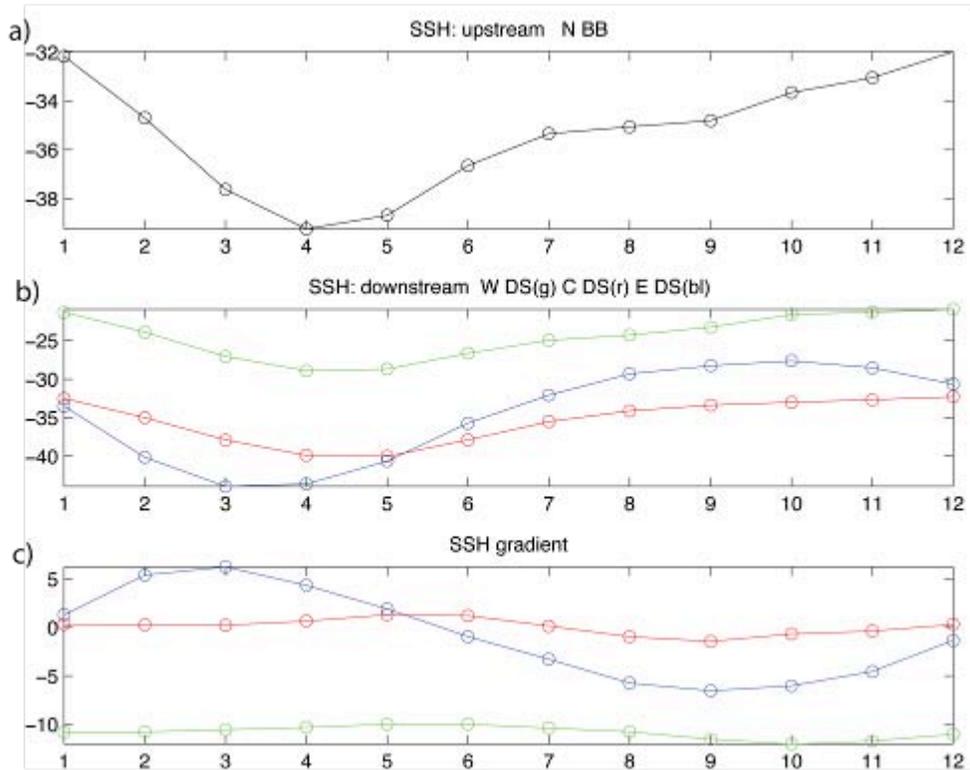
Figure 27. Annual cycle of SSH in a) northern Baffin Bay, b) three points along Davis Strait section, and c) the gradient between them. Green=western Davis Strait, Red=central Davis Strait, and Blue=eastern Davis Strait.

In contrast to the SSH gradient between northern Baffin Bay and eastern Davis Strait, the gradient measured from northern Baffin Bay to western Davis Strait is always negative (western Davis Strait has higher SSH than northern Baffin Bay). However, flow here is continually in the direction opposite to the sense of the gradient. The large volume input (~1.5 Sv) that enters from Nares Strait and Lancaster Sound is dynamically confined to the shelf and piles up water to its right (on the western side of Baffin Bay) as it moves southward in the Baffin Island Current. When it reaches Davis Strait, the sea floor rises at the sill, constricting the flow and causing a further increase in SSH. In this region, the flow drives the gradient rather than the opposite regime in eastern Baffin Bay where the flow responds to the gradient.

The time series of SSH gradient anomalies measured from northern Baffin Bay to various points along the Davis Strait section are presented in Figure 28. Numerous combinations of points between northern Baffin Bay and across the width of Davis Strait were considered and a few are shown here for illustration. As one goes from west to east, the time series of SSH gradient anomalies become increasingly similar in shape to the time series of net volume flux anomalies through Davis Strait (Figure 29) with correlations at locations in western Davis Strait, central Davis Strait, and eastern Davis Strait of R=0.53, 0.61, and 0.86 respectively. To monitor the flow through the CAA one could possibly observe the SSH gradient from northern Baffin Bay to the eastern Davis Strait. Furthermore, to estimate the net volume export into the Labrador Sea one could even just monitor the SSH in eastern Davis Strait. The time series of SSH anomaly in eastern Davis Strait correlated with net volume flux anomalies through Davis Strait into the Labrador Sea yields a value of R= -0.83.
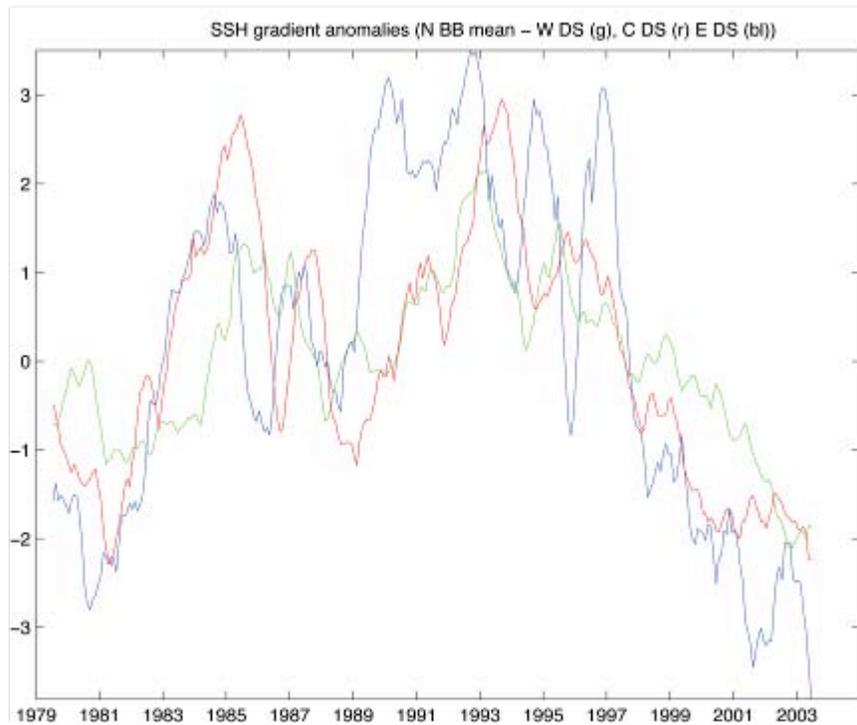
Figure 28.   SSH gradient anomalies (13-month running mean) measured from northern Baffin Bay to several locations along the Davis Strait section. Green=western Davis Strait, Red=central Davis Strait, and Blue=eastern Davis Strait.
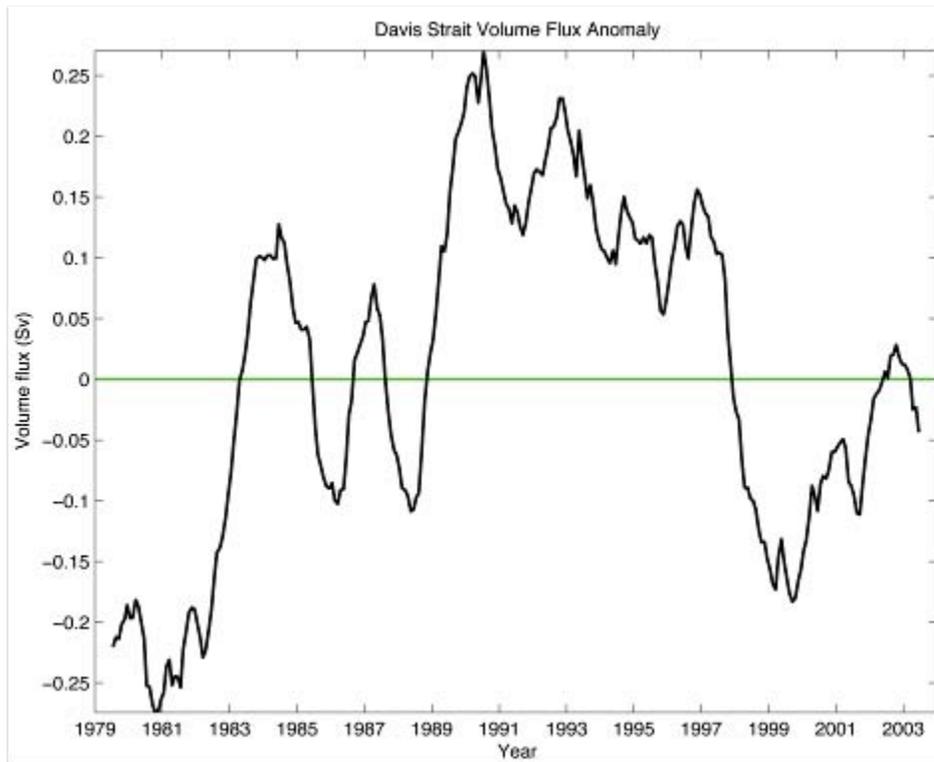
Figure 29.   Davis Strait net volume flux anomaly (13-month running mean).

As freshwater export from the Arctic Ocean via the CAA was one of the main goals of this overall study, its final movement southwards through Davis Strait was examined.   The best correlation (R=0.52) between Davis Strait net freshwater flux (liquid) anomalies and Baffin Bay N-S SSH gradient anomalies occurred when the downstream endpoint of the gradient was in eastern Davis Strait, just as was the case for volume flux anomalies.   When considering ice fluxes as well, the combined freshwater flux anomalies correlated even better with the N-S Baffin Bay SSH gradient anomalies (R=0.65).   This increase in correlation does not suggest that the SSH gradient anomalies push ice through Davis Strait, but rather that anomalies in winds which may cause anomalies in the gradient may also drive an increase in the ice flux.   For example, an anomalous northerly wind could drive more recirculation offshore from the Greenland shelf, reduce SSH there, and cause an increased SSH gradient.   That same northerly wind could also drive extra ice southwards through Davis Strait.

What drove the SSH gradient (between northern Baffin Bay and eastern Davis Strait) anomalies and Davis Strait net volume flux anomalies to such a high values in early-mid 1990's is still an open question. Correlation with AO and NAO indices explain little of the variance (~20% and ~15% respectively). As this study has shown the importance of control by the West Greenland Current, perhaps the cause could be traced back to that region.

In summary, variations in the northward flow in eastern Davis Strait provide a significant control on the flow moving from the Arctic Ocean through the CAA to Baffin Bay. Dunlap and Tang (2006) also found a connection between CAA outflow and the flow strength in eastern Davis Strait but determined the opposite: flow through the CAA regulated the northbound inflow to Baffin Bay. Our model has demonstrated the opposite, where flow in eastern Davis Strait regulates CAA outflow. However, their solution was based solely on September simulation and many of the details presented here (i.e. seasonal cycles in WGC and recirculating branches, etc) would not have been available to resolve the cause/effect nature of the processes.

G.   CONCLUSIONS

This study examined the controls on the 1979-2004 volume and freshwater fluxes through the Canadian Arctic Archipelago using a high-resolution (~9 km) numerical model. Volume flux anomalies were controlled by the SSH gradient anomalies across the straits and FW anomalies were highly correlated with the volume anomalies. At least half of the variance in the time series of SSH gradient anomaly was due to SSH anomalies in northern Baffin Bay. The West Greenland Current exhibits seasonality, with cross shelf flow (into the Labrador Sea) peaking in January/February/March, causing reduced northward flow across eastern Davis Strait. The decreased northwards flow contributes to decreases in the volume and SSH in Baffin Bay. This maximizes the SSH gradients between the Arctic Ocean and Baffin Bay, leading to maximum volume fluxes through Nares Strait and Lancaster Sound. The net flow through Davis Strait

towards the Labrador Sea is at a maximum in winter when the WGC is at its weakest and volume anomalies are most correlated with the SSH gradient anomalies measured from northern Baffin Bay to eastern Davis Strait.

Given these new findings, it becomes apparent that modeling of the CAA with a limited domain (one which does not include the western Greenland shelf) could significantly impact the flow northwards through Davis Strait which in turn drives volume and SSH variations in Baffin Bay. This could subsequently alter the SSH gradients and flow through the CAA. Ultimately, this would distort the exchange of volume and freshwater between the Arctic Ocean and the Labrador Sea. Additionally, model bathymetry and horizontal resolution are critical because they play significant roles in representing passages within the CAA as well as determining where the recirculating branches separate from the western Greenland shelf into the Labrador Sea interior. Near Cape Desolation, this is also associated with the formation of eddies (Katsman et al. 2004; Chanut et al. 2008), which again are resolution dependent.

THIS PAGE INTENTIONALLY LEFT BLANK

V.   IMPACT OF SHELF-BASIN FRESHWATER TRANSPORT ON DEEP CONVECTION IN THE LABRADOR SEA

Labrador Sea deep convection helps make up the downward part of the AMOC "conveyor," where water sinks from the surface to depth, sometimes exceeding 2000m (e.g. Dickson et al. 1996; Lazier et al. 2002; Yashayev 2007). The water sinks in the winter when extremely cold air sweeps from the Canadian landmass over the Labrador Sea, cooling the surface waters and increasing the density enough to render the water column unstable. This atmospheric forcing of deep convection is a link between the high-latitude atmosphere and the mid-depth ocean (Pickart et al. 2002). Curry et al. (1998) even tracked climate signals from the surface of the Labrador Sea to the deep ocean near Bermuda. The product of convection is Labrador Sea Water (LSW), an important water mass in the Atlantic Ocean which itself plays a role in the formation of another major water mass, Northeast Atlantic Deep Water (NEADW). Additionally, the Labrador Sea, via the process of deep convection is a location where atmospheric pollutants such as CFC's and carbon dioxide can be removed and injected into the intermediate ocean (Lazier et al. 2002).

However, atmospheric forcing alone is not enough to trigger deep convection. Density is dependent on both salinity and temperature so there is a constant competition between the destabilizing effect of atmospheric cooling and the stabilizing effect of freshwater in the surface layers. Schmidt and Send (2007) partitioned the contributions of temperature and salinity to total buoyancy in the Labrador Sea and showed that for seasonal stratification salinity is equally if not more important than temperature. Freshwater anomalies have been observed to disrupt or even shutdown deep convection in the Labrador Sea. The Great Salinity Anomaly (Dickson et al. 1988) was a low salinity signal which propagated around the North Atlantic, resulting in the shutdown of deep convection between 1968-1972, with mixed layer depths limited to 200m (Lazier 1980).

The modeled circulation of the Labrador Sea (Figure 30b) is in good qualitative agreement with previous studies (Lazier and Wright 1993; Cuny et al. 2002). The

Labrador Sea is a deep basin, surrounded by a system of currents that travel cyclonically along its rim. To the east, the West Greenland current flows northward carrying cool low salinity water near the surface and warm salty Atlantic Water slightly deeper and offshore (this component is often referred to as the Irminger Current). Near Cape Desolation, the current fractures into several branches that follow the bathymetry, some moving west and recirculating along the top of the northern Labrador Sea (Cuny et al. 2002) and the remainder continuing north into Baffin Bay. Once across, these branches merge with the southward flowing Baffin Island Current and become the Labrador Current that continues southward along the Canadian shelf and out of the Labrador Sea. This current has even lower salinity than the West Greenland Current because of the more direct connection to the Arctic Ocean and its low salinity outflow. During the cycle of convection and restratification, the central Labrador Sea experiences large fluxes of heat and freshwater. During the restratification period in particular there is evidence of strong lateral exchange between the interior and boundary currents, where interior properties shift towards values found in the boundary currents (Straneo 2006). Mesoscale eddies have been proposed as the mechanism for this flux (Lilly et al. 1999; Straneo 2006).

Deep convection in the Labrador Sea is sparse, both in time and space. Some years have none while others have extremely deep convection because of the "memory" of the water column which allows a series of cold winters to affect progressively deeper layers (Lazier et al. 2002). This intermittence of convection, along with the harsh environment (which includes high wind speeds, low temperatures, rough seas, and the presence of sea ice) makes observation of convective episodes in the wintertime Labrador Sea very difficult. Furthermore, the eddies thought to play an important role in preconditioning and restratification processes are also difficult to observe because of their relatively short life span and small size. However, there have been a number of studies focused on the observation of convection and eddies which have yielded valuable insight into the Labrador Sea.

Since the 1960's, there has been occupation of the site designated Ocean Weather Station Bravo (OWSB) in the central Labrador Sea. Also, since the start of the World Ocean Circulation Experiment in 1990, there has been regular measurement of the

transect AR7W, from Cape Desolation, Greenland to Misery Point, Canada. The data gleaned has been valuable for monitoring long-term changes in the Labrador Sea. However, OWSB is not ideally positioned to measure the deepest convection and AR7W is usually surveyed after the convective season has ended (Yashayev 2007).
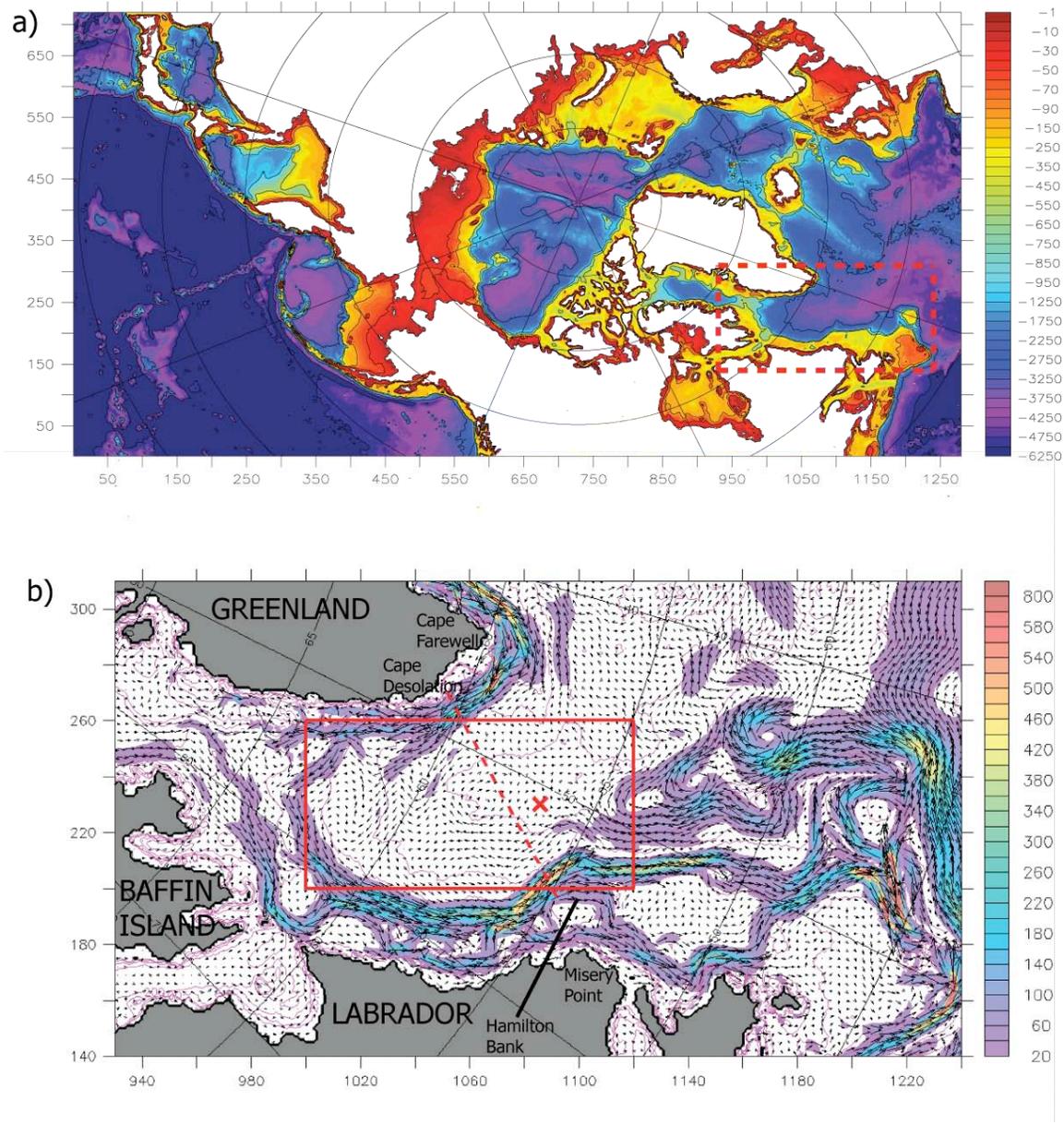
Figure 30.   a) domain bathymetry with Labrador Sea bathymetry (m) and red dashed box denoting Labrador Sea region; b) Labrador 26 year 0-122m mean TKE (cm2/s2) (shading) and velocity (vectors). Red box is convective study area, dashed line is AR7W section and x is OWSB.

From 1996-1998, the U.S. Office of Naval Research sponsored the Deep Convection Experiment in the Labrador Sea. Included in these extensive measurements was a research cruise in February and March of 1997, which yielded a comprehensive dataset of the Labrador Sea during the winter period of active convection. Pickart et al. (2002) found the area of deepest convection to be in the central western Labrador Sea. Simultaneously, Lavender et al. (2002) measured circulation and mixed layer depths with a series of subsurface floats with similar findings. However, they observed convection further to the north than previously reported (above 60°N) and for the first time southwest of Cape Farewell. Furthermore, they diagnosed a recirculation pattern flowing anticyclonically around the Labrador basin, counter to both the surface current system and the Irminger Current (Lavender et al. 2000).

Prater (2002) used RAFOS floats and satellite altimetry to describe and track eddies formed near the west Greenland coast. He identified seasonal peaks in SSH variability corresponding to eddy activity near Cape Desolation and in the central Labrador Sea. He speculated that eddies played a role in the restratification of the central Labrador Sea after convection. Cuny et al. (2002) used drifters to create a map of EKE for the Labrador Sea. There was again a peak near Cape Desolation in addition to the main EKE maximum well to the south associated with the "NW Corner" of the North Atlantic Current. They also investigated effects of eddies on the modification and mixing of Irminger water as it circled the Labrador Sea.

Lilly et al. (1999) used floats and a mooring at OWSB to describe the annual cycle of convection in the Labrador Sea. Restratification was rapid and there were high frequency variations in temperature and salinity, suggesting the highly variable spatial distribution of convective depths. Rapid ejection of floats from the boundary currents into the interior supported the possibility of pulsation in the currents being a source of eddies and therefore cross-shelf transport of water properties into the interior.

Cuny et al. (2005b) used a series of moorings to show that convection takes place within the Labrador Current itself over the slope. The temporal and spatial variability of convection between these moorings was analyzed. They also discussed the possibility of slantwise convection that can support mixing while maintaining significant stratification.

Hatun (2007) used gliders and altimetry to investigate eddies entering the Labrador Sea from the western shelf of Greenland. He observed eddies that had buoyant freshwater tops with Irminger water below, providing resistance to deep convection. He reasoned that the tracks of these eddies are what confines deep convection to the western side of the central Labrador Sea (instead of in the region of most intense forcing to the NW) and are responsible for much of the restratification at the end of the convective season.

Schmidt and Send (2007) examined the annual freshwater cycle in the central Labrador Sea using data from moorings at OWSB. They observed two pulses of freshwater, one from April to May and the other July to September. The source of the second pulse was attributed to West Greenland Current but the origin of the first pulse during the initial restratification period was unclear. They also observed a mixing down of freshwater from the surface waters from December to January, indicative of preconditioning before the onset of deep convection.

There have also been a number of modeling studies that have yielded valuable insight into the Labrador Sea. Some of the most relevant studies to this chapter are discussed here.

Eden and Boning (2002) used two models to recreate the seasonal EKE pattern of the Labrador Sea observed with altimetry. They determined the source of eddies shed at Cape Desolation was not purely variations in wind but the modulation of the seasonal instability of the West Greenland Current.

Katsman et al. (2004) used an idealized model to examine the restratification of the Labrador Sea after convection. Warm buoyant eddies shed near Cape Desolation were efficient in restratifying the central Labrador. Unfortunately the study only considered temperature and neglected the role of salinity, the other major contribution to buoyancy. Straneo (2006) considered both temperature and salinity and showed that the exchange between the boundary currents and the central Labrador Sea was a function of the lateral density gradient, not the temperature or salinity gradient alone.

Boning et al. (2003) used a $1/3^o$ high-resolution model of the North Atlantic to show that chlorofluorocarbon (CFC) inventories can be used to calculate the rate of LSW formation. The variations in CFC uptake were due to pulses in LSW formation responding to the varying atmospheric forcing.

Gerdes et al. (2005) used a $1/4^o$ horizontal resolution model to recreate the convection rates in the Greenland and Labrador Seas. Labrador Sea convection was dominated by large-scale atmospheric forcing and heat fluxes, and showed high correlation with the positive phase of the North Atlantic Oscillation.

Chanut et al. (2008) were able to recreate realistic deep convection in a high-resolution model of the North Atlantic. Interestingly, it was found that there was anomalous convection in the northern Labrador Sea when the bathymetry was smoothed to the point where no eddies were shed at Cape Desolation. These eddies inhibited convection and their paths confined its area.

Myers (2005) used an eddy permitting $1/3^o$ horizontal resolution model to examine the role of freshwater from the CAA. They showed that freshwater exported through Davis Strait was mostly confined to the Labrador shelf and very little of it moved into the Labrador Sea interior. A further experiment with a 2/3 increase in the freshwater flux through Davis Strait did not show significant changes in the formation of Labrador Sea water or the freshwater content of the Labrador Sea interior.

Over time the Labrador Sea has undergone profound changes of salinity and temperature. The entire basin has seen large changes in heat and freshwater content. Since 1994, the sea has changed from an extremely cold, fresh and weakly stratified body of water to one that is warmer, saltier and more stratified (Yashayev 2007). The observed variation in convection and water mass properties has raised concerns over their effects on MOC and ultimately climate variability itself (Dickson et al. 2002; Myers and Donnelly 2008).

This chapter is an effort towards understanding some of the interplay between freshwater transport from the Arctic Ocean, deep convection, and the role of eddies and sea ice. This model's high resolution is key to realistic simulation. Due to the decreasing

Rossby radius of deformation at higher latitudes (~5-10 km in the Labrador Sea; e. g. Gascard and Clark 1983; Marshall and Schott 1999; Lilly et al. 1999), high resolution is required to represent these small eddies and their processes (Maslowski et al. 2008a). These eddies may be very important, transporting Arctic outflowing freshwater to areas of open ocean convection and affecting deep-water formation and properties.

However, high resolution alone is not the answer. Most high-resolution regional models that include the Labrador Sea have domains that are North Atlantic focused (Boning et al. 1996; Myers 2005; Brandt et al. 2007; Chanut et al. 2008). They resolve neither the upstream events in the Arctic nor both freshwater pathways to the Labrador Sea, relying on the prescribed (fixed climatological) lateral boundary conditions for ocean fluxes and often climatology for sea ice.

This model resolves events in the Arctic, both pathways between it and the Labrador Sea, has boundary conditions located well away from the Labrador Sea, and features a coupled ice-ocean model that responds to atmospheric forcing. The modeled hydrography, dynamics, and sea ice variability in the Labrador Sea are analyzed in an effort to understand the interactions of eddies with freshwater outflow and their effect on deep convection. Due to the memory storage requirements and size of data files involved, the available model outputs for this section were limited to monthly mean fields, a 3-D snapshot of the end of each month, and daily selected fields and levels. These data constraints determined the capability and course of this section.

A.   EVALUATION OF MODELED LABRADOR SEA HYDROGRAPHY AND CURRENTS

In an earlier study, this model previously showed skill in the Labrador Sea, where the modeled eddy kinetic energy compared well to observations (Maslowski et al. 2008a). Additionally, the model showed skill in simulating eddies in the Gulf of Alaska and their effects on shelf-basin exchange of mass and properties (Maslowski et al. 2008b). Specifically, it showed how the modeled eddies transported freshwater off of the continental shelf and into the deep basin in accordance with observations.

79

Detailed comparisons of modeled current speed and temperature with values obtained from multiple moorings with several instrumented depths for a cumulative period of over 10 years on the Labrador shelf and slope (Lazier and Wright 1993) show that the model is slightly faster (with a mean difference of +1.2cm/s) and warmer (with a mean difference of +0.79°C) for the same time periods.

The modeled currents also compared well to drifter observations in other regions of the study area. The modeled West Greenland Current with a speed of 30-35 cm/s is in agreement with the Cuny et al. (2002) value of 35 cm/s. The recirculation region along the top of the Labrador Sea had slightly slower modeled values of surface flow (5-10 cm/s in the southern branch and 10-15 cm/s in the northern branch) than the observations (12 cm/s in the southern branch and 20 cm/s in the northern branch) (Cuny et al. 2002). At 700m, the current along the recirculation region was modeled at 4-10 cm/s, which is in reasonable agreement with the Lavender et al. (2002) observation of less than 5cm/s. The modeled Labrador Current was 30-35 cm/s on either side of Hamilton Bank compared to observed values of 20 cm/s to the north and 30 cm/s to the south of it (Cuny et al. 2002). It was acknowledged that the current was undersampled north of Hamilton Bank (Cuny et al. 2002), possibly explaining some of the difference between the modeled and observed values there.

Comparisons of modeled upper water column salinity to the observations of Schmidt and Send (2007) show that the modeled central Labrador Sea is approximately 0.1-0.15 psu higher than in reality. The West Greenland Current and Labrador Currents both have high spatial variability in salinity. The seasonal patterns of 0-25m salinity for the observations and model are similar but their magnitudes can alter by as much as 1.0 psu depending on the change of only a few model grid cells. Qualitatively, it can be said that the modeled 0-25m salinity west of Greenland shows minimum in October instead of the observed minimum in September and a maximum in February instead of the observed maximum in March/April. The Canadian Labrador slope shows a minimum in June instead of the observed minimum in August and maximum in February instead of the observed maximum in May. The effects of surface salinity restoring are not readily available for analysis from the model output. However, as this investigation focuses on

determining mechanisms driving Arctic-Labrador fluxes and physical processes of shelf-basin exchange, the analysis of surface salinity restoring effects is not of primary relevance.

The magnitudes of the positive temperature bias (as compared to the observations of Lazier and Wright 1993) and positive salinity bias largely cancel out when determining potential density.

Referenced analyses suggest no evidence that the boundary conditions affect the modeled dynamics in the Labrador Sea. In particular, the model does realistically resolve the NW Corner of the North Atlantic Current (Figure 30b) (Maslowski et al. 2008a), a feature located near the edge of the domain.

B.   EDDY DYNAMICS

1.   Formation Regions

Eddies in the Labrador Sea have two distinct formation regions: Cape Desolation and the "NW Corner" of the North Atlantic Current (Figure 30b). The Cape Desolation formation region is well documented from observations (Prater 2002; Cuny 2002; Hatun 2007). Modeling studies show that eddies are formed due to the West Greenland Current flowing over the increased steepness of the bottom slope and the long narrow extent of the shelf (Eden and Boning 2002; Katsman et al. 2004; Bracco et al. 2008). Eddy formation has also been reported in the region of the NW Corner (Woityra and Rossby 2008).

2.   Eddy Kinetic Energy (EKE) Distributions

The Labrador Sea EKE produced by this model was previously validated in Maslowski et al. (2008a). It was found that the spatial distribution is well represented compared to observations (Prater 2002; Cuny et al. 2002). The levels of EKE corresponded well in the southern Labrador Sea, while those to the north were underestimated by 20-30%. The importance of resolution was also highlighted, where the 9 km model showed more than an order of magnitude increase in EKE compared to

the 18 km variant of the model. The modeled EKE for the winters of 1998 and 2002 (Figure 31) are presented as background for 2 case studies discussed later. Our analysis suggests that the high levels to the NE are due to eddies shed near Cape Desolation while those to the south are due to eddies shed from the "NW Corner" of the North Atlantic Current which transit into the southern Labrador Sea.
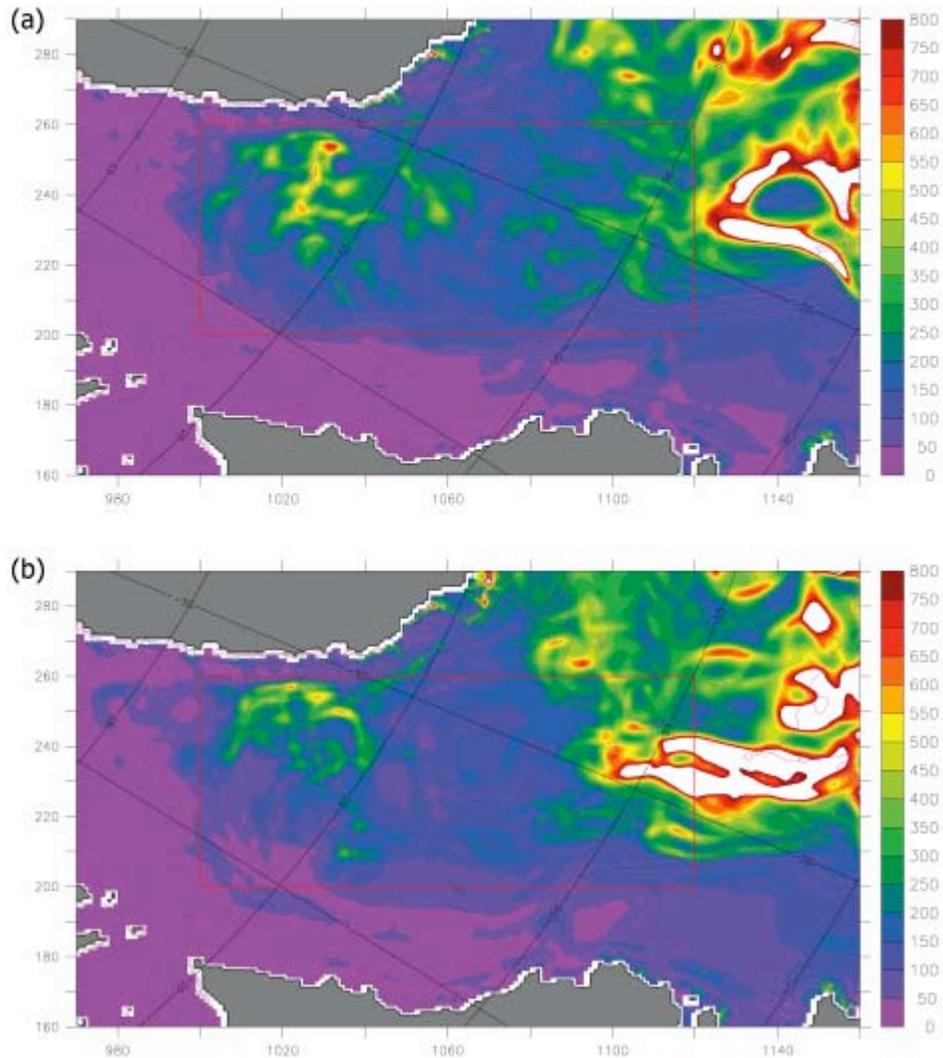
Figure 31.   Model eddy kinetic energy (EKE) (cm^2/s^2) for the winter (January-March) of a) 1998 and b) 2002.

3.   Eddy Processes

Based on our model results, the Labrador Sea surface experiences large annual changes in temperature and salinity. During the winter convection season (January-March) the sea surface is cool (~4 ^{o}C) and has relatively high salinity (~35). During the period of restratification starting in April, the surface remains cool but salinity begins to decrease, with the changes starting on the western side of the basin and propagating eastward towards Greenland. By June the entire basin has a freshwater cap (~34.8) and the SST begins to increase. SST increases until September (~6-7 ^{o}C) when it begins to decrease again towards a minimum in November (~3 ^{o}C). Salinity decreases until the beginning of November when it too reaches a minimum (~34.6). With the sea surface at its coolest and freshest point of the year, air temperatures decrease and winds increase, rapidly mixing the cold freshwater cap with warmer and higher salinity water below during November and December. At that time, the upper ocean is homogenized and ready for deep convection again.

Eddies are found to play an important role in these annual temperature and salinity cycles of the Labrador Sea. The cold freshwater cap is preferentially mixed down by eddies, reducing the buoyancy of the upper water column and preconditioning it immediately before the onset of the convective season (Figure 32). Cross sections of salinity and temperature anomalies on 30 Nov 2002 (anomaly calculated as the value on that day minus the monthly mean) clearly show increasing salinities above 50m and a band of decreasing salinity centered around 50m, indicative of the freshwater being mixed down across the Labrador Sea (Figure 33). This is more pronounced under the eddies, where cold freshwater is mixed much deeper with anomalies reaching depths of almost 300m.
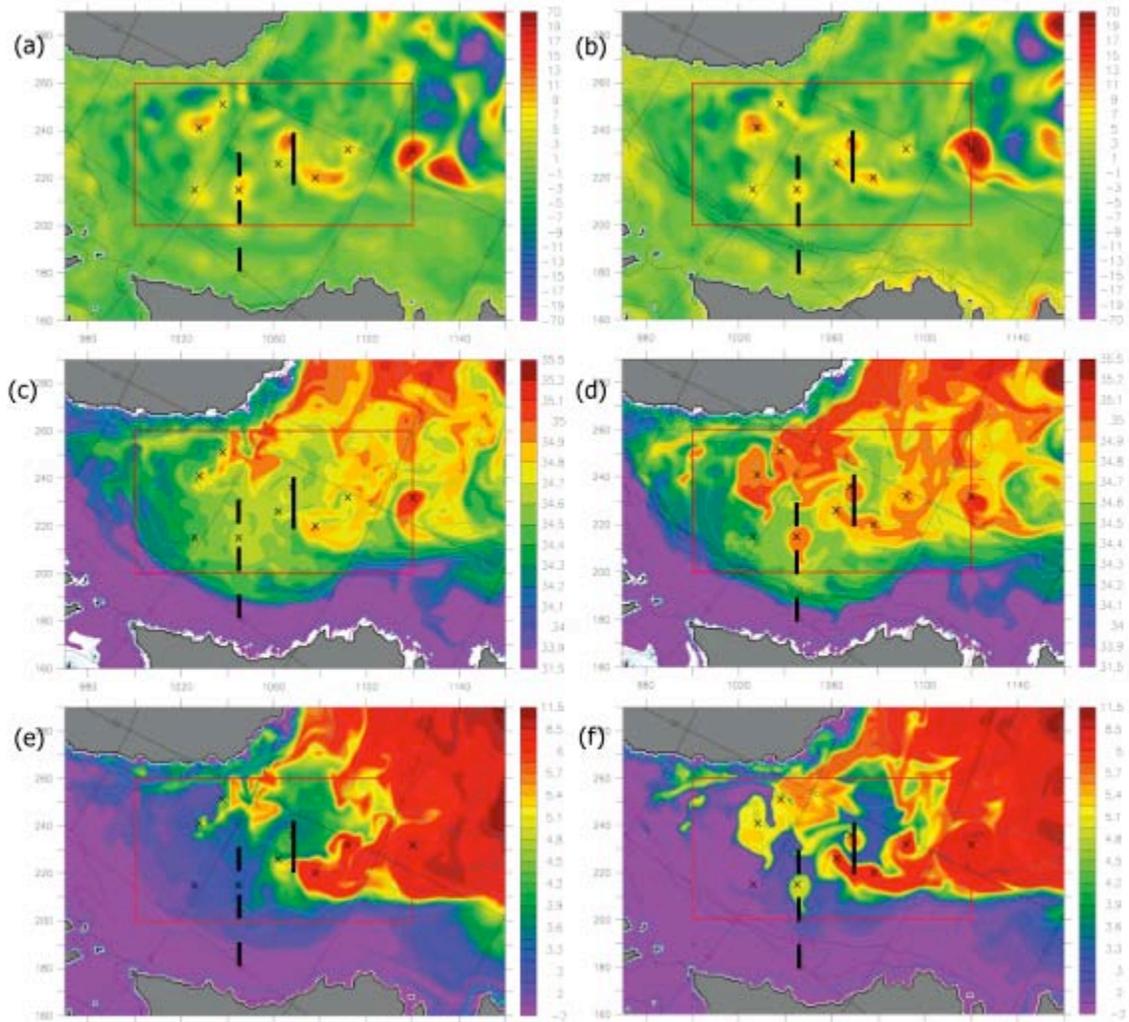
Figure 32.   26 Nov 2002 a) SSHA (cm), c) SSS, e) SST (deg C). 06 Dec 2002 b) SSHA (cm), d) SSS, and SST (deg C).
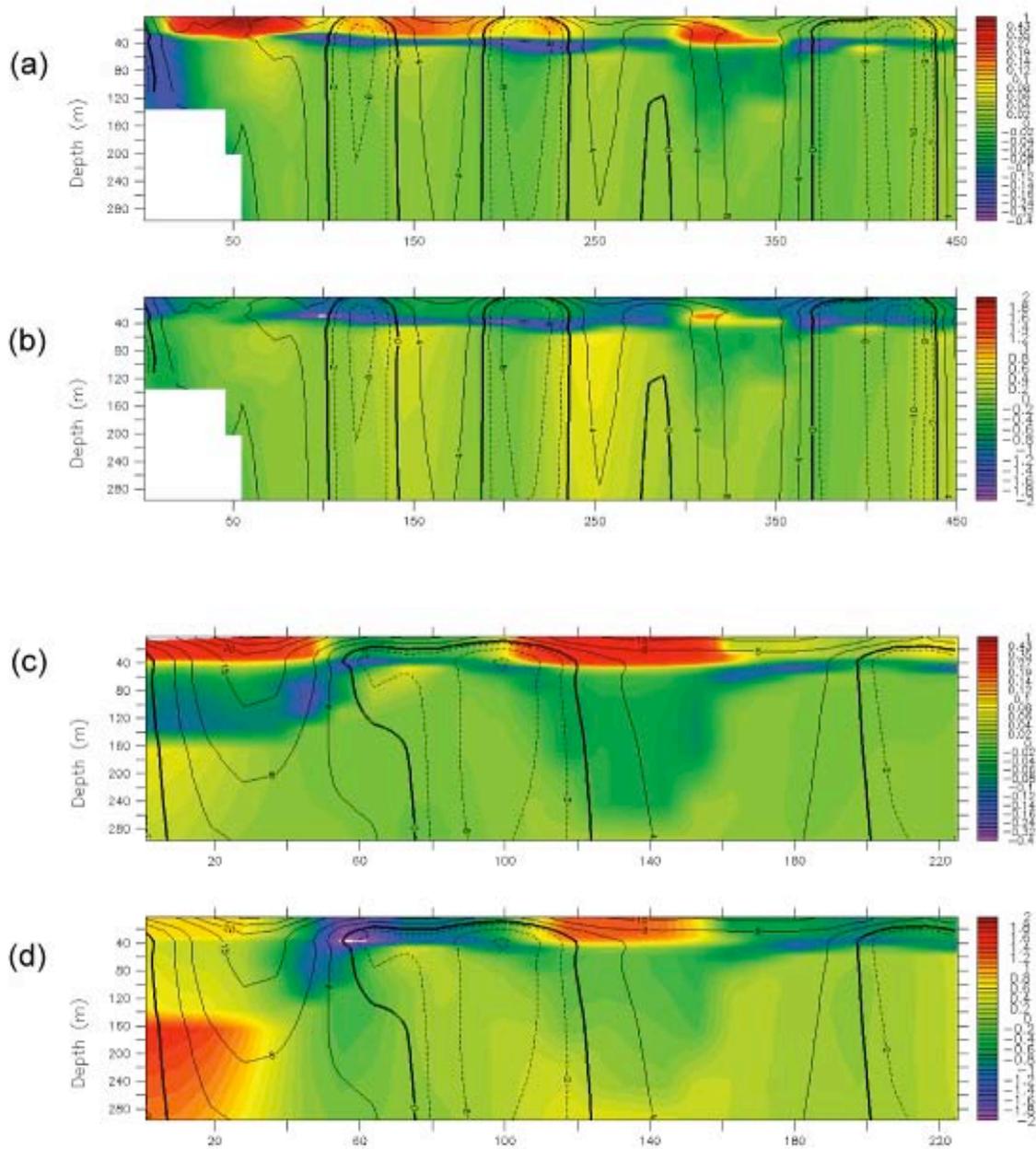
Figure 33. a), c) S anomalies and b), d) T anomalies (deg C) on 20 Nov 2002 along two cross sections shown in Figure 32 a), b) are from the dashed line while b), d) are from solid line. Anomalies were calculated as the values on the date minus the monthly mean for that month (i.e., negative anomalies mean the last day of the month was colder/fresher than the mean for the month).

Schmidt and Send (2007) observed this negative FW flux (increasing S) in the surface layers near OWSB in the central Labrador Sea from December to January, consistent with the model results.

An interesting feature shown in Figure 33a is the strong positive salinity anomaly near the surface at approximately 50 km on the cross section. Our results suggest this is due to the brine rejection during sea ice formation as the ice edge is extending seaward. This illustrates a benefit of the coupled ice-ocean model, where the ice and ocean actually interact (as discussed more in section F) instead of a climatological ice representation with no interaction.

4. Eddy Tracks

It appears that eddies shed near Cape Desolation tend to follow the bathymetry across the basin along two preferred paths (Cuny et al. 2002). Similar eddy tracks (Figure 34a) have been observed (Prater 2002; Cuny et al. 2002; Hatun 2007). The two paths form the sides of an "eddy corridor." Note that the region of the deepest mixed layer depth (Figure 34b) is underneath the "eddy corridor" hinting at some eddy influence on the modeled convection in this region.
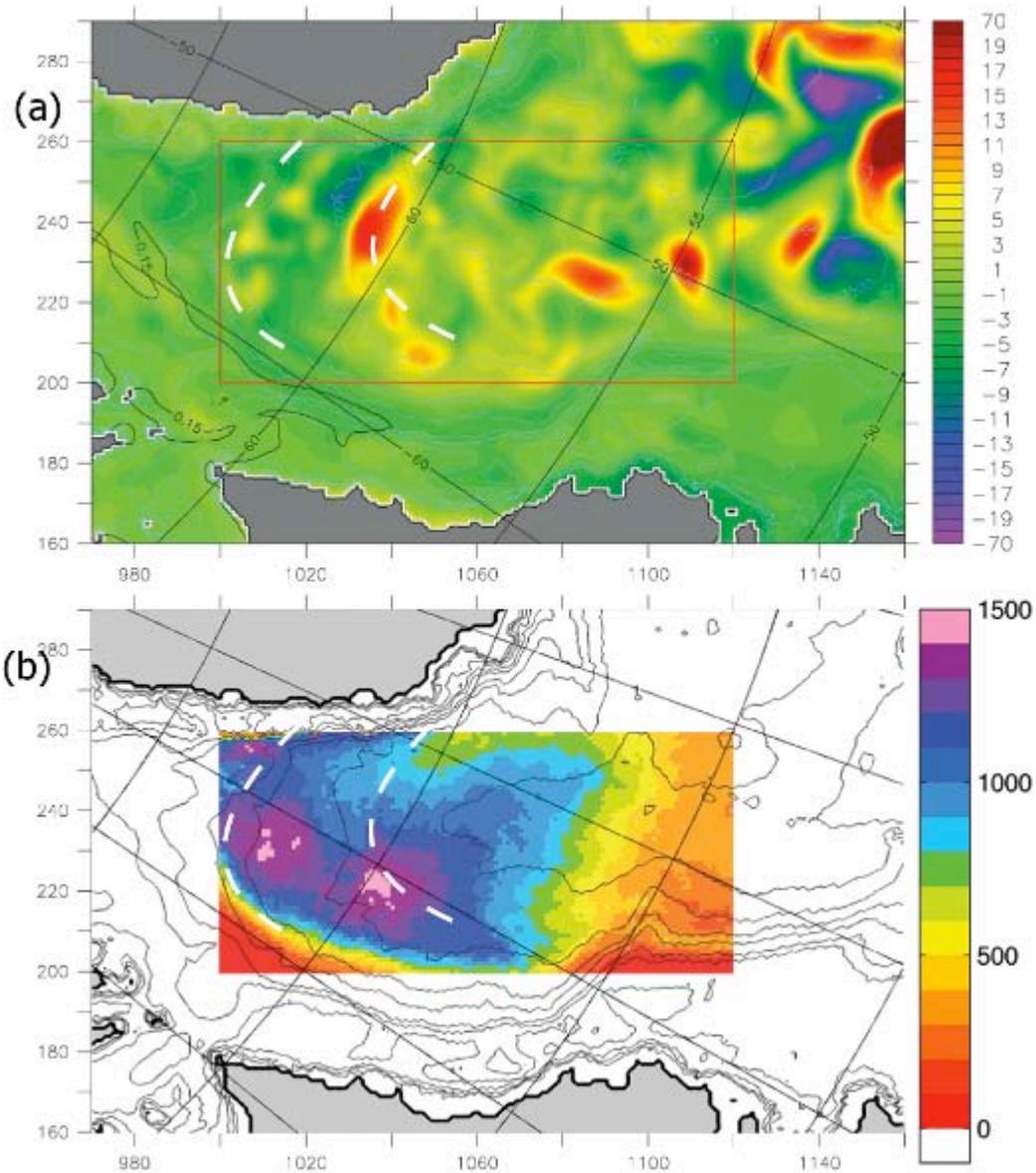
Figure 34.   a) Typical model derived tracks for eddies shed from the west Greenland shelf near Cape Desolation and b) 25 year mean (January-March) mixed layer depth (m).

C.   MIXED LAYER DEPTHS

In this study, mixed layer depth is used as a proxy for convection. Pickart et al. (2002) derived mixed layer depth from observed CTD data using a procedure which

included visual estimation of the approximate mixed layer extent, determination of the mean value over that extent and bracketing it with a two standard deviation envelope, and finally recording the depth where the profile crossed out of that envelope. While this process works well for a finite number of CTD casts, the preliminary step involving visual estimation makes this method impractical for use with large amounts of modeled data. Chanut et al. (2008) defined mixed layer depth as the depth where potential density exceeds its surface value by 0.005 kg m^{-3}. Several model profiles were analyzed using the methods of both Pickart et al. (2002) and Chanut et al. (2008) and the resulting mixed layer depths were very similar. Other methods for defining mixed layer depth were also considered. Kara et al. (2002) defined mixed layer depth as the depth where the observed density departed from its surface value by the amount equal to the change in density due to a temperature difference of 0.8 ^{o}C. Using their definition yielded mixed layer depths much deeper than the profiles actually showed. It is important to note that many of the other thresholds used to determine mixed layer depth (summarized in Kara et al. 2000; de Boyer Montegut et al. 2004) were optimized to deal with data in other regions and therefore do not apply here. Mixed layer depth can also be based on the gradient of the density profile. However, in the case of an unstable profile, this could underestimate the depth of mixing and convection. Another reason against using the gradient method is that the model-derived profiles are not continuous, but rather are a collection of points at different depth levels. What would in reality be a sharp density gradient at the base of the mixed layer could become smoothed due to level spacing, thereby not reaching the required gradient criteria and giving an erroneously deep mixed layer. Furthermore, it adds another step in the process of determining the gradient, therefore slowing the calculations. It was decided to use the method of Chanut et al. (2008) because it provided depths similar to those based on purely visible inspection of the profiles, was in good agreement with depths obtained using the method of Pickart et al. (2008) (against whose observations we would make comparisons), and it allowed for easy automation of the mixed layer depth calculations. It is also important to note that the magnitude of convection may be slightly overestimated here because of the decreased vertical resolution in the model at depth (below 850m, layer thickness becomes 200m).

1.   Time Series

The time series of deep convection is represented here (Figure 35) as the fraction of cells within the study area (Figure 30b) that show mixed layer depths exceeding various thresholds. The values are for the winter months only, defined as January, February and March. The observed patterns of deep convection (Lazier et al. 2002; Pickart et al. 2002) are reproduced, especially the early to mid-1990s. During 1989-1993 a series of severe winters was experienced which allowed the mixed layer depth to increase year by year due to the "memory" of the water column. 1993 and 1994 had some of the deepest convection ever reported, with mixed layer depths measured to 2320 m and 2300 m respectively. Later winters were warmer, leading to progressively shallower mixed layer depths with some cooling and deep convection in 1997. This variability is well represented in the model, with the deepest mixed layer depths for the period between 1979 and 2003 occurring in 1993 and 1994.
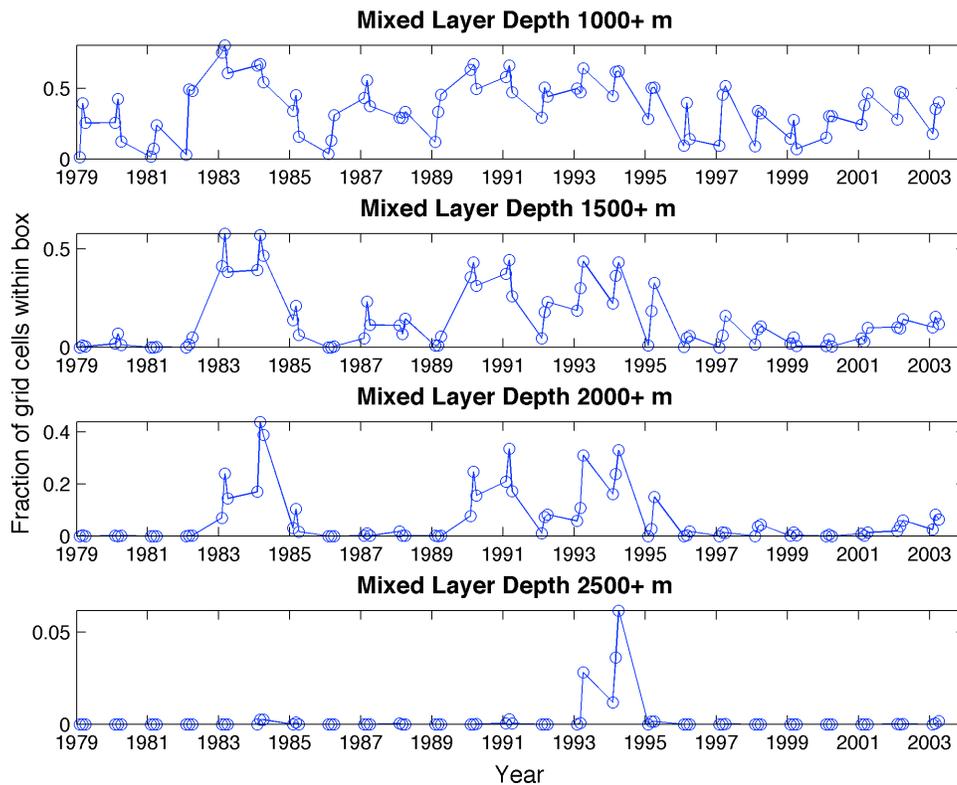
Figure 35.   Fraction of grid cells within study box (Figure 30b) with mixed layers exceeding depth thresholds.

89

2.   Individual Event

For March 1997 (Figure 36a), the bulk of deep convection observed by Pickart et al. (2002) (circled area) is well represented by the model with similar timing, depths, and locations. The same is true for the regions of maximum mixed layer depth (Feature A) and deep convection at the SW edge of the observed area (Feature B). The model also reproduces deep convection in the regions observed during this same period by Lavender et al. (2002). Specifically, they found deep convection further north than previously observed and for the first time SW of Cape Farewell, both of which are demonstrated in the model output (Features C, D and E).

However, the model also shows anomalous deep convection occurring north and east of the observed area. Exceptionally deep mixed layers from 2300 to 2400m have been observed (Gascard and Clarke 1983; Dickson et al. 1996; Lazier et al. 2002) near the middle of the AR7W CTD line, making the modeled magnitudes possible but most likely they are too large. A modeling study by Chanut et al. (2008) determined that excessive deep convection was present in these areas when Irminger Rings were not formed at Cape Desolation. These eddies act to inhibit convection in the region. This model does resolve the rings, but they tend to enhance convection by quickly eroding the seasonal stratification, as they are composed entirely of saline water, whereas Hatun (2007) and Rykova (2010) observed some eddies with freshwater tops. If many of these eddies do in fact have low salinity caps, they would act to add buoyancy and inhibit convection in the NE region, making the overall picture closer to the observations. This would also explain why the model has skill in the western Labrador Sea where the freshwater effects decrease farther from the Greenland coast; at some point the model is no longer "missing" freshwater.

The AR7W cross-section of the model for this same time period (Figure 36c) qualitatively compares well to the observed salinity (Figure 36d), especially on the Canadian side with similar spatial distribution but differing magnitudes. However, the large freshwater cap extending ~150 km from the western coast of Greenland is present only near the coast.   The cross sections show that overall the modeled salinities are too

high, with a bias of around $O(0.15$ psu) near the surface decreasing to $O(0.1$ psu) at depth. A similar bias was observed by Chanut et al. (2008), perhaps indicating a common problem between the models. The model bias may be due to errors in the surface salinity fields used in restoring, lack of runoff from Greenland, and/or insufficient resolution to represent buoyancy-driven narrow coastal flow along west Greenland.
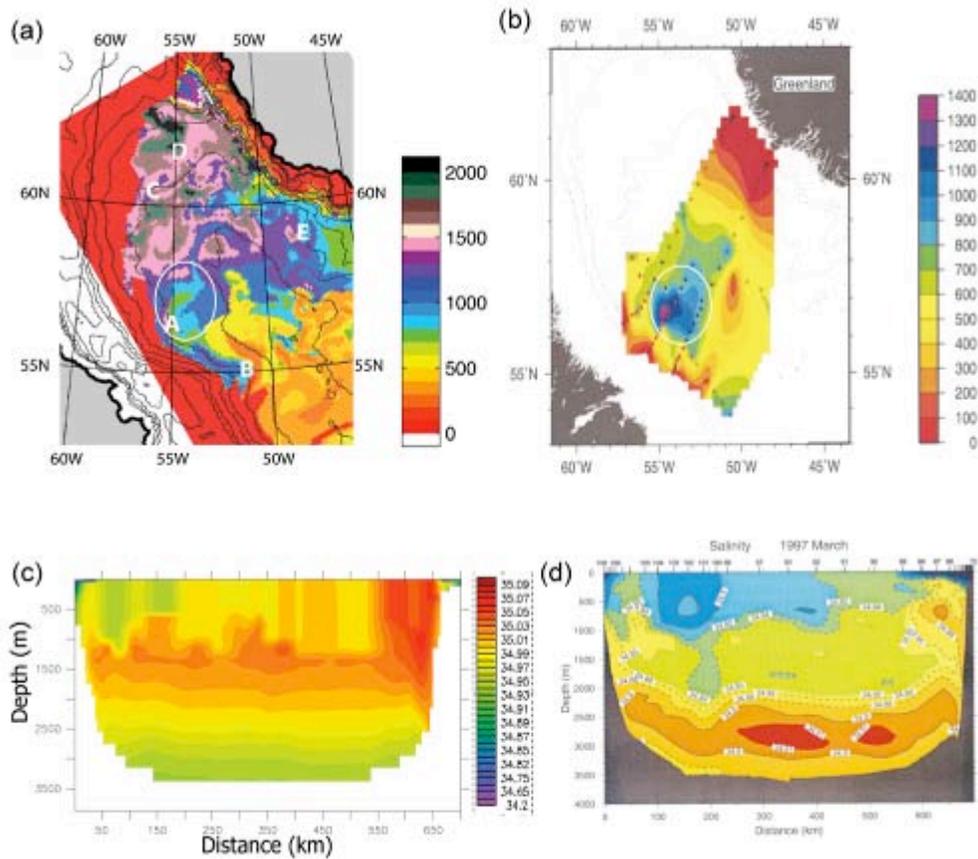
Figure 36.   Mixed layer depth (m) for a) model 31 Mar 1997 and b) observed Mar 1997 (from Pickart et al. 2002). A, B, C, D, E, and circle correspond to specific features discussed in the text. Cross sections of S along AR7W transect for c) model 31 Mar 1997 and d) observed Mar 1997 (from Pickart et al. 2002).

Interestingly, a transient feature similar to the freshwater cap missing in early March is resolved by the model but on 30 November 1996, 90 days before it is observed in reality. This could indicate an error in timing instead of a missing freshwater source altogether. The observed freshwater cap could be the result of an intermittent event.

Prater (2002) included a satellite derived IR image showing a jet of shelf water forced offshore from a location similar to the observed cap.

Another possible explanation for the missing freshwater is that although 9 km resolution is high, it is not high enough to resolve the coastal flow along Greenland. This coastal flow may be responsible for the fresh tops observed on some eddies. Alternatively, eddies forming in this region might not themselves be fresh but may redistribute some of the freshwater from the shelf to the interior as they propagate.

Preliminary results from a new model version configured at horizontal resolution of ~2.36 km (1/48°) suggest that eddies with fresh tops do form off Cape Desolation, even without the inclusion of Greenland's meltwater. The model produces the stronger coastal flow but so far does not include any Greenland runoff. Those results also indicate that the freshwater tops do not survive the transit across the top of the Labrador Sea but rather the freshwater is dissipated as it moves. Further 1/48° model details are discussed in Chapter VII.

Given the unknown source and phasing of the missing freshwater signal, coupled with its integrated effect over many years of convective cycles which would redistribute this freshwater vertically, our modeled mixed layer depth is not considered fully reliable in the northern Labrador Sea. However, the central and southern portions of the Labrador Sea are reproduced well.

D.   WATER MASS PROPERTIES

1.   Observed Deep Convection Region

The time series shown in Figure 37 represents the a 3 x 3 grid cell square (about 900 km^2) located within the area of deep convection identified by both Pickart et al. (2002) and this model (circled area of Figure 36a) for the months of the winter season. In order to represent the properties of the deep mixed layer, we use the 0-2000m mean potential density, salinity, and potential temperature. As deep convection occurs (Figure 35), the entire water column freshens and cools while potential density increases (Figure 37). This concurs with the observed signature of deep convection (Yashayev 2007). The

θ-S diagram (Figure 38) is another representation of the same trend for the 0-2000m mean, but it shows annual averages for each winter (mean of January, February and March for each year). It also clearly shows the cooling and freshening in times of increased density. Removal of the 0.1 psu estimated bias from the salinity shifts the distribution of points on the T-S diagram to yield potential densities corresponding to Classical Labrador Sea Water (Brandt 2007) during deep convection years and Upper Labrador Sea Water (Kieke et al. 2006) in the early 2000's, in agreement with observations.

A feature worthy of note is the increasing salinity between 1989 and 1991 while density is increasing. Yashayev (2007) describes a similar feature in his observations, where progressively deepening winter convection from 1988-1993 resulted in entrainment of more saline NEADW into the bottom of the mixed layer, overcompensating for the freshening from above.
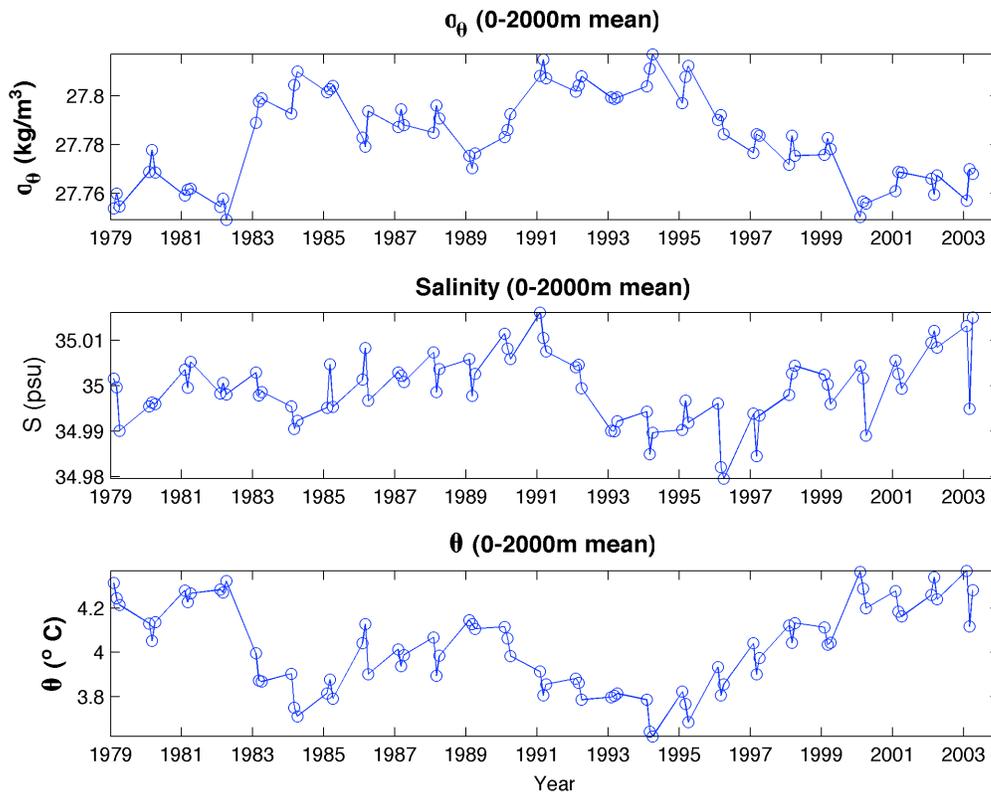
Figure 37.   Time series (JFM of each year) of potential density anomaly, salinity, and potential density (0-2000m mean) for a 3x3 grid cell box located within the circled convection region of Figure 36a.

93
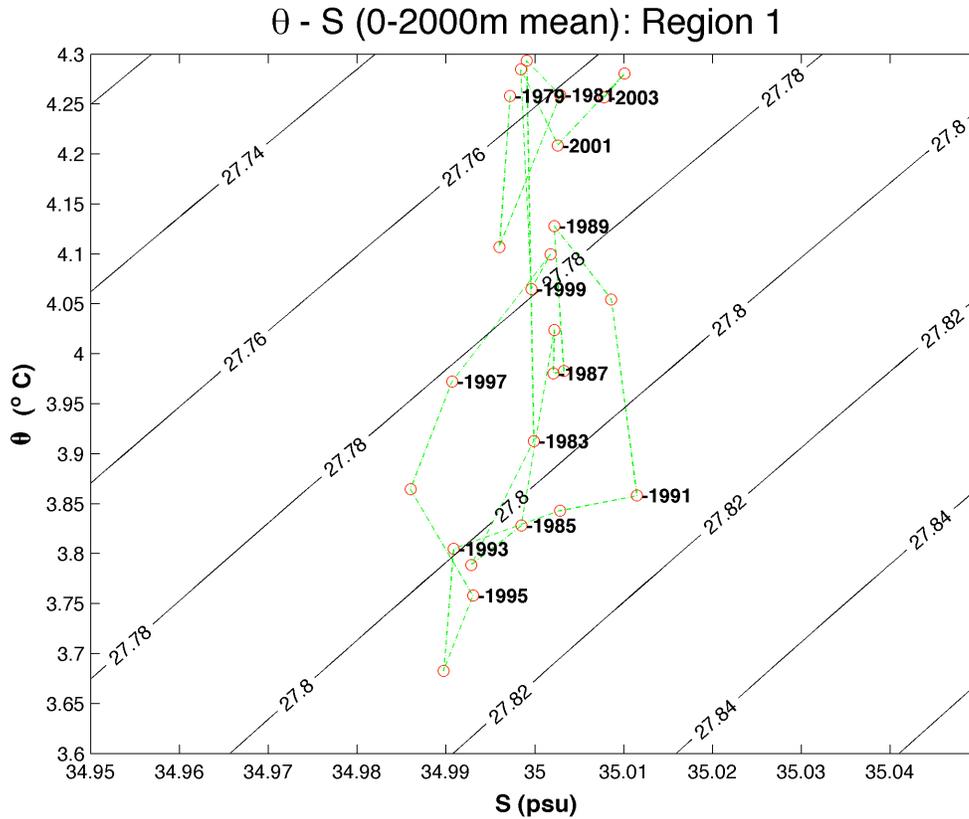
Figure 38.   θ-S diagram of data in Figure 37 but for each winter (average of JFM).

2.   Comparing Other Regions

In a comparison of several regions across the Labrador Sea, the T-S diagrams follow a general pattern of cooling, freshening and increasing density, agreeing with Yashayev's (2007) assertion that the entire Labrador Sea undergoes these fluctuations. However, the coolest, freshest and most dense waters are found in the observed deep convection region along Labrador slope, with the water column becoming warmer and saltier towards Greenland.

In summary, this model has shown reasonable skill in recreating the general circulation, eddy dynamics, deep convection and water mass properties of the Labrador Sea. However, the question is what can we say about the interaction of processes and their relative importance to deepwater formation in the Labrador Sea?   Section E

describes a case where eddies move freshwater from the shelf to influence deep convection. Section F describes a different case that illustrates the role of the ice cover and ice edge.

E.   CASE 1: SHELF-BASIN TRANSPORT OF FRESHWATER

1.   Into Observed Convection Region

This event from the winter of 1998 (Figure 39a) shows two counter-rotating eddies forcing a jet of freshwater (of approximately 70 m depth and 50 km width) in between them almost 200 km from the Labrador shelf into the observed deep convection region of the deep basin. It subsequently spreads to create counter-rotating vortices and form a "mushroom" shape. The origin of these eddies cannot be readily determined because of their weak initial SSHA signatures (Figure 40c). The anticyclonic eddy appears to come from the area immediately to the SE and then moves into the area via a recirculation pathway. The cyclonic eddy is induced between the edge of this eddy and another anticyclonic one to the NW. The cyclonic eddy is very weak with little SSHA signature (Figure 40d) but is visible in the surface circulation (Figure 40b). Before the event, both locations have moderately deep mixed layers, down to ~400 and ~1100 m (Figure 40e, Figure 41a). After the freshwater moves offshore, cold and fresh water covers the shallow layers of the offshore site, whereas the mixed layer of the inshore site deepens (Figure 40f, Figure 41b). The effect of the freshwater intrusion is visible where it adds sufficient buoyancy at the surface to halt deep convection, drastically reducing the mixed layer depth. The additional fingers of freshwater extending offshore (Figure 40b) to the NW (left) of the main plume (which also limit convection) are indications that this sort of event might be common. One of these upstream events is described in more detail in the next section.
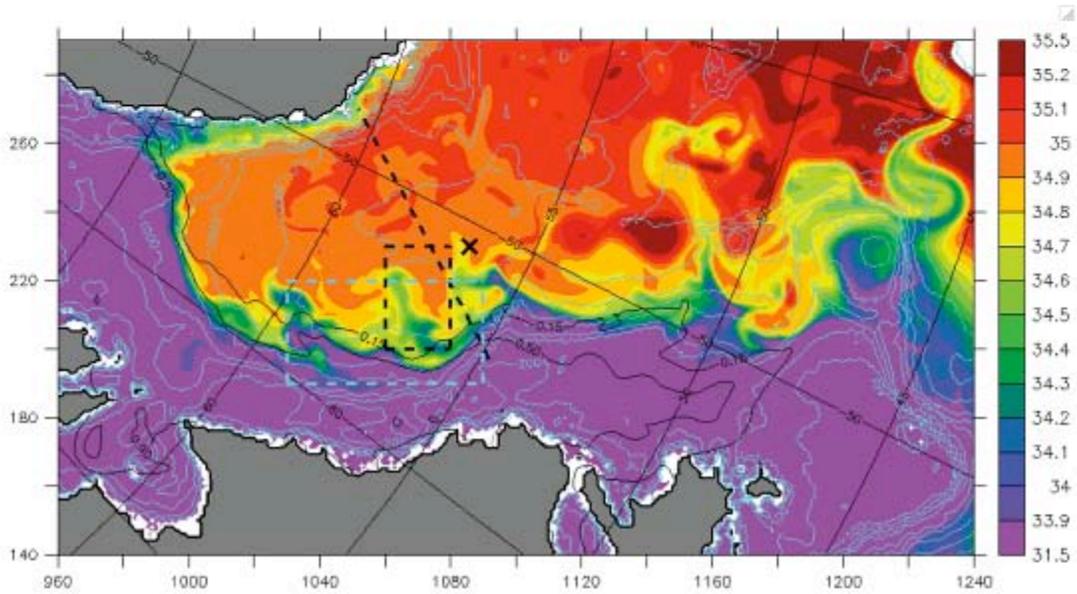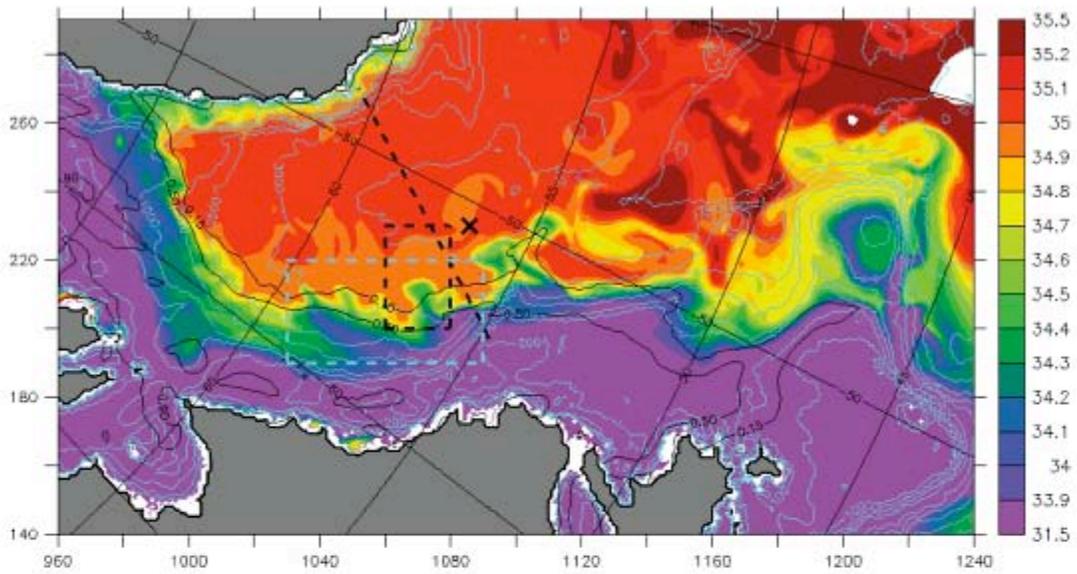
Figure 39.   SSS a) 31 Mar 1998 and b) 30 Apr 1998. Light blue dashed box delineates
the area of focus for this case, dashed black box is the convective area observed
by Pickart et al. (2002), dashed black diagonal line is AR7W transect, and black x
is OWSB.
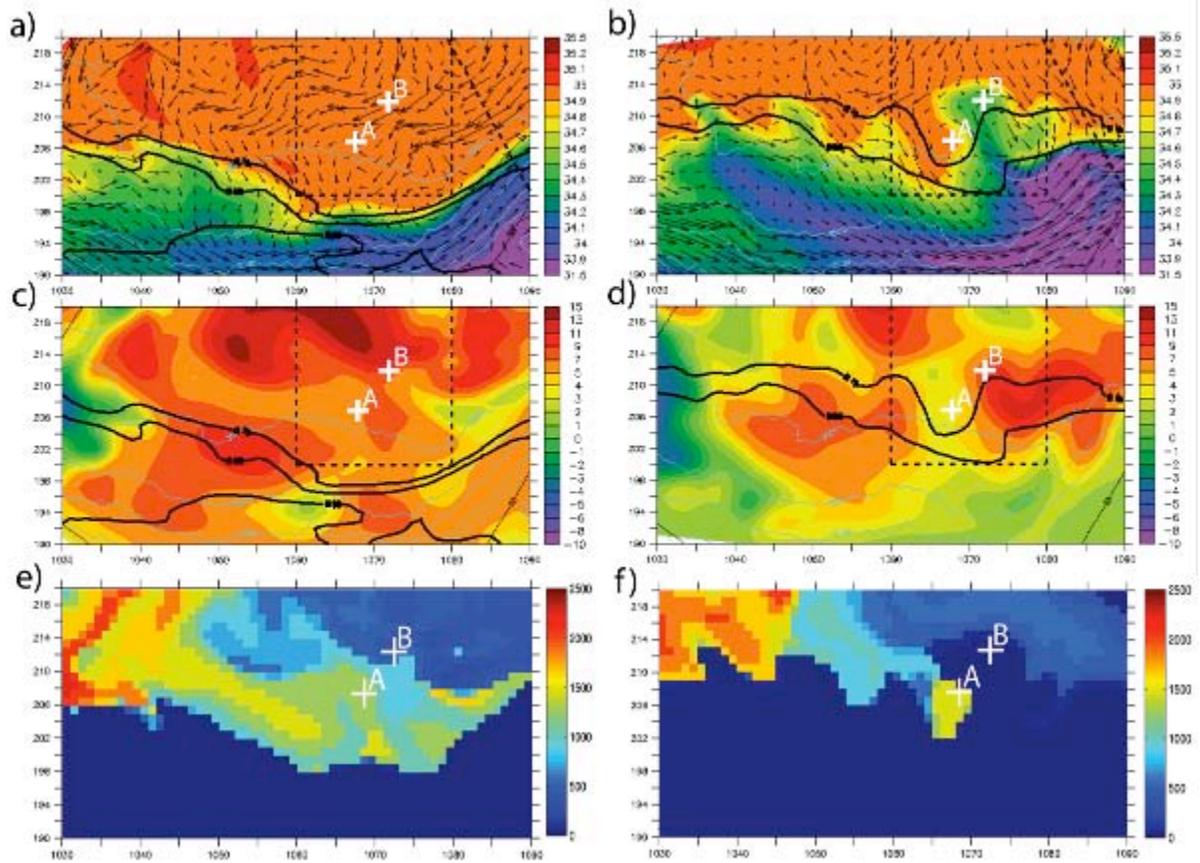
Figure 40.   28 Feb 1998 (left) and 31 Mar 1998 (right) modeled a) and b) SSS, c) and d) SSHA (cm), e), f) mixed layer depths (m). Dashed black box is the convective area observed by Pickart et al. (2002) and + symbols denote profile locations.
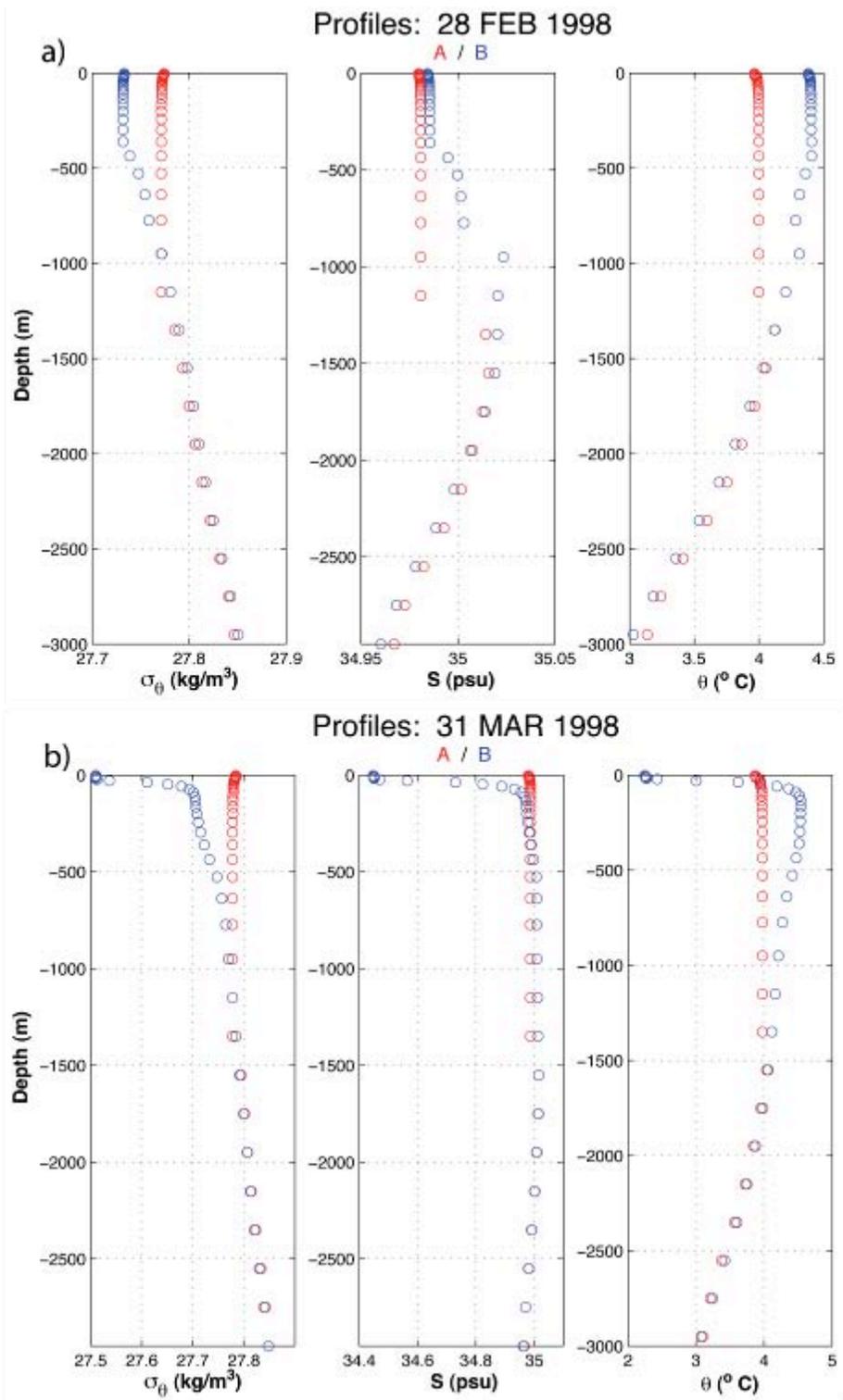
Figure 41.   Potential density, salinity and potential temperature profiles for a) 28 Feb
1998, and b) 31 Mar 1998 at the locations specified in previous figure.

The notion of counter-rotating eddies forcing a jet of freshwater off of the Labrador shelf has supporting evidence. The RADARSAT image in Figure 42 appears to show a similar mushroom shaped vortices occurring along the same part of the Labrador coast. The image, albeit from a different time (07 June 2009), features the broken and melting ice that acts as a tracer of the surface circulation. The dimensions of the larger vortex are consistent with the model results.
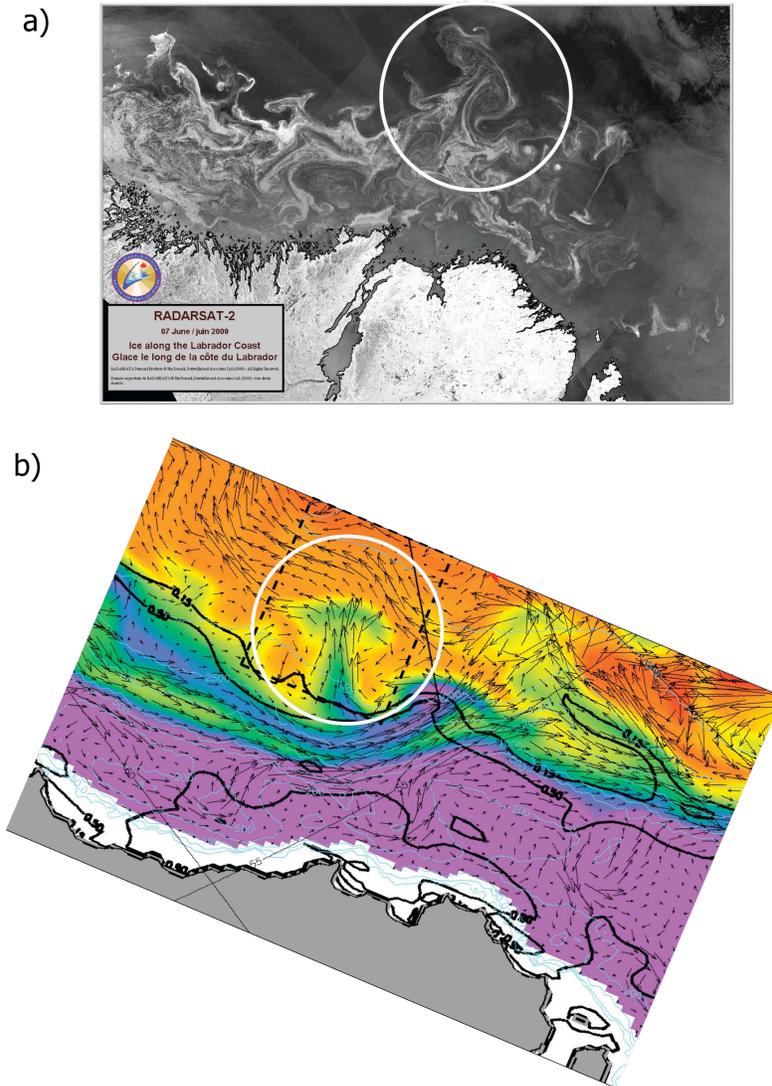
Figure 42.   a) RADARSAT-2 image 07 Jun 2009 and b) model SSS (shading) and surface velocity (vectors) 08 Apr 1998. Circled areas are discussed in the text.

Afterwards, the freshwater continues offshore (Figure 39b), following a meandering path back towards Greenland, similar to the anticyclonic recirculation documented by Lavender et al. (2000). Observations of upper water column salinity show two annual pulses of freshwater into the central Labrador Sea (in the vicinity of OWSB), the first of which occurs from April to May and is of unknown origin (Schmidt and Send 2007) but definitely not the West Greenland Current (Khatiwala et al. 2002). Animations of model output show freshwater coming off of the Labrador shelf and propagating half way to Greenland during the same months, suggesting that this may be the previously undetermined source of the observed freshening possibly acting in concert with sea ice melt.

2.   Upstream of Observed Convection Region

This 2002 event (Figure 43) is similar to the previous example, where 2 counter-rotating eddies force a jet of freshwater offshore. The location is slightly upstream of the traditional convection site, which is a region logistically more difficult to access. This time the origin of the anticyclonic eddy can be determined from animations of model output. The eddy is formed in July 2001 at Cape Desolation and crosses the northern Labrador Sea along the 3000 m contour. Shortly before it approaches the ice edge on the Labrador slope, a weaker cyclonic eddy is induced between this eddy and another anticyclonic one transiting behind it. The larger anticyclonic eddy sheds several smaller anticyclonic eddies which begin to interact with the MIZ and wrap ice and freshwater around them and move it offshore (Figure 44a,c). Then, the cyclonic eddy moves next to the anticyclonic one, both along the ice edge (Figure 44d). The counter-rotating eddies combine to force a jet of freshwater (~40 m deep and 40 km wide) approximately 150 km across the surface of the basin that eventually makes a "mushroom" shape as in Case 1a (Figure 44b).
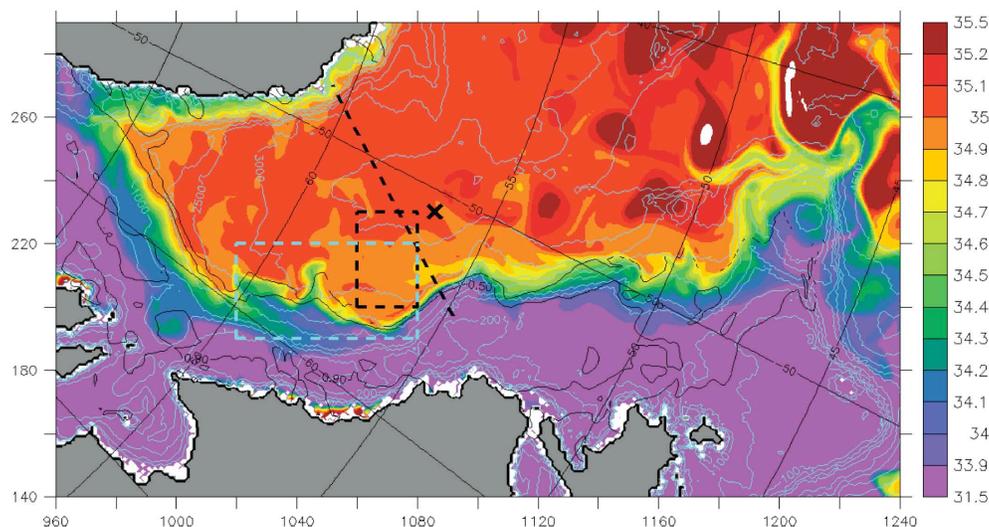
Figure 43.   SSS 31 Mar 2002. Light blue dashed box delineates area of focus for this case, dashed black box is the convective area observed by Pickart et al. (2002), dashed black diagonal line is AR7W transect, and black x is OWSB.

The ice edge position illustrates some of the dynamics involved. On 31 March (Figure 44b), there is no ice over the cyclonic eddy, which is expected because of the divergent flow that forces the ice outwards. The surface is ice free and exposed to the strong atmospheric cooling very close to the ice edge. Conversely, ice accumulates over the anticyclonic eddy due to its convergent flow.   Model profiles show that the characteristics of the two locations change drastically. On 28 February, profile A (Figure 45a) is along the edge of cold and fresh water that is being forced off of the shelf in a small episode which makes the upper water column buoyant and inhibits deep convection (Figure 44e). Profile B is primed for convection down to 800m. One month later on 31 March, profile A (Figure 45b) is under the influence of the cyclonic eddy with a deepening mixed layer to about 1500 m and the profile B is receiving the cold fresh cap which shuts down convection in that location (Figure 44f).
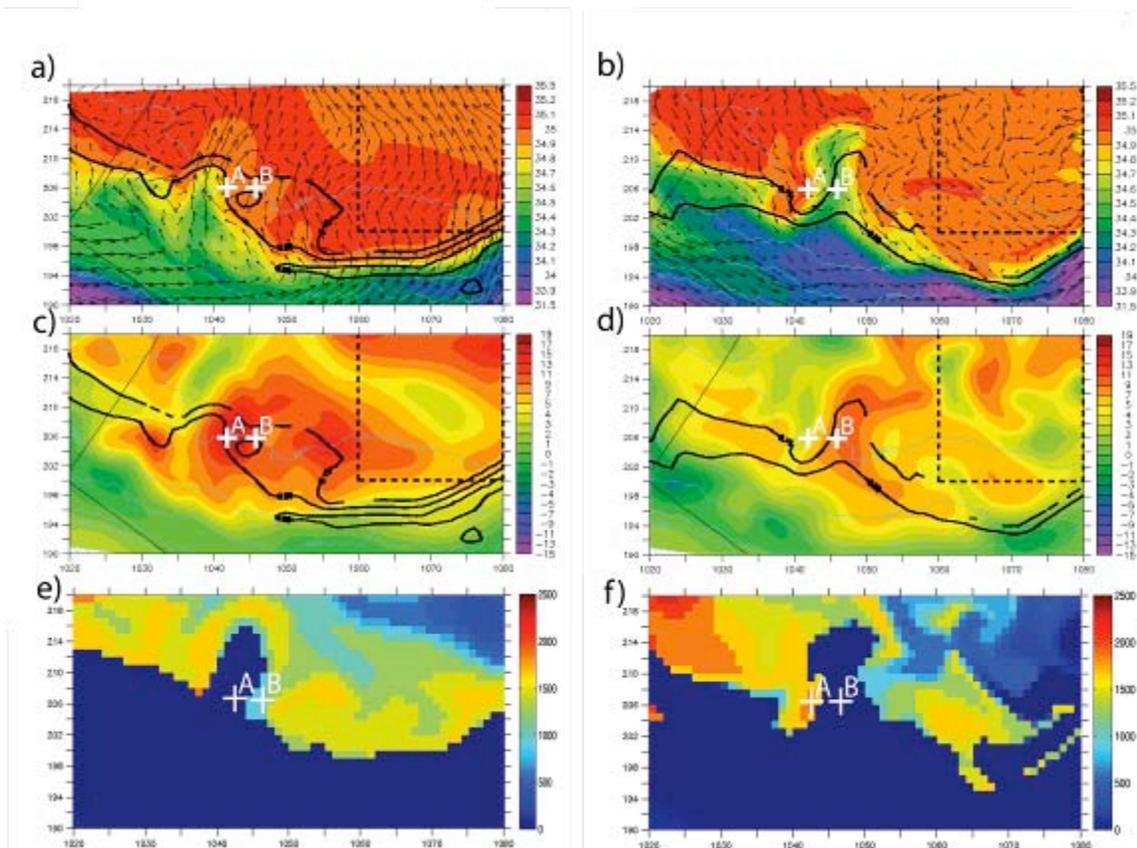
Figure 44.   28 Feb 2002 (left) and 31 Mar 2002 (right) modeled a), b) SSS, c), d) SSHA (cm), e),f) mixed layer depths (m). Dashed black box is the convective area observed by Pickart et al. (2002) and + symbols denote profile locations.
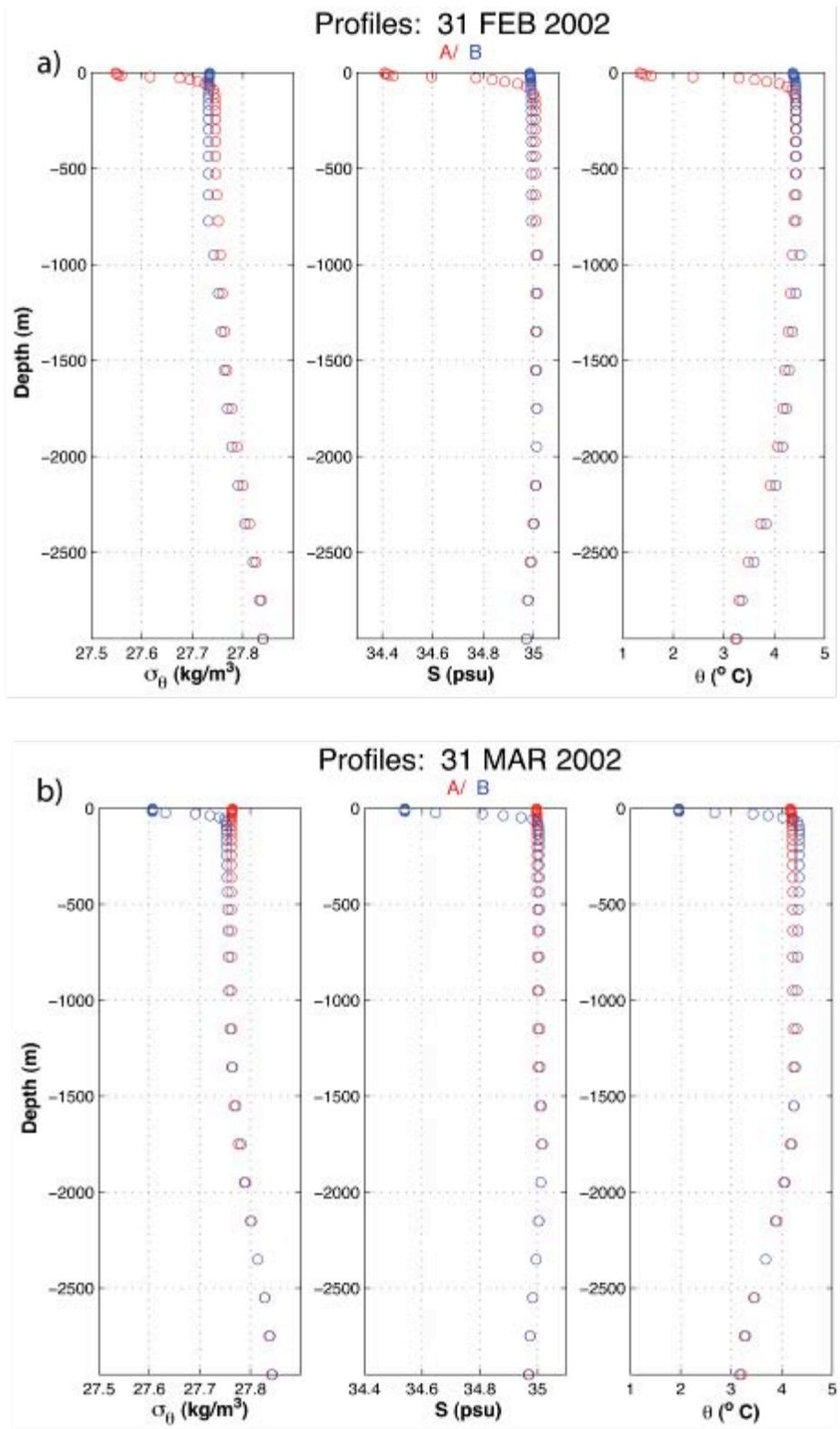
Figure 45. Potential density, salinity and potential temperature profiles for a) 28 Feb 2002, and b) 31 Mar 2002 at the locations specified in previous figure.

F.   CASE 2: SEA ICE MODULATION OF CONVECTION

This case (Figure 46a) shows the effects of sea ice cover and its edge position on locations of deep convection.   On 31 December, there is no evidence of convection (Figure 47a,b, Figure 48a,b) and the ice edge is towards shore. During the first half of January freshwater in the surface layers is mixed down by an eddy. This mixing and homogenization of the water column is clearly visible in the profiles (Fig 48a) and theta-S diagram (Fig 48b). The stage is set for deep convection, which occurs in concert with the advance of the ice edge by 31 January (Figure 47c,d). The strong forcing from the cold dry winds immediately adjacent to the ice edge is reflected in the thin band of deep convection (Figure 47d). By 28 February, the ice edge has continued to advance, now over the location of the profiles. Fresh water, insulated by the sea ice cover from atmospheric forcing advances offshore with sea ice (Figure 47e), restratifies the water column as it goes (Figure 48a,b) and subsequently halts convection (Figure 47f).
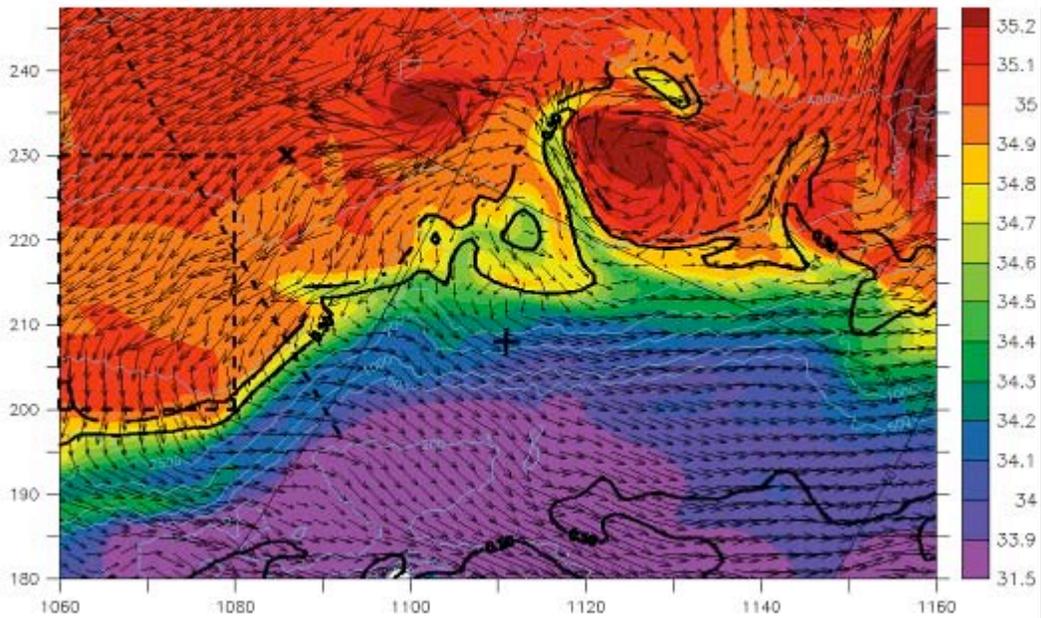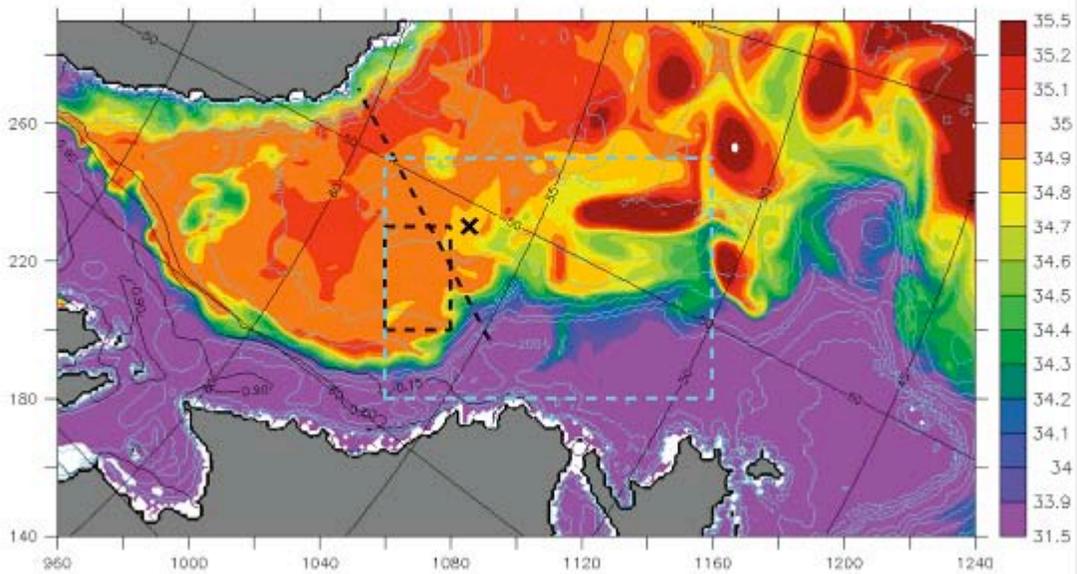
Figure 46.   a) SSS 31 Dec 2001. Light blue dashed box delineates the area of focus for
this case, shown in the lower panel. Dashed black box is the convective area
observed by Pickart et al. (2002), dashed black diagonal line is AR7W transect,
and black x is OWSB. b) SSS (shading) 16 Mar 2002, surface velocity (vectors),
and ice concentration (contours).
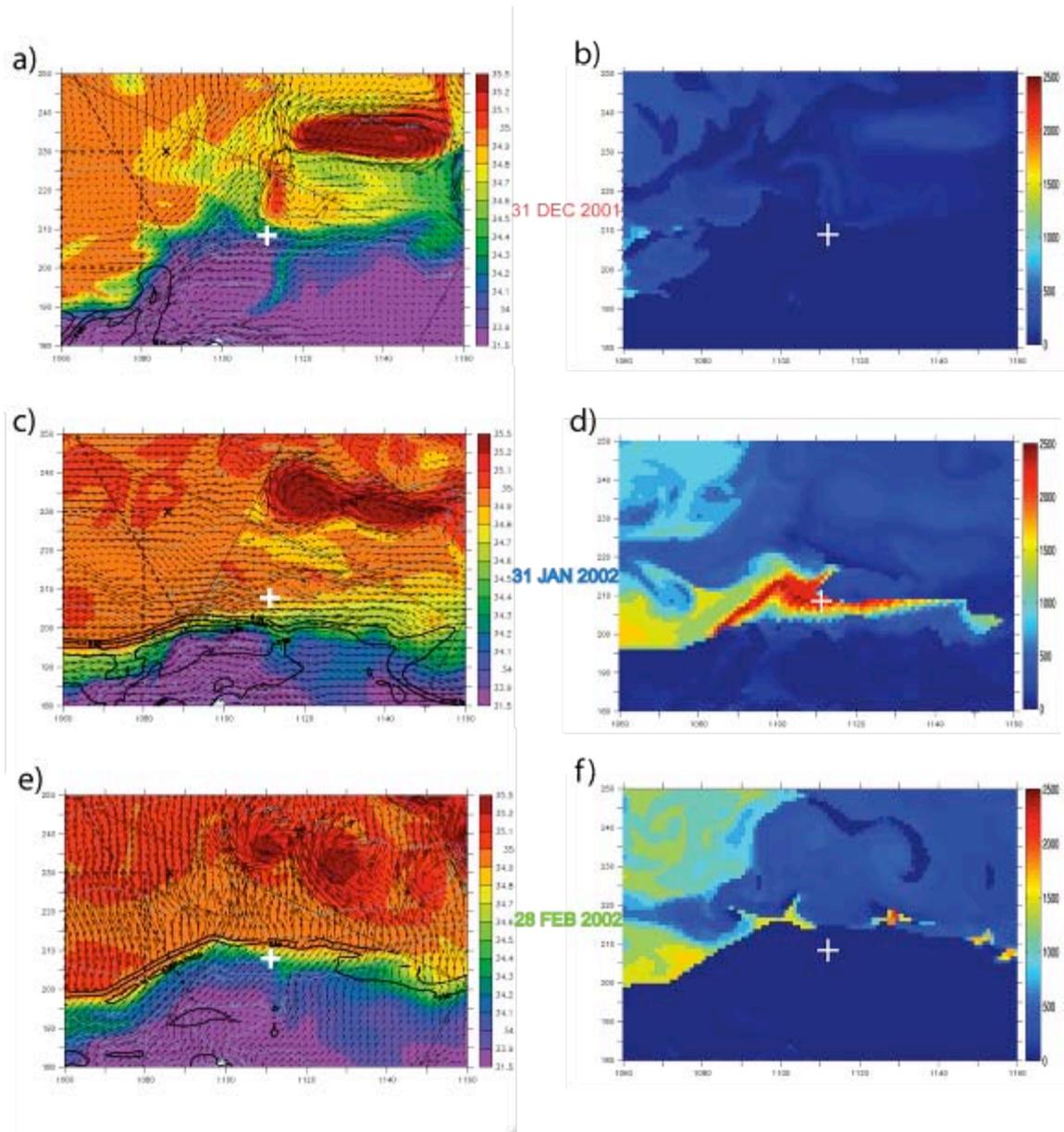
Figure 47.   SSS (shading) (with velocity (vectors) and ice concentration (contours)) (left) and mixed layer depth (m) (right) for a), b) 31 Dec 2001, c), d), 31 Jan 2002, and e), f) 28 Feb 2002. Dashed black box is the convective region observed by Pickart et al. (2002) and + symbol denotes profile location.
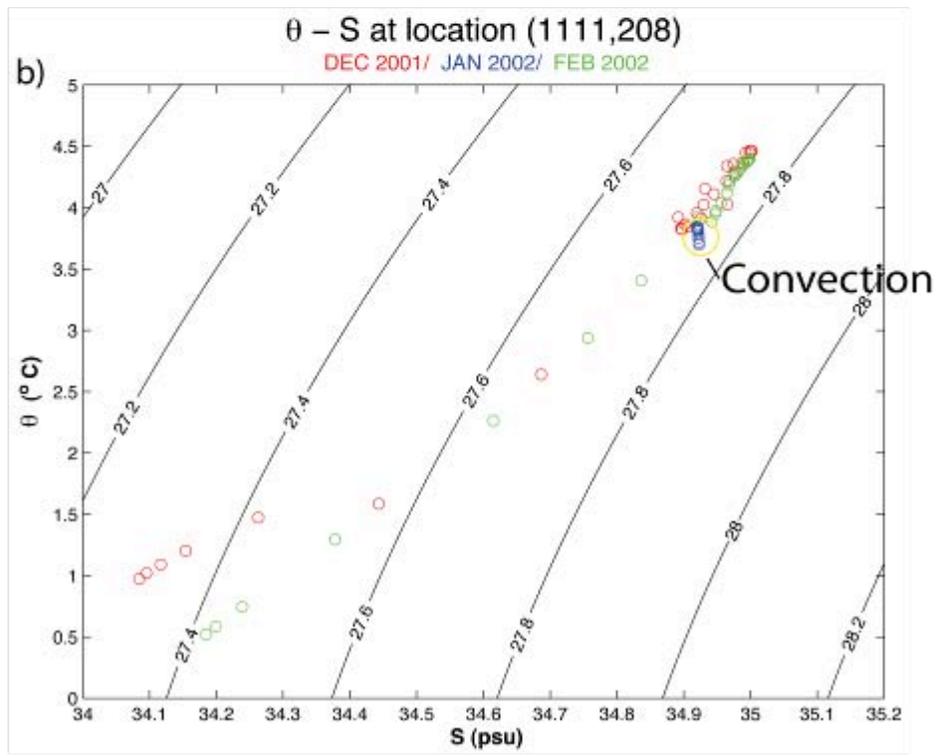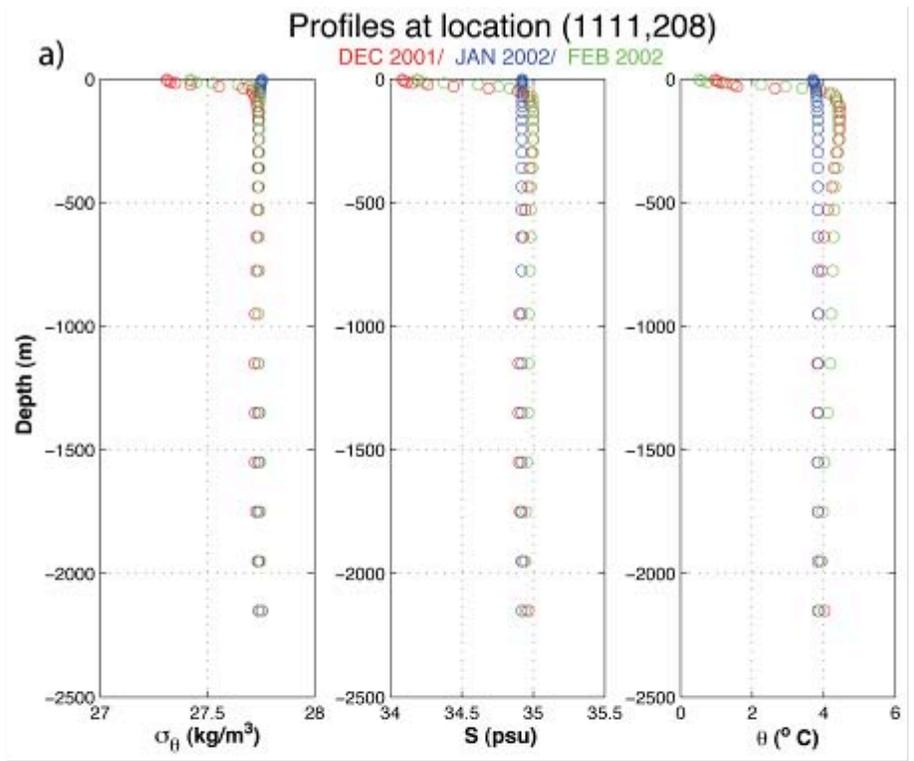
Figure 48.   a) Profiles and b) Theta-S diagram for location on 31 Dec 2001, 31 Jan 2002, and 28 Feb 2002.

Shortly afterwards, on 16 March, an anticyclonic eddy is seen to actively pull freshwater and ice away from the ice edge and redistribute it ~ 200 km away in the deep basin (Figure 46b). This eddy (and the one that removed the seasonal stratification before the onset of convection) originated from the NW Corner of the North Atlantic Current.

Mixed layer depths exceeding 1500m are simulated in this region (over the slope to the south of AR7W) in every year examined (1979-2003). However, they tend to occur earlier in the season (i.e. December or January) and then drastically decrease during the rest of the winter. As in this example, later in the winter (February and March) the ice cover and freshwater underneath moved over this convective area and halted convection. Deep convection has been observed in this region (Cuny et al. 2005; Vage et al. 2009). In fact, the recent paper by Vage et al. (2009) detailing the observed return of deep convection showed deepest mixed layer depths in this area, not in the region of strongest forcing (to the northwest).

This and the previous two cases emphasize the need for a coupled and high-resolution ice-ocean model to accurately represent the Labrador Sea dynamics. The convective event discussed here is highly dependent on the ice edge position and timing, and would not likely be reproduced with a prescribed climatological ice edge. A fully interactive sea ice model is needed. As well the model domain must allow for realistic representation of the NW Corner of the North Atlantic Current and it must be configured at high enough resolution to resolve the eddies it sheds into the Labrador Sea.

G.   FRESHWATER FLUXES

To quantify the shelf-basin exchange, annual freshwater fluxes from the Canadian Labrador shelf to interior are calculated (Table 2, Table 3). The fluxes are calculated separately for the Northern/Central Gates and Southern Gates (Figure 49). For the 25 year mean of the Northern/Central shelf, the ratio of solid to liquid freshwater flux is ~3:1, whereas for the Southern gates the ratio is nearly reversed. The Northern/Central net fluxes are surprising because they are negative for both the liquid and combined freshwater (more freshwater moving from interior to shelf than vice versa). The Southern

gates have positive liquid, solid and combined freshwater fluxes, with consistent shelf to interior transport. Therefore, the main freshwater exchange is to the south of AR7W, where the freshwater crosses from the southbound Labrador Current to the northbound recirculation and spreads into the central Labrador Sea. This region has strong current shear and high levels of TKE (Figure 30b) and EKE (Figure 31). Large eddies, such as those described in Case 2 can move freshwater and ice off of the shelf into the basin (Figure 46b). Mooring M9 from Lazier and Wright (1993) is located here as well. Their observations show it to have very weak mean flow (0-1cm/s) from the surface down to 2200m. However, the N/S and E/W components of the flow at 50m show high variability, with standard deviations of 10 and 9 cm/s respectively. This could be indicative of eddy activity near the mooring, where exchange can occur between the southbound and northbound currents. A modeling study by Myers (2005) showed what freshwater exchange there was between the Labrador shelf and interior was confined mostly to the south of Hamilton Bank, which is in the region of our Southern Gates and in agreement with our findings.
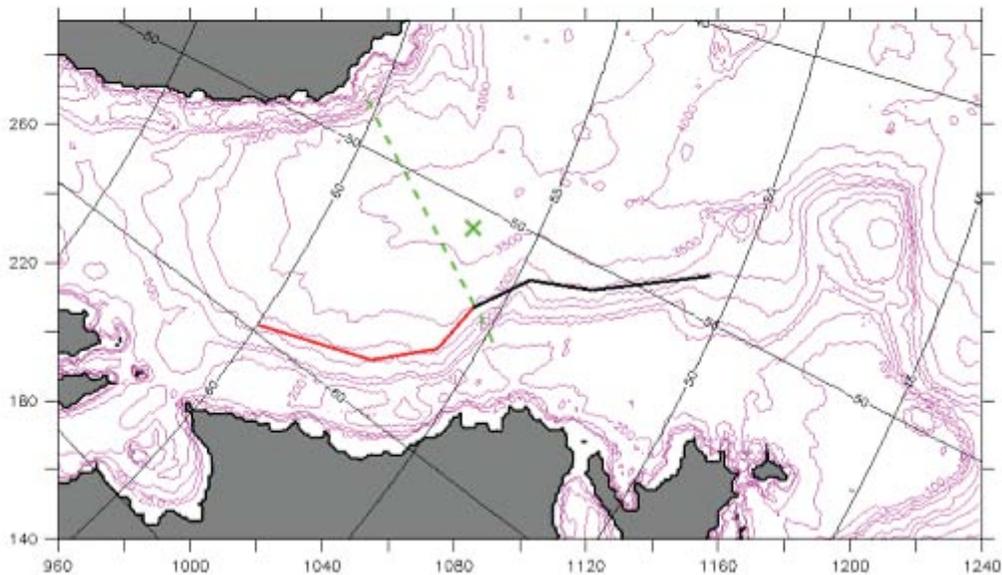
Figure 49.   Positions of Northern/Central (red) and Southern (black) gates. Dashed green diagonal line is AR7W transect and green x is OWSB.

	Northern/Central Gates (LCCS1, LCCS2, LCCS3)								
	Liquid Freshwater Flux, mSv			Solid Freshwater Flux, mSv			Combined Freshwater Flux, mSv		
Year	Net	To Interior	To Shelf	Net	To Interior	To Shelf	Net	To Interior	To Shelf
1979	-57.71	10.73	-68.44	17.00	23.16	-6.15	-40.71	33.88	-74.59
1980	-55.79	6.52	-62.31	6.61	14.39	-7.78	-49.17	20.91	-70.09
1981	-44.78	5.74	-50.52	15.12	20.28	-5.16	-29.66	26.01	-55.68
1982	-48.76	6.29	-55.05	14.79	24.98	-10.19	-33.97	31.27	-65.24
1983	-48.24	7.89	-56.14	4.28	12.63	-8.35	-43.97	20.52	-64.49
1984	-50.55	4.19	-54.74	13.28	25.69	-12.41	-37.27	29.88	-67.15
1985	-45.72	4.20	-49.93	-4.98	3.99	-8.97	-50.70	8.19	-58.89
1986	-38.36	10.81	-49.17	5.42	9.76	-4.34	-32.94	20.57	-53.51
1987	-46.86	8.84	-55.70	11.08	21.24	-10.16	-35.78	30.08	-65.86
1988	-32.94	3.46	-36.40	14.12	19.94	-5.83	-18.82	23.41	-42.22
1989	-71.17	0.09	-71.25	17.00	35.93	-18.94	-54.17	36.02	-90.19
1990	-67.40	1.91	-69.30	30.36	48.26	-17.90	-37.03	50.17	-87.20
1991	-42.00	1.00	-43.00	6.33	23.07	-16.74	-35.67	24.07	-59.73
1992	-43.13	4.12	-47.25	8.74	23.02	-14.28	-34.39	27.15	-61.54
1993	-27.72	10.45	-38.17	14.46	28.61	-14.15	-13.26	39.06	-52.32
1994	-52.37	9.19	-61.56	4.83	26.33	-21.50	-47.54	35.52	-83.06
1995	-46.07	6.77	-52.84	-4.90	12.78	-17.68	-50.97	19.56	-70.52
1996	-65.37	5.20	-70.57	21.53	26.28	-4.74	-43.84	31.48	-75.32
1997	-41.60	6.68	-48.27	11.69	25.67	-13.98	-29.90	32.35	-62.25
1998	-34.24	13.47	-47.71	5.51	15.67	-10.16	-28.74	29.13	-57.87
1999	-18.24	8.58	-26.82	7.57	10.10	-2.54	-10.67	18.68	-29.35
2000	-15.05	11.68	-26.73	23.31	27.22	-3.91	8.26	38.90	-30.63
2001	-21.86	4.46	-26.32	5.47	6.57	-1.10	-16.39	11.04	-27.42
2002	-35.73	3.35	-39.08	5.41	12.32	-6.90	-30.31	15.67	-45.98
2003	-33.42	5.04	-38.47	8.88	13.28	-4.40	-24.54	18.33	-42.87
25yr Mean	-43.40	6.43	-49.83	10.52	20.45	-9.93	-32.89	26.87	-59.76

Table 2.   Cross-Shelf Freshwater Fluxes (liquid, solid, combined) for Northern/Central Gates. Positive values indicate flow off of the shelf towards the interior.

	Southern Gates (LC2RC1, LC2RC2, LC2RC3)								
	Liquid Freshwater Flux, mSv			Solid Freshwater Flux, mSv			Combined Freshwater Flux, mSv		
Year	Net	To Interior	To Shelf	Net	To Interior	To Shelf	Net	To Interior	To Shelf
1979	-2.98	19.48	-22.46	2.16	2.24	-0.08	-0.82	21.72	-22.54
1980	18.03	28.69	-10.66	4.15	4.15	0.00	22.17	32.83	-10.66
1981	21.82	28.27	-6.45	8.76	8.78	-0.02	30.58	37.05	-6.47
1982	10.81	28.48	-17.67	4.79	4.80	-0.01	15.60	33.27	-17.68
1983	10.14	22.18	-12.04	0.34	0.42	-0.08	10.47	22.59	-12.12
1984	6.08	17.45	-11.37	3.11	3.22	-0.12	9.18	20.67	-11.48
1985	1.21	18.95	-17.74	1.27	1.27	0.00	2.47	20.22	-17.75
1986	6.00	26.07	-20.07	5.94	5.95	-0.01	11.93	32.01	-20.08
1987	25.97	32.20	-6.23	7.29	7.34	-0.05	33.26	39.54	-6.28
1988	24.23	29.39	-5.16	4.51	4.57	-0.06	28.73	33.96	-5.23
1989	-2.51	12.76	-15.26	6.82	7.00	-0.17	4.32	19.75	-15.44
1990	5.93	20.85	-14.92	14.66	14.79	-0.13	20.60	35.65	-15.05
1991	1.81	10.88	-9.08	9.44	9.63	-0.18	11.25	20.51	-9.26
1992	2.29	19.69	-17.40	16.15	16.29	-0.13	18.44	35.97	-17.53
1993	11.96	25.74	-13.78	14.14	14.25	-0.11	26.09	39.99	-13.89
1994	1.14	17.60	-16.46	13.21	13.22	0.00	14.35	30.81	-16.46
1995	9.80	17.98	-8.19	0.74	0.87	-0.13	10.53	18.85	-8.32
1996	12.91	23.59	-10.68	18.30	18.30	0.00	31.21	41.89	-10.68
1997	11.90	21.82	-9.92	8.33	8.37	-0.04	20.23	30.18	-9.96
1998	35.63	41.51	-5.88	1.06	1.06	0.00	36.68	42.57	-5.88
1999	5.46	13.31	-7.85	0.10	0.10	0.00	5.57	13.41	-7.85
2000	18.48	27.39	-8.91	7.79	7.79	-0.01	26.27	35.18	-8.91
2001	23.49	29.22	-5.73	0.07	0.08	0.00	23.56	29.30	-5.73
2002	3.75	10.89	-7.13	0.74	0.83	-0.10	4.49	11.72	-7.23
2003	20.30	26.98	-6.68	1.07	1.14	-0.07	21.37	28.13	-6.75
25yr Mean	11.35	22.85	-11.51	6.20	6.26	-0.06	17.54	29.11	-11.57

Table 3.   Cross-Shelf Freshwater Fluxes (liquid, solid, combined) for Southern Gates. Positive values indicate flow off of the shelf towards the interior.

These fluxes need to be regarded with caution though. They are mean annual net values so short duration events are filtered out in relation to the lower frequency yearly signals. Also, negative flux does not necessarily imply that the freshwater moving from the interior to Canadian shelf came from an alternate pathway (West Greenland Current via Fram Strait). Much of the water came through Davis Strait. The meandering of the Labrador Current and advection of meltwater from sea-ice just seaward of the gates can cause an apparent onshore flow of freshwater from the interior. Furthermore, the location and orientation of the gates can influence the results.

Straneo (2006) noted that the restratification period results in an excess of freshwater in the surface layer that cannot be balanced by current estimates of P-E or vertical transport. The proposed methods to remove this excess freshwater from the

central Labrador Sea were increased evaporation or lateral surface fluxes. The negative freshwater fluxes (interior to shelf) as determined by this model for the Northern Gates point to the latter possibility. It is important to remember that although the flux of freshwater appears to be dominated by onshore flow from the interior, small localized events (Cases 1 and 2) of freshwater moving offshore at the right time and location can and do affect deep convection.

H.   CORRELATIONS OF OUTSIDE FACTORS WITH CONVECTION

The relationships between the time series of deep convection and the time series of several other variables were examined. These variables included the North Atlantic Oscillation (NAO) index, Labrador Sea ice area, and volume and freshwater fluxes through Davis Strait. All time series were converted to 13-month running means and then correlated. It should be kept in mind that convection is a wintertime event, and that the mixed layer depth time series has significant amplitudes during those times. As such, the anomalies (annual cycle removed) of convective indices (the fraction of cells with mixed layer depths exceeding 1000m and 1500m) were used. It was found that NAO correlated with the anomaly of the 1000m index with R=0.63, where the convection lagged the NAO by 4 months. Correlating the NAO with the 1500m index (anomaly) yielded R=0.56, again with convection lagging the NAO by 4 months. It is not surprising that the NAO would lead convection because the increased cold northwesterly winds that are present during positive phases of the NAO would act for some time before homogenizing the upper water column before the occurrence of deep convection. The Labrador Sea ice area anomaly correlated with the 1000m index (anomaly) at R=0.62 (0 lag) and with the 1500m index (anomaly) at R=0.61 (0 lag). There has been speculation that positive anomalies in ice area can support convection because the wind from Canada does not absorb heat from an open ocean below, causing more intense forcing farther across the shelf into convective areas (Vage et al. 2009). Conversely, this could simply be the result of colder temperatures and winds, which happen to both extend the ice edge and support convection. The surprising finding was that the net combined freshwater flux anomaly through Davis Strait correlated positively with the 1000m and 1500m

112

convective indices (anomalies) with values of R=0.53 and R=0.55 respectively (both at zero lag). That is, more freshwater exited Baffin Bay when there was increased convection. This enhanced freshwater flux could be partly responsible for the enhanced ice area anomaly. This freshwater flux was largely a function of volume flux. The Davis Strait volume flux anomaly time series had very similar correlations with the 1000m and 1500m convective indices, with R=0.58 at zero lag for each. This could be due to an enhanced Northerly wind which would help push volume out of Baffin Bay (possibly by the mechanism discussed at the end of Chapter IV), but also stimulate convection. Regardless of the cause, freshwater still has a distance to travel after it crosses Davis Strait before it can possibly affect the convection regions. Hence it appears that freshwater flux anomalies that start in the Arctic, transit the CAA, and proceed through Baffin Bay do not have a large scale impact on Labrador Sea convection.

I.   CORRELATIONS OF WATER PROPERTIES WITH CONVECTION

In light of limited sampling resources and the sparse nature of deep convection (both in space and time), it would be advantageous to identify for future field studies which small areas within the Labrador Sea best represent the entire region in terms of deep convection. To this end, the time series of 0-2000m mean potential temperature, salinity, and potential density for every grid cell in the study area was correlated with the time series of convection (fraction of cells with mixed layer depth exceeding 2000m) for the entire region.

The potential temperature correlated best with the convection (Figure 50c), with high correlations along the southern Canadian Labrador slope and also southwest of Cape Farewell, Greenland. Potential density followed a similar pattern (Figure 50a), with the region southwest of Cape Farewell slightly more correlated than the Canadian side. A surprise was the highest correlation near Cape Desolation where R^2 ~0.7. The salinity correlation (Figure 50b) was lowest but had its maximum in the southeast of the study area and numerous slightly weaker maxima offshore of the southern Canadian Labrador slope. The reason for this maximum is unclear, but other maxima interestingly appear in the region where the freshwater is exchanged from the boundary to the interior of the

Labrador Sea. This suggests that freshwater signal in this area can alone explain up to 50% of the variance in deep convection over the entire Labrador Sea. The temperature signal in this area can explain almost 70% of the variance. From these three correlation plots, it appears that one of the most advantageous locations to measure potential density, potential temperature, and salinity signals representative of the entire Labrador Sea convection is along the southern Canadian Labrador slope, approximately 100 km southwest of OWSB.
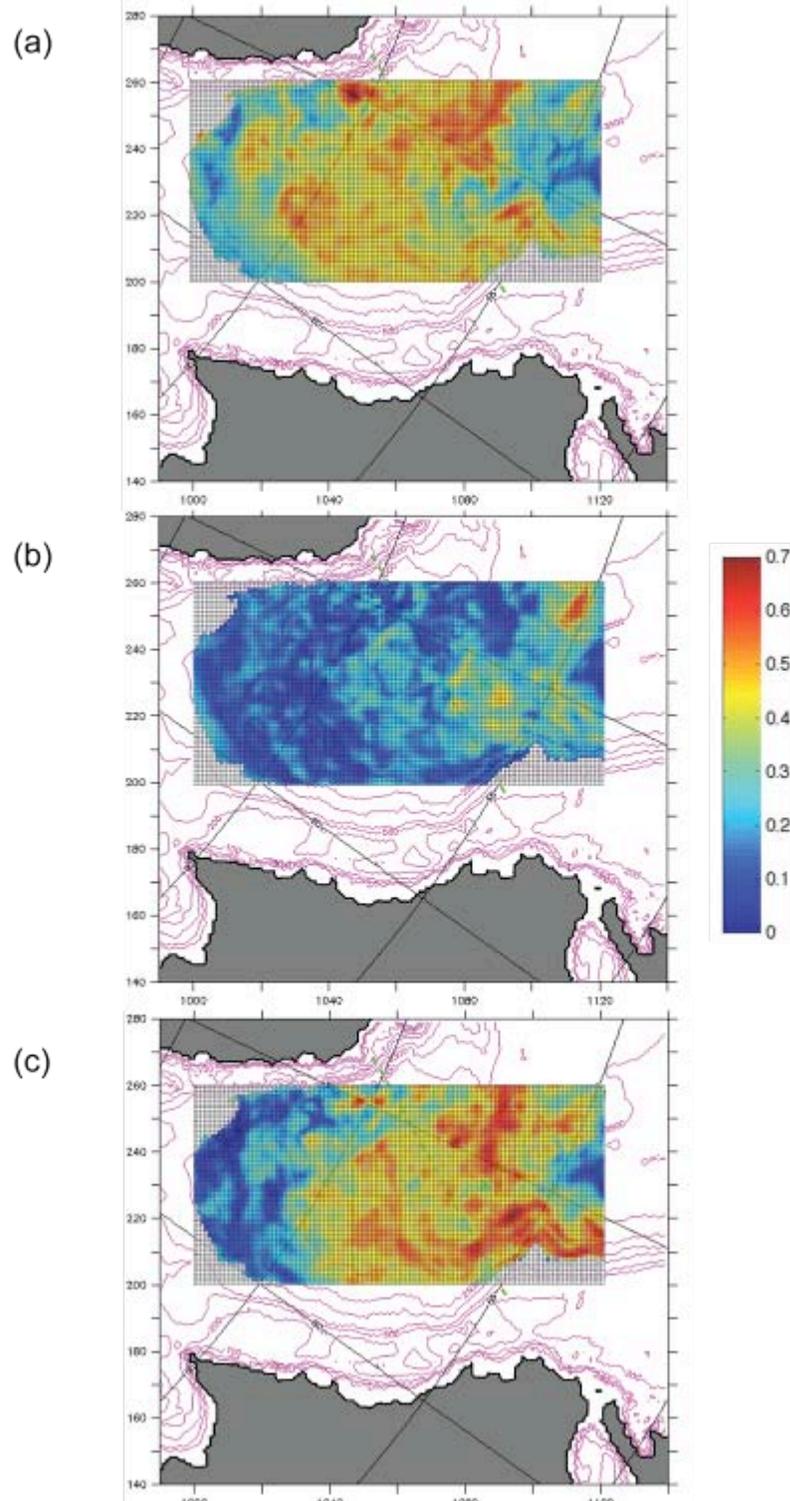
Figure 50. R^2 correlation for time series at each point with convection for entire Labrador Sea. a) potential density, b) salinity, and c) potential temperature.

J.   CONCLUSIONS

This high-resolution regional model (which includes both a realistic CAA freshwater outflow and the Fram Strait freshwater pathway) shows skill in simulating properties and processes of the Labrador Sea. The EKE distributions, eddy formation regions and pathways, time series of mixed layer depth and water mass properties, and individual deep convection episodes show agreement with observations. Inconsistencies with observations, most notably the anomalous deep convection occurring to the north, lack of the freshwater cap observed off of western Greenland, and a general high salinity bias of O (0.1-0.15 psu) may be indicative of a missing freshwater source on the Greenland side of the Labrador Sea which is not accounted for in the model (such as Greenland's glacial meltwater).

Eddies play an important role in mixing down the cold freshwater from the surface layers and in homogenizing the upper water column immediately before the start of the convective season. Eddies also transport buoyant low salinity water off of the Labrador shelf into convective regions of the deep basin in the late winter, thereby "capping" the water column and halting deep convection. The subsequent transport and spreading of this freshwater may be a principle agent of basin wide annual restratification as well as the previously unknown origin of the pulse of low salinity water observed annually from April to May in the central Labrador Sea. Convection is also modulated by the position of the ice edge, highlighting the critical need for a coupled eddy-resolving ice-ocean model.

The major shelf to interior freshwater flux on annual time scales occurs from Hamilton Bank southwards. Enhanced freshwater fluxes exiting Davis Strait do not immediately disrupt convection. Correlation analysis showed that the area most representative of basin wide convection is offshore of southern Canadian Labrador slope. Finally, the size of eddies and the short duration of events in Cases 1 and 2 demonstrate the need for high resolution, both spatial and temporal.

VI. CHANGES IN CANADIAN ARCTIC ARCHIPELAGO ICE CONDITIONS

> The navigation of the Polar seas, which is peculiar, requires in a practical manner, an extensive knowledge of the nature, properties and usual motions of the ice, and it can only be performed to the best advantage by those who have long experience with working a ship in icy conditions.
>
> -William Scoresby, 1820

The thickest and oldest ice in the Arctic has been observed in the northern Canadian Arctic Archipelago (Bourke and McLaren 1992). There, thick multiyear ice of Arctic origin encounters land, converges and deforms. This region is predicted to be the last bastion of multiyear ice (Lindsay and Zhang 2006). Its southern portion, the Northwest Passage has already been observed to lose much of its summertime ice cover. This part of our study examines the changes during 1979-2004 in sea ice conditions for three regions: CAA (covering the entire Canadian Arctic Archipelago), NWP (covering the Northwest Passage), and CAS (covering the Canadian Arctic Slope) as delineated in Figure 51. Parameters determined are sea ice area and volume (26-year long term mean and standard deviation, 26-year September mean and standard deviation, 26-year April mean and standard deviation). Furthermore, recent sea ice area and volume losses were calculated (comparing the mean of the last 5 years to the overall mean). Tabulated results for each region are presented in Table 4.

A. REGIONAL CHANGES IN ICE AREA AND VOLUME

All three areas showed almost no change (less than 1%) in ice area in April. This is due to the formation of first year sea ice each year that entirely covers the fixed extent of each region (Figure 52). There is an upward boundary to how much ice can fit in each area and that is achieved with ice formation each winter. However, there is a significant difference in the September sea ice area in all three regions. The decreases in end of summer ice area for the CAA, NWP, and CAS are 14.27%, 25.08%, and 14.22% respectively. It is expected that the Northwest Passage will have the most change and

melt as it traditionally has the thinnest ice and is located furthest south. The changes in ice volume (Figure 53) are more telling as they include thickness. The September decreases in ice volume for the CAA, NWP, and CAS are 29.01%, 39.21%, and 33.94%. This indicates that the Northwest Passage has lost the most (%) both area and thickness (which is no surprise) but that the CAS lost more of its volume than the CAA did (which included the large losses in the Northwest Passage). The April volume loss might provide the key to understanding this. The April decreases in ice volume for the CAA, NWP, and CAS are10.35%, 8.02%, and 13.66%. This shows that the CAS cannot replenish itself as well as the CAA or NWP.
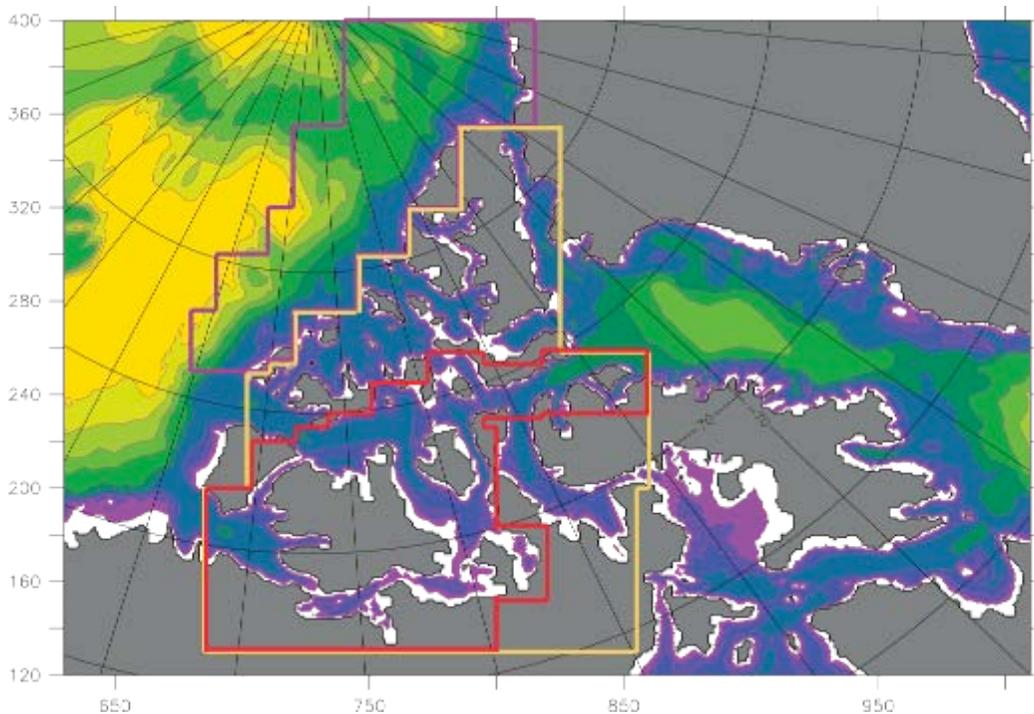
Figure 51.   Boxes enclosing CAA region (tan), b) NWP region (red), and c) C A Slope region (purple).

All three regions have shown large decreases in ice area and volume at the end of the summer for the period 2000-2004 as compared to the period 1979-2004. The Northwest Passage showed the largest changes. The end of winter ice area is nearly constant in all regions (Figure 52). The end of winter ice volume decreases for all

regions, especially for the Canadian Arctic Slope (Figure 53). This implies that the last bastion of multiyear sea ice is losing the ability to replenish itself first.

	CAA	NWP	CAS
Area-26yr mean (km^2)	9.4078e+05	4.6185e+05	1.0093e+06
Area-26yr std (km^2)	2.0048e+05	1.4167e+05	8.0510e+04
Area-SEP mean (km^2)	5.2317e+05	1.7018e+05	8.6918e+05
Area-SEP std (km^2)	7.8769e+04	4.7237e+04	9.6046e+04
Area-APR mean (km^2)	1.0823e+06	5.6355e+05	1.0623e+06
Area-APR std (km^2)	3.6152e+03	2.3612e+03	3.3555e+03
Volume-26yr mean (km^3)	2.2940e+03	819.5323	3.4757e+03
Volume -26yr std (km^3)	736.9697	431.8434	655.0537
Volume -SEP mean (km^3)	1.1807e+03	171.3985	2.8334e+03
Volume -SEP std (km^3)	240.5922	71.6048	608.4947
Volume -APR mean (km^3)	3.1732e+03	1.3536e+03	4.0467e+03
Volume -APR std (km^3)	210.2065	81.1722	408.8652
Area loss*-SEP (%)	14.27	25.08	14.22
Area loss*-APR (%)	0.26	0.21	0.30
Volume loss*-SEP (%)	29.01	39.21	33.94
Volume loss*-APR (%)	10.35	8.02	13.66

Table 4.   Sea ice area and volume statistics for the CAA as a whole (CAA), Northwest Passage (NWP), and Canadian Arctic Slope (CAS) (* The loss is calculated for the mean of the last 5 years against the overall mean).
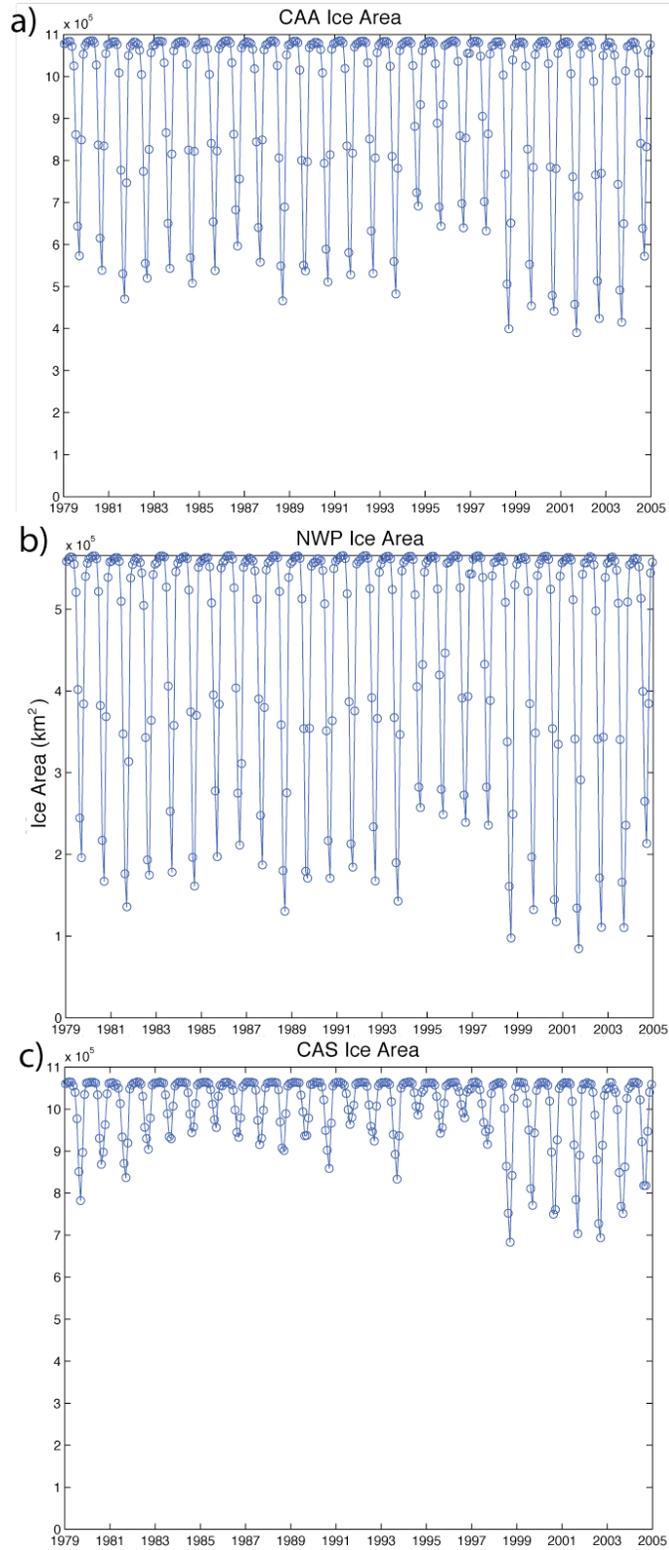
Figure 52.   Time series of ice area (km^2) a) Canadian Arctic Archipelago (CAA), b) Northwest Passage (NWP) and c) Canadian Arctic Slope (CAS).
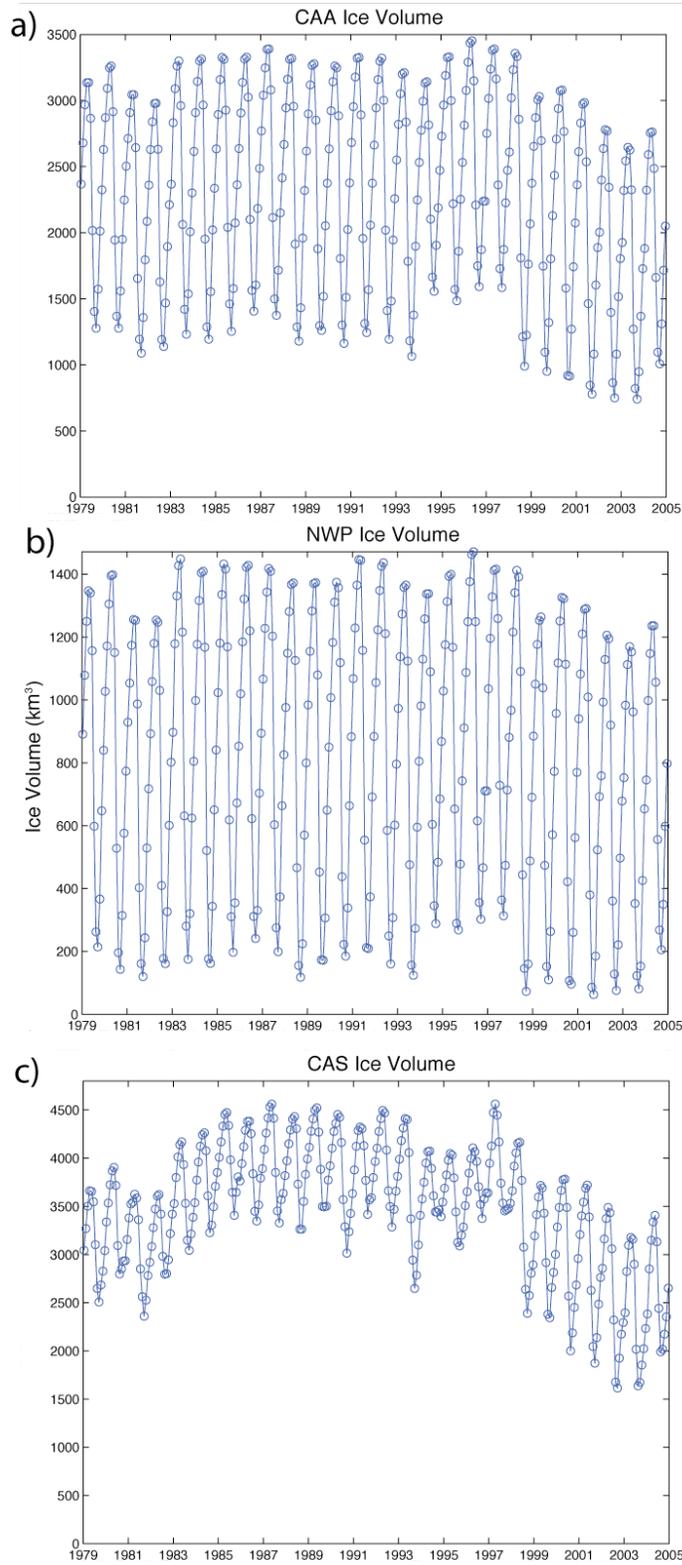
Figure 53. Time series of ice volume (km^3) a) Canadian Arctic Archipelago (CAA), b) Northwest Passage (NWP) and c) Canadian Arctic Slope (CAS).

B.   NORTHWEST PASSAGE TRAFFICABILITY

For this study, an area was considered trafficable if it had less than 60% ice concentration and less than 1 m average thickness for a period of 2 months (after Sou and Flato 2009). This definition was used as benchmark where commercial shipping may be feasible yet still require extra measures and/or support. The 2-month requirement is used to provide a reasonable window for a shipping season.   Using these constraints, trafficability was determined for the Northwest Passage from 1979-2004 (Figure 54). It was found that the Northwest Passage was trafficable via the shallow water route through Peel Sound (see Figure 7 in Chapter III) 3 times: 1980, 1993, and 2001 (Figure 54b). It was only trafficable via the deep-water route through Prince of Wales Strait in 2001 (Figure 54c). McClure Strait itself was never a viable exit region due to the influx of thick ice. These findings are consistent with a study by Howell and Yackel (2004) who assessed shipping conditions through different Northwest Passage routes using Canadian Ice Service charts from 1969-2002. Their study showed that McClure Strait was the most difficult route (due to old ice blocking the way) and Peel Sound was the least difficult.

However, it is important to note that the definition used above is different than the ones used frequently. The World Meteorological Organization (WMO) defines "open" as less than 1/10 sea ice concentration with no ice of land origin (landfast ice or icebergs). The term "freely navigable" is equivalent. The sea ice charts produced by the analysts at the National Ice Center (Suitland, MD) and the Canadian Ice Service (Ottawa, ON) follow the WMO convention for ice concentration and stage of development.   The National Ice Center defines "ice-free" only where its analysts determine there is no ice of any origin present. Hence, while one may hear in the news of the Northwest Passage being "open" that is not the same as the analysis performed above. Applying the WMO definition, our model results do not show any period where the Northwest Passage is "open" nor is it ever "ice-free" (Figure 55). This is consistent with observations from 1979-2004.
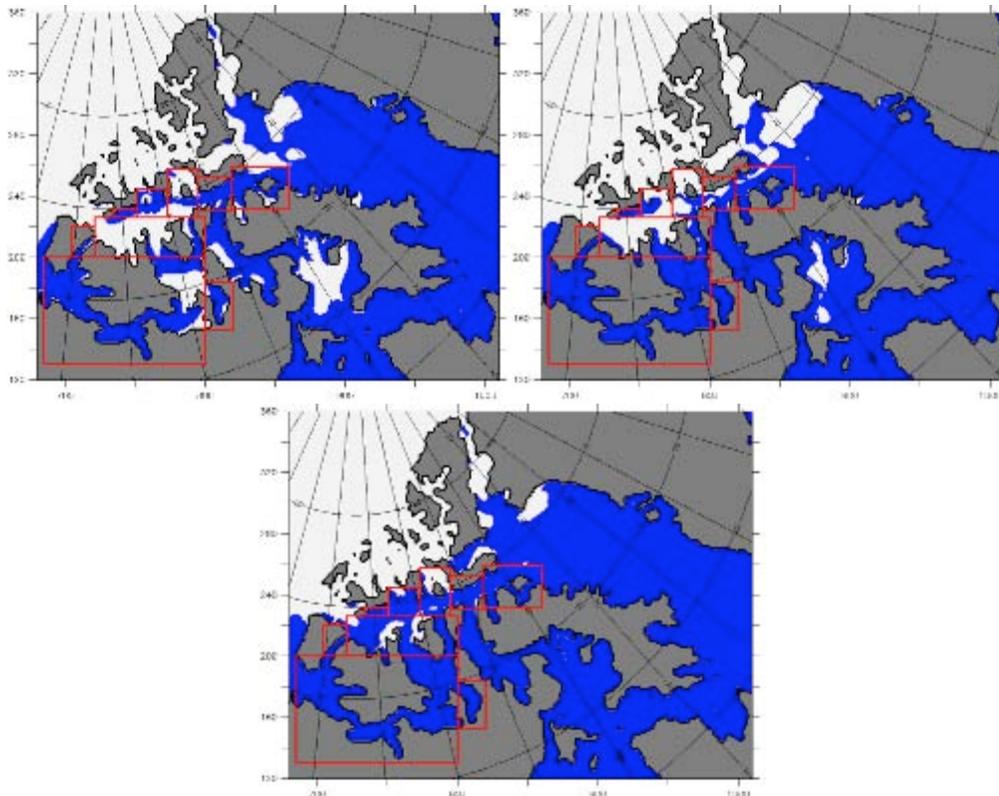
Figure 54.   White areas are untrafficable due to sea ice while the blue areas are passable.
a) August 1987: example of an untrafficable Northwest Passage. b) August
1980: example of a trafficable Northwest Passage via the southern "shallow water
route." c) August 2001: example of trafficable Northwest Passage by both
"shallow water route" and "deep water route."
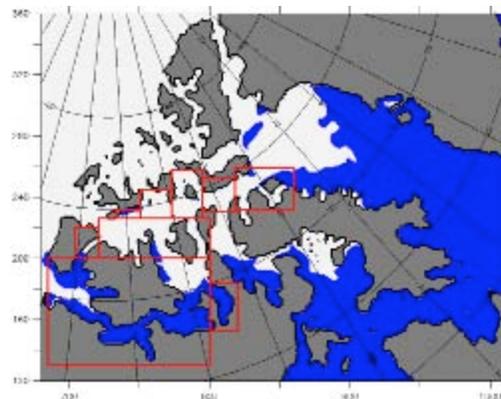
Figure 55.   Open water conditions. Blue areas are "open" (< 1/10 ice concentration) and
white are not. This is from August 2001, when both routes through the Northwest
Passage were trafficable. However, neither route fit the definition of "open."

C.   PREDICTABILITY

Knowing that shipping was possible after the season had already passed is not useful. As such, it would be useful if there was some way of determining if a passage would be open based on some sort of climate index, such as the Arctic Oscillation (AO) or North Atlantic Oscillation (NAO). These indices were analyzed for years with summers of trafficable conditions. The AO was negative in 1980 and 1993 but positive in 2001, showing no apparent preference for even the sign of the index. The NAO was strongly negative in the summers of 1980, 1993, and weakly negative in 2001 (but it stayed negative for that entire year) (Figure 56). If a strong negative summer NAO alone controlled the trafficability, it would be expected that the Northwest Passage would have been passable in the summer of 1998 when the NAO was strongly negative as well. The model did simulate that it was trafficable that summer but only for one month, not long enough for a full shipping season. However, these relationships are tenuous because trafficability is a discrete yes/no variable, while the NAO has continuous degrees of variation. A simpler approach of examining the surface air temperatures revealed that the summers (July/August/September) of the trafficable years (1980, 1993, and 2001) were anomalously warm. Figure 57 is a composite made for the summers of those three years; it reveals a positive temperature anomaly centered south of Baffin Island. Temperatures along the Northwest Passage were up to 1.2 $^{\circ}$C above normal that could have led to slightly more mild ice conditions. However, examination of the preceding winters (January/February/March of 1980, 1993, and 2001) revealed much larger warm temperature anomalies in the central/western CAA. Figure 58 is a composite made for the winters of those three years; it reveals a positive temperature anomaly of up to 4 $^{\circ}$C running the length of the Northwest Passage. This could have hindered ice growth, effectively preconditioning the Northwest Passage to have more benign conditions the following summer.
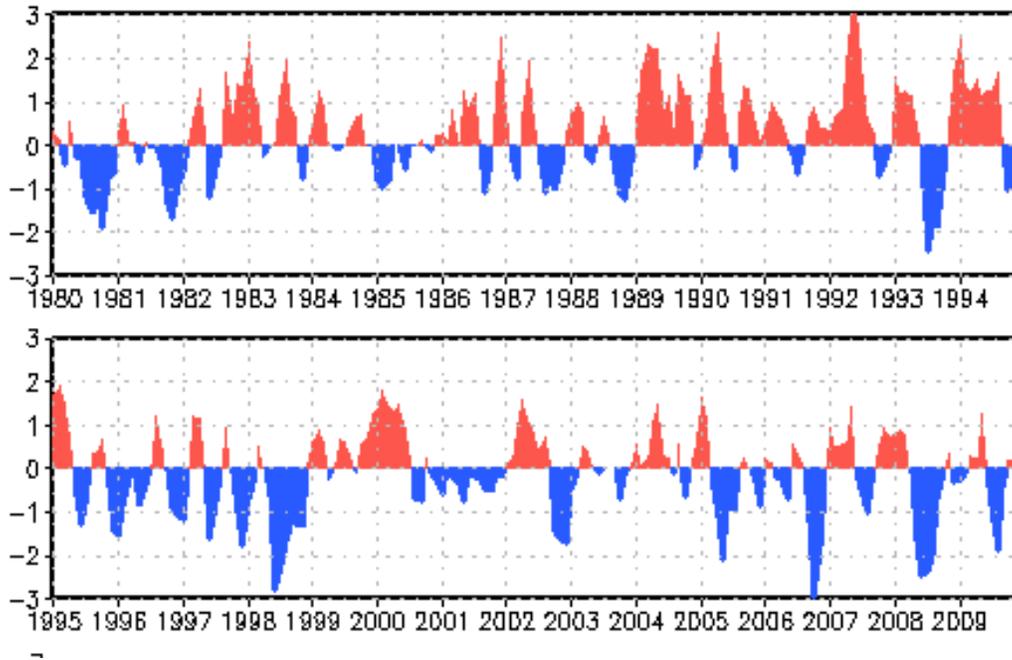
Figure 56.   Standardized 3-month running mean NAO Index (From NOAA 2010).

Jul to Sep: 1980,1993,2001
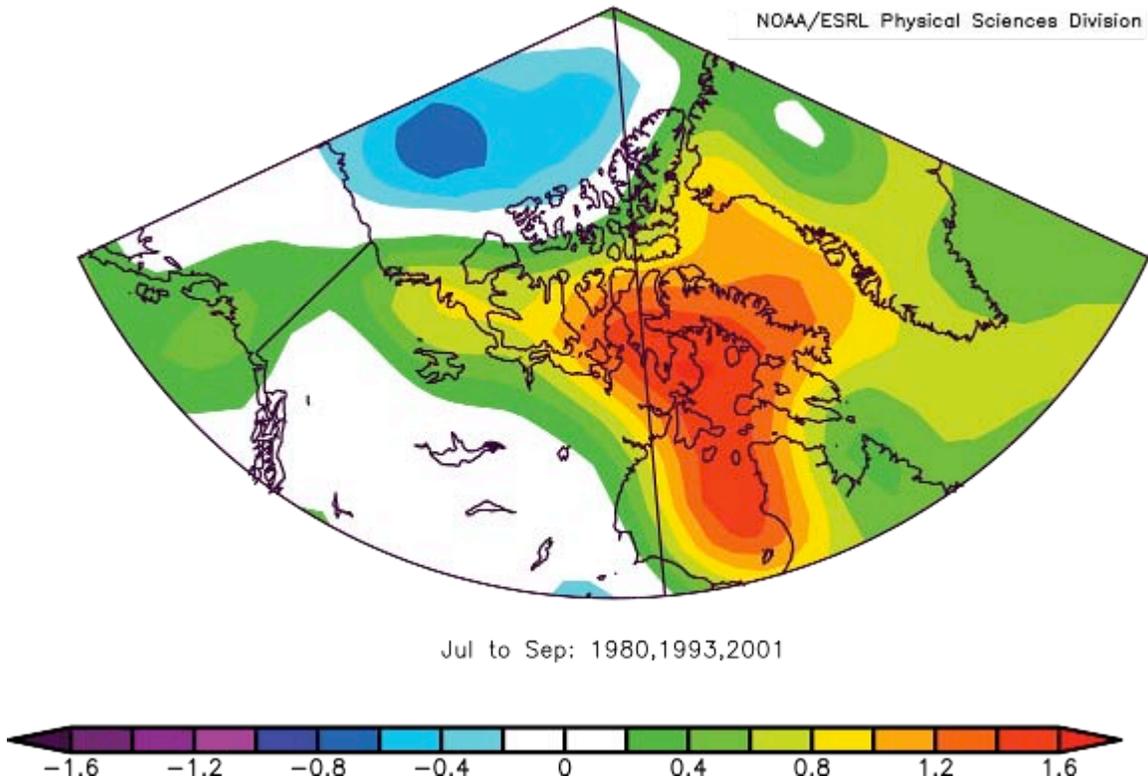
Figure 57.   NCEP/NCAR Reanalysis 1000mb air temperature composite anomaly for
summers (JAS) during trafficable conditions in the Northwest Passage.
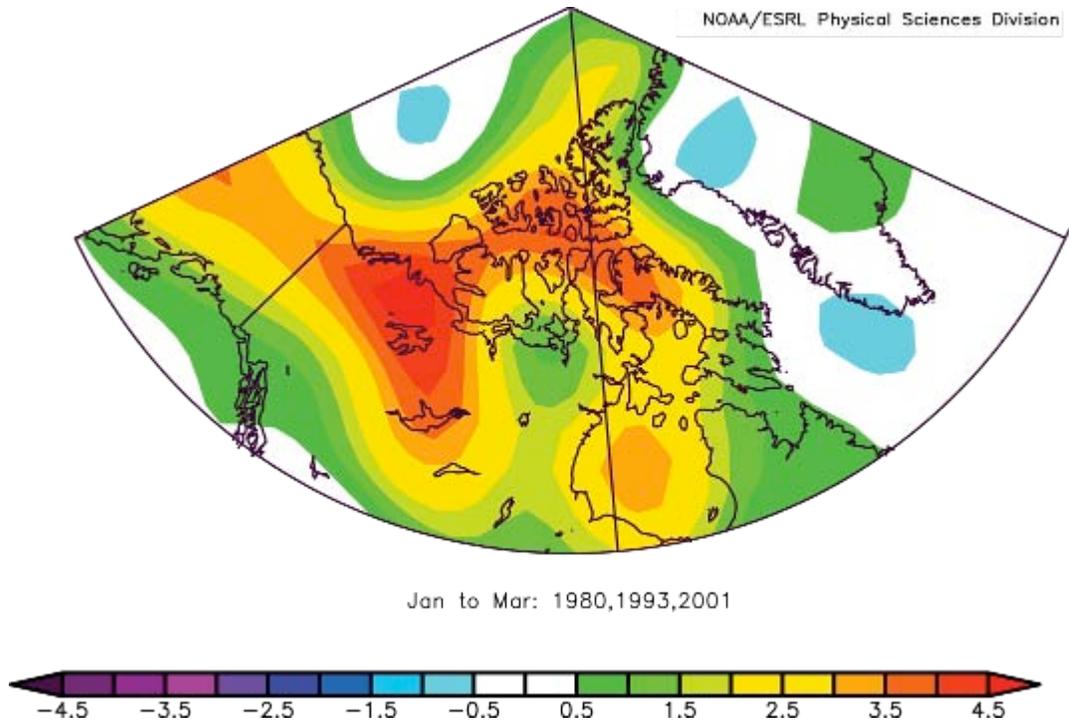
Figure 58. NCEP/NCAR Reanalysis 1000mb air temperature composite anomaly for winters (JFM) preceding trafficable conditions in the Northwest Passage (note the scale difference from the preceding figure).

D. ICE ARCHES IN THE CANADIAN ARCTIC ARCHIPELAGO

In the Queen Elizabeth Islands, thick multiyear sea ice often converges above narrow straits, resulting in the formation of ice arches that act as plugs, preventing the thick ice from flowing southwards into the Northwest Passage (Melling 2002). In a warming climate with longer melt seasons, ice strength will decrease due to ice thinning, which may lead to collapse of the ice arches and influx of thick multiyear ice into the Northwest Passage (Melling 2002). There has already been observed multiyear ice moving into the Northwest Passage where it can survive a melt season (Howell et al. 2008). This older and thicker ice could present a major danger to shipping. Furthermore, if the rest of the water is ice free it can be highly mobile, possibly collecting at other choke points and to further hinder shipping (Wilson et al. 2004).

The modeled ice does show ice arches north of Byam Martin Channel and Penny Strait during the summer that separate thicker immobile ice to the north from the thinner

mobile ice to the south in the Northwest Passage (Figure 59a, Figure 60a, Figure 61a). Over the course of the study period, all of the ice thins and the separation between thick ice to the north and the thin ice to the south becomes less clear. Likewise, the differential in ice strength between the arch and the thin ice to the south becomes less defined (Figure 61). By the end of the period, areas of nearly open water are adjacent to the remaining thick ice that has extended further south (particularly near Byam Martin Channel) (Figure 59b). A stream of mobile ice extends to the north out of the top of the CAA (Figure 60b). Our study period stops in 2004 so recent events of thick ice entering the Northwest Passage cannot be analyzed. However, the model conditions do tend towards a situation where the stage has been set for thick ice to start leaking into the Northwest Passage.

Information about ice conditions and the formation of ice arches in Nares Strait was presented in Chapter III.
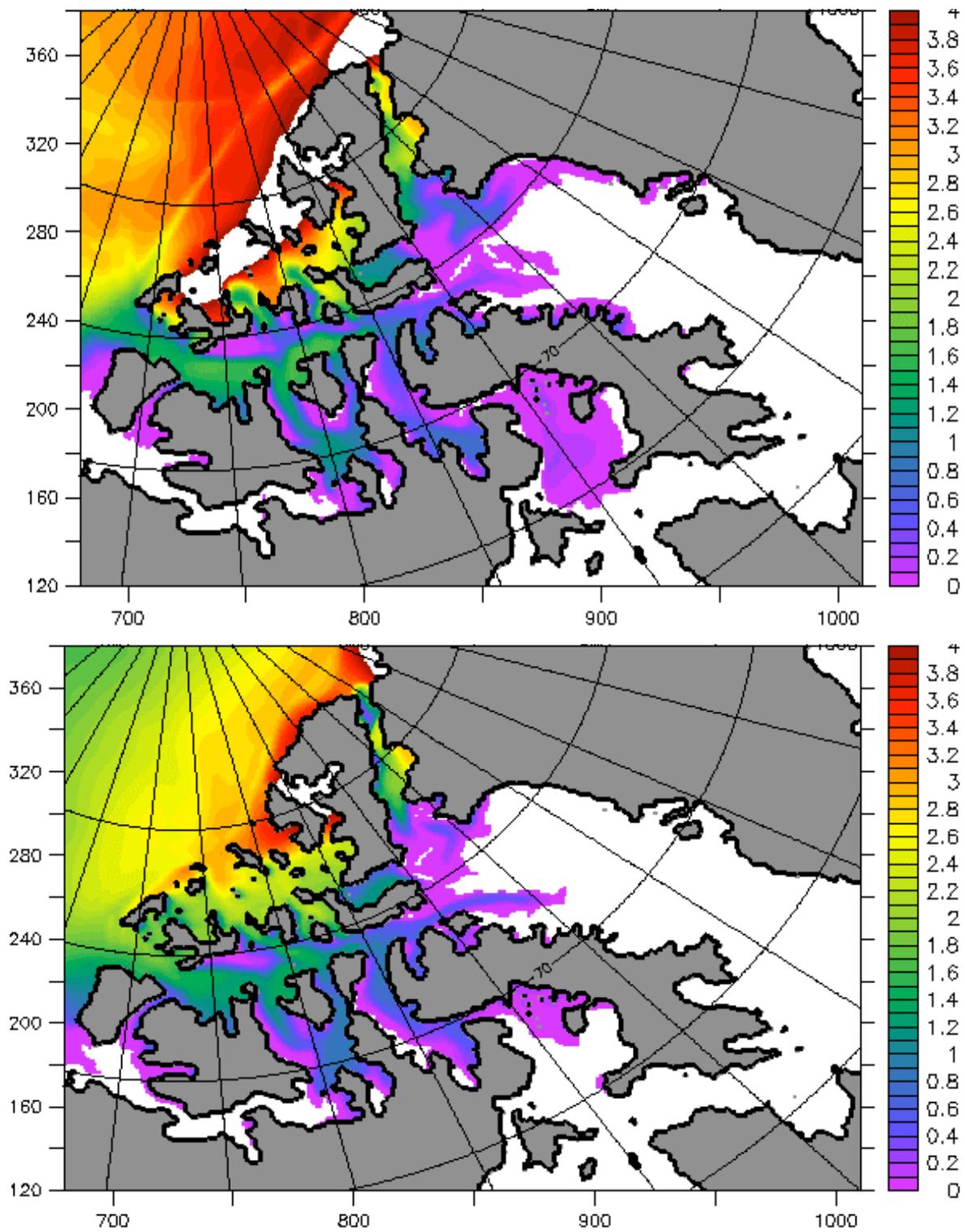
Figure 59.   September ice thickness (m) distribution. a) 1979, and b) 2004.
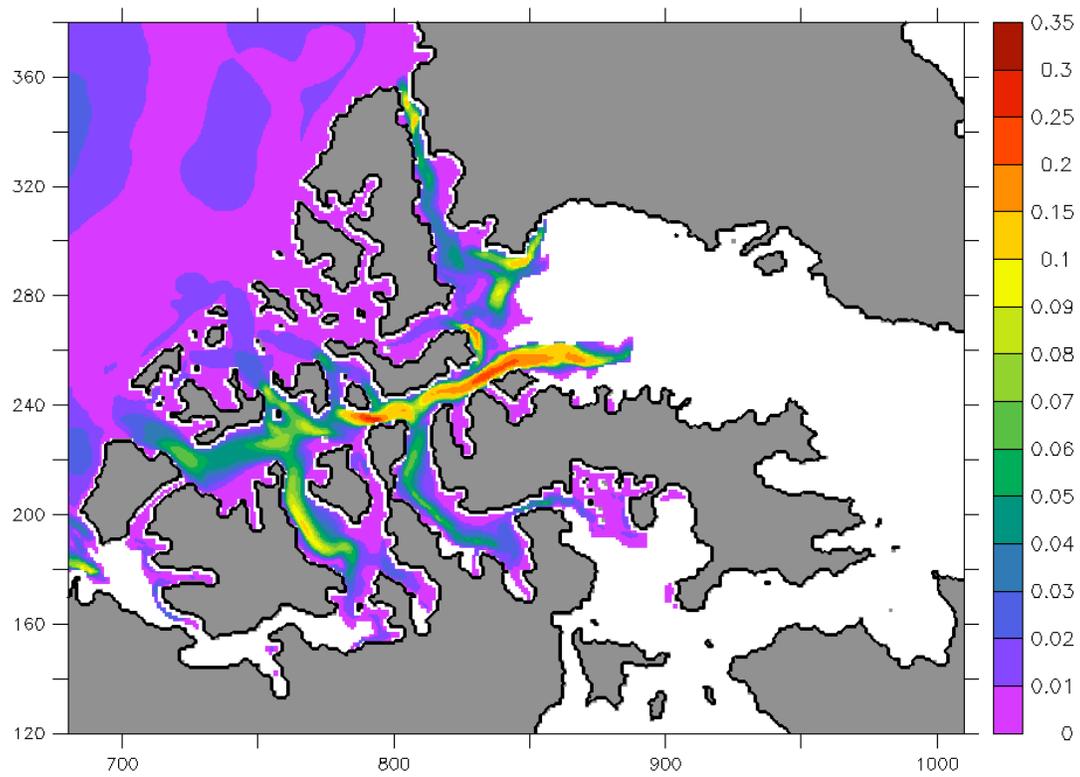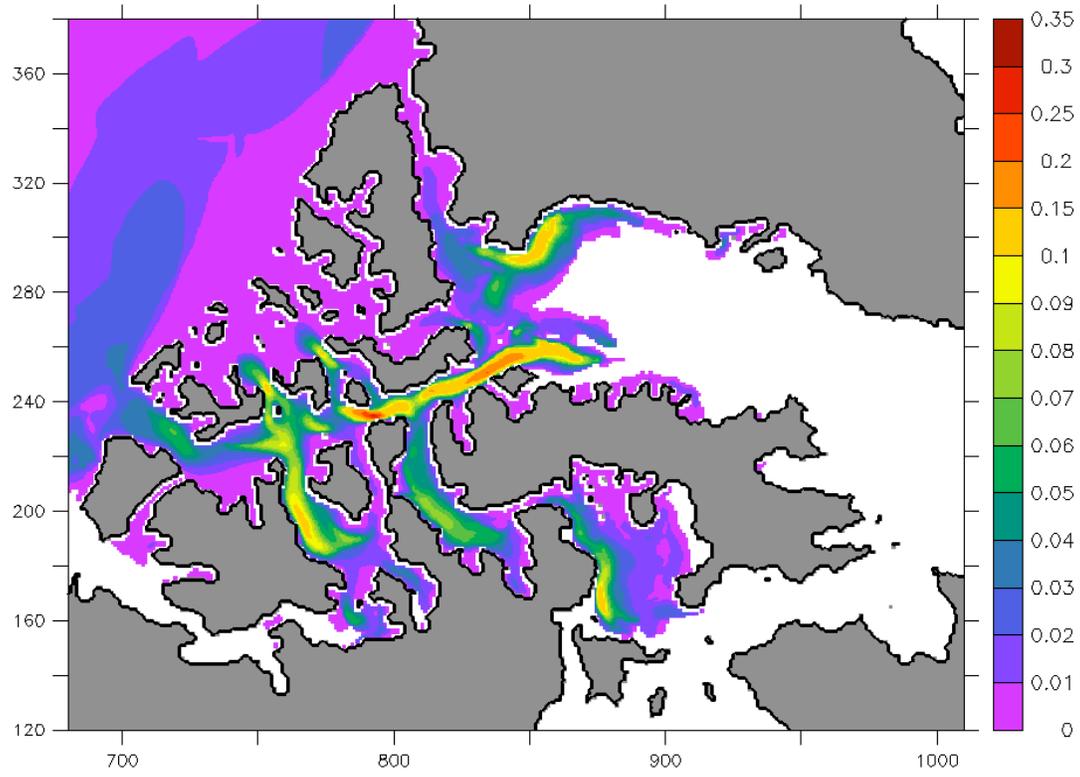
Figure 60.   September ice speed (m/s). a) 1979, and b) 2004.
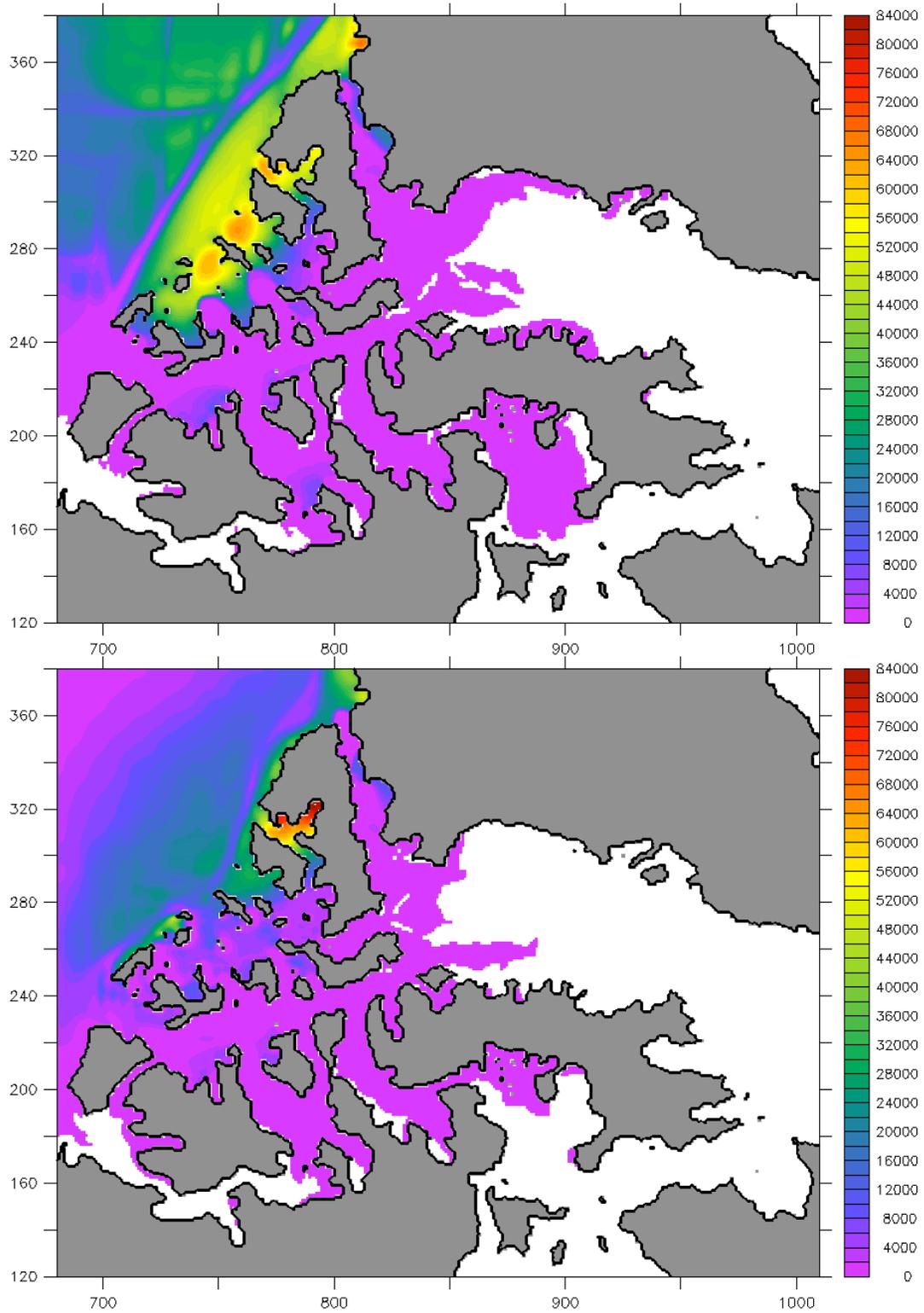
Figure 61.   September ice strength (N/m^2). a) 1979, and b) 2004.

E.   CONCLUSIONS

The simulated CAA and surrounding regions had lost significant amounts of ice by the end of the period 1979-2004. Furthermore, the thick multiyear ice towards the north shows the least ability to replenish itself during winter. The model does produce years with ice conditions meeting certain criteria for a viable Northwest Passage shipping route. However, the Northwest Passage never qualifies as "open" or "ice-free" based on WMO definitions. Furthermore, the deepwater route required by larger ships is only trafficable once during that period. Anomalously warm air temperatures over the Northwest Passage were observed each winter before the route was trafficable. Ice arches that traditionally hold multiyear ice out of the CAA weaken towards the end of the simulation and may lead to the influx of the remaining thick ice into the Northwest Passage.

THIS PAGE INTENTIONALLY LEFT BLANK

VII. EFFECTS OF INCREASED RESOLUTION ON LABRADOR SEA SIMULATION

The first generation of the NPS pan-Arctic coupled ice-ocean model was developed and run at a horizontal resolution of ~18 km. Years later, when the 9 km version became available, it was apparent that there were immediate benefits, some of which were in the simulation of the Labrador Sea (Marble 2001; Maslowski et al. 2008a). Specifically, the EKE increased an order of magnitude and the circulation was closer to the observations. Now, a newer model running at ~2.3 km is being tested. Comparison of parameters is summarized in Table 5. This chapter examines the new model and its most current output to understand the role of even higher resolution, particularly in simulating the Labrador Sea dynamics.

Parameter		$1/6^o$ model	$1/12^o$ model	$1/48^o$ model
ocean model		LANL POP, free surface	LANL POP, free surface	LANL POP, free surface
ice model		Hibler (1979)	Zhang and Hibler (1997)	LANL CICE
grid cell size		~18 km	~9.3 km	~2.3 km
horizontal grid		368x304	1280x720	5120x2880
vertical levels		30	45	48
bathymetry		modified ETOPO5	IBCAO+ETOPO5	AOOS+ETOPO1
initialization fields		PHC 1.0	PHC 2.0	PHC 2.0
atmospheric forcing		ECMWF	ECMWF	ECMWF
restoring fields	surface	PHC 1.0 monthly mean	PHC 2.0 monthly mean	PHC 2.0 monthly mean
	Lat. Bdry	PHC 1.0 annual mean	PHC 2.0 annual mean	PHC 2.0 annual mean
restoring timescale	surface	Temp-365 d, Sal-120 d	Temp/Sal-30 d	Temp/Sal-30 d
	Lat. Bdry	30 d	10 d	10 d
timestep	ocean	20 min	8 min	2 min
	ice	120 min	48 min	6 min
horizontal diffusion coefficients	tracer	-4.00E+18	-5.00E+17	-6.25E+16
	momentum	-1.00E+19	-1.25E+18	-1.56E+17
vertical diffusion coefficients	bkgd diff.	0.1	0.05	0.05
	bkgd visc.	1	0.2	0.2
approximate integration time		~28 hr/yr on 64 pe, ARSC T3E-900	~168 hr/yr on 128 pe, ARSC T3E-900	~7 days/yr on 2048 pe, NAVO Einstein XT5

Table 5.   Comparison of $1/6^o$ (~ 18 km), $1/12^o$ (~ 9.3 km), and $1/48^o$ (~ 2.3 km) model parameters (After Maslowski et al. 2009).

A. MODEL PREPARATIONS

1. New Grid

The 2 km model utilizes an entirely new bathymetric grid. The bathymetry for the entire domain was derived from the new ETOPO1 dataset at one-minute resolution, except for the Alaskan region which came from an even higher resolution dataset compiled by the Alaskan Ocean Observing System (AOOS) at 1 km resolution. The new model domain is 5120x2880 points. As with the 9 km bathymetry, the new grid had to be examined manually to ensure that narrow passages were not closed during the process of interpolating the new data onto the grid. Changing the grid from 9 km to 2 km allowed even better representation of narrow passages, particularly in the CAA. This higher resolution further minimizes the effect of the no slip boundary condition on volume fluxes. Additionally, three levels have been added in the vertical for additional resolution near the sea surface.

2. Ice and Ocean Models

Another improvement is the new sea ice model, CICE from the Los Alamos National Laboratory (LANL), adapted for a regional application over the pan-Arctic region. This new model uses five thickness categories in each grid cell, allowing a more physical representation of sea ice deformation processes. An improved ice strength parameterization is based on the amount of thin ice in a grid cell, instead of depending on the mean grid cell ice thickness as in the previous model (Maslowski and Lipscomb 2003). The ocean model remains a regional adaptation of the LANL POP code, including recent improvements in the vertical mixing parameterization, KPP, instead of the previous convective adjustment scheme as well as the use of shaved bottom cells to more realistically represent steep bottom topography, such as the shelf slopes of Greenland.

3. Optimization

Scalability tests were conducted to determine the optimal number of processors to integrate the model most efficiently. It was determined that running on 2048 cores was

most efficient for Einstein, the Navy's Cray XT5 located at the Naval Oceanographic Office in Bay St. Louis, MS. At this most optimal configuration, a year of model integration can be completed in about 7 days (Figure 62). This would at first appear to be a demonstration of Amdahl's Law, where there is an upper limit to the speed of parallel calculations due to non-parallelizable functions; hence adding processors does not increase the speed. However, it was found that using more than 2048 processors actually slowed the integration. If the problem was Amdahl's Law, the speed of integration would have leveled off with the addition of more processors, not decreased. This suggests another issue, possibly due to inefficiency of communication between the processors (which gets worse as more processors are added) and or a large load imbalance as many processors cover only land points and do nothing while the ones assigned to the ocean work continuously. Additional test runs were conducted to determine optimal ice strength coefficients for this resolution, crucial to achieving realistic ice thickness and concentration and their interannual variability.

The previous 9 km model was integrated for 48 years in the spinup mode. To attempt that length of spinup with the 2 km model in its present configuration would take about 48 weeks of continuous runs, which in a wall clock time would take ~96 weeks just to reach a fully spun up model. Then, a 30 year simulation would take ~ another 60 weeks. The implication is that the full spinup and production period for the 2 km model will take about 3 years to achieve. An option currently pursued is to use the end of the 48-year spinup results from the 9 km model to significantly shorten the 2 km spinup. Other improvements that can either speed the integration or increase the scalability of this code are also being pursued.
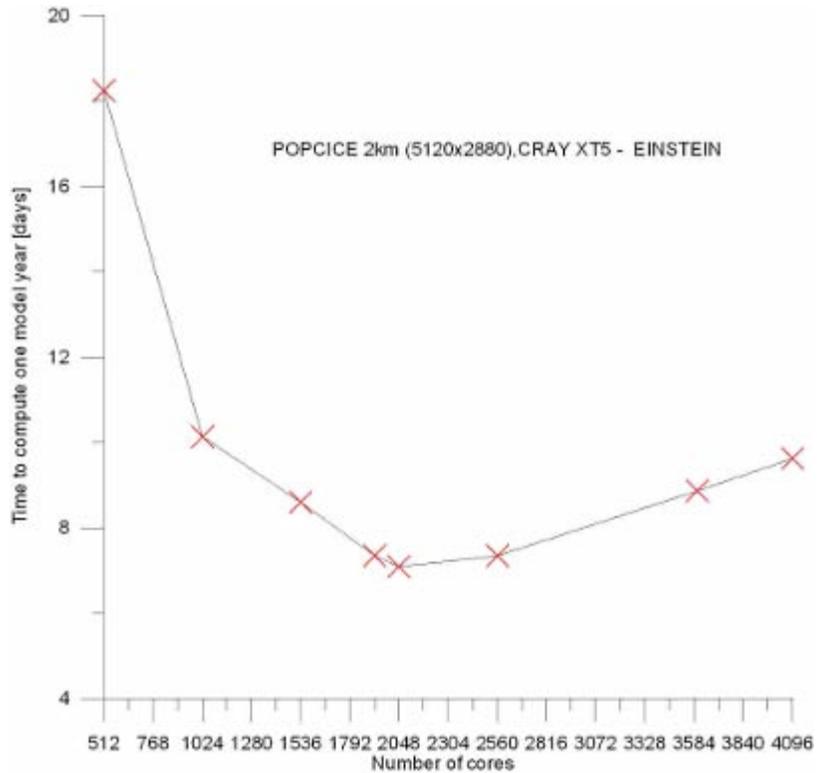
Figure 62.   Time to compute one model year as a function of number of cores used.

B.   RESULTS

The 2 km model output presented many challenges due to its size. The output files are so large that one of the few ways to access them for analyses is by the newest netcdf format, which is still not available on many computer platforms. The daily files are on the order of 11.5 GB, whereas they were less than 600 MB for the 9 km files. The files are so large that standard data processing and plotting programs such as Ferret and Matlab cannot be used at this time. The data files must be stored remotely at the supercomputing sites and data processing must be done using their computers.

The results presented here are from the most recent year of spinup, using daily realistic forcing for 1983. It is important to note that due to an early spinup phase those results may not reflect full energy levels expected in this eddy-resolving model configuration.

1. Total Kinetic Energy

Plots comparing 2 km to 9 km model results for 1983 annual 0-122m mean total kinetic energy (TKE) reveal that the 2 km model has larger maximum values, especially in the southern portion of the West Greenland Current (Figure 63a,b). Also, the 2 km model has more energetic flow across the top of the Labrador Sea and its recirculation into the Labrador Current. Narrow bands of high energy adjacent to the Greenland and Labrador coasts represent buoyancy-driven coastal currents, the width of which can be more realistically represented by the model with a smaller grid size. Finally, the 2 km model shows narrow bands of energy along the coasts between Hudson Strait and the Labrador shelf, indicative of opposing currents there that are not apparent in the 9 km model.

On the other hand, the 2 km model has less energy on either side of Davis Strait, with little evidence of a northbound branch of the WGC or southbound Baffin Island Current. Also, the strong maximum TKE value to the south associated with the NW Corner of the NAC is much weaker in the 2 km model. The lower magnitude of these features is believed to be due to the early phase of model spinup and they will be re-evaluated at a later time of model integration.
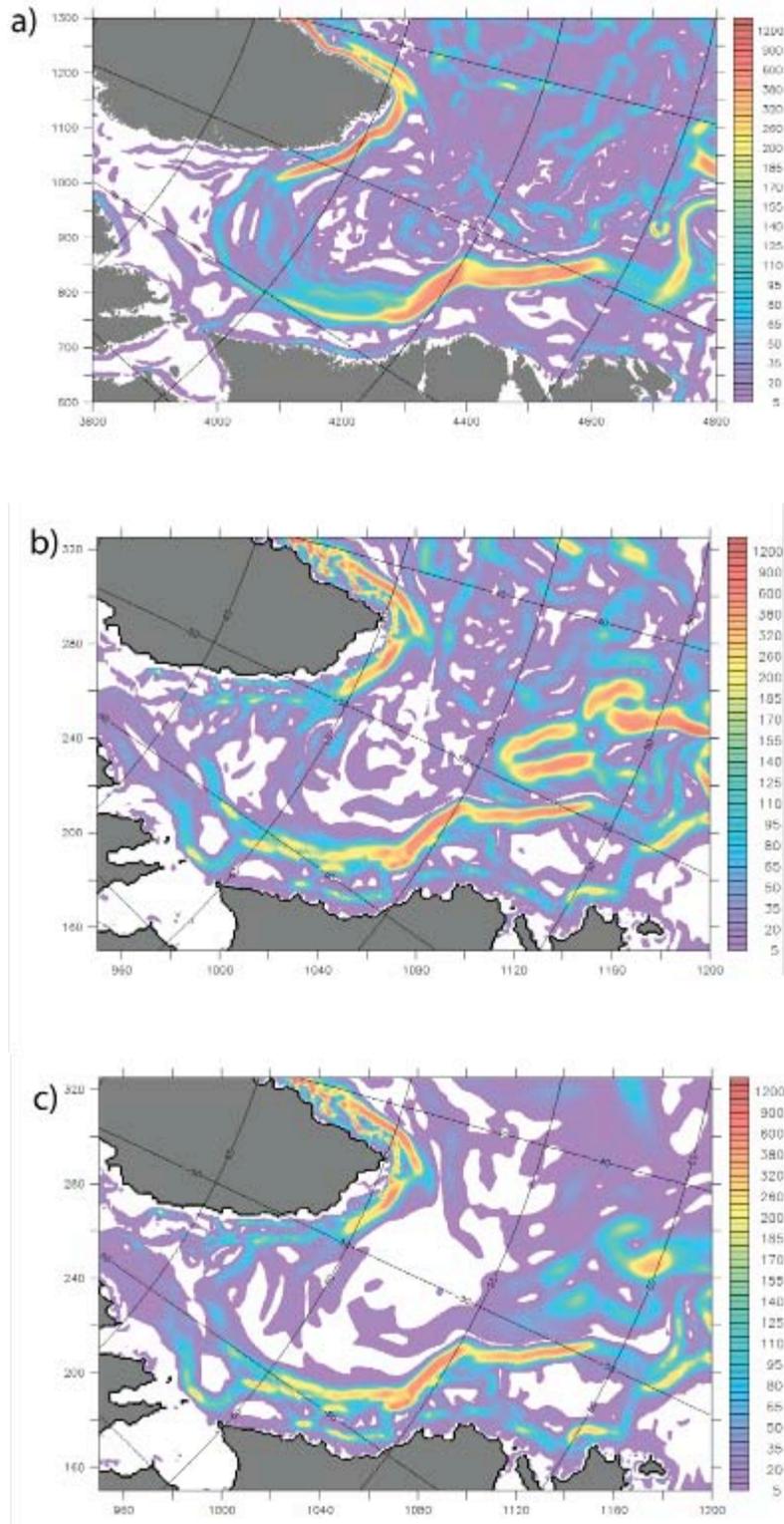
Figure 63. 0-122 mean TKE (cm2/s2) a) 2 km model 1983, b) 9 km model 1983, and c)
9 km model 26 year mean.

138

2.   Eddy Kinetic Energy

The plot of seasonal surface EKE reveals that the patch of high values near Cape Desolation lies further to the north than it did in the 9 km model (Figure 64). Coastal currents are prominent on both sides of the Labrador basin. Perhaps increased EKE there is in part the result of increased roughness with the higher resolution coastline as well as the smaller grid cell size to represent the width of those narrow currents. The other peak value in EKE associated with the NW Corner of the NAC is similar in location and magnitude with the 9 km model. However, the region extending northeast of that has much lower values in the 2 km model; values range from 300-600 cm^2s^{-2} where they were 500-1000 cm^2s^{-2} in the 9 km model.
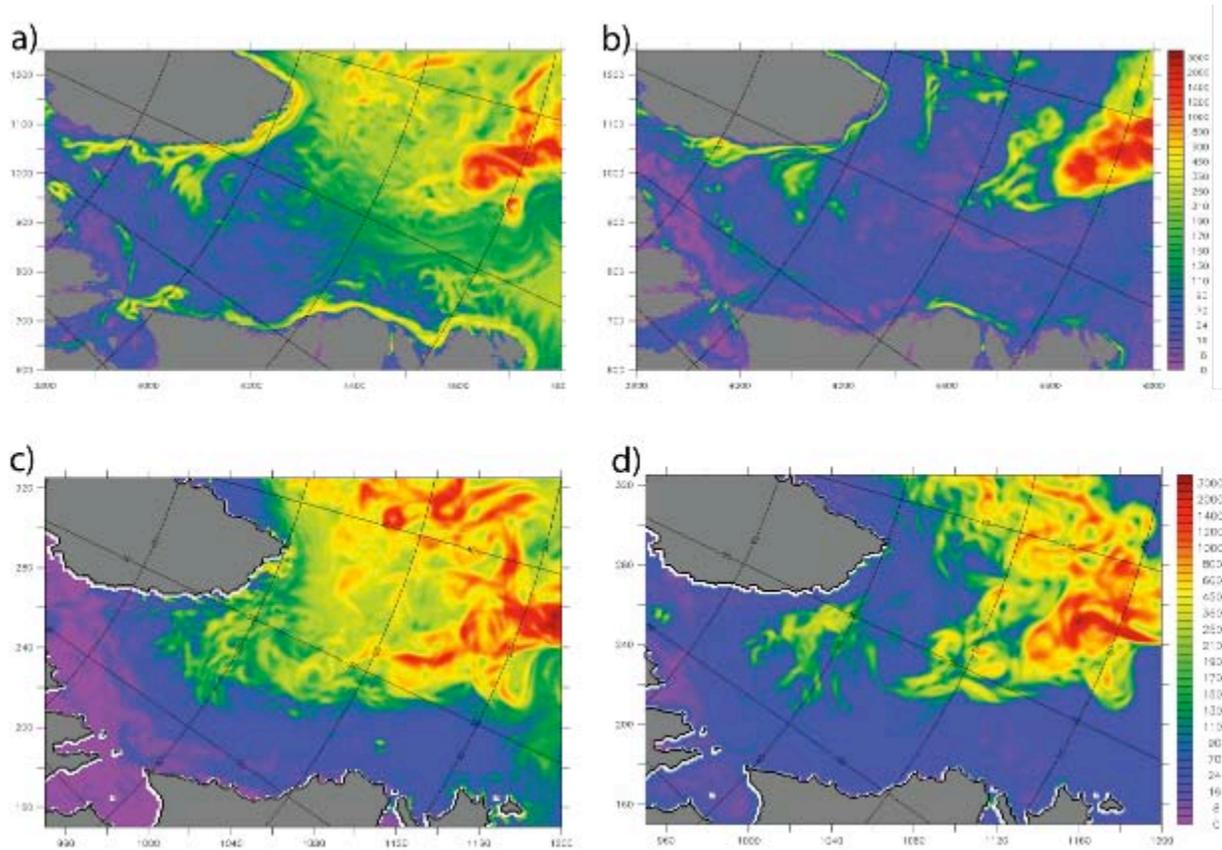
Figure 64.   EKE (cm^2s^{-2}). a) 1983 JFM 2 km, b)1983 JAS 2 km, c) 1983 JFM 9 km, d) 1983 JAS 9 km.

3. Circulation

There are noticeable changes in the modeled circulation (Figure 65). The coastal currents are more narrow and defined. The flow into and out of Hudson Strait is stronger in the 2 km model. Surprisingly the Labrador Current is wider than in the 9 km model, apparently due to two separate cores in the northern Labrador Current from different recirculation branches merging together. The West Greenland Current bifurcates near Cape Desolation but the branches are not as spread as they are in the 9 km model (Figure 65b).

The recirculation described by Lavender (2002) that flows opposite to the Labrador Current has not developed yet (Figure 65a). In the 9 km model, this appeared to be the result of eddies propagating into the Labrador Sea from the Northwest Corner of the North Atlantic Current (Figure 65b) in agreement with (Myers 2005). Perhaps this feature is not yet fully defined with the limited spinup period.
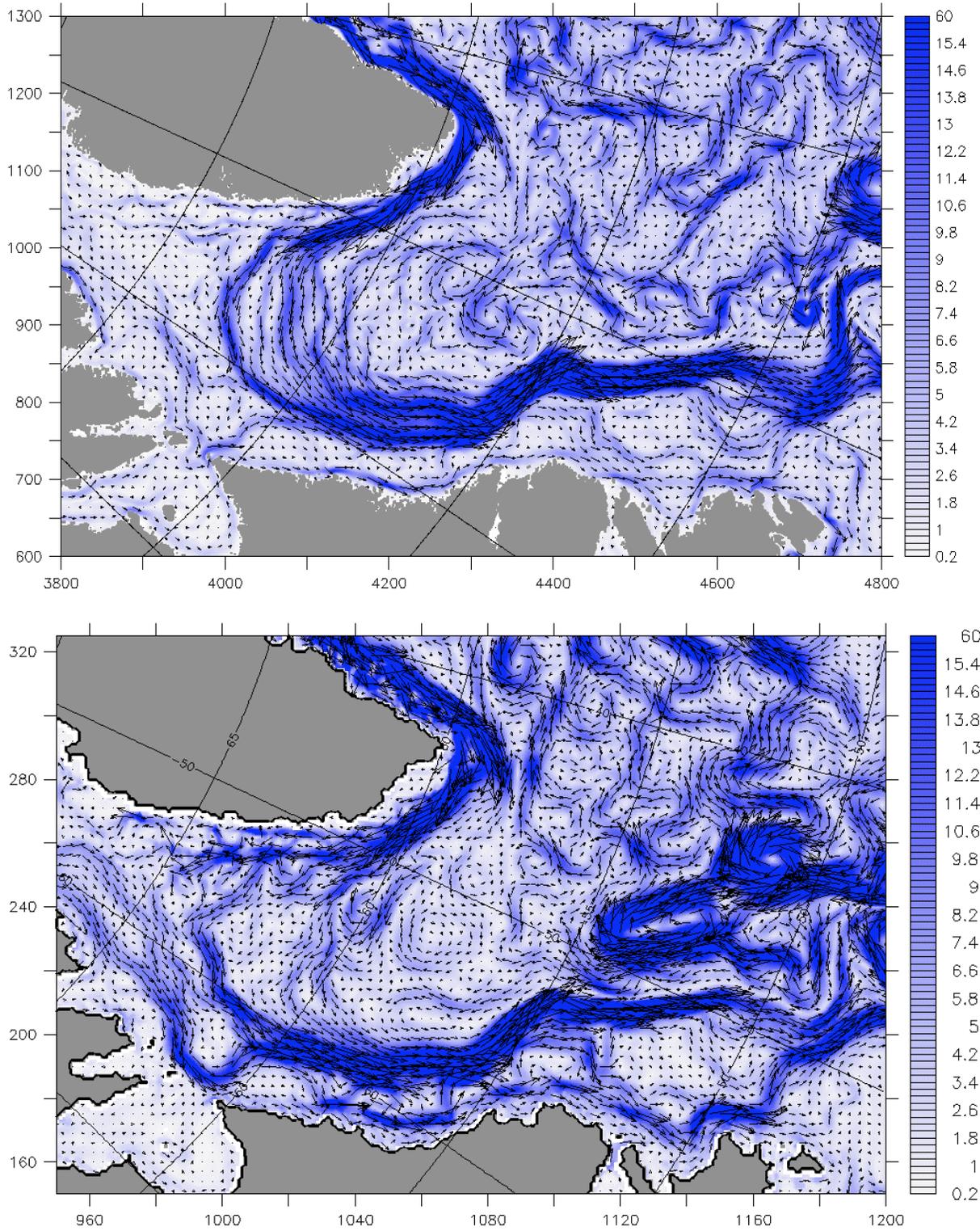
Figure 65.   0-122 mean circulation; speed (shading) (cm/s) and velocity (vectors) top) 2 km model 1983, bottom) 9 km model 1983.

4.   Eddies

It is difficult to investigate eddies produced in the 2km model because of the short run. Eddies were identified in the 9 km model primarily using their sea surface height anomaly (SSHA) fields. Here, there is no long-term annual cycle to remove in order to get anomalies. Hence, the background SSH variation contaminates the picture in the Labrador Sea making the SSH field of limited reliability. However, some eddies can be deduced here by their salinity and velocity characteristics, especially below the frictional upper layer, as well as from their effects on the ice thickness and concentration fields (as was done in analyses of the 9 km results).

a.   *From the West Coast of Greenland*

Eddies are formed near Cape Desolation, but they take a more northern propagation route instead of directly to the west into the Labrador Sea interior. Additionally, they are not as frequent as they were in the 9 km model, perhaps due to the West Greenland Current not yet attaining high enough speed to become sufficiently unstable over the narrowing shelf to allow frequent formation of eddies. Another explanation could be that the instabilities are resolved at smaller scales, with smaller, shorter lived eddies. However, some of the simulated eddies do have low salinity tops (Figure 66). A cross section of one of these anticyclonic eddies reveals its low salinity cap and approximate size (Figure 67) similar to the eddies described by Hatun (2007) and Rykova (2010).

If they survive the transit along the rim of the Labrador basin, these eddies break up and are absorbed into the Labrador Current. Many do not and are simply dissipated along the way. In any event, they do represent a flux of low salinity water to the northeastern Labrador Sea that would act to suppress convection there. The presence of convection in that region was a shortcoming of the 9 km model and it was thought to be due to a missing freshwater source. Perhaps the source was a low salinity coastal flow, rather than Greenland's glacial melt (which is not yet specified in this new model either).
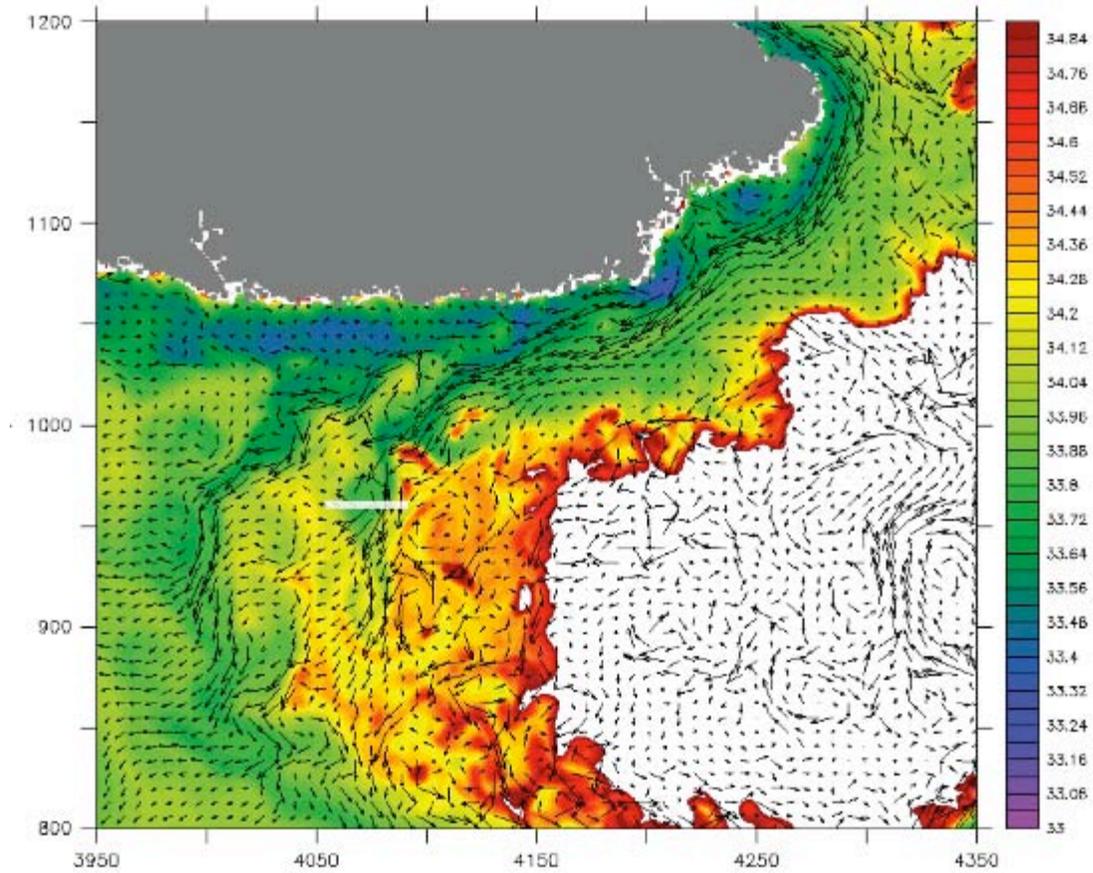
Figure 66.   Fresh top eddy being injected into the Labrador Sea interior from the West
          Greenland Current. Salinity (shading) and velocity (vectors) from depth of 10-15
          m. White line indicates the location of the cross section in the following figure.
          Note that the S shading scale was chosen to accentuate the lower salinity water,
          leaving much of the higher salinity Labrador Sea interior unshaded.
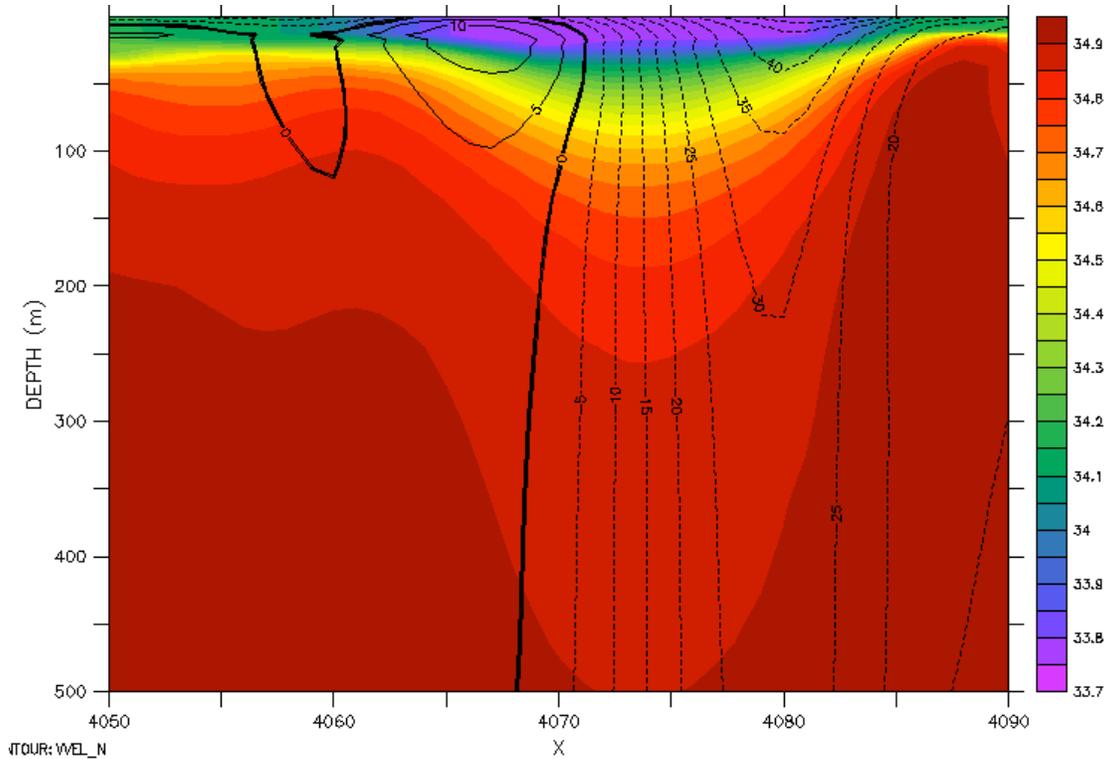
Figure 67.   Cross-section of anticyclonic eddy S (shading) and velocity (contours).

b.   *On the Canadian Labrador Shelf/Slope*

On the Canadian Labrador slope, model eddies do interact with freshwater, moving it towards the interior during the convective season. However, instead of injecting freshwater hundreds of kilometers offshore and having a lifespan measured in months, these eddies have ~1 week lifespan and are much smaller. The 9 km model eddies that moved the freshwater as described in Chapter V had radii ~ 25 km. Here, eddies are found with radii ~ 10 km. Many of these eddies appear to form along the ice edge due to barotropic instabilities along the ice edge resulting from shear between the wind accelerated ice free water and the adjacent ice covered water. The instabilities create waves which grow and pinch off eddies which are quickly dissipated. However, they provide a means of moving freshwater offshore, albeit ~70 km instead of 200 km as produced in the 9 km model. As this water moves offshore, the ice edge follows behind it. This process of local formation of eddies was lacking in the 9km

144

model; instead the eddies which did the work in that model were advected either from the WGC or the Northwest Corner of the North Atlantic Current.

Figure 68 shows two plots of Labrador SSS less than two weeks apart. The freshwater has advanced offshore due to the actions of a number of small eddies. Figure 69 shows these actions in a series of plots of S and velocity at 10-15 m depth (each 2 days apart) where numerous small eddies propagate along the ice edge and move freshwater towards the interior of the Labrador basin. Three of the more prominent eddies are labeled A, B, and C. A and C are anticyclonic while B is cyclonic. Not only do these eddies move the front of freshwater offshore, they also provide a mechanism for extending the ice edge (Figure 70). Figure 71, a RADARSAT image from the Canadian Ice Center, reveals a signature in the Labrador Ice edge that is similar to how the modeled smaller eddies (~ 10 km) interacted with the modeled ice edge.
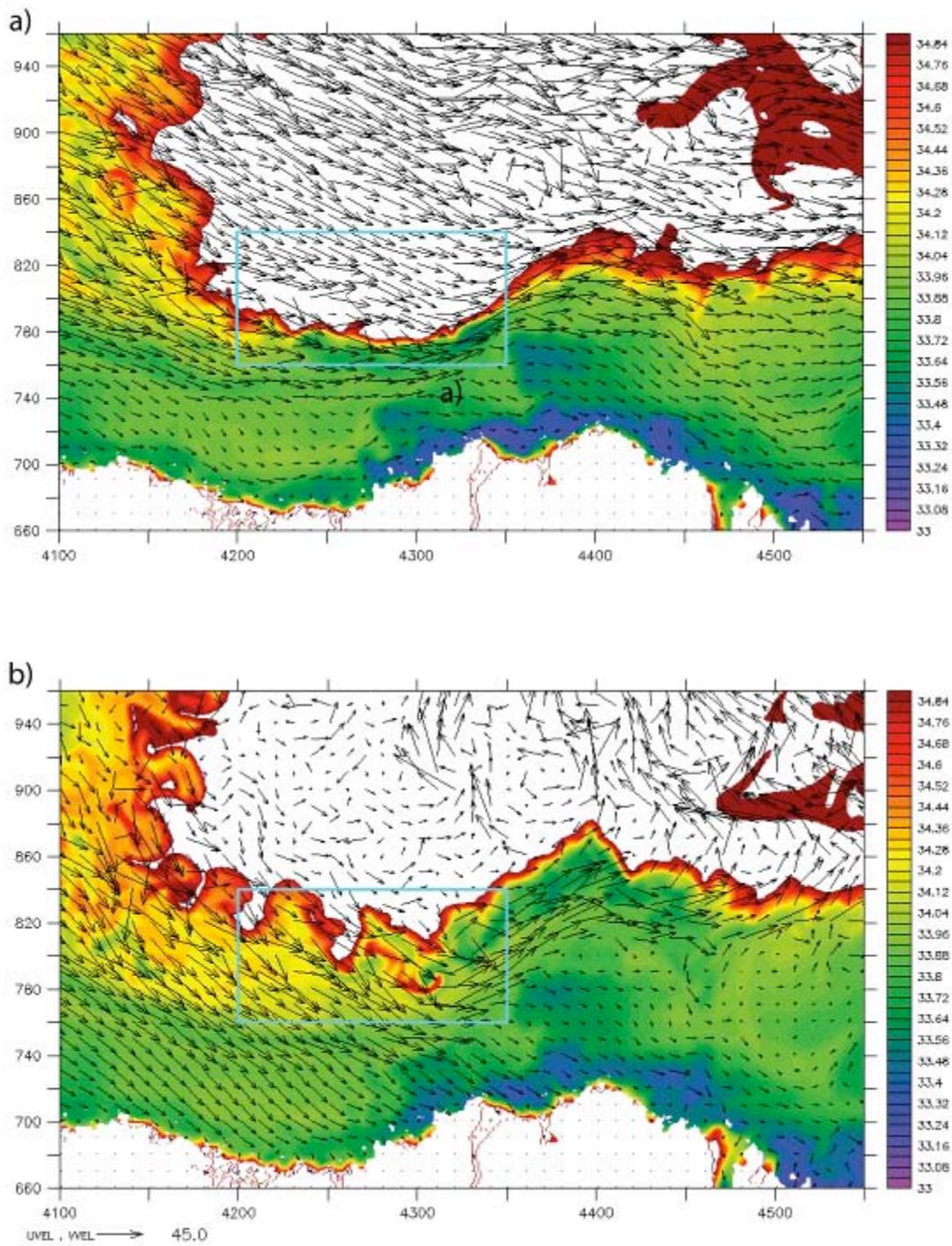
Figure 68.   SSS (shading) and velocity (vectors). a) 25 January, and b) 08 February.
Light blue box denotes the area examined in next figure.

146
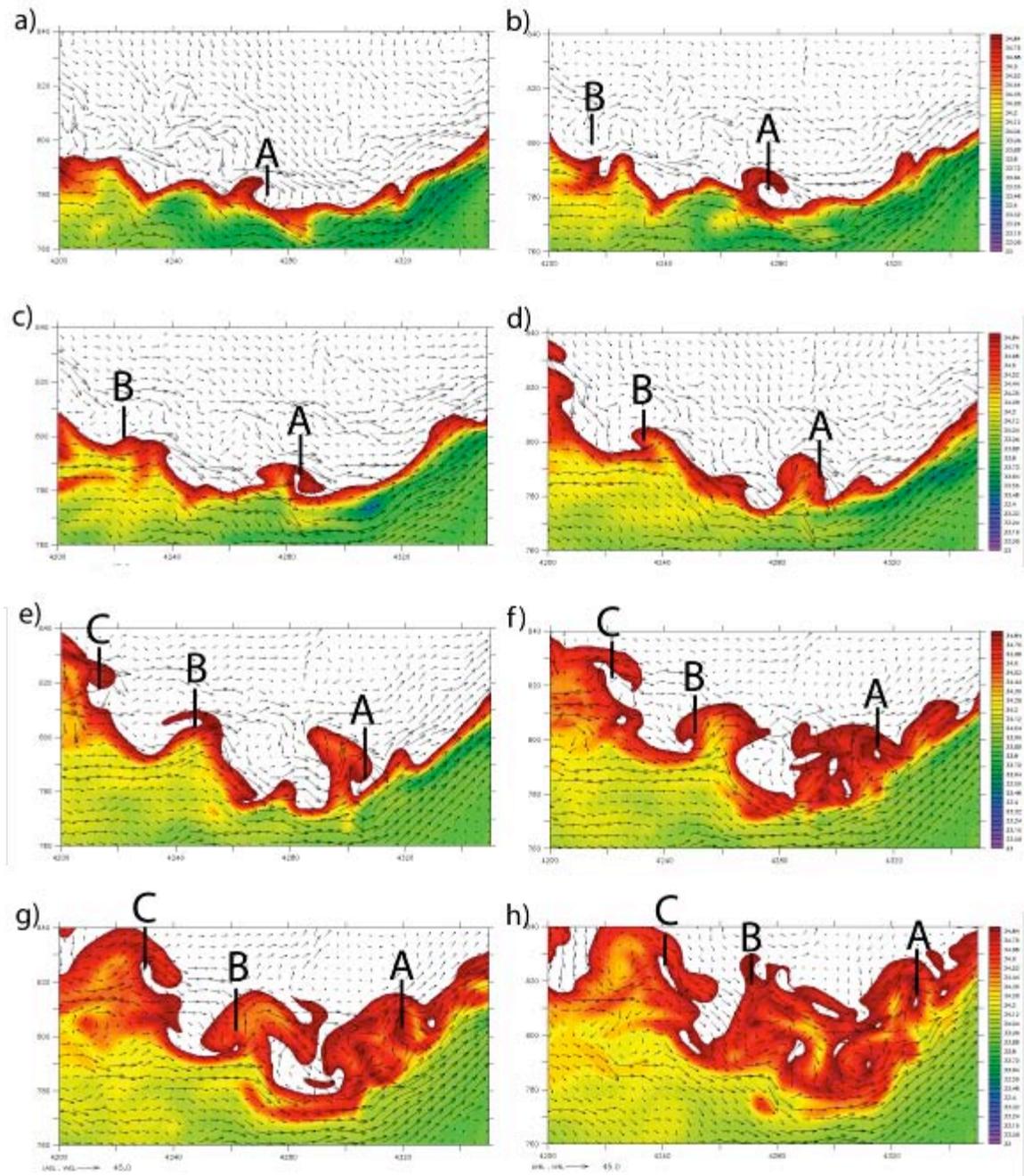
Figure 69.   S (shading) and velocity (vectors) at 13 m depth. a) 25 January, b) 27 January, c) 29 January, d) 31 January, e) 02 February, f) 04 February, g) 06 February, and h) 08 February. A, B, C correspond to specific eddies described in the text.

147
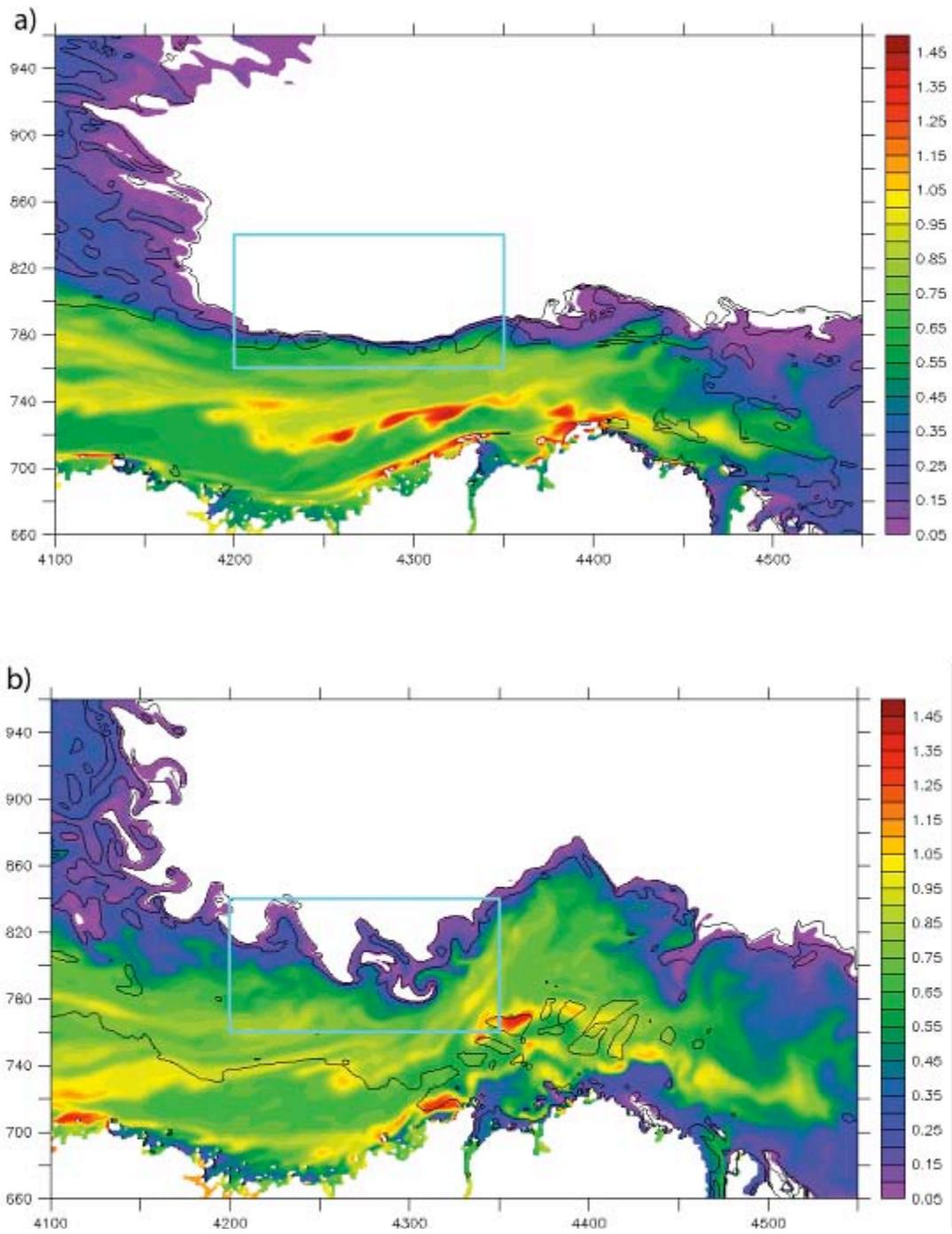
Figure 70.   Ice thickness (shading) and concentration (contours). a) 25 January and b) 08
             February. Light blue box denotes region examined in previous figure.
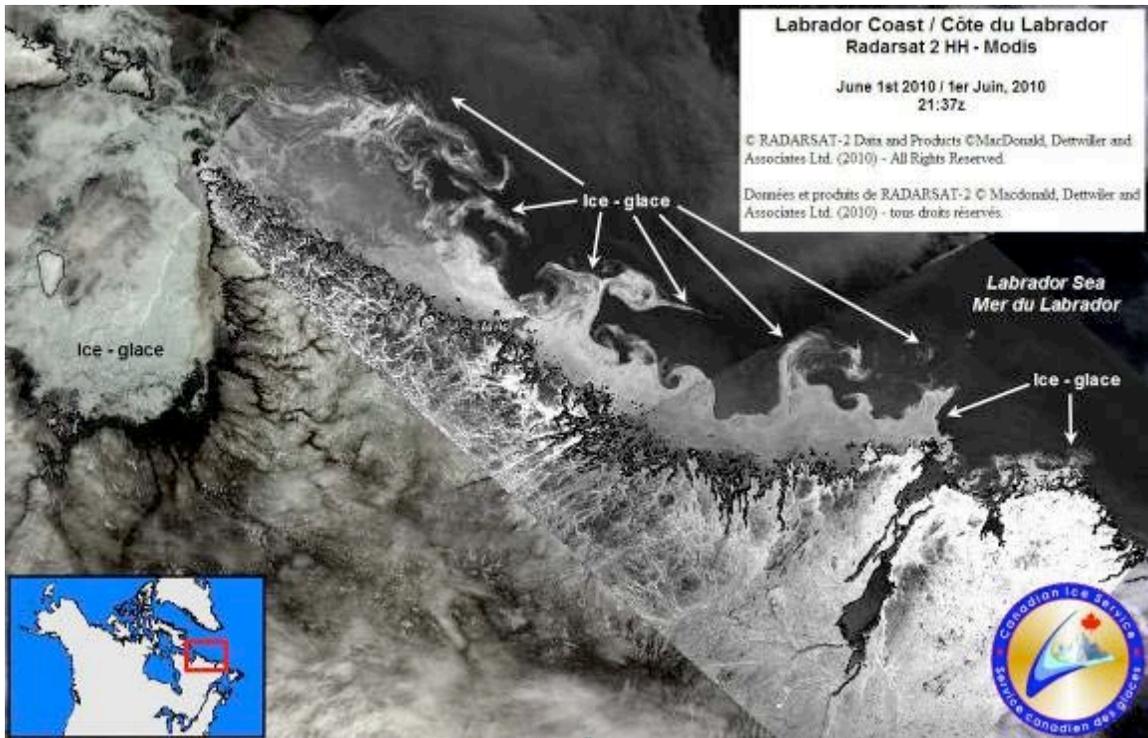
Figure 71.   Canadian Ice Center image of possible small eddies (radius ~10 km)
interacting with the Labrador Sea ice edge.

South of the convection region, there is an instance where freshwater is moved offshore by an eddy (Figure 72). The eddy that is responsible appears to have formed locally as the result of horizontal shear between the Labrador Current as it (is rounding Hamilton Bank) and the western edge of an anticyclonic eddy (the current is moving south and the edge of that eddy was moving northwards) (not shown). This induced a cyclonic eddy that just over a week later is depicted in Figure 72b. The eddy has a radius of ~ 25 km, similar in size to the eddies performing similar functions in the 9 km model. This eddy moves a parcel of freshwater ~ 100 km into interior. In the 9 km model (and in reality) this is where the recirculating branch (identified by Lavender et al. 2000) would be moving up to the north and would receive the freshwater returning it to the central Labrador Sea. However, as was previously mentioned, there is no such northbound recirculation branch in the 2 km model at this point in the spinup.
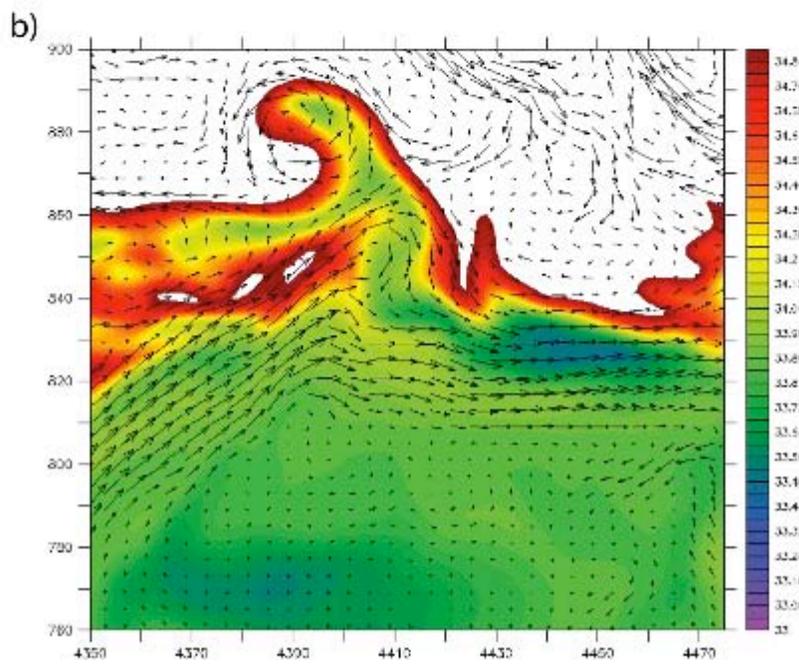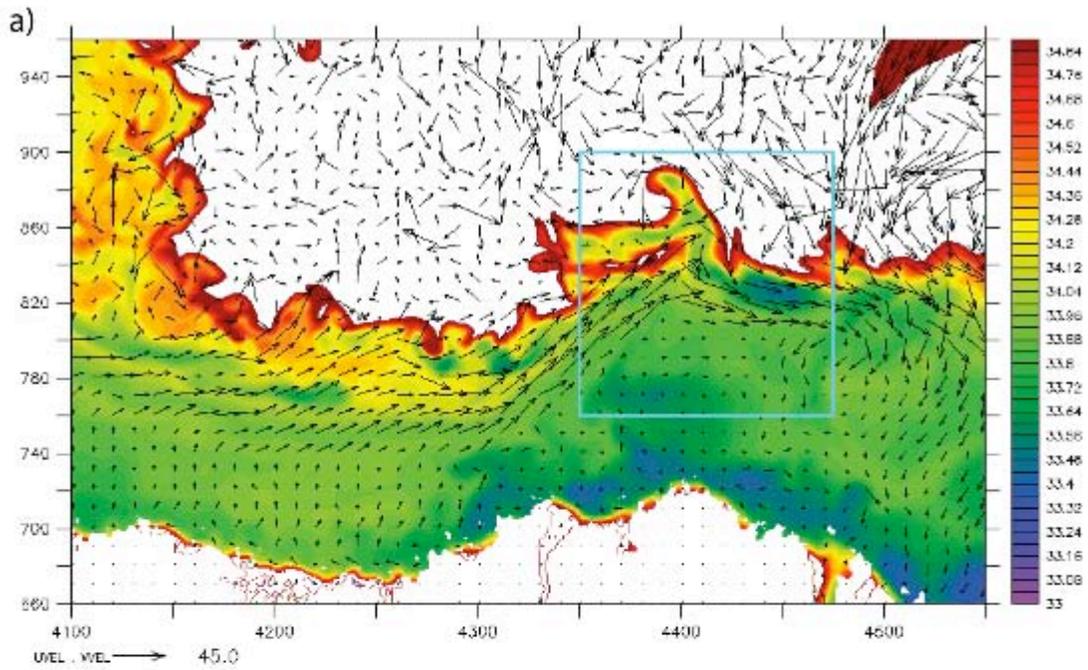
Figure 72.   19 February. a) surface S (shading) and velocity (vectors), b) 13 m S (shading) and velocity (vectors).

C. CONCLUSIONS

Although still in spinup mode, the new 2 km model shows promise for improved representation and understanding of the Labrador Sea dynamics. Improvements, especially in simulating the coastal flows are most striking at this point. Eddies perform similar functions that they did in the 9 km model but they appear to act on smaller scales. The larger eddies from the 9 km model, although present, are not as common. They do separate from Greenland near Cape Desolation and some have low salinity tops, which would inhibit deep convection downstream of their transit. Thus, the problems of anomalous convection produced in the 9 km model may be eliminated in the near future. On the Canadian side of the Labrador Sea, model eddies do interact with the freshwater on the slope, moving it towards the interior during the winter convective season. They even appear to provide a mechanism to extend the ice edge. The RADARSAT images in Figures 42 and 71 show that both large and small eddies play a role in the cross shelf fluxes.

However, there are certainly challenges associated with the new 2 km model. The output files are large and more difficult to analyze especially locally. Flows have not yet fully developed in Davis Strait, the NW Corner of the NAC, or the northbound recirculation (Lavender et al. 2000), requiring more spinup time to realize. The long time required to integrate the model from a "cold start" (i.e. a motionless ocean) could possibly be reduced by using output from the 9 km model to give the integration a "jump start." Fine scale features such as coastal flows will not be there in the coarser startup file but should develop quicker. Finally, scalability tests suggest that further optimization is possible hopefully leading to faster and more efficient model integration in the future.

THIS PAGE INTENTIONALLY LEFT BLANK

VIII. CONCLUSIONS AND RECOMMENDATIONS

Nothing is so fatal to the progress of mankind as to suppose our views of science are ultimate; that there are no mysteries in nature; that our triumphs are complete; and that there are no new worlds to conquer.

-Humphry Davy, 1810

Specific conclusions relevant to each chapter have already been discussed. Here a more general summary of conclusions and recommendations based on all chapters is presented.

This study used a high-resolution (9 km) coupled ice-ocean numerical model to examine the volume and freshwater fluxes from the Arctic Ocean, through the Canadian Archipelago and ultimately to the Labrador Sea. Fluxes from the Arctic Ocean through the CAA were quantified and their controls were diagnosed as a series of processes leading back to the West Greenland Current branching near Cape Desolation. Freshwater transport from the shelf to the interior of the Labrador Sea was determined to occur mostly in the southern Labrador Sea, but eddies provided a mechanism to move freshwater into active convective regions and shut down deep convection. Finally, the Northwest Passage was determined to be a viable shipping route in three summers, but only once via the deep-water route.

None of these questions could have been addressed to this detail with the coarse resolution of a global model. The volume and freshwater fluxes through the CAA benefited from the ability to represent narrow channels (while still satisfying the no slip boundary condition). Forcing of the fluxes could be addressed because of the extended domain including upstream conditions in the Arctic Ocean and the high resolution, which allowed the West Greenland Current to bifurcate in the correct place. The convective analysis was heavily reliant on eddies which play many roles in the Labrador Sea. Finally, the trafficability study required high resolution to not only resolve the passages themselves but also to reveal if one side or the other of a particular channel could be passed.

Despite its successes, the 9 km model still had limitations. Preliminary data from the new 2 km model suggest that some of them may be overcome by this higher resolution. The 9 km model was unable to resolve coastal buoyancy currents but the 2 km model might. The missing freshwater source to the NE Labrador Sea may just be due to the 9 km model's inability to simulate a low salinity coastal flow that supports eddies with fresh tops. These have been created in the 2 km model. This may solve the 9 km model's anomalous convection problems in that region. Furthermore, the 2km model will be eddy resolving in the Labrador Sea. It may allow examination of the processes controlling oceanic conditions in the narrow Greenland fjords that appear to be particularly important to Greenland's recent ice loss.

However, resolution alone is not the answer. Higher resolution is computationally expensive. The model code needs to be optimized to run on increasingly higher number of processors. If it can scale to more processors, additional computer resources and computing hours could be justified. Furthermore, additional resolution increases could approach non-hydrostatic conditions. While this would allow for the explicit depiction of convective processes, such models are not readily available for regional and global ocean applications and they would be even more computationally intensive and therefore would have to be efficient.

There are several environmental variables that could help improve modeling of the Canadian Arctic Archipelago and Labrador Sea dynamics even more. Higher resolution atmospheric forcing would allow more realistic high intensity wind events, such as those through Nares Strait, which are currently not available for forcing ice-ocean models. This could affect both the ocean and ice (fluxes and deformation). The incorporation of tides may further improve the regional fluxes and mixing throughout the CAA in particular. Incorporation of Greenland's glacial runoff will also allow a more complete representation of buoyancy sources in the subpolar North Atlantic Ocean.

Aside from model improvements and computer resources, it is critical to have more observational data for model verification. Regular, sustained, Eulerian and Langrangian observations will be integral to the development of future quality models as the environment changes. Parameterizations based on data from the 1970's for one

154

model resolution may not be up to the task of representing current processes at much higher resolutions. Large-scale and long-term ice thickness observations for the upstream Arctic are key to understanding the region's changes. A resurgence of the SCICEX submarine observations would be greatly beneficial. However, unmanned undersea vehicles represent an emerging technology that may be able to do the job more consistently and possibly even more economically. In the CAA, an increased network of tide gauges would allow better understanding of SSH patterns and the forcing of through flow. Additional moorings, especially on the northern end of the western Lancaster Sound mooring array could shed light on the winter volume flux maximum in that region. Increased monitoring of the Labrador Sea should be undertaken to compliment the annual hydrographic sections along AR7W and the sustained mooring efforts such as the one at OWSB. Ocean glider sampling campaigns could be expanded to cover the Labrador Sea to monitor deep convection in the winter as it happens. This would allow a much more thorough understanding of the process.

In closing, there is still much to learn about the Arctic Ocean and its downstream oceanic effects. Numerical models are valuable tools to "fill the gaps" between sparse temporal and spatial observational data. High resolution is crucial, not only to represent bathymetric features that affect flow but also to resolve motions governed by a decreasing Rossby radius of deformation at high latitudes. Without high model resolution, most of this study could not have been undertaken.

THIS PAGE INTENTIONALLY LEFT BLANK

IX. APPENDIX 1: ADDITIONAL CANADIAN ARCTIC ARCHIPELAGO FLUXES AND CIRCULATION

If you stare into the Abyss long enough, the Abyss stares back at you.

-Friedrich Nietzsche

The two major pathways for fluxes to transit through the CAA are Nares Strait and Lancaster Sound, described in Chapter III. However, data regarding the volume and freshwater fluxes through other CAA passages may be of some use to other researchers. Hence, they are being made available here along with other possibly pertinent data.

A. AMUNDSEN GULF

Amundsen Gulf undergoes an annual change in its circulation pattern. The flow changes from being weak with an anticyclonic sense of rotation in winter to a stronger flow with cyclonic rotation in summer. This is visible in Figure 73, which shows the monthly changes in a cross section of velocity across the mouth of Amundsen Gulf. Perhaps the annual change in circulation is connected to its annual cycle of ice cover, going from complete coverage in winter to open water in summer. Also, towards the end of the study period (1979-2004) the speed of rotation is at its maximum, especially in the summer (Figure 74). This coincides with longer ice free seasons. The summertime cyclonic regime corresponds to an annual flux to the east through Dolphin Union Strait; the wintertime anticyclonic regime corresponds to inflow from Dolphin Union Strait (Figure 75). There is evidence of a strong exchange of volume and freshwater across the mouth of Amundsen Gulf (Figure 76). However, they nearly cancel out and the resulting net fluxes are very small (especially compared to the flow through Lancaster Sound or Nares Strait) and do not appear significant to understanding the connection from the Arctic Ocean to the North Atlantic.
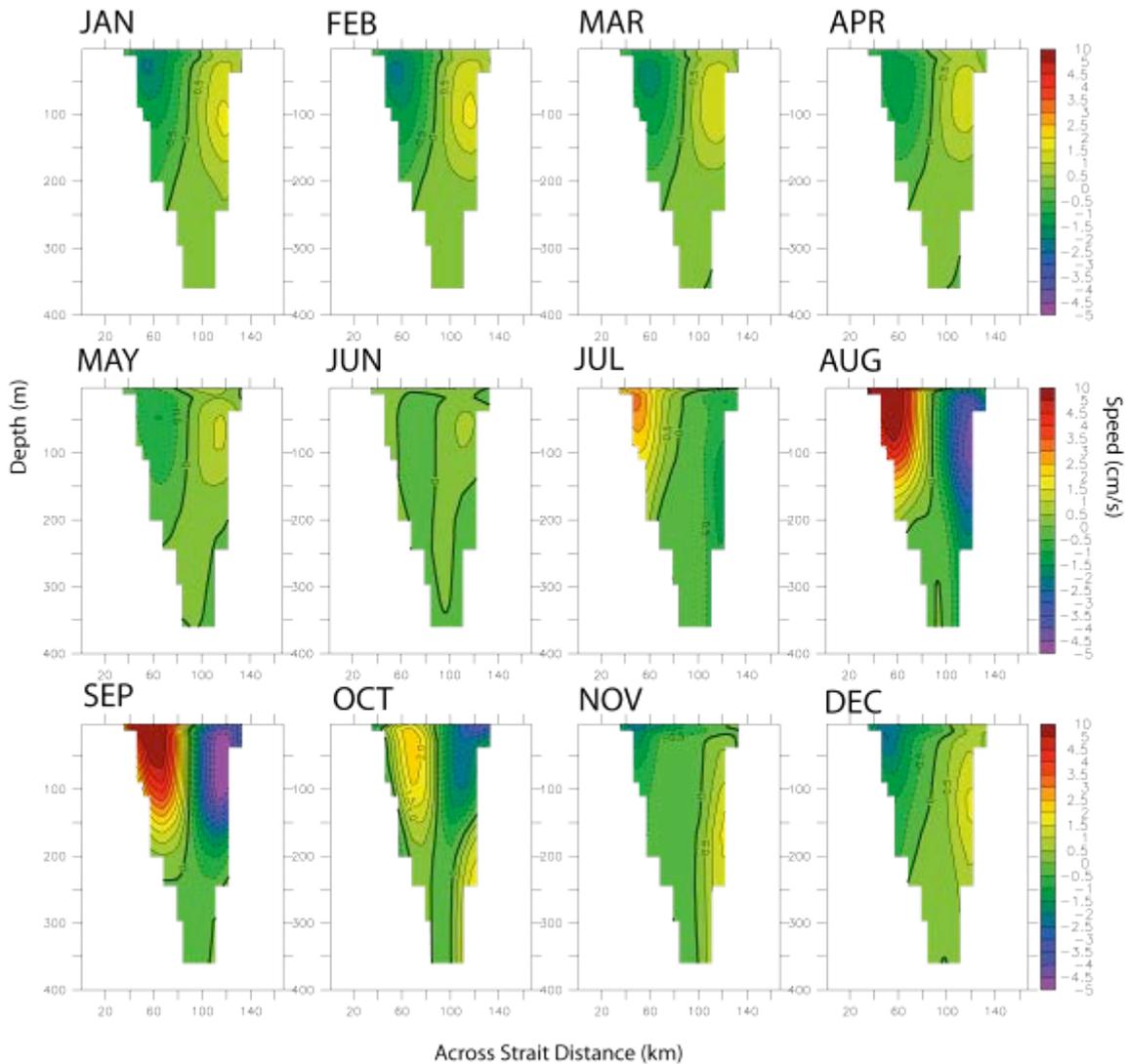
Figure 73.   Cross section of velocity across the mouth of Amundsen Gulf (orientation is with the southern end on the left hand side, northern end on the right hand side, and positive flow is moving from west to east; it is as if the observer is standing in Amundesn Gulf and looking towards the Beaufort Sea).
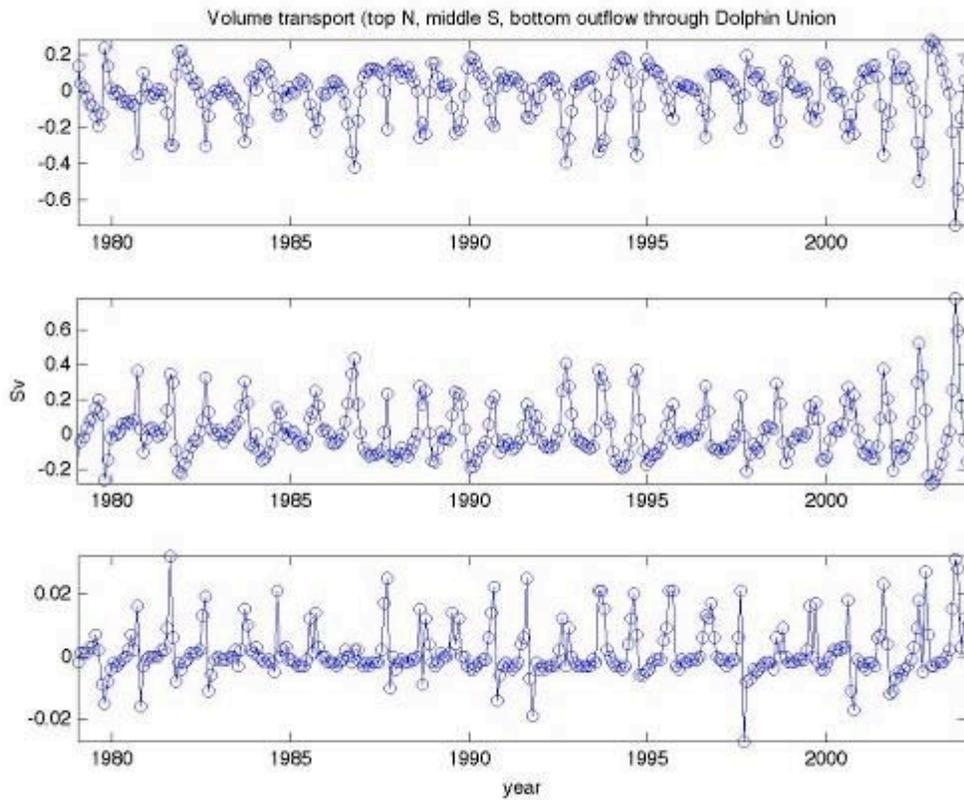
Figure 74. Volume Transport. a) N half of the mouth of Amundsen Gulf, b) S half of the mouth of Amundsen Gulf, and c) flow out of Amundsen Gulf into Dolphin Union Strait. Positive values indicate flow from the Beaufort Sea to Amundsen Gulf and negative flow is from Amundsen Gulf to the Beaufort Sea.
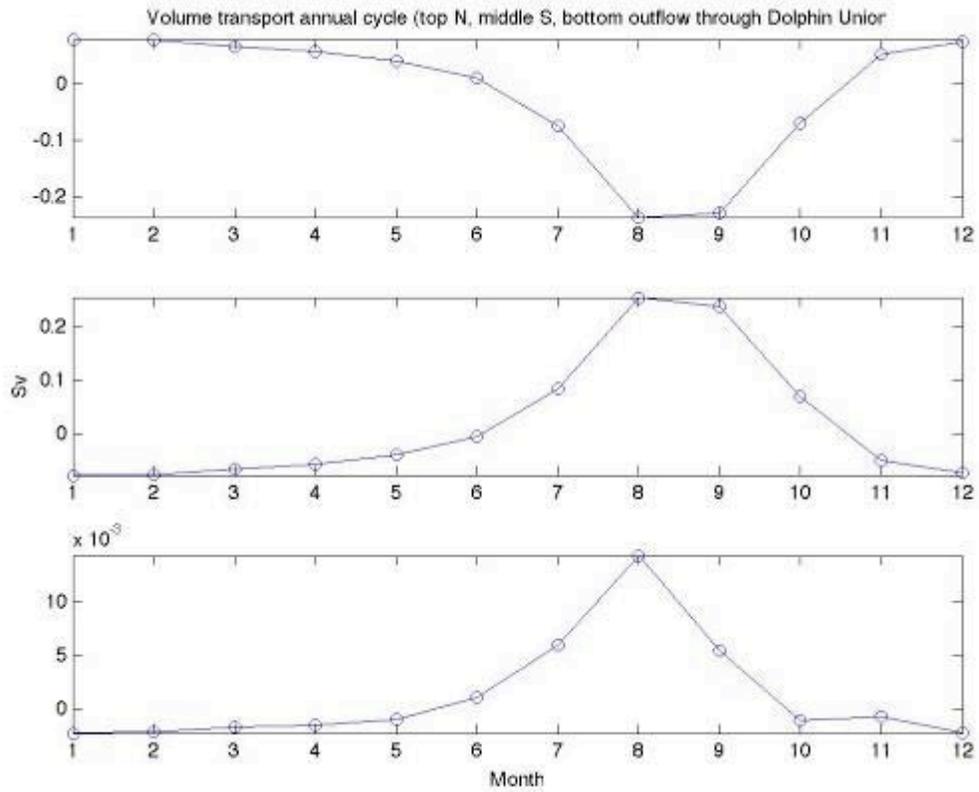
Figure 75.   Annual cycle of volume transport. a) N half of the mouth of Amundsen Gulf,
b) S half of the mouth of Amundsen Gulf, and c) flow out of Amundsen Gulf into
Dolphin Union Strait. Positive values indicate flow from the Beaufort Sea to
Amundsen Gulf and negative flow is from Amundsen Gulf to the Beaufort Sea.
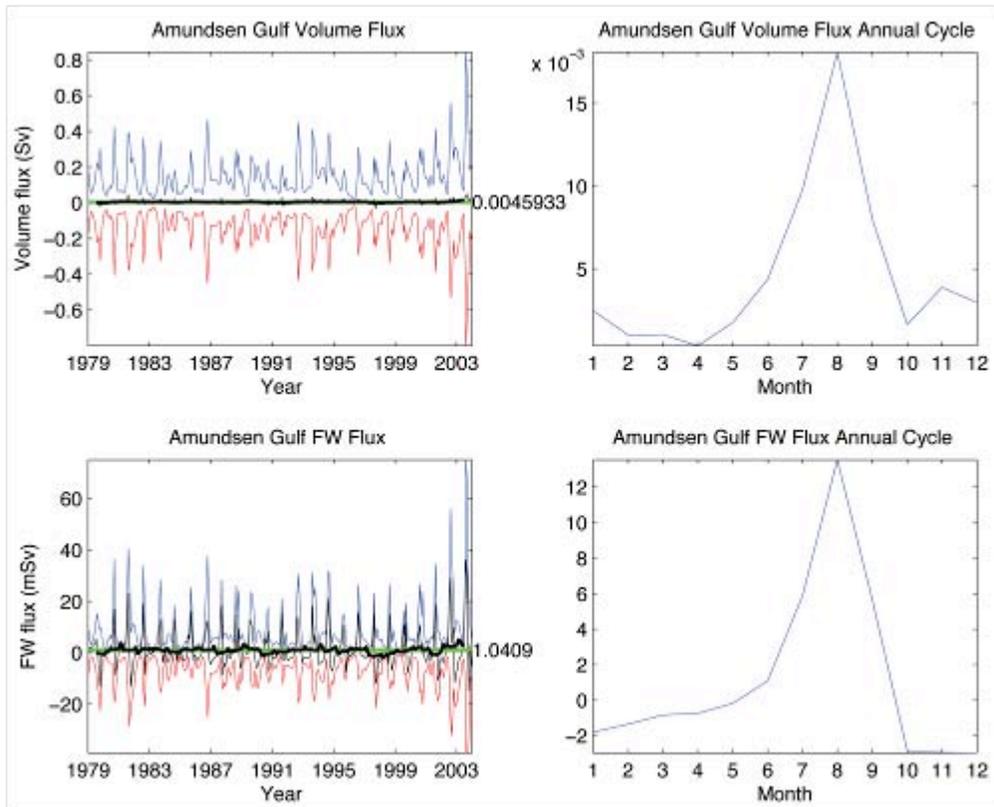
Figure 76.   Amundsen Gulf fluxes. a) volume 26-year time series, b) volume annual cycle, c) freshwater 26-year time series, and d) freshwater annual cycle. For a) and c), blue=flux from west to east, red=flux from east to west, black=net, thick black=13-month running mean of the net. b) and d) are net only.

B.   DOLPHIN UNION STRAIT

Flow through Dolphin Union Strait is controlled by the flux to and from Amundsen Gulf. Net fluxes nearly cancel out, with a small positive flux from moving eastwards from Amundsen Gulf. Maximum transports are in the summertime and negative for most of the rest of the year.
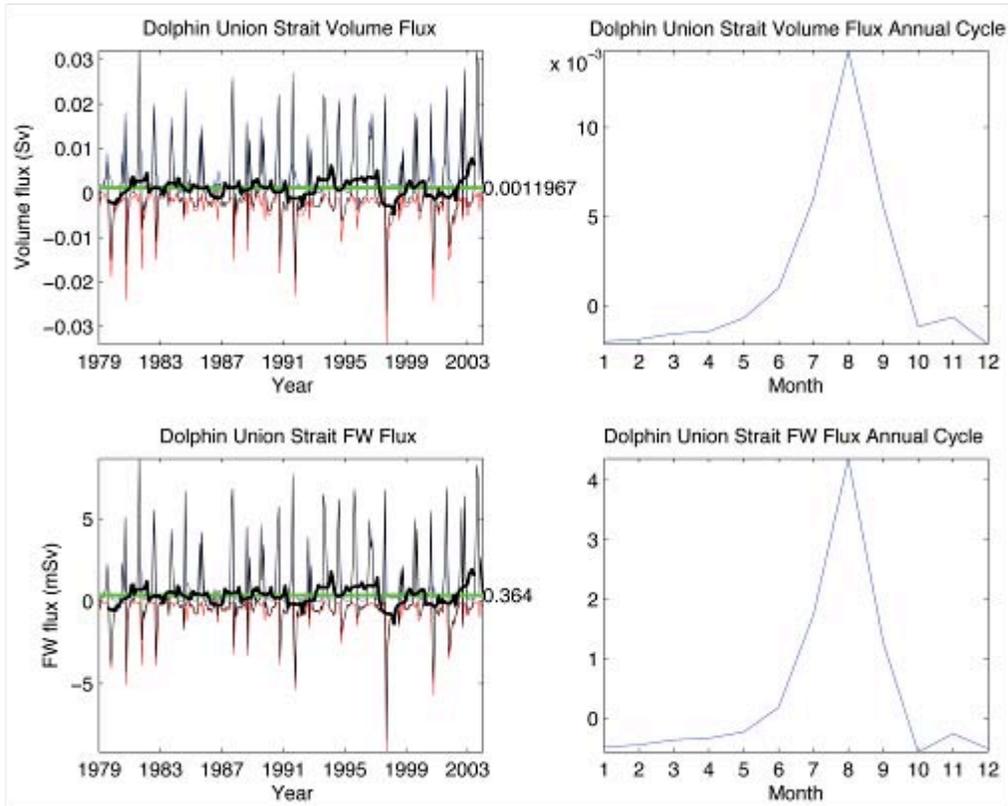
Figure 77.   Dolphin Union Strait fluxes. a) volume 26-year time series, b) volume annual cycle, c) freshwater 26-year time series, and d) freshwater annual cycle. For a) and c), blue=flux from west to east, red=flux from east to west, black=net, thick black=13-month running mean of the net. b) and d) are net only.

C.   DEASE STRAIT

Dease Strait fluxes are very similar to Dolphin Union Strait. It also appears to be ultimately controlled by the fluxes from Amundsen Gulf. These fluxes are seasonal and appear to be dependent on the direction of rotation in Amundsen Gulf.
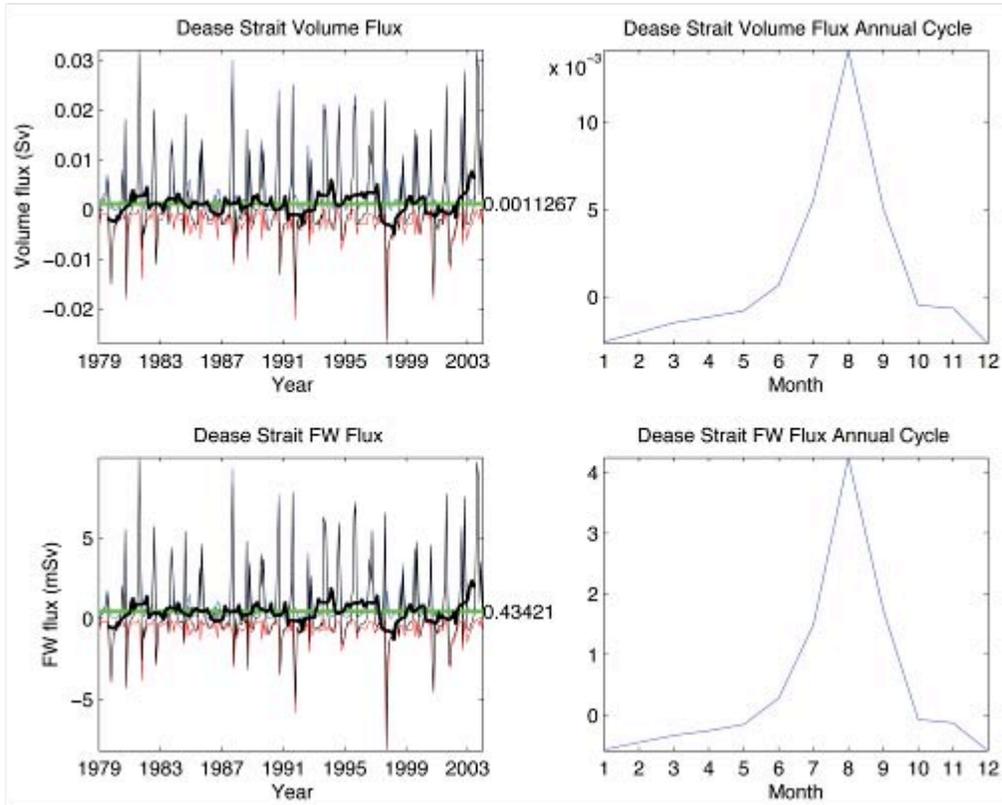
Figure 78.   Dease Strait fluxes. a) volume 26-year time series, b) volume annual cycle, c) freshwater 26-year time series, and d) freshwater annual cycle. For a) and c), blue=flux from west to east, red=flux from east to west, black=net, thick black=13-month running mean of the net. b) and d) are net only.

D.   VICTORIA STRAIT

The volume flux through Victoria Strait follows the same pattern as its upstream locations, Dolphin Union Strait and Dease Strait.   However, it experiences a large negative freshwater flux in summer. This could be due to winds pushing surface waters to the south while flow at depth was directed to the north.
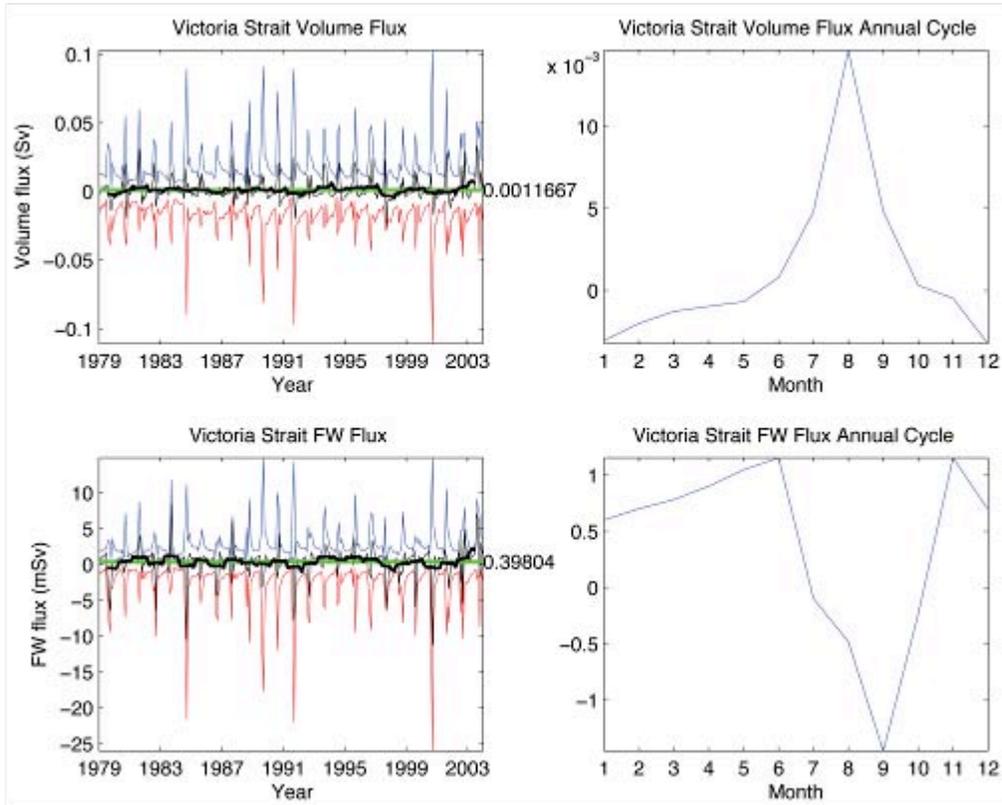
Figure 79.   Victoria Strait fluxes. a) volume 26-year time series, b) volume annual cycle, c) freshwater 26-year time series, and d) freshwater annual cycle. For a) and c), blue=flux from west to east, red=flux from east to west, black=net, thick black=13-month running mean of the net. b) and d) are net only.

E.   BYAM MARTIN CHANNEL

Byam Martin Channel empties southwards into the Northwest Passage. Its volume flux is significant but its freshwater flux is even more so. It supplies more freshwater than Nares Strait. It has dual peaks in the annual cycles of volume and freshwater flux.
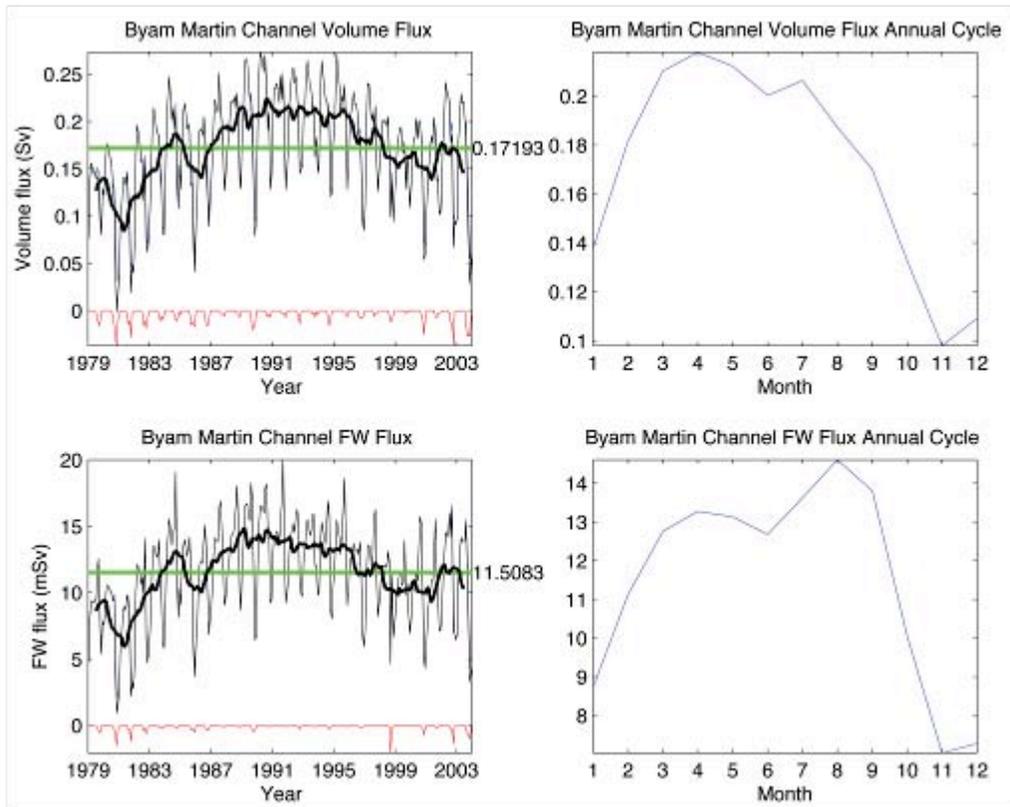
Figure 80. Byam Martin Channel fluxes. a) volume 26-year time series, b) volume annual cycle, c) freshwater 26-year time series, and d) freshwater annual cycle. For a) and c), blue=flux from north to south, red=flux from south to north, black=net, thick black=13-month running mean of the net. b) and d) are net only.

F. PENNY STRAIT

Penny Strait also provides a southwards flux into the Northwest Passage. It has dual peaks in the annual cycles of volume of freshwater flux. Its volume and freshwater contributions are even large than those of Byam Martin Channel.
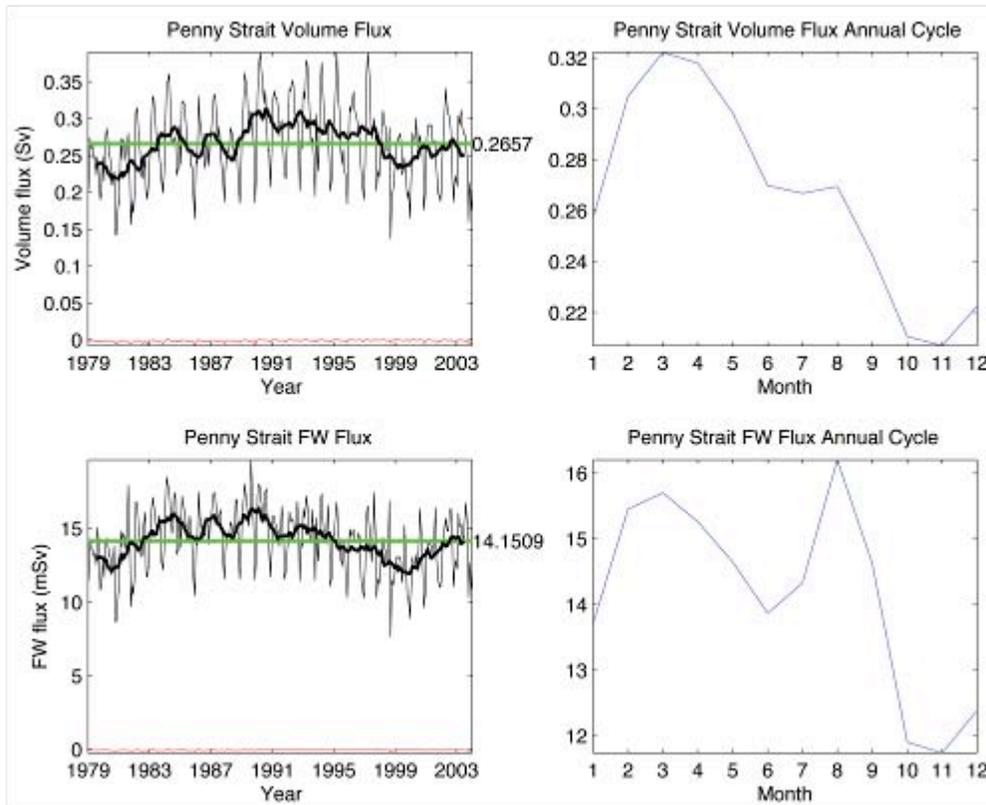
Figure 81.   Penny Strait fluxes. a) volume 26-year time series, b) volume annual cycle, c) freshwater 26-year time series, and d) freshwater annual cycle. For a) and c), blue=flux from north to south, red=flux from south to north, black=net, thick black=13-month running mean of the net. b) and d) are net only

G.   PRINCE REGENT INLET

Prince Regent Inlet lies just east of Barrow Strait/ western Lancaster Sound mooring array line. It is an area where the flow turns direction from anticyclonic to cyclonic. This is due to the changing bathymetry and conservation of potential vorticity; as the flow goes over the sill it rotates anticyclonically; in the deeper water it rotates cyclonically again. As such there is strong flow in both directions across the mouth of the inlet but only a small net volume flux southwards. The annual cycles of volume and freshwater flux show dual peaks for each, consistent with other locations along the Northwest Passage.

166
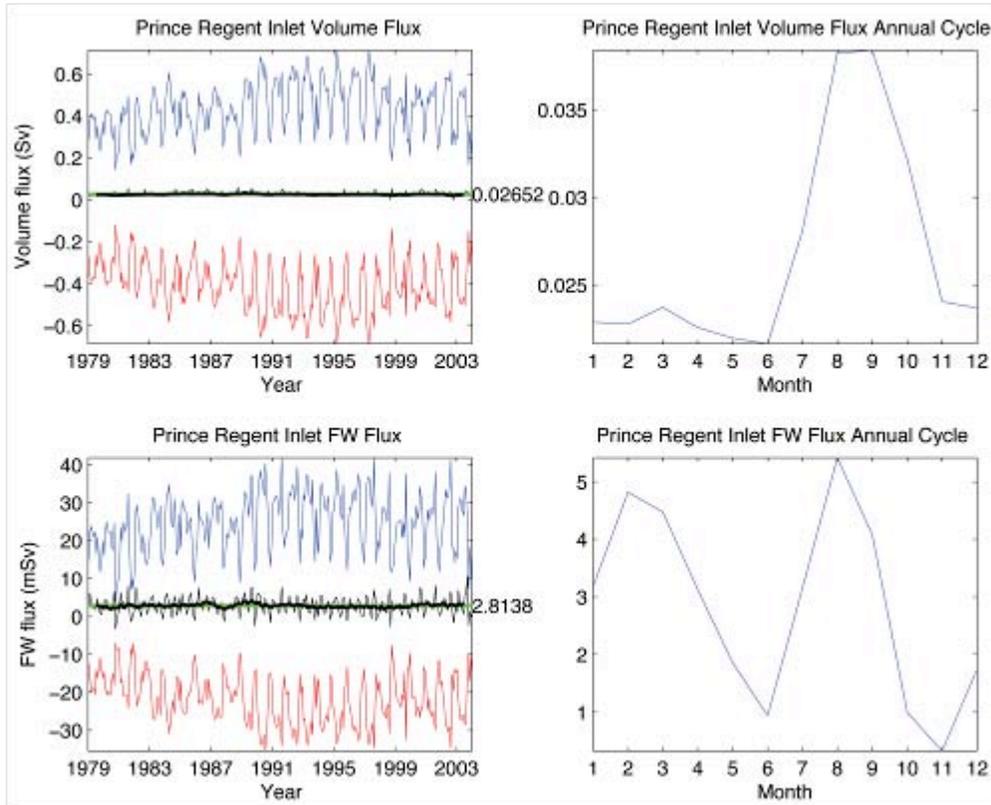
Figure 82.   Prince Regent Inlet fluxes. a) volume 26-year time series, b) volume annual cycle, c) freshwater 26-year time series, and d) freshwater annual cycle. For a) and c), blue=flux from north to south, red=flux from south to north, black=net, thick black=13-month running mean of the net. b) and d) are net only.

H.   FURY-HECLA STRAIT

Fury-Hecla Strait is a small but important passage linking the Canadian Arctic Archipelago with Hudson Bay. It shows evidence of a dual peak in volume flux but only a single peak in freshwater.
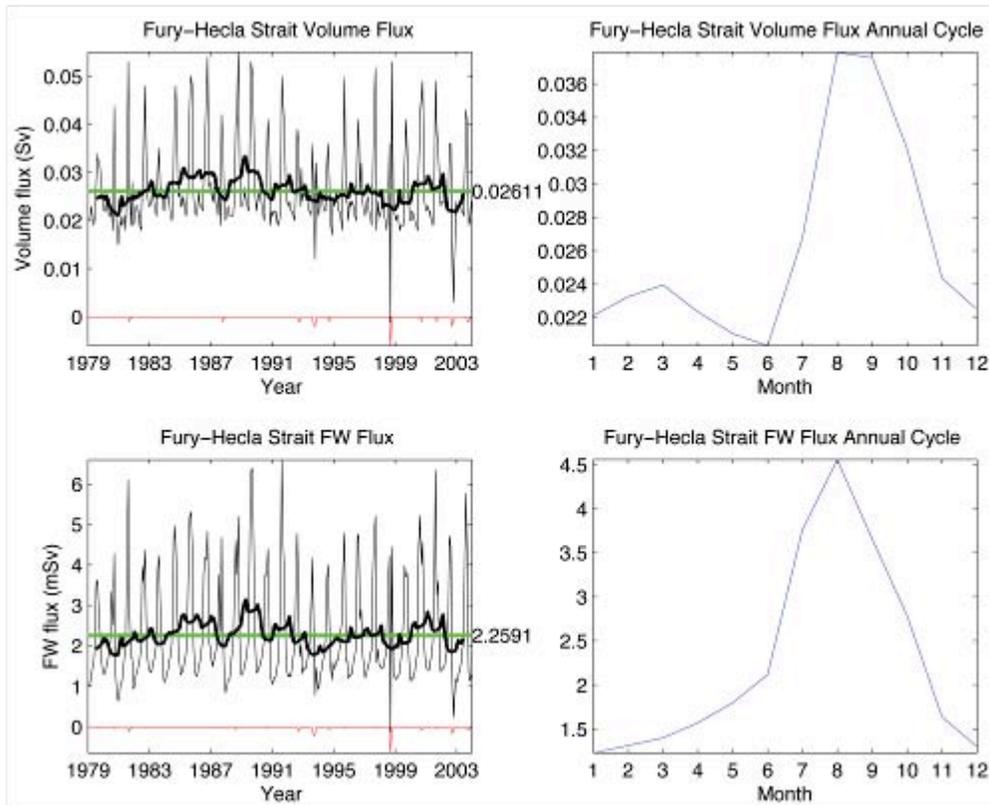
Figure 83.   Fury-Hecla Strait fluxes. a) volume 26-year time series, b) volume annual cycle, c) freshwater 26-year time series, and d) freshwater annual cycle. For a) and c), blue=flux from west to east, red=flux from east to west, black=net, thick black=13-month running mean of the net. b) and d) are net only.

I.   JONES SOUND

Jones Sound empties into northern Baffin Bay. Its fluxes are small and contribute to the total transports between the Arctic Ocean and Baffin Bay. Its volume flux shows a single peak in March just like for Nares Strait. The annual peak in the freshwater cycle is in the summer.
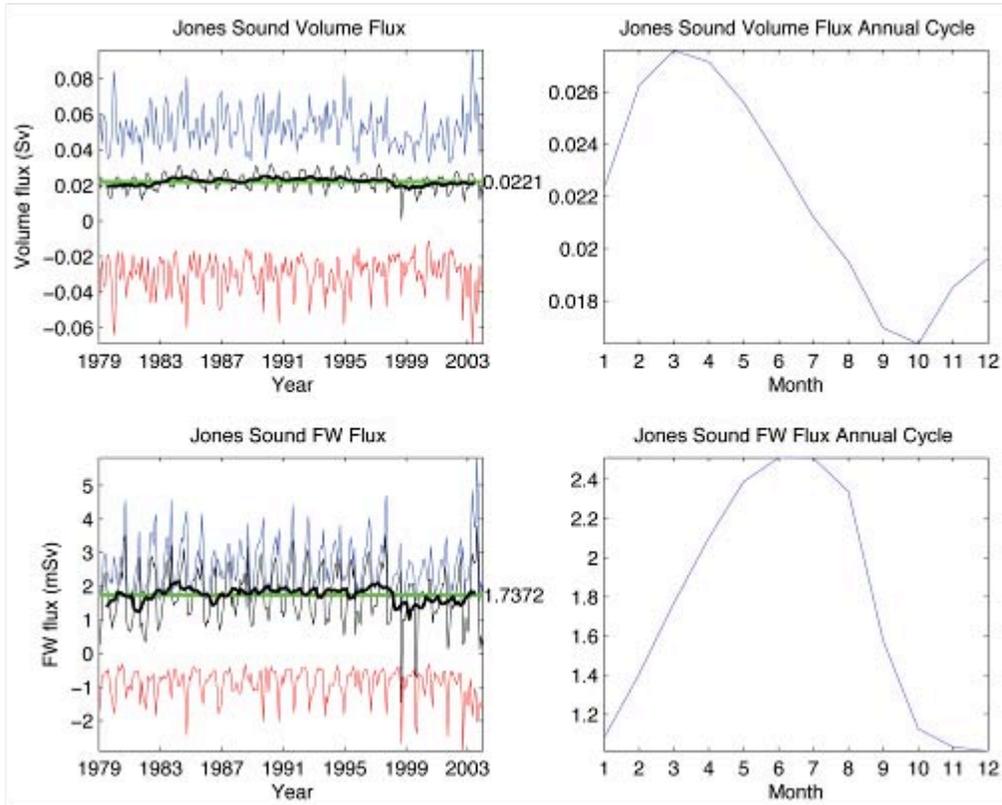
Figure 84.   Jones Sound fluxes. a) volume 26-year time series, b) volume annual cycle, c) freshwater 26-year time series, and d) freshwater annual cycle. For a) and c), blue=flux from west to east, red=flux from east to west, black=net, thick black=13-month running mean of the net. b) and d) are net only.

THIS PAGE INTENTIONALLY LEFT BLANK

LIST OF REFERENCES

Agnew, T., A. Lambe, and D. Long, 2008: Estimating sea ice area flux across the Canadian Arctic Archipelago using enhanced AMSR-E. *J. Geophys. Res.*, **113**, C10011, doi:10.1029/2007JC004582, 2008.

Allen, T. W., 2009: The Emerging Arctic- Security on the Last Frontier. *3ʳᵈ Symposium on the Impacts of an Ice-Diminishing Arctic on Naval and Maritime Operations*, Annapolis, MD, U.S. National Ice Center and the U.S. Arctic Research Commission, 1-18.

Andres, R. B., 2009: Prospective U. S. Strategy in the Face of Increasing Military Tension in the Arctic Over Emerging Energy Resources. *3ʳᵈ Symposium on the Impacts of an Ice-Diminishing Arctic on Naval and Maritime Operations*, Annapolis, MD, U.S. National Ice Center and the U.S. Arctic Research Commission.

Baker, B. B., 2010: Law, Science, and the Continental Shelf: The Russian Federation and the Promise of Arctic Cooperation. American *University International Law Review*, **25**(2), 251-281.

Barber, D. G., J. M. Hanesiak, W. Chan, and J. Piwowar, 2001: Sea-Ice and Meteorological Conditions in Northern Baffin Bay and the North Water Polynya between 1979 and 1996. *Atmosphere-Ocean* **39**(3), pp. 343-359.

BBC, 2007: Canada to strengthen Arctic claim. BBC News. [Available online at http://news.bbc.co.uk/2/hi/americas/6941426.]

BBC, 2010: Russia and Norway sign maritime border agreement. BBC News. [Available online at http://www.bbc.co.uk/news/business-11316430.]

Belkin, I. M., S. Levitus, J. Antonov, S. Malmberg, 1998: "Great Salinity Anomalies" in the North Atlantic. *Prog. Oceanogr.*, **41**, 1-68.

Boning, C. W., F. O. Bryan, W. R. Holland, and R. Doscher, 1996: Deep-Water Formation and Meridional Overturning in a High-Resolution Model of the North Atlantic. *J. Phys. Oceanogr.*, **26**, 1142-1164.

Boning, C. W., M. Rhein, J. Dengg, and C. Dorow, 2003: Modeling CFC inventories and formation rates of Labrador Sea Water. *Geophys. Res. Lett.*, **30(2)**, 22.1–22.4.

Borgerson, S. G., 2008: Arctic Meltdown- The Economic and Security Implications of Global Warming. *Foreign Affairs*, **87**(2), 63-77.

Bourke, R. H., and A. S. McLaren, 1992: Contour mapping of Arctic Basin ice draft and roughness parameters. *J. Geophys. Res*., **97**(C11), 17715-17728.

Bowes, M. D., 2009: *Impact of Climate Change on Naval Operations in the Arctic*. Center for Naval Analyses, 52 pp.

Bracco, A., J. Pedlosky, and R. S. Pickart, 2008: Eddy Formation near the West Coast of Greenland. *J. Phys. Oceanogr*., **38**, 1992-2002.

Brandt, P., A. Funk, L. Czeschel, C. Eden, and C. Boning, 2007: Ventilation and transformation of Labrador Sea Water and its rapid export in the deep Labrador Current. *J. Phys. Oceanogr*., **37**, 946-961.

Broecker, W., 1991: The great ocean conveyor. *Oceanography*, **4**, 79-89.

CBC, 2008: Federal government blocks sale of MDA space division. CBC News. [Available online at http://www.cbc.ca/money/story/2008/04/10/mdablock.html.]

Chanut, J., B. Barnier, W. Large, L. Debreu, T. Penduff, J. M. Molines, and P. Mathiot, 2008: Mesoscale Eddies in the Labrador Sea and Their Contribution to Convection and Restratification. *J. Phys. Oceanogr*., **38**, 1617-1643.

Cheng, W., and P. B. Rhines, 2004: Response of overturning circulation to high-latitude fresh-water perturbations in the North Atlantic. *Clim. Dyn*., **22**, 359-372.

Cuny, J., P Rhines, S. Niiler, and S. Bacon, 2002: Labrador Sea boundary currents and the fate of the Irminger Sea Water. *J. Phys. Oceanogr*., **32**, 627-647.

Cuny, J., P. B. Rhines, and R. Kwok, 2005a: Davis Strait volume, freshwater and heat fluxes. *Deep-Sea Res. I,* **52**, 519–542.

Cuny, J., P. Rhines, F. Schott, and J. Lazier, 2005b: Convection above the Labrador Continental Slope. *J. Phys. Oceanogr*., **35**, 489-511.

Curry, R. G., M. S. McCartney, and T. M. Joyce, 1998: Oceanic transport of subpolar climate signals to mid-depth subtropical waters. *Nature*, **391**, 575-577.

De Boyer Montegut, C., G. Madec, A. S. Fischer, A. Lazar, and D. Iudicone, 2004: Mixed layer depth over the global ocean: An examination of profile data and a profile-based climatology. *J. Geophys. Res*., **109**, C12003, doi:10.1029/2004JC002378.

Dickson, R., J. Meincke, S. Malmberg, and A. J. Lee, 1988: The "great salinity anomaly" in the Northern North Atlantic 1968-1982. *Prog. Oceanog*. **20**, 103-151.

Dickson, R., J. Lazier, J. Meincke, P. Rhines, and J. Swift, 1996: Long-term coordinated changes in the convective activity of the North Atlantic. *Prog. Oceanog*. **38**, 241-295.

Dickson, R., I. Yashayaev, J. Meincke, B. Turrell, S. Dye, and J. Holfort, 2002: Rapid freshening of the deep North Atlantic Ocean over the past four decades. *Nature*. **416**, 832-836.

Dickson, R., S. Dye, M. Karcher, J. Meincke, B. Rudels, and I. Yashayaev, 2007: Current estimates of freshwater flux through arctic and subarctic seas. *Prog. Oceanog*., **73**, 210-230.

Doney, S. C., W. M. Balch, V. J. Fabry, and R. A. Feely, 2009: Ocean Acidification- A Critical Emerging Problem for the Ocean Sciences. *Oceanography*, **22**(4), 18-25.

DOS, 2009: Status of Wrangel and Other Arctic Islands. U.S. Department of State Fact Sheet. [Available online at http://www.state.gov/p/eur/rls/fs/128740.htm.]

Dunbar, M., 1973: Ice regime and ice transport in Nares Strait. *Arctic*, **26**, 282-291.

Dunlap, E., and C. C. L. Tang, 2006: Modelling the Mean Circulation of Baffin Bay. *Atmosphere-Ocean* **44**(1), pp. 99-110.

Eden, C., and C. Boning, 2002: Sources of Eddy Kinetic Energy in the Labrador Sea. *J. Phys. Oceanogr*., **32**, 3346-3363.

Ellis, B. and L. Brigham, Eds., 2009: *Arctic Marine Shipping Assessment 2009 Report*. Arctic Council, 194 pp.

Fabry, V. J., J. M. McClintock, J. T. Mathis, and J. M Grebmeier, 2009: Ocean Acidification at High Latitudes: The Bellwether. *Oceanography*, **22**(4), 160-171.

Falkingham, J. C., 2000: Sea ice in the Canadian Arctic in the 21st Century. Canadian Ice Service report, 5 pp.

Federoff, G. E., 2009: NSPD Panelist. *3rd Symposium on the Impacts of an Ice-Diminishing Arctic on Naval and Maritime Operations*, Annapolis, MD, U.S. National Ice Center and the U.S. Arctic Research Commission.

Feely, R. A., S. C. Doney, and S. R. Cooley, 2009: Ocean Acidification- Present Conditions and Future Changes in a High-CO2 World. *Oceanography*, **22**(4), 36-47.

Fissel, D. B., D. D. Lemon, and J. R. Birch, 1982: Major Features of the Summer Near-Surface Circulation of Western Baffin Bay, 1978 and 1979. *Arctic*, **35**, 180-200.

Gascard, J. C., and R. A. Clarke, 1983: The formation of Labrador Sea water. Part II: Mesoscale and smaller-scale processes. *J. Phys. Oceanogr*., **13**, 1779-1797.

Gerdes, R., J. Hurka, M. Karcher, F. Kauker, and C. Koberle, 2005: Simulated History of Convection in the Greenland and Labrador Seas, 1948-2001, in *The Nordic Seas: An Integrated Perspective, Geophys. Monogr. Ser.*, vol. 158, edited by H. Drange, T. Dokken, T Furevik, R. Gerdes, and W. Berger, pp. 221-238, AGU, Washington, D.C.

Goosse, H., T. Fichefet, and J. M. Campin, 1997: The effects of the water flow through the Canadian Archipelago in a global ice-ocean model. *Geophys. Res. Lett*., **24**, 1507–1510.

Gove, D., 2009: Arctic Melt: Reopening a Naval Frontier. *Proceedings of the U. S. Naval Institute*, **135**(2), 1,272.

Hakkinen, S., 1999: A simulation of Thermohaline effects of a Great Salinity Anomaly. *J. Clim*., **12**, 1781-1795.

Hatun, H., 2007: Buoyant eddies entering the Labrador Sea observed with gliders and altimetry. *J. Phys. Oceanogr*., **37**, 2838–2854.

Hester, K. C., E. T. Peltzer, W. J. Kirkwood, and P. G. Brewer, 2008: Unanticipated consequences of ocean acidification: A noisier ocean at lower pH. *Geophys. Res. Lett*., **35**, L19601, doi:10.1029/2008GL034913.

Holland, D. M., R. H. Thomas, B. de Young, M. H. Ribergaard, and J. Lyberth, 2008: Acceleration of the Jakobshavn Isbrae triggered by warm subsurface ocean waters. *Nat. Geo*., **1**, 659-664.

Holland, P., 2010: Climate change: Warm bath for an ice sheet. *Nat.Geo*., **3**, 147-148.

Houghton, R. W., and M. H. Visbeck, 2002: Quasi-decadal Salinity Fluctuations in the Labrador. *J. Phys. Oceanogr*., **32**, 687–701.

Howell, S. E. L., and J. J. Yackel, 2004: A vessel transit assessment of sea-ice variability in the Western Arctic, 1969-2002: implications for ship navigation. *Can. J. Remote Senseing*, **30**(2), 205-215.

Howell, S. E. L, A. Tivy. J. J. Yackel, B. G. T. Else, and C. R. Duguay, 2008: Changing sea ice melt parameters in the Canadian Arctic Archipelago: Implications for the future presence of multiyear ice. *J. Geophys. Res*., **113**, C09030, doi:10.1029/2008JC004730.

Hu, A., B. L. Otto-Bliesner, G. A. Meehl, W. Han, C. Morrill, E. C. Brady, and B. Briegleb, 2008: Response of Thermohaline Circulation to Freshwater Forcing under Present-Day and LGM Conditions. *J. Clim.*, **21**, 2239-2258.

Hufford, G., 2009: National Weather Service Alaska Region Sea Ice Program. *3rd Symposium on the Impacts of an Ice-Diminishing Arctic on Naval and Maritime Operations*, Annapolis, MD, U.S. National Ice Center and the U.S. Arctic Research Commission, 1-39.

Jakobsson, M., N. Cherkis, J. Woodward, R. Macnab, and B. Coakley, 2000: New grid of Arctic bathymetry aids scientists and mapmakers. *Eos Trans. AGU*, **81**(9), 89.

Jakobsson, M., R. Macnab, L. Mayer, R. Anderson, M. Edwards, J. Hatzky, H. W. Schenke, and P. Johnson, 2008: An improved bathymetric portrayal of the Arctic Ocean: Implications for ocean modeling and geological, geophysical and oceanographic analyses. *Geophys. Res. Lett.*, doi: 10.1029/2008gl033520.

Jahn, A., L. B. Tremblay, R. Newton, M. M. Holland, L. A. Mysak, and I. A. Dmitrenko, 2010: A tracer study of the Arctic Ocean's liquid freshwater export variability. *J. Geophys. Res.*, **115**, C07015, doi:10.1029/2009JC005873.

Jones, B. M., C. D. Arp, M. T. Jorgenson, K. M. Hinkel, J. A. Schmutz, and P. L. Flint, 2009: Increase in the rate and uniformity of coastline erosion in Arctic Alaska. *Geophys. Res. Lett.*, **36**, L03503, doi:10.1029/2008GL036205.

Joyce, T. M., and A. Proshutinsky, 2007: Greenland's Island Rule and the Arctic Ocean circulation. *J. Mar. Res*, **65**, 639-653.

Jungclaus, J. H., H. Haak, M. Latif, U. Mikolajewicz, 2005: Arctic-North Atlantic Interactions and Multidecadal Variability of the Meridional Overturning Circulation. *J. Clim.*, **18**, 4013-4031.

Kara, A. B., P. A. Rochford, and H. E. Hurlburt, 2000: An optimal definition for ocean mixed layer depth. *J. Geophys. Res.*, **105**, C7, 16,803-16,821.

Kara, A. B., P. A. Rochford, and H. E. Hurlburt, 2002: Naval Research Laboratory Mixed Layer Depth (NMLD) Climatologies. *Naval Research Laboratory Report*. NRL/FR/7330-02-9995, 29pp.

Katsman, C. A., M. A. Spall, and R. S. Pickart, 2004: Boundary Current Eddies and Their Role in the Restratrication of the Labrador Sea. *J. Phys. Oceanogr.*, **34**, 1967–1983.

Kauker, F., T. Kaminski, M. Karcher, R. Giering, R. Gerdes, and M. VoBbeck, 2009: Adjoint analysis of the 2007 all time Arctic sea-ice minimum. *Geophys. Res. Lett.*, **36**, L03707, doi:10.1029/2008GL036323.

Khatiwala, S. P., P. Schlosser, and M. Visbeck, 2002: Rates and mechanisms of water mass transformation in the Labrador Sea as inferred from tracer observations. *J. Phys. Oceanogr*., **32**, 666–686.

Kieke, D., M. Rhein, L. Stramma, W. M. Smethie, D. A. LeBel, and W. Zenk, 2006: Changes in the CFC inventories and formation rates of Upper Labrador Sea Water, 1997-2001. *J. Phys. Oceanogr*., **36**, 64-86.

Kliem, N., and D. A. Greenberg, 2003: Diagnostic Simulations of the Summer Circulation in the Canadian Arctic Archipelago. *Atmosphere-Ocean* **41**(4), 273-289.

Koberle, C., and R. Gerdes, 2007: Simulated Variability of the Arctic Ocean Freshwater Balance 1948-2001. *J. Phys. Oceanogr*., **37**, 1628–1644.

Koenigk, T., U. Mikolajewicz, H. Haak, and J., 2007: Arctic freshwater export in the 20th and 21st centuries. *J. Geophys. Res*., **112**, G04S41, doi:10.1029/2006JG000274.

Komuro, Y., and H. Hasumi, 2005: Intensification of the Atlantic Deep Circulation by the Canadian Archipelago Throughflow. *J. Phys. Oceanogr*., **35**, 775–789.

Kramer, A. E., and A. C. Revkin, 2009: Arctic Shortcut Beckons Shippers as Ice Thaws. *The New York Times*, A1, 11 Sep 2009.

Kruse, D. M., 2009: U. S. National / Naval Ice Center (NIC) Support to Naval and Maritime Operations. *3rd Symposium on the Impacts of an Ice-Diminishing Arctic on Naval and Maritime Operations*, Annapolis, MD, U.S. National Ice Center and the U.S. Arctic Research Commission, 1-39.

Kwok, R., G. F. Cunningham, and S. S. Pang, 2004: Fram Strait sea ice outflow. *J. Geophys. Res.*, **109**, C01009, doi:10.1029/2003JC001785.

Kwok, R., 2005: Variability of Nares Strait ice flux. *Geophys. Res. Lett.*, **32**, L24502, doi:10.1029/2005GL024768.

Kwok, R., 2006: Exchange of sea ice between the Arctic Ocean and the Canadian Arctic Archipelago. *Geophys. Res. Lett.*, **33**, L16501, doi:10.1029/2006GL027094.

Kwok, R., 2007: Baffin Bay ice drift and export: 2002-2007. *Geophys. Res. Lett.*, **34**, L19501, doi:10.1029/2007GL031204.

Kwok, R., E. C. Hunke, W. Maslowski, D. Menemenlis, and J. Zhang, 2008: Variability of sea ice simulations assessed with RGPS kinematics. *J. Geophys. Res.*, **113**, C11012, doi:10.1029/2008JC004783.

Kwok, R., 2009: Thinning and volume loss of the Arctic Ocean sea ice cover: 2003-2008. *J. Geophys. Res.*, **114**, C07005, doi:10.1029/2009JC005312.

Kwok, R., and D. A. Rothrock, 2009: Decline in Arctic sea ice thickness from submarine and ICESat records: 1958-2008. *Geophys. Res. Lett.*, **36**, L15501, doi:10.1029/2009GL039035.

Kwok, R., L. T. Pedersen, P. Gudmandsen, and S. S. Pang, 2010: Large sea ice outflow into Nares Strait in 2007. *Geophys. Res. Lett.*, **37**, L03502, doi:10.1029/2009GL041872.

Lavender, K., R. E. Davis, and W. B. Owens, 2002: Observations of Open-Ocean Deep Convection in the Labrador Sea from Subsurface Floats. *J. Phys. Oceanogr.*, **32**, 511–525.

Lavender, K., R. E. Davis, and W. B. Owens, 2000: Mid-depth recirculation observed in the interior Labrador and Irminger Seas by direct velocity measurements. *Nature*, **407**, 66–69.

Lazier, J.R.N., 1980: Oceanographic conditions at Ocean Weather Ship Bravo, 1964-1986. *Atmos. Ocean*, **18**, 227 - 238.

Lazier, J. R. N., and D. G. Wright, 1993: Annual Velocity Variations in the Labrador Current. *J. Phys. Oceanogr.*, **23**, 659–678.

Lazier, J., R. Hendry, A. Clarke, I. Yashayaev, and P. Rhines, 2002: Convection and restratification in the Labrador Sea, 1990-2000. *Deep-Sea Res., I*, **49**, 1819-1835.

Lehane, B., 1981: *The Northwest Passage*. Time-Life Books, 176 pp.

Lietaer, O., T. Fichefet, and V. Legat, 2008: The effects of resolving the Canadian Arctic Archipelago in a finite element sea ice model. *Ocean Modelling*, **24**, 140-152.

Lilly, J. M., P. B. Rhines, M. Visbeck, R. Davis, J. R. N. Lazier, F. Schott, and D. Farmer, 1999: Observing Deep Convection in the Labrador Sea during Winter 1994/1995. *J. Phys. Oceanogr.*, **29**, 2065–2098.

Lilly, J. M., P. B. Rhines, F. Schott, K. Lavender, J. Lazier, U. Send, and E. d'Asaro, 2003: Observations of the Labrador Sea eddy field. *Prog. Oceanogr.*, **59**, 75–176.

Lindsay, R. W., and J. Zhang, 2006: Arctic Ocean Ice Thickness: Modes of Variability and the Best Locations from Which to Monitor Them. *J. Climate*, **22**, 165-176.

Lindsay, R. W., J. Zhang, A. Schweiger, M. Steele, and H. Stern, 2009: Arctic Sea Ice Retreat in 2007 Follows Thinning Trend. *J. Phys. Oceanogr.*, **29**, 2065–2098.

Logerwell, L., 2008: Cruise Report for the 2008 Beaufort Sea Survey. NOAA, U.S. Department of Commerce, National Marine Fisheries Service, Alaska Fisheries Science Center.

Lubchenko, J., 2009: A Changing Arctic: An Urgent Call for Collaborative and Cooperative Action. *3rd Symposium on the Impacts of an Ice-Diminishing Arctic on Naval and Maritime Operations*, Annapolis, MD, U.S. National Ice Center and the U.S. Arctic Research Commission, 1-13.

Marble, D. C., 2001: Simulated Annual and Seasonal Arctic Ocean and Sea-Ice Variability from a High Resolution, Coupled Ice-Ocean Model. PhD Thesis, Naval Postgraduate School, 181 pp.

Marshall, J., and F. Schott, 1999: Open-ocean convection: Observations, theory, and models. *Rev. Geophys*. **37**, 1-64.

Maslowski, W., W. H. Lipscomb, 2003: High-resolution simulations of Arctic sea ice during 1979-1993. *Polar Research* 22, 67-74.

Maslowski, W., D. Marble, W. Walczowski, U. Schauer, J. L. Clement, A. J. Semtner, 2004: On climatological mass, heat, and salt transports through the Barents Sea and Fram Strait from a pan-Arctic coupled ice-ocean model simulation. *J. Geophys. Res*., **109**, C03032, doi:10.1029/2001JC001039.

Maslowski, W., J. C. Kinney, J. Jakacki, 2007: Toward Prediction of Environmental Arctic Change. *Computing in Science & Engineering*, **9**(6), 29-34.

Maslowski, W., J. C. Kinney, D. Marble, J. Jakacki, 2008a: Towards eddy-resolving models of the Arctic Ocean, in *Ocean modeling in an eddying regime, Geophys. Monogr. Ser.*, vol. 177, edited by M. W. Hecht, and H. Hasumi, pp. 241-264, AGU, Washington, D.C.

Maslowski, W., R. Roman, and J. C. Kinney, 2008b: Effects of mesoscale eddies on the flow of the Alaskan Stream. *J. Geophys. Res*., **113**, C07036, doi:10.1029/2007JC004341.

Mazzetti, M., and T. Shanker, 2009: *Russian Subs Patrolling Off East Coast of U.S. The New York Times.* A5.

McBean, G., G. Alekseev, D. Chen, E. Forland, J. Fyfe, P. Y. Groisman, R., King, H. Melling, R. Vose, and P. H. Whitfield, 2005: *Arctic Climate Impact Assessment Chapter 2- Arctic Climate: Past and Present*. Cambridge University Press, 40 pp.

Melling, H., 2002: Sea ice of the northern Canadian Arctic Archipelago. *J. Geophys. Res.*, **107**(C11), 3181, doi:10.1029/2001JC001102.

Melling, H., T. A. Agnew, K. K. Falkner, D. A. Greenberg, C. M. Lee, A. Munchow, B. Petrie, S. J. Prinsenberg, R. M. Samelson, R. A. Woodgate, 2008: Fresh-Water Fluxes via Pacific and Arctic Outflows Across the Canadian Polar Shelf, in *Arctic-Subarctic Ocean Fluxes*, edited by R. R. Dickson et al., pp.193-247, Springer Science and Business Media B. V., Netherlands.

Mote, T. L., 2007: Greenland surface melt trends 1973-2007: Evidence of a large increase in 2007. *Geophys. Res. Lett.*, **34**, L22507, doi:10.1029/2007GL031976.

Munchow, A., H. Melling, and K. K. Faulkner, 2006: An Observational Estimate of Volume and Freshwater Flux Leaving the Arctic Ocean through Nares Strait. *J. Phys. Oceanogr.*, **36**, 2025-2041.

Munchow, A., K. K. Faulkner, and H. Melling, 2007: Spatial continuity of measured seawater and tracer fluxes through Nares Strait, a dynamically wide channel bordering the Canadian Archipelago. *J. Mar. Res*, **65**, 759-788.

Munchow, A., and H. Melling, 2008: Ocean current observations from Nares Strait to the west of Greenland: Interannual to tidal variability and forcing. *J. Mar. Res*, **66**, 801-833.

Myers, P. G., 2005: Impact of freshwater from the Canadian Arctic Archipelago on Labrador Sea Water formation. *Geophys. Res. Lett*., **32**, L06605.

Myers, P. G., and C. Donnelly, 2008: Water Mass Transformation and Formation in the Labrador Sea. *J. Climate*, **21**, 1622-1638.

Newton, G. B., 2009: A Concept from a Concern: The Arctic Emergency Liaison Office. *3rd Symposium on the Impacts of an Ice-Diminishing Arctic on Naval and Maritime Operations*, Annapolis, MD, U.S. National Ice Center and the U.S. Arctic Research Commission, 1-21.

NOAA, 2010: Monitoring Weather & Climate. [Available online at http://www.cpc.noaa.gov/products/precip/CWlink/pna/month_nao_index.shtml.]

Noble, P. G., 2009: Recent and Planned Oil & Gas Exploration, Development, Production, and Transportation Activity in Arctic Regions. *3rd Symposium on the Impacts of an Ice-Diminishing Arctic on Naval and Maritime Operations*, Annapolis, MD, U.S. National Ice Center and the U.S. Arctic Research Commission, 1-33.

NSF, 2010: Methane Releases From Arctic Shelf May Be Much Larger and Faster Than Anticipated. NSF Press Release 10-036.

NSIDC, 2009: Arctic sea ice extent remains low; 2009 sees third-lowest mark. [Available online at http://nsidc.org/news/press/20091005_minimupr.html.]

NSIDC, 2010a: All About Sea Ice- Processes: Thermodynamics: Albedo. [Available online at http://nsidc.org/seaice/processes/albedo.html.]

NSIDC, 2010b: Arctic sea ice extent falls to third-lowest extent; downward trend persists. [Available online at http://nsidc.org/news/press/20101004_minimumpr.html.]

Overland, J., J. Turner, J. Francis, N. Gillett, G. Marshall, and M. Tjernstrom, 2008: The Arctic and Antarctic: Two faces of climate change. *Eos Trans. AGU*, **89**(19), doi:10.1029/2008EO190001.

Perovich, D. K., J. A. Richter-Menge, K. F. Jones, and B. Light, 2008: Sunlight, water, and ice: Extreme Arctic sea ice melt during the summer of 2007. *Geophys. Res. Lett.*, **35**, L11501, doi:10.1029/2008GL034007.

Peterson, I. K., S. J. Prinsenberg, J. Hamilton, R. Pettipas, 2008: Variability of Oceanographic and Ice Properties of the Canadian Arctic Archipelago. *ICES*, CM2008/B:16.

Pickart, R. S., D. J. Torres, and R. A. Clarke, 2002: Hydrography of the Labrador Sea during active convection. *J. Phys. Oceanogr*., **32**, 428–457.

Prater, M. D., 2002: Eddies in the Labrador Sea as observed by profiling RAFOS floats and remote sensing. *J. Phys. Oceanogr*., **32**, 411–427.

Prinsenberg, S. J., E. B. Bennett, 1987: Mixing and transports in barrow Strait, the central part of the Northwest Passage. *Continental Shelf Research*, **7**(8), pp. 913-935.

Prinsenberg, S. J., J. Hamilton, 2005: Monitoring the volume, freshwater and heat fluxes passing through Lancaster Sound of the Canadian Arctic Archipelago. *Atmosphere-Ocean* **43**(1), pp. 1-22.

Prinsenberg, S., J. Hamilton, I. Peterson, and R. Pettipas, 2009: Observing and interpreting the seasonal variability of the oceanographic fluxes passing through Lancaster Sound in the Canadian Arctic Archipelago, in *Influence of Climate Change on the Changing Arctic and Sub-Arctic Conditions*, edited by C. J. Nihoul and A. G. Kostianoy, pp.125-143, Springer Science and Business Media B. V., Netherlands.

Reynolds, R., 2005: Who Owns Hans Island? National Public Radio. [Available online at http://www.npr.org/templates/story/story.php?storyId=4797368.]

Rignot, E., M. Koppes, and I. Velicogna, 2010: Rapid submarine melting of the calving faces of West Greenland glaciers. *Nat. Geo.*, **3**, 187-191.

Roberts, K., 2008: Russian bomber again intercepted near U.S. Navy ship. *Reuters*. [Available online at http://www.reuters.com/article/idUSN0564833620080305.]

Rocchio, L., 2006: Landsat Island [Available online at http://landsat.gsfc.nasa.gov/news/news-archive/dyk_0001.html.]

Rykova, T., 2010: The Seasonal and Interannual Variability of the West Greenland Current System in the Labrador Sea. PhD Thesis, Massachusetts Institute of Technology and Woods Hole Oceanographic Institution, 159 pp.

Samelson, R. M., T. Agnew, H. Melling, and A. Münchow, 2006: Evidence for atmospheric control of sea–ice motion through Nares Strait. *Geophys. Res. Lett.*, **33**, L02506, doi:10.1029/2005GL025016.

Samelson, R. M., P. L. Barbour, 2008: Low-Level Jets, Orographic Effects, and Extreme Events in Nares Strait: A Model-Based Mesoscale Climatology. *Mon. Wea. Rev.*, **136**, 4746–4759.

Schauer, U., E. Fahrbach, S. Osterhus, and G. Rohardt (2004), Arctic warming through the Fram Strait: oceanic heat transport from 3 years of measurements, *J. Geophys. Res.*, **109**, 14 pp., doi:10.1029/2003JC001823.

Schmidt, S., and U. Send, 2007: Origin and composition of seasonal Labrador Sea freshwater. *J. Phys. Oceanogr.*, **37**, 1445–1454.

Shimada, K., T. Kamoshida, M. Itoh, S. Nishino, E. Carmack, F. McLaughlin, S. Zimmermann, and A. Proshuinsky, 2006: Pacific Ocean inflow: Influence on catastrophic reduction of sea ice cover in the Arctic Ocean. *Geophys. Res. Lett.*, **33**, L08605, doi:10.1029/2005GL025624.

Sigler, M., 2009: Climate Change and Arctic Fisheries. *3rd Symposium on the Impacts of an Ice-Diminishing Arctic on Naval and Maritime Operations*, Annapolis, MD, U.S. National Ice Center and the U.S. Arctic Research Commission, 1-28.

Silversides, A., 2010: Inuit health system must move past suicide prevention to "unlock a better reality," conference told. *Canadian Medical Association Journal*, **182**(1). [Available online at http://www.ncbi.nlm.nih.gov/pmc/articles/PMC2802645.]

Smith, R., and P. Gent, 2002: Reference Manual for the Parallel Ocean Program (POP). National Center for Atmospheric Research, May 2002.

Snyder, J., 2009: Tourism: A Growing Presence in an Ice Diminishing Arctic. *3rd Symposium on the Impacts of an Ice-Diminishing Arctic on Naval and Maritime Operations*, Annapolis, MD, U.S. National Ice Center and the U.S. Arctic Research Commission, 1-20.

Solomon, S., D. Qin, M. Manning, Z. Chen, M. Marquis, K. B. Averyt, M. Tignor, and H. L. Miller, Eds., 2007: *Climate Change 2007: The Physical Science Basis*. Cambridge University Press, 996 pp.

Sou, T., and G. Flato, 2009: Sea Ice in the Canadian Arctic Archipelago: Modeling the Past (1950-2004) and the Future (2041-60). *J. Phys. Oceanogr*., **22**, 2181-2198.

Steele, M., R. Morley, and W. Ermold, 2000: PHC: A global ocean hydrography with a high quality Arctic Ocean. *J. Clim.,* **14**(9), 2079-2087.

Steele, M., and W. Ermold, 2007: Steric Sea Level Change in the Northern Seas. *J. Clim.,* **20**, 403-417.

Straneo, F., 2006: Heat and Freshwater Transport through the Central Labrador Sea. *J. Phys. Oceanogr*., **36**, 606-628.

Straneo, F., and F. Saucier, 2008: The outflow from Hudson Strait and its contribution to the Labrador Current. *Deep-Sea Res. I*, **55**, 926-946.

Straneo, F., G. S. Hamilton, D. A. Sutherland, L. A. Stearns, F. Davidson, M. O. Hammill, G. B. Stenson, and A. Rosing-Asvid, 2010: Rapid circulation of warm subtropical waters in a major glacial fjord in East Greenland. *Nat. Geo*., **3**, 182-186.

Stroeve, J., M. M. Holland, W. Meier, T. Scambos, and M. Serreze, 2007: Arctic sea ice decline: Faster than forecast. . *Geophys. Res. Lett.*, **34**, L09501, doi: 10.1029/2007GL029703.

Tang, C. L., C. K. Ross, T. Yao, B. Petrie, B. M. DeTracey, E. Dunlap, 2004: The circulation, water masses and sea-ice of Baffin Bay. *Prog. Ocn*., **63**, 183-228.

University of Delaware, 2010: Greenland glacier calves island 4 times the size of Manhattan, UD scientist reports. [Available online at http://www.edel.edu/udaily/2011/aug/greenland080610.html.]

USGS, 2008: Circum-Arctic Resource Appraisal: Estimates of Undiscovered Oil and Gas North of the Arctic Circle. USGS Fact Sheet 2008-3049, 4 pp.

Vage, K., R. S. Pickart, V. Thierry, G. Reverdin, C. M. Lee, B. Petrie, T. A. Agnew, A. Wong, and M. H. Ribergaard, 2009: Surprising return of deep convection to the subpolar North Atlantic Ocean in winter 2007-2008. *Nat. Geo*. **2**, 67-72 (2009).

VanderKlippe, N., 2006: Northwest Passage Gets Politcal Name Change. Ottawacitizen.com. [Available online at http://www.canada.com/ottawacitizen/news/story.html? id=6d4815ac-4fdb-4cf3-a8a6-4225a8bd08df&k=73925.]

Vellinga, M., B. Dickson, and R. Curry, 2008: The Changing View on How Freshwater Impacts the Atlantic Meridional Overturning Circulation, in *Arctic-Subarctic Ocean Fluxes*, edited by R. R. Dickson et al., pp.289-313, Springer Science and Business Media B. V., Netherlands.

Wadley, M. R., and G. R. Bigg, 2002: Impact of flow through the Canadian Archipelago and Bering Strait on the North Atlantic and Arctic circulation: An ocean modeling study. *Quart. J. Roy. Meteor. Soc*., **128**, 2187–2203.

Willett, L., 2009: Security Implications of Increased International Commercial and Military Activity in the Arctic. *3rd Symposium on the Impacts of an Ice-Diminishing Arctic on Naval and Maritime Operations*, Annapolis, MD, U.S. National Ice Center and the U.S. Arctic Research Commission, 1-18.

Williams, K., 2004: The Circulation and Fluxes from the Arctic into the North Atlantic Ocean: 1979-2002 Model Results. MS Thesis, Department of Oceanography, Naval Postgraduate School, 111 pp.

Wilson, K. J., J. Falkingham, H. Melling, and R. De Abreu, 2004: Shipping in the Canadian Arctic- Other Possible Climate Change Scenarious. *IGARSS04*, Anchorage, AK, IEEE Geoscience and Remote Sensing Society, 1-4.

Woityra, W., and T. Rossby, 2008: Current broadening as a mechanism for anticyclogenesis at the northwest corner of the North Atlantic Current. *Geophys. Res. Lett.*, **35**, L05609.

Wu, B., J. Wang, and J. E. Walsh, 2006: Dipole anomaly in the winter Arctic atmosphere and its association with sea ice motion. *J. Clim.*, **19**, 210–225.

Wu, B. Y., R. H. Zhang, and R. D'Arrigo, 2008: Arctic dipole anomaly and summer rainfall in Northeast China. *Chinese Science Bulletin*, **53**(14), 2222-2229.

Yashayev, I., 2007: Hydrographic changes in the Labrador Sea, 1960-2005. *Prog. Oceanogr.*, **73**(3-4), 242-276.

Yeager, S. G., and M. Jochum, 2009: The connection between Labrador Sea buoyancy loss, deep western boundary current strength, and Gulf Stream path in an ocean circulation model. *Ocean Modelling*, 30, 207-224.

Zhang, J., and W. D. Hibler, 1997: On an efficient numerical method for modeling sea ice dynamics. *J. Geophys. Res.*, **102**, C4, 8691-8702.

Zhang, J., R. Lindsay, M. Steele, and A. Schweiger, 2008: What drove the dramatic retreat of arctic sea ice during summer 2007? *Geophys. Res. Lett.*, **35**, L11505, doi:10.1029/2008GL034005.

INITIAL DISTRIBUTION LIST

1.   Defense Technical Information Center
        Ft. Belvoir, Virginia

2.   Dudley Knox Library
        Naval Postgraduate School
        Monterey, California

3.   Wieslaw Maslowski
        Oceanography Dept., Naval Postgraduate School
        Monterey, California

4.   Peter Chu
        Oceanography Dept., Naval Postgraduate School
        Monterey, California

5.   Timothy Stanton
        Oceanography Dept., Naval Postgraduate School
        Monterey, California

6.   Rebecca Stone
        Oceanography Dept., Naval Postgraduate School
        Monterey, California

7.   Peter Guest
        Meteorology Dept., Naval Postgraduate School
        Monterey, California

8.   CNMOC
        Stennis Space Center, Mississippi

9.   Oceanographer of Navy
        Washington, D.C.

10.   Chief Scientist
        National/Naval Ice Center
        Suitland, Maryland

11.   CAPT Timothy Gallaudet
        Task Force Climate Change
        Washington, D.C.

12.   CAPT Douglas Marble
        Office of Naval Research
        Arlington, Virginia